


Yasheng Zhang · Yanli Xu
Haijun Zhou

Theory and Design Methods of Special Space Orbits

 国防工业出版社
National Defense Industry Press

 Springer

Theory and Design Methods of Special Space Orbits

Yasheng Zhang · Yanli Xu
Haijun Zhou

Theory and Design Methods of Special Space Orbits

 國防工業出版社
National Defense Industry Press

 Springer

Yasheng Zhang
Department of Space Equipment
Academy of Equipment
Beijing
China

Haijun Zhou
Department of Space Equipment
Academy of Equipment
Beijing
China

Yanli Xu
Department of Space Equipment
Academy of Equipment
Beijing
China

Funded by the B&R Program.

ISBN 978-981-10-2947-9 ISBN 978-981-10-2948-6 (eBook)
DOI 10.1007/978-981-10-2948-6

Jointly published with National Defense Industry Press, Beijing, China

Library of Congress Control Number: 2016954624

Translation from the *Chinese* language edition: 空间特殊轨道理论与设计方法 by Yasheng Zhang, Yanli Xu and Haijun Zhou, © National Defense Industry Press 2015. All Rights Reserved.

© National Defense Industry Press and Springer Nature Singapore Pte Ltd. 2017

This work is subject to copyright. All rights are reserved by the Publishers, whether the whole or part of the material is concerned, specifically the rights of translation, reprinting, reuse of illustrations, recitation, broadcasting, reproduction on microfilms or in any other physical way, and transmission or information storage and retrieval, electronic adaptation, computer software, or by similar or dissimilar methodology now known or hereafter developed.

The use of general descriptive names, registered names, trademarks, service marks, etc. in this publication does not imply, even in the absence of a specific statement, that such names are exempt from the relevant protective laws and regulations and therefore free for general use.

The publishers, the authors and the editors are safe to assume that the advice and information in this book are believed to be true and accurate at the date of publication. Neither the publishers nor the authors or the editors give a warranty, express or implied, with respect to the material contained herein or for any errors or omissions that may have been made.

Printed on acid-free paper

This Springer imprint is published by Springer Nature

The registered company is Springer Nature Singapore Pte Ltd.

The registered company address is: 152 Beach Road, #22-06/08 Gateway East, Singapore 189721, Singapore

Preface

A space orbit refers to the route along which a celestial body travels in space. It can also be called a trajectory or an orbit for short. Generally, there are three types, namely, launch orbit, operational orbit, and re-entry orbit. It follows that space orbit theory is about the principles and methods that the design of a space orbit should comply with, while orbit design is one of the key technologies in spacecraft system design.

Orbit design needs to take many factors into consideration, such as orbit dynamics, space environment, mission requirement, and capability of effective payload, among others. Theories regarding orbit design were proposed long before the first man-made satellite was launched into space.

With the growing demands in space application and the advancements in space technology, classical orbit theories and design methods can no longer meet the requirements of new space missions. There is an urgent need for new space orbit theories which can effectively bring advanced space technology into full play.

On the basis of decade-long research findings, this book aims to answer the call of these new developments. There are eight chapters in this book. The first part consists of the first two chapters, which are a general review of recursive orbit, synchronous orbit, frozen orbit, stay orbit, and other classical orbits, together with their design methods. Based on this review, the focus of this book, i.e., concepts, types, and applications of special space orbits are introduced. The second part is from chapter three to chapter eight. Each chapter is about a specific orbit, together with its concepts, characteristics, design methods, and applications. So altogether, there are six special space orbits which are elaborated, namely, hovering orbit, spiral cruising orbit, multi-target rendezvous orbit, initiative approaching orbit, responsive orbit, and earth pole-sitter orbit.

This book is based on the findings of our research team over the years. We want to thank Profs. Zhi Li and Lei Wang, postgraduate students Xiaojing Xu, Yuanfei Li, and Haijun Zhou, for their contributions to this book.

Theories of space orbit design are closely related to other fast-changing areas of study and develop along with new space applications. The authors are fully aware

of the limitations of this book and warmly welcome comments in order to improve their work.

This book can be used as a technical reference for people engaged in the strategic studies of space development and engineering applications. It can also be used as a textbook for students majoring in space sciences and technologies.

Beijing, China
January 2014

Yasheng Zhang

Contents

1 Overview of Classical Orbits	1
1.1 Recursive Orbit.	1
1.1.1 Recursive Orbit: Definition	2
1.1.2 Different Orbital Periods	2
1.1.3 Geostationary Earth Orbit and Its Applications	4
1.2 Sun-Synchronous Orbit.	5
1.2.1 Sun-Synchronous Orbit: Definition	6
1.2.2 Sun-Synchronous Orbit: Characteristics.	7
1.2.3 Sun-Synchronous Regression Orbit and Its Applications	9
1.3 Frozen Orbit	10
1.3.1 Frozen Orbit: Definition	10
1.3.2 Molniya Orbit and Its Applications.	12
1.4 Stay Orbit.	13
1.4.1 Stay Orbit: Definition	13
1.4.2 Stay Orbit: Applications	15
1.5 Summary	17
2 Special Space Orbit: Concept and Application	19
2.1 Special Space Orbit: Concept	19
2.1.1 Differences in Orbit Design Concepts	20
2.1.2 Coupling of Orbit Control and Orbit Design.	21
2.1.3 Requirements for Special Space Application.	23
2.2 Types of Special Orbit	25
2.2.1 Hovering Orbit	25
2.2.2 Cruising Orbit	25
2.2.3 Multi-Target Rendezvous Orbit.	28
2.2.4 Initiative Approaching Orbit	29
2.2.5 Fast Responsive Orbit	31
2.2.6 Earth Pole-Sitter Orbit.	31

2.3	Description of Special Space Orbit	32
2.3.1	Orbit Element	32
2.3.2	Non Singularity Orbit Elements	33
2.3.3	Rectangular Coordinate Component	34
2.4	Summary	35
3	Theory and Design Method of Hovering Orbit	37
3.1	Hovering Orbit: Concept	37
3.2	Design of Fixed-Point Hovering Orbit	38
3.2.1	Dynamic Model	39
3.2.2	Open-Loop Control	47
3.2.3	Closed Loop Control	52
3.3	Design of Regional Hovering Orbit	56
3.3.1	Analysis of Confined Area Configuration	56
3.3.2	Control of Regional Hovering Orbit	63
3.3.3	Regional Hovering Orbit of Single-Pulse Trust	76
3.3.4	Regional Hovering Orbit of Multi-Pulse Trust	82
3.4	Design of Displaced Geostationary Orbit	83
3.4.1	Displaced Orbit Deviating from Orbit Plane	86
3.4.2	Displaced Orbit in Orbit Plane	88
3.4.3	Energy Analysis of Orbit Displacement	88
3.5	Summary	90
4	Theory and Design Method of Spiral Cruising Orbit	91
4.1	Spiral Cruising Orbit: Concept	91
4.2	Precision Analysis of Relative Motion Model	94
4.2.1	Accurate Relative Motion Dynamics Equation	94
4.2.2	Simplification of Relative Motion Dynamics Equation	96
4.2.3	Precision Analysis of Relative Motion Dynamics Model	98
4.2.4	Analysis of Relative Motion Dynamics Model of Cruising Spacecraft	99
4.3	Traversal Cruising Orbit: Design	103
4.3.1	Design Method Based on Hill Equation	104
4.3.2	Design Method Based on E/I Vector Method	106
4.3.3	Design Constraint	107
4.3.4	Simulation Analysis	110
4.4	Design of the Round-Trip Itinerant Orbit	114
4.4.1	Design Method	114
4.4.2	Design Constraints	117
4.4.3	Simulation Analysis	118
4.5	Controllable Cruising Orbit: Design	121
4.5.1	Spiral Ring: Design	122
4.5.2	Entry Corridor: Design	124
4.5.3	Single-Pulse Control Strategy	127

4.5.4	Fast Cruising Control Strategy	133
4.6	Summary	137
5	Theory and Design Method of Multi-Target Rendezvous	
	Orbit Based on Traversing Points	139
5.1	Multi-Target Orbital Rendezvous: Problem Description	139
5.2	Traversing Point: Concept and Determination Method	142
5.2.1	Traversing Point: Concept.	142
5.2.2	Traversing Point: Determination Method.	144
5.3	Orbital Rendezvous: Strategies Based on Traversing Point.	147
5.3.1	Design Principles Based on Traversing Point	147
5.3.2	Rendezvous Orbit: Design Method	148
5.3.3	Orbital Rendezvous: Control Method	150
5.4	Non-Coplanar Homogeneous Multi-Target Rendezvous Orbit: Design Method.	153
5.5	Non-Coplanar Heterogeneous Multi-Target Rendezvous Orbit: Design Method.	157
5.5.1	Design Procedures.	158
5.5.2	Rendezvous Orbit: Design Method	158
5.5.3	Traversing Point Set: Determination Method.	161
5.5.4	Rendezvous Trajectory: Design Method	162
5.6	Simulation Analysis and Method Correction.	166
5.6.1	Simulation of Orbital Rendezvous Based on Traversing Point.	166
5.6.2	Method Correction of Orbital Rendezvous Based on Traversing Point.	169
5.7	Summary	173
6	Theory and Design Method of Initiative Approaching Orbit.	175
6.1	Initiative Approaching Orbit: Concept	175
6.2	Approaching Orbit: Design.	176
6.2.1	Phasing Orbit	176
6.2.2	Short-Range Approaching Orbit	180
6.3	Dynamics Model of Relative Position and Attitude	181
6.3.1	Dynamics Model of Relative Attitude.	182
6.3.2	Dynamics Model of Relative Position.	184
6.4	Ultimate Approaching Orbit: Design	187
6.4.1	The Final Approach for Three-Axis-Stabilized Target Spacecraft	187
6.4.2	Final Approach to the Target Without Attitude Control	191
6.4.3	Simulation and Realization	194
6.5	Summary	196

7	Theory and Design Method of Responsive Orbit	199
7.1	Fast Responsive Orbit: Concept	199
7.2	Circular Fast Flying-Around Orbit	203
7.2.1	Circular Fast Flying-Around Orbit: Design	203
7.2.2	Target Forbidden Zone: Definition	208
7.2.3	Safety Analysis	209
7.3	Fast Access Orbit	218
7.3.1	Low-Earth-Orbit Fast Access Orbit: Design	219
7.3.2	Cobra Orbit: Design	221
7.4	Summary	223
8	Theory and Design Method of Earth Pole-Sitter Orbit	225
8.1	Earth Pole-Sitter Orbit: Concept	225
8.2	Earth Pole-Sitter Orbit: Design Method	226
8.2.1	Dynamic Model in Circular Restricted Three-Body Problem.	226
8.2.2	Design of Earth Pole-Sitter Orbit with Fixed Residence Distance	228
8.2.3	Design of Earth Pole-Sitter Orbit with Unfixed Residence Distance	230
8.3	Optimization Design of Earth Pole-Sitter Orbit.	233
8.4	Summary	235
Appendix A: Optimization Design of Rendezvous Orbit with MATLAB		237
References		243

Abstract

The book focuses on the theory and design method of special space orbit. With the development human need and the progress in space technique, the classical orbit theory and design method cannot satisfy the new needs anymore. In this book, the concept of special space orbit is put forward, theory and design methods of hovering orbit, spiral cruising orbit, multi-target rendezvous orbit, initiative approaching orbit are expatiated; also, responsive orbit and polar stay is introduced simply.

Hopefully, it would be useful for engineers and scientists working in related fields.

Chapter 1

Overview of Classical Orbits

The operation orbit of a spacecraft directly determines the observational geometry and operating environment of a space mission, and largely determines the payload performance of a spacecraft. Ever since the successful launch of the first artificial satellite in 1957, humankind has spared no effort in exploring the relationship between space missions and spacecraft orbits. Concepts such as recursive orbit, sun-synchronous orbit, frozen orbit, stay orbit, and others, have been successively brought forward and applied in communication, navigation, reconnaissance, meteorological exploration and other space missions. These orbits, with their unique advantages and application having been tested in various space missions and widely acknowledged around the globe, are generally known as classical orbits.

In this chapter, the concepts, characteristics and applications of four classical orbits, i.e., recursive orbit, sun-synchronous orbit, frozen orbit and stay orbit, will be introduced briefly.

1.1 Recursive Orbit

Among the many different kinds of spacecraft, reconnaissance and remote sensing satellites and missile early-warning satellites are responsible for the detection and early warning of hot spots, while communication satellites are required to provide communication support for other particular areas. All these determine that the recursive orbit is the most commonly adopted orbit in space missions.

The geosynchronous orbit, as a unique type of recursive orbit, is subject to stricter constraint conditions. Within each regression period, satellites travelling in the recursive orbit pass all of its coverage areas in sequence, dynamically monitoring these areas and capturing any changes to the targets within the period.

1.1.1 Recursive Orbit: Definition

Recursive orbit refers to the spacecraft orbit with periodically-repeated ground tracks. The time interval of the said repetition is called a regression period, and the time a spacecraft spends on travelling one lap along the orbit is called an orbital period.

The precession resulted from the earth's rotation and the perturbation of its orbit plane keeps a spacecraft's orbit plane rotating relative to a specific longitude line on the Earth. Specifically speaking, a precession angular velocity of the spacecraft's orbit plane relative to the Earth, $\vec{\omega}_e$, is generated because of the earth's rotation. And the impact of the earth's perturbation, especially the earth's non-spherical perturbation, results in $\vec{\Omega}$, a precession angular velocity of the spacecraft's orbit plane relative to the Earth. Hence, by adding the two precession angular velocities, i.e., $\vec{\omega}_e + \vec{\Omega}$, the angular rate of the spacecraft's orbit plane relative to the Earth can be obtained. The time interval, during which an orbit plane completes one rotation relative to a particular longitude line on the Earth, can be calculated and obtained by Eq. (1.1):

$$T_e = \frac{2\pi}{|\vec{\omega}_e + \vec{\Omega}|} \quad (1.1)$$

It takes the Earth one sidereal day to complete one rotation, i.e., to rotate 360° . We can denote a spacecraft orbital period as T, if there are two relatively prime positive integers D and N that satisfy:

$$NT = DT_e \quad (1.2)$$

Then the ground tracks, which start to overlap after the spacecraft travels N laps in D days, is defined as a recursive orbit. N is the minimum number of laps and D the minimum numbers of days required for the repetition of ground tracks to take place. If $D = 1$, then the ground tracks repeat day by day, and their serial numbers are arranged from east to west. Within each day, the equator is equally divided by the ascending and descending of orbits respectively. Figure 1.1 demonstrates a typical division of the equator. If $D > 1$, then the ground tracks repeat every D days instead of every day.

1.1.2 Different Orbital Periods

Under the influences of different perturbations, a spacecraft orbit changes constantly. The period of the corresponding osculating orbit, similarly, changes with time. The period of a spacecraft's osculating orbit determined at any time is defined

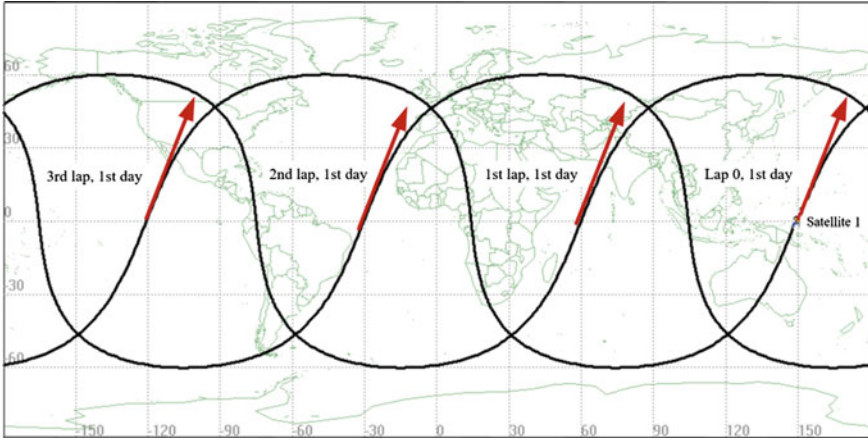


Fig. 1.1 Order of ground tracks when $N/D = 4$

as an osculating period, a time interval that cannot be measured directly. Hence, other two measurable periods, i.e., the nodal period and the perigee period, are more frequently used in real work. Their definitions are as follows:

Nodal period is the time interval it takes a satellite to travel across the ascending nodes twice successively.

Perigee period refers to the time interval it takes a satellite to travel across the perigees twice successively.

If we do not take the influence of perturbation into consideration, the osculating orbit overlaps with the actual orbit and the osculating period, nodal period and perigee period, which can be calculated and obtained by Eq. (1.3), are equivalent:

$$T = 2\pi\sqrt{\frac{a^3}{\mu}} \tag{1.3}$$

Nevertheless, when perturbation is taken into account, the three periods vary from each other.

Specifically speaking, the integral expression of a nodal period is:

$$T_{\Omega} = \int_0^{2\pi} \left(\frac{dt}{du} \right) du \tag{1.4}$$

Here, u represents the argument of latitude, or the argument of the ascending node. When only J_2 -perturbation is taken into account, Eq. (1.4) can be expanded and transformed until $O(J_2e^2)$ exists in the expression. The transformation equation between a nodal period and an osculating period can then be expressed as:

$$T_{\Omega} = T_0 \left\{ 1 - \frac{3J_2}{8a^2} [(12 + 34e^2) - (10 + 20e^2) \sin^2 i - (4 - 20 \sin^2 i)e \cos \omega + (18 - 15 \sin^2 i)e^2 \cos 2\omega] \right\} \quad (1.5)$$

Here, T_0 stands for the osculating period, and α , e , i and ω are the osculating orbit elements of a spacecraft when $u = 0$ (i.e., at the ascending node).

The perigee period can be expressed as:

$$T_{\omega} = \int_0^{2\pi} \left(\frac{dt}{dM} \right) dM \quad (1.6)$$

Here, M represents the mean anomaly. When only J_2 -perturbation is taken into account, Eq. (1.6) can be expanded and transformed until $O(J_2 e^2)$ exists in the expression. The transformation equation between a perigee period and an osculating period can then be expressed as:

$$T_{\omega} = T_0 \left[1 - \frac{3J_2}{2a^2} (1 - e)^{-3} \left(1 - \frac{3}{2} \sin^2 i + \frac{3}{2} \sin^2 i \cos 2\omega \right) \right] \quad (1.7)$$

Here, T_0 stands for the osculating period, and α , e , i and ω are the osculating orbit elements of a spacecraft when $M = f = 0$ (i.e., at the perigee).

1.1.3 Geostationary Earth Orbit and Its Applications

Geostationary Earth Orbit (GEO) is a unique type of recursive orbit, on which the spacecraft completes one lap around the Earth per day. Its orbital period is one day and its regression period is also one day. As a circular orbit, the GEO has an orbit altitude of 35,786 km and an orbit inclination of 0° . A satellite that travels on the GEO is stationary relative to the surface of the Earth. That is to say, a GEO satellite is fixed to a certain location above the earth's equator, as shown in Fig. 1.2.

However, a GEO satellite is by no means fixed in space as it is actually travelling at a speed of 3.07 km per second. It appears stationary relative to the earth's surface simply because it shares the same rotational angular rate and direction with the Earth when it rotates around the earth's axis. Theoretically speaking, there is only one GEO, on which many satellites are distributed above the equators at different longitudes. The fixed location of each GEO satellite is the geographic longitude at the very moment when the satellite enters the GEO. A high precision is required for the positioning of the GEO since the satellite may drift even if there is only a minor error. If the satellite drifts northward or southward, the orbit inclination will no longer be 0° , and the orbit plane will stop overlapping with the equatorial plane. In

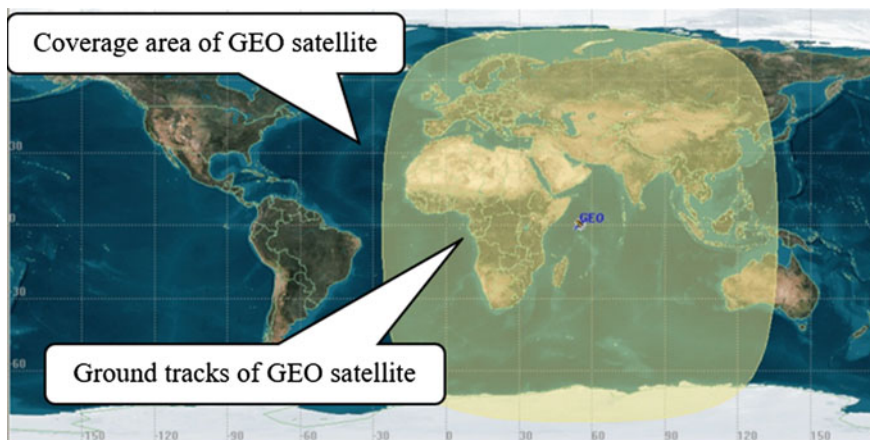


Fig. 1.2 Ground tracks and coverage area of GEO

this case, the satellite moves along the latitude direction once every day and the ground tracks form a shape of “8”, pointing to the north and the south.

One GEO satellite can cover approximately 40 % of the earth’s surface. Therefore, three satellites, distributed equidistantly along the equator, can achieve a global coverage of the earth’s surface, excluding the polar regions. As GEO satellites are relatively stationary, the antennas of ground stations can easily trace them, making the GEO more preferable for communication satellites, broadcast satellites and meteorological satellites.

GEO is the most widely used type of orbit so far. However, we need to consider the strict restrictions and safety factors of GEO satellites in normal operating conditions. For controlled satellites, it is required by the *Radio Regulations* that the position-keeping precision of GEO satellites should not be larger than $\pm 1^\circ$, indicating that the orbital separation between two satellites should be kept larger than 2° .

In 1979, the *Radio Regulations* further ruled that the drift should be kept no larger than $\pm 0.1^\circ$. Thanks to the advancement in space technology, GEO satellites can now be deployed at an even smaller longitude separation. Figure 1.3 demonstrates the spatial distribution of GEO controlled satellites up to December, 2012, offered by the European Space Agency (ESA).

1.2 Sun-Synchronous Orbit

As its name implies, a sun-synchronous orbit is closely related to the Sun. The well-known resources satellites, meteorological satellites, ocean satellites and so on, including the American IKONOS satellite and the French Helios reconnaissance satellite, all adopt sun-synchronous orbits.

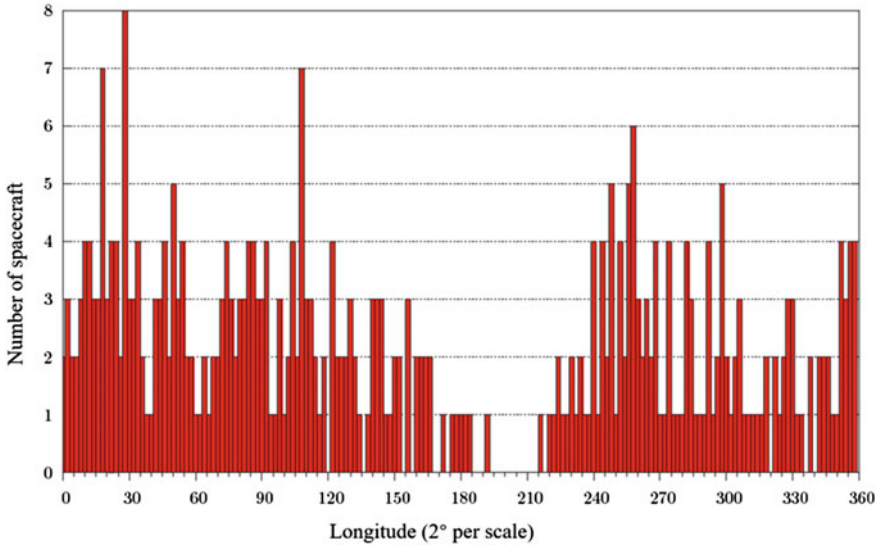


Fig. 1.3 Spatial distribution of GEO spacecraft (Controlled satellites) (Classification of Geosynchronous objects, issue 15 [R]. European Space Agency, European Space Operations Center 2013.)

1.2.1 Sun-Synchronous Orbit: Definition

A sun-synchronous orbit refers to the orbit in which the precession angular velocity of the spacecraft's orbit plane is equal to the angular velocity of the mean Sun when it moves along the equator.

Influenced by the non-spherical perturbation of the Earth, the spacecraft's orbit plane keeps a precession angular velocity of $\dot{\Omega}$. If only the long-term J_2 -perturbation is taken into account, $\dot{\Omega}$ can be expressed by Eq. (1.8):

$$\dot{\Omega} = -\frac{9.97}{(1-e^2)^2} \left(\frac{R_e}{a}\right)^{3.5} \cos i(^{\circ}/d) \quad (1.8)$$

A tropical year is defined as the time interval it takes for the mean Sun to move across the vernal equinox twice successively during its apparent annual motion along the equator. And it is equal to 365.2422 mean solar days. Hence, the angular velocity of the mean Sun moving along the equator is:

$$\frac{360}{365.2422} = 0.9856^{\circ}/d$$

In accordance with its definition, the sun-synchronous orbit can be described as:

$$-\frac{9.97}{(1-e^2)^2} \left(\frac{R_e}{a}\right)^{3.5} \cos i = 0.9856 \quad (1.9)$$

If the orbital eccentricity $e = 0$, then the satellite orbit is a circular orbit, Eq. (1.9) can be further transformed and simplified into:

$$-9.97 \left(\frac{R_e}{a}\right)^{3.5} \cos i = 0.9856 \quad (1.10)$$

The relation between the semi-major axis of a sun-synchronous circular orbit and the orbit inclination can thus be obtained. It is manifest that the orbit inclination of a sun-synchronous orbit is always larger than 90° .

1.2.2 Sun-Synchronous Orbit: Characteristics

The spacecraft on the sun-synchronous orbit always have a constant local mean solar time, or the sun elevation angle when they travel past areas with the same latitude from the same direction. This feature of the sun-synchronous orbit makes it a favorable choice for sun-related satellites. For instance, by adopting the sun-synchronous orbit, a visible reconnaissance satellite receives preferable illumination conditions and achieves better optical reconnaissance results when it passes specific target areas during each ascending or descending movements.

The included angle between the direction of the Sun and the local horizontal plane of a sub-satellite point is called the Sun elevation angle. If we suppose the distance between the Sun and the Earth is infinite, then the sunlight can be considered as parallel light. In Fig. 1.4, S, O_e and p are the sub-satellite point, the Earth center-of-mass (CM), and the local horizontal plane in which the sub-satellite point locates respectively.

We can denote the sun elevation angle of a sub-satellite point as h_Θ according to its definition. As the sunlight is parallel, the incident angle of any spot in plane p remains the same. Hence,

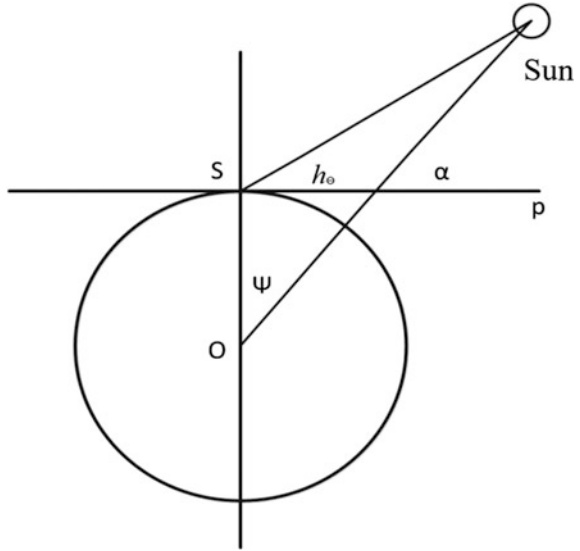
$$h_\Theta = \alpha = \frac{\pi}{2} - \Psi \quad (1.11)$$

In accordance with the equation of spherical triangle, Eq. (1.12) can be obtained:

$$\sin h_\Theta = \cos \Psi = \sin \delta \sin \delta_\Theta + \cos \delta \cos \delta_\Theta \cos(\alpha_\Theta - \alpha) \quad (1.12)$$

Given that the mean Sun moves in the equatorial plane, i.e., $\delta_\Theta = 0$, Eq. (1.12) can be transformed into

Fig. 1.4 Sun elevation angle

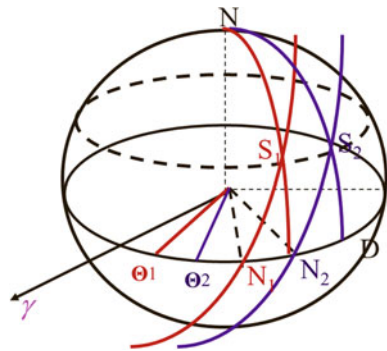


$$\sinh_{\Theta} = \cos \delta \cos(\alpha_{\Theta} - \alpha) \tag{1.13}$$

As is shown in Fig. 1.5, a spacecraft travels in the orbit for a complete cycle T . It descends and travels across the same circle of latitude twice consecutively, the two descending nodes of which are denoted as S_1 and S_2 . The corresponding ascending nodes at which the spacecraft crosses are denoted as N_1 and N_2 , and the corresponding locations of the mean Sun as Θ_1 and Θ_2 .

In accordance with the equation of spherical triangle, the right ascensions of S_1 and S_2 , i.e., α_1 and α_2 , can be determined by the orbit inclination and the local latitude, i.e.,

Fig. 1.5 Satellite travelling past areas with the same latitude from the same direction



$$\alpha_1 - \alpha_{N1} = a \sin\left(\frac{\cos i}{\cos \delta}\right) \quad (1.14)$$

$$\alpha_2 - \alpha_{N2} = a \sin\left(\frac{\cos i}{\cos \delta}\right) \quad (1.15)$$

Here, α_{N1} and α_{N2} stand for the right ascensions of N_1 and N_2 respectively. Formula (1.15) minus (1.14) is Eq. (1.6).

$$\alpha_2 - \alpha_1 = \alpha_{N1} - \alpha_{N2} \quad (1.16)$$

In accordance with the definition of the sun-synchronous orbit,

$$\alpha_{N1} - \alpha_{N2} = \alpha_{\Theta 2} - \alpha_{\Theta 1} \quad (1.17)$$

Here, $\alpha_{\Theta 2}$ and $\alpha_{\Theta 1}$ are the corresponding right ascensions of Θ_1 and Θ_2 respectively. Hence,

$$h_{\Theta 1} = h_{\Theta 2} \quad (1.18)$$

1.2.3 Sun-Synchronous Regression Orbit and Its Applications

The design of a sun-synchronous orbit usually involves two steps. The first step is to design the orbit altitude, or the semi-major axis for a circular orbit, which depends on the demands of the satellite's overall design for coverage, resolution and coverage period. Once the orbit altitude is determined, the orbit inclination can be confirmed. The second step is to design the right ascension of ascending node (RAAN), or to decide the proper launch time, satisfying the demands for the relative location of the satellite orbit and the Sun. For a sun-synchronous orbit, satisfying the demand for the sun elevation angle is the first priority.

In practical application, the sun-synchronous regression orbit, which is a combination of the sun-synchronous regression orbit and the recursive orbit, is more frequently adopted. The design of a sun-synchronous regression orbit involves the following three procedures:

- (1) Determine the orbital period that satisfies certain regressive conditions, i.e., $T = D$ mean Sun day/ N . Here, N refers to the number of laps the satellite travels in D mean Sun days;
- (2) Calculate the semi-major axis of the orbit according to the orbital period Formula, Eq. (1.3);
- (3) Determine the orbit inclination in accordance with Eq. (1.10), i.e., the constraint conditions of a sun-synchronous orbit.

1.3 Frozen Orbit

A frozen orbit is also known as apsidal line frozen orbit. Like the sun-synchronous orbit, it has many valuable properties. For instance, the shape of a frozen orbit, its 90° perigee argument, and the altitude of spacecraft when it travels above areas with the same latitude from the same direction all maintain unchanged. These properties provide favorable conditions for ground inspection and the scientific measurement of the vertical section.

1.3.1 Frozen Orbit: Definition

The non-spherical perturbation of the Earth results in the rotation of a space orbit plane in inertial space, i.e., the precession of the orbit plane and the rotation of the apsidal line. A frozen orbit refers to the orbit whose semi-major axis, or the apsidal line, consistently points in the same direction. In other words, frozen orbits are orbits with constant eccentricity and perigee argument. Therefore, this kind of orbit can be described as follows:

$$\begin{cases} \frac{d\omega}{dt} = 0 \\ \frac{de}{dt} = 0 \end{cases} \quad (1.19)$$

If only the long-term J_2 -perturbation is taken into account, then Eq. (1.19) can be expressed as:

$$\begin{cases} \frac{d\omega}{dt} = \frac{3nJ_2a_E^2}{a^2(1-e^2)^2} \left(1 - \frac{5}{4}\sin^2 i\right) = 0 \\ \frac{de}{dt} = 0 \end{cases} \quad (1.20)$$

Here, n , a_E , a , e , and i refer to the mean angular rate of the orbit, semi-major axis of the Earth, semi-major axis of the orbit, eccentricity, and orbit inclination respectively.

When we suppose that the apsidal line does not rotate, it can be gained from the first equation of Eq. (1.20) that

$$i = 63.4^\circ \quad \text{or} \quad 116.4^\circ$$

Here, orbit inclinations of 63.4° and 116.4° are called critical inclinations. If J_2 and J_3 perturbations are taken into account, then it is required that:

$$\begin{cases} \frac{d\omega}{dt} = \frac{3nJ_2a_E^2}{a^2(1-e^2)^2} \left(1 - \frac{5}{4}\sin^2 i\right) \left[1 + \frac{J_3a_E}{2J_2a(1-e^2)} \frac{(\sin^2 i - e \cos^2 i) \sin \omega}{e \sin i}\right] = 0 \\ \frac{de}{dt} = \frac{-3na_E^3 J_3 \sin i}{2a^3(1-e^2)^2} \left(1 - \frac{5}{4}\sin^2 i\right) \cos \omega = 0 \end{cases} \quad (1.21)$$

It can be gained by solving Eq. (1.12) that when $i = 63.4^\circ$ or $i = 116.4^\circ$, the requirements for a frozen orbit are still met. In addition, if $\omega = 90^\circ$ and $\omega = 270^\circ$, then $de/dt = 0$. The rotation of the apsidal line can also be stopped if i satisfies:

$$1 + \frac{J_3a_E}{2J_2a(1-e^2)} \frac{\sin^2 i - e \cos^2 i}{e \sin i} = 0 \quad (1.22)$$

Figure 1.6 illustrates the relationship between the eccentricity, the orbit altitude, and the orbit inclination of a frozen orbit.

The computational accuracy of a frozen orbit, which is actually the product of zonal harmonics' balance, depends on the order of the zonal harmonic. The larger the order is, the more precise the calculation is and the more computational effort it takes. Generally speaking, only J_2 and J_3 should be considered when the orbit inclination is smaller than 50° . Zonal harmonics higher than J_3 should be taken into account when the orbit inclination is larger than 50° .

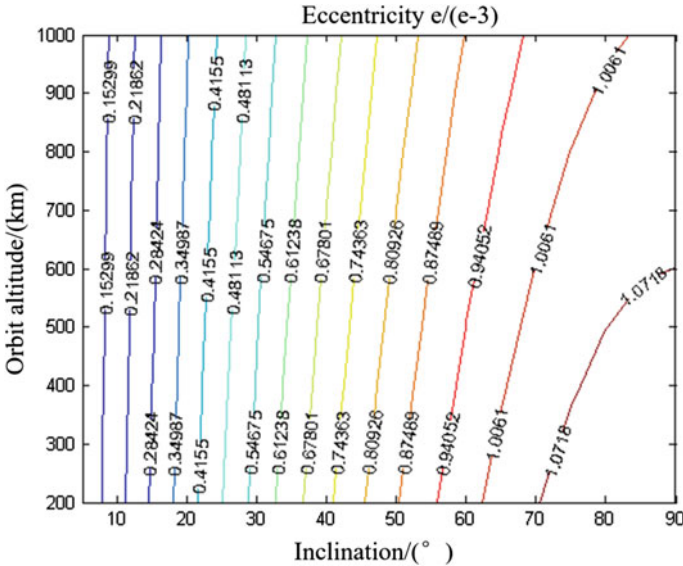


Fig. 1.6 Relationship between eccentricity, orbit altitude, and orbit inclination of a frozen orbit

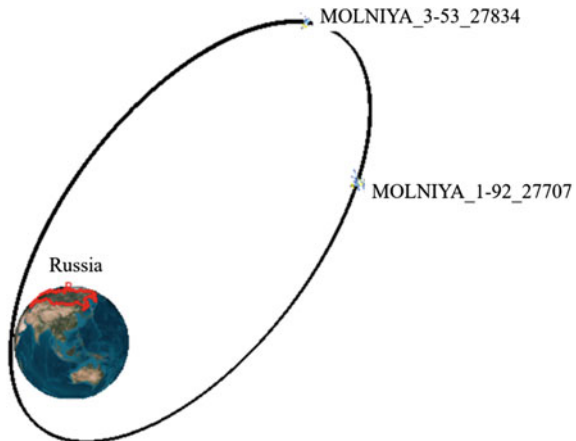
1.3.2 Molniya Orbit and Its Applications

A Molniya Orbit is a highly elliptical orbit with frozen characteristics, the major feature of which is the relatively long time it stays in space in the northern or southern hemisphere. The Russian Molniya (Russian: Молния) communications satellite system, a communications satellite system for both civil and military uses, is a typical Molniya orbit. Molniya satellites operate at an orbit altitude of $400 \text{ km} \times 40,000 \text{ km}$, with an orbit inclination of 63.4° and an orbital period of 12 h. See Fig. 1.7 for details.

Russia (USSR) is located at a relatively high latitude, many areas of which cannot be fully covered by a GEO satellite. In comparison, the Molniya Orbit has its apogee positioned above the northern hemisphere. A Molniya satellite spends around $2/3$ of its operating time per lap in the said area. Moreover, its relatively slow velocity relative to the movement of the earth's surface makes it easy to be tracked by ground stations. This is very favorable for satellite communications in high latitudes.

The Molniya communications satellites, initially launched in 1964, have now been developed for three generations. The current system in commission is of the third generation, with some improved first-generation satellites still being launched and used simultaneously. The whole constellation consists of 8 satellites, with a 45° included angle between every two orbit planes, providing constant communication coverage for high latitude areas. The first generation of the Molniya satellite was developed with a military communication payload. This satellite weighs 1600 kg, with 500–700 W power and a designed life of two years, and carries more than one 40 W military transponders. The third generation of the Molniya satellite is mainly used for civil communication domestically. The satellite has a weight of 1750 kg, with 1200 W power and a designed life of four years, and carries three 30 W traveling wave tube amplifiers, with two in use and one for back up. The uplink and downlink frequencies are 5.975–6.225 GHz and 3.650–3.900 GHz respectively.

Fig. 1.7 Molniya satellites



The satellite adopts C-band global beam antenna with circular polarization. Earlier Molniya satellites used to carry meteorological sensors, and were even responsible for the U.S.-USSR presidents' hotline communications during the Cold War.

1.4 Stay Orbit

Generally speaking, there are three statuses for the ground tracks of spacecraft, i.e., eastward movement, westward regression and stay. The so-called stay, as its name implies, refers to the long-time stop over a certain area. Therefore, the stay orbits can be used by missile early-warning satellites or communication satellites, and the key coverage areas can be the high latitudes which are out of reach for GEOs.

1.4.1 Stay Orbit: Definition

We can denote the geographic longitude of the ground track of a spacecraft as $\lambda(t)$, if points that satisfy the following conditions exist in the geographic longitude of the ground track, then the orbit is called a stay orbit, and the points are called staying points.

$$\frac{d\lambda}{dt} = 0 \quad (1.23)$$

Given the equation of the satellites' ground tracks as:

$$\lambda = \lambda_{\Omega} + \arctg(tgu \cos i) - \omega_e t \quad (1.24)$$

Here, λ_{Ω} refers to the geographic longitude of the ascending nodes at a certain time t_0 ; u and i are the argument of the ascending node and the orbit inclination of the orbit respectively; ω_e refers to the angular rate of earth rotation.

When we take derivatives of Eq. (1.24) on both sides and substitute Eq. (1.23) into it, the following can be obtained:

$$\frac{d\lambda}{dt} = \frac{\cos i}{1 - (\sin i \sin u)^2} \frac{du}{dt} - \omega_e = 0 \quad (1.25)$$

Since

$$\begin{cases} \frac{du}{dt} = \frac{h}{r^2} = \frac{\sqrt{\mu P}}{r^2} = \left(\frac{\mu}{a^3}\right)^{\frac{1}{2}} \frac{[1 + e \cos(f)]^2}{\sqrt{(1-e^2)^3}} = \frac{2\pi}{T} \frac{[1 + e \cos(u-\omega)]^2}{\sqrt{(1-e^2)^3}} \\ \omega_e = \frac{2\pi}{24} \end{cases} \quad (1.26)$$

Here, T stands for the orbital period of a spacecraft, with hour as the unit of measurement; f refers to the true perigee angle; and ω refers to the perigee argument.

When we substitute Eq. (1.26) into Eq. (1.25), the following can be obtained:

$$\frac{\cos i}{1 - (\sin i \sin u)^2} \frac{[1 + e \cos(\omega + f)]^2}{\sqrt{(1 - e^2)^3}} \frac{2\pi}{T} = \frac{2\pi}{24} \quad (1.27)$$

If the spacecraft orbit is a circular one, i.e., $e = 0$, then the condition for the stay points is transformed into:

$$\frac{\cos i}{1 - (\sin i \sin u)^2} = \frac{T}{24} = \frac{1}{k} \Rightarrow \sin u = \pm \frac{(1 - k \cos i)^{\frac{1}{2}}}{\sin i} \quad (1.28)$$

It can be obtained by analyzing Eq. (1.28) that, if the equation is to have a solution, then the following conditions have to be satisfied:

$$\begin{cases} 0^\circ \leq i \leq 90^\circ \\ \cos i \leq \frac{1}{k} \\ \sin i \geq (1 - k \cos i)^{1/2} \end{cases} \quad (1.29)$$

Combining the above conditions, the following can be gained:

$$\cos i \leq \min\left(k, \frac{1}{k}\right) \quad (1.30)$$

Apparently, if $k = 4$, then the condition for the existence of stay points is $73^\circ \leq i \leq 90^\circ$; if $k = 1$, then the condition for the existence of stay points is $i \leq 90^\circ$; if $k = 16$, then the condition for the existence of stay points is $86.4^\circ \leq i \leq 90^\circ$.

The locations of the stay points on the stay orbits are:

$$\cos \varphi = \pm \sqrt{\frac{24}{T} \cos i} \quad (1.31)$$

For elliptical orbits, if the semi-major axis of orbit a is relatively large, then the orbital period T is correspondingly large and the ratio k is relatively small. Therefore, it is more probable that there exists a stay point. If the eccentricity e is relatively small, then it is more probable that there exists a stay point near the perigee or the apogee. If the eccentricity e is relatively large, then the stay points are not likely to be discovered near the perigee when they are found near the apogee.

1.4.2 Stay Orbit: Applications

The spacecraft travelling in the stay orbits can stay for a long time near the stay points, enabling the spacecraft to conduct itinerating observation of a certain longitude line or latitude line of the Earth.

In fact, the GEO and Molniya orbit introduced earlier in this chapter both belong to a unique type of the stay orbits. We can denote the orbit altitude of a Molniya satellite as $39,850.5 \text{ km} \times 500 \text{ km}$ and the orbit inclination as 63.4° , then the stay point is located at 89°E . The ground tracks of the satellite are shown in Fig. 1.8.

The longitudes of the satellite's ground tracks change with time during one orbital period, as shown in Fig. 1.9. It is manifest from the figure that the satellite can conduct long-term itinerating observation at the 89°E longitude.

The orbital period of the said stay orbits is 12 h. We can denote that the spacecraft is a communications satellite which demands a minimum elevation of 15° for communication requirements, correspondingly then the satellite can provide Russia (the red area in Fig. 1.8) with as long as 11 h of communication services within each orbital period, as shown in Fig. 1.10.

Since the GEO cannot cover high latitude areas, it is difficult to achieve constant coverage of the said areas. Generally speaking, a constellation consisting of several satellites are required for this mission. Nevertheless, the use of a stay orbit makes it

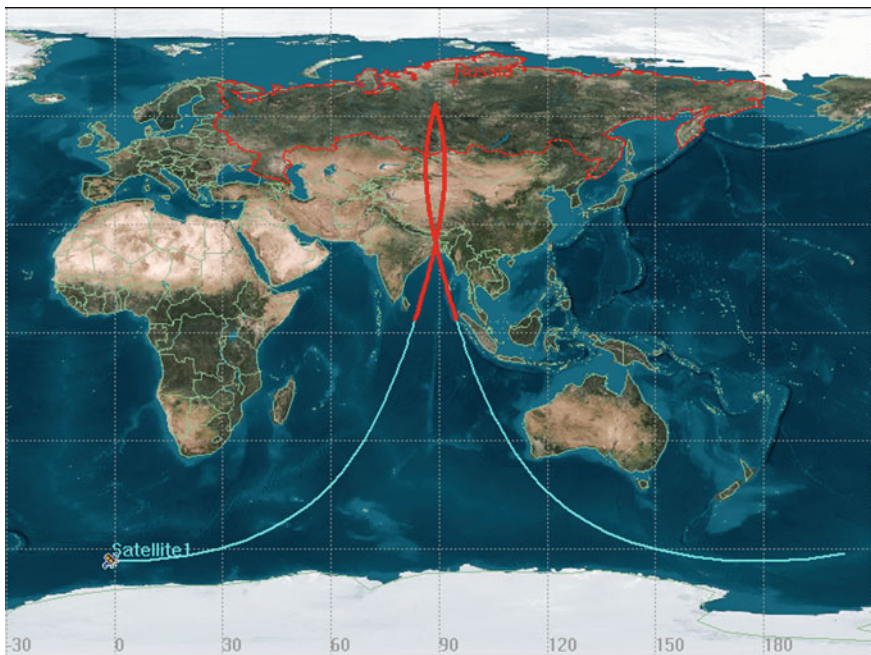


Fig. 1.8 Ground tracks and stay point of Molniya satellite

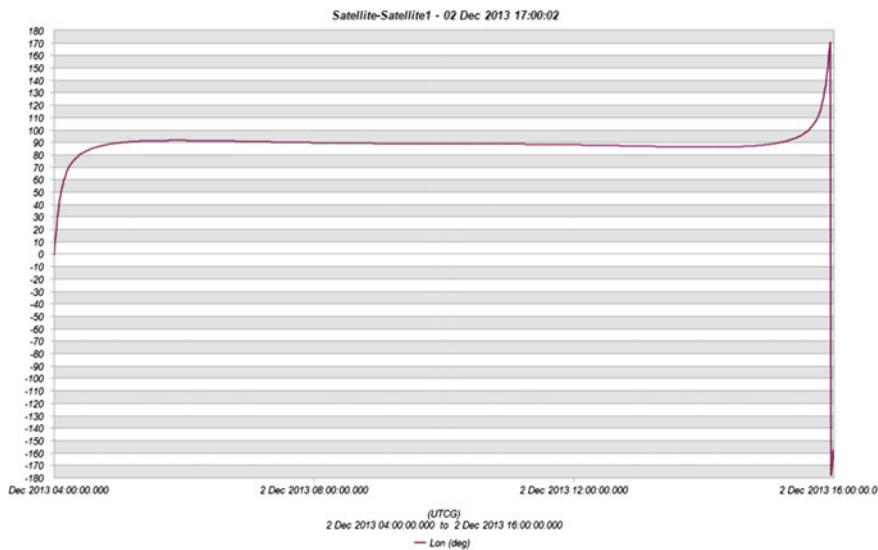


Fig. 1.9 Variation curve of the longitudes of the stay orbit’s ground tracks as time changes

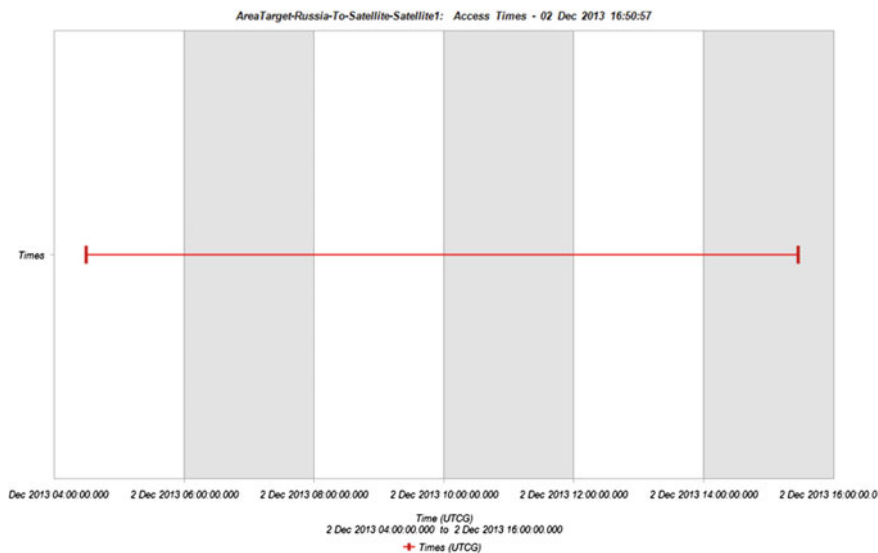


Fig. 1.10 Valid service time of communication satellite for Russia

possible for a single satellite to hover over the high latitudes for a long time, effectively reducing the number of satellites needed. Hence, the stay orbits are highly valuable for countries located in this area.

1.5 Summary

Tested by years of astronautical practices, the application value and practicability of the typical orbits have been widely recognized. Currently, the majority of the satellites used for earth observation, communications, navigation, and others, still adopt these orbits.

Actually, the typical orbits introduced in this chapter are mainly orbits that rotate around the Earth and regard the Earth as their references. Orbits that are beyond the Earth's gravitational field and used to conduct lunar exploration, interplanetary exploration or even galaxy exploration, as well as orbit formations that regard spacecraft operating in the space as references, are not included in this book. Nevertheless, these orbits have also developed maturely, with systematic orbit theories and design methods. Readers interested in them may refer to relative papers and books for more information.

Chapter 2

Special Space Orbit: Concept and Application

Since the beginning of the 21st century, mankind has been carrying out various space activities, especially new types of space missions such as space-based space target surveillance, on-orbit service, and so on. These activities have brought about increasingly higher requirements for orbits with special space motion characteristics. However, traditional orbit theories and design methods can no longer satisfy these special application demands. Therefore, in this chapter, the concepts and characteristics of a special space orbit will be introduced and analyzed, with six typical special space orbits elaborated in accordance with their specific application requirements.

2.1 Special Space Orbit: Concept

A spacecraft orbit refers to the motion trajectory of the centroid of an operating spacecraft. In the light of different flight missions, orbits can be generally classified into three categories, i.e., the artificial earth satellite trajectory, the Earth-to-Moon flight trajectory and the interplanetary flight trajectory. Typical orbits are usually Keplerian ones, which satisfy the fundamental motion equations of the restricted two body problem. Taking advantage of the typical orbit equations, such as the above fundamental motion equations and the Kepler Equation, these orbits can be precisely predicted.

$$r = \frac{a(1 - e^2)}{1 + e \cos f} \quad (2.1)$$

Here, a , e , r and f refer to the semi-major axis, the eccentricity, the geocentric distance and the true anomaly of an orbit, respectively.

The concept of special space orbit was put forward relative to the currently widely applied typical space orbit. Compared to typical orbits, special space orbits have the following unique features.

2.1.1 Differences in Orbit Design Concepts

With the successful launch of the first artificial earth satellite in the 1950s, design theories and methods of spacecraft orbit have been developing rapidly. The primary missions of a spacecraft at that time were to conduct reconnaissance and surveillance of hotspot areas, and to provide communications and navigation support for the army, the navy and the air force. Hence, the design of a spacecraft orbit at that time focused mainly on the relative motion between the spacecraft and the ground area, and the absolute orbit design methods, which take the Earth as the reference, were adopted, e.g., the sun-synchronous orbit, the recursive orbit, the stay orbit, and so on.

In addition, mankind has spared no efforts in exploring untapped areas in space. In the 1960s, there were many lunar exploration projects with burgeoning interplanetary explorations to Venus, Mercury, Mars, and other planets. Meanwhile, theories and design methods in interplanetary exploration orbits have become increasingly mature. The mid and late 1990s witnessed another round of upsurge in lunar exploration and interplanetary exploration with well-established theories and design methods.

With the continuous development of astronautical technology and the heightened military status of space, the functions of spacecraft, such as providing on-orbit service, conducting space-based space target surveillance and so on, have become the focus of all countries. To support these missions, the concept of relative orbit, which takes spacecraft as the reference point, started to emerge. In the 1990s, the idea of distributed satellites led to the explicit proposal of theories and design methods of a spacecraft relative motion orbit, which have matured in the last 20 years.

To sum up, the well-developed spacecraft orbit theories and the corresponding typical orbits today are shown in Table 2.1.

Nevertheless, there are major distinctions in the theories and design methods between special space orbits and the above typical orbits. Moreover, completely different space orbits are required by different missions, resulting in the discrepancy in the theories, principles and methods when designing these special space orbits. For instance, the hovering orbit is a type of relative orbit that regards the target spacecraft as a reference; the spiral cruising orbit is a kind of relative orbit that takes the target orbit as a reference; and the non-coplanar multi-target rendezvous orbit is a fitting orbit based on several traversing points in the rendezvous orbit plane. Hence, it is necessary to introduce the theories and design methods of special space orbits in combination with the specific mission requirements and orbit types.

Table 2.1 Well-developed spacecraft orbit theories and design methods at present

Initial time	Orbit theory	Type of typical orbit
1950s	Theory and design method of absolute orbit	Recursive orbit Sun-synchronous orbit Frozen orbit Stay orbit...
1960s	Theory and design method of interplanetary orbit	Lunar probe orbit (Chang'e Lunar probe satellite, China) Mars probe orbit (Curiosity Mars Rover, U.S.) ...
Mid-and-late 1990s	Relative orbit design method that takes spacecraft as the reference point	Formation flight (Cluster II, European space agency, ESA) (TanDEM-X/TerraSAR-X formation flying satellite of synthetic aperture radar, Germany)

2.1.2 Coupling of Orbit Control and Orbit Design

At the early stages of astronomical technological development, restricted by immature technologies in space marching, fueling, and others, spacecraft orbit control was cautiously applied in the following four areas:

(1) Launching GEO satellites

Restricted by the geographic latitudes of spacecraft launching spots, GEO satellites are unlikely to be launched directly into their orbits. Generally speaking, a GEO satellite is usually firstly sent up into the parking orbit with an altitude of 200–400 km. As the satellite approaches the space above the equator, the upper stage rocket is ignited, and the satellite breaks away from the tail stage rocket after the brennschluss. The satellite enters the highly elliptical transfer orbit there, with both the perigee and the apogee of the orbit above the equator. Usually, the altitudes of the perigee and the apogee equal those of the orbit-insertion point and the GEO respectively. At the apogee of the highly elliptical transfer orbit, the apogee engine on the satellite is ignited, driving the satellite into the GEO ultimately (Fig. 2.1).

(2) Orbit maintenance

Affected by a variety of perturbations including the Earth's non-spherical perturbation, atmospheric drag, lunisolar attraction, solar radiation pressure, and other factors, the spacecraft eventually deviate from their originally designed orbits after long-term operation. As shown in Fig. 2.2, a GEO satellite with a fixed point longitude of 100° east at a certain Epoch time experiences a longitude drift under the influence of perturbation. For satellites deviated from their preset orbits, it is necessary to conduct orbit maintenance to ensure that they remain in the correct orbits. As only a limited amount of fuel can be carried by the satellites, the service

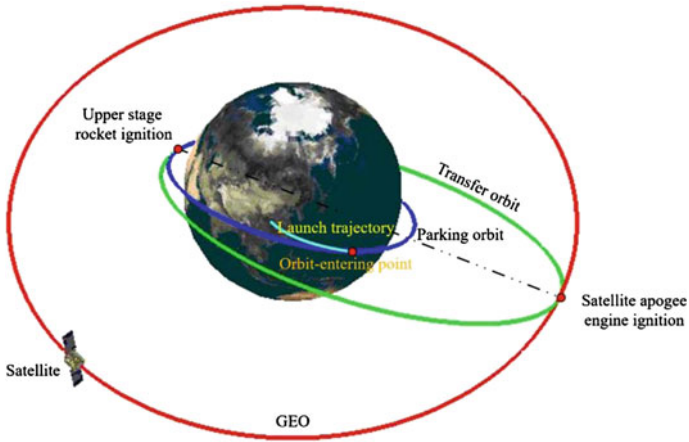


Fig. 2.1 Schematic figure of the launching process of GEO satellites

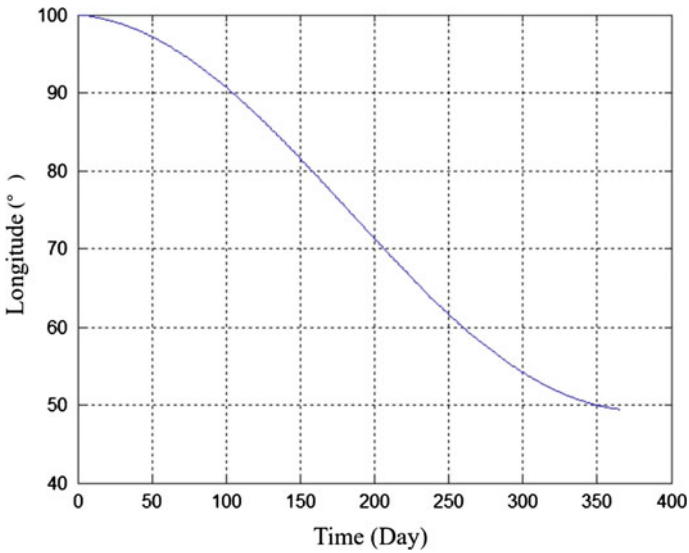


Fig. 2.2 Longitude drift of GEO satellite within a year

of many spacecraft has to be terminated because of fuel exhaustion. Hence, a rigorous plan of satellite orbit control has to be made.

(3) Earth-to-Moon flight and interplanetary exploration

We can take Earth-to-Moon flight as an example. Firstly, the lunar probe is launched into the Earth-Moon transfer orbit (or into the parking orbit first, and then the orbit is maneuvered into the Earth-Moon transfer orbit). During this process,

orbit adjustments may be required. Then, after the lunar probe enters the lunar sphere of influence, orbit control should be conducted to transfer the lunar probe from an Earth satellite into a lunar satellite that circles the Moon. If the lunar probe is designed to be recalled, then orbit control is conducted again to transfer it from the lunar orbit back into the Moon-Earth transfer orbit finally bringing it back to Earth.

(4) Space rendezvous and docking

During the process of space rendezvous and docking, the tracking spacecraft experiences a series of orbit control and also attitude control, consistently bringing down the relative position and relative velocity between the tracking spacecraft and its target spacecraft, and meeting the initial conditions of docking in a relative attitude angle and angular rate. Space rendezvous and docking requires a high precision in both orbit control and attitude control.

In these applications, orbit control is primarily used in the transfer between the initial orbit and the target orbit. It is in essence an intermediate state, rather than the final state of an orbit. Some special space orbits, however, regard orbit control as an integral part of their orbit design, i.e., the special space orbit itself is possibly a type of controlled orbit. For instance, the hovering orbits must be subject to the successive monitoring of an orbit control system, thus maintaining the relative position between the spacecraft and its target unchanged or just making relative movements in a minimal range during a certain period.

Thanks to the development of modern space marching technology, long-term, highly-precise and low-thrust orbit control has become a reality. Special space orbits are thus free from the conventional restrictions of Keplerian orbits, and are enabled to provide on-orbit service and meet the application requirements of new space missions.

2.1.3 Requirements for Special Space Application

During the past decade or so, a large number of new-concept space application experiments have been conducted at home and abroad, including the already completed Orbital Express (OE) Program, the Micro-Satellite Technology Experiment (MiTeX) Program, the Deep Impact Program, the X-37B space maneuvering vehicle program in the United States, the still on-going Phoenix Program, and other typical ones. The major details of these experiments are shown in Table 2.2.

In the above space experiments, the main purpose of a spacecraft is no longer to provide reconnaissance, communications, navigation and other information support for the ground, rather, it is to provide flexible and various services in space, including on-orbit supply, close inspection, space interception, rapid maneuver, component replacement in space, and so on. Apparently, these space service missions can hardly, or never, be accomplished on the basis of the current typical

Table 2.2 New-concept space application experiments conducted in the U.S

Space experiments	Details
Orbital express (OE) program	A space service operation experiment conducted by the U.S. Defense Advanced Research Projects Agency (DARPA) in 2007, including four major parts: <ol style="list-style-type: none"> (1) Testing small space robot orbiters which can provide services for satellites (2) Testing target satellites that can be upgraded and repaired (3) Testing interfaces between the two satellites during the process of docking (4) Operating the on-orbit satellites
Micro-satellite technology experiment (MiTEx) program	In December 2008, the U.S. Department of Defense utilized two MiTEx satellites to examine the on-orbit malfunctioning missile early-warning satellite of the defense support program (DSP-23)
Deep impact program	At Beijing time 13:2:4 on July 4, 2005, the impactor of the deep impact program conducted by the U.S. National Aeronautics and Space Administration (NASA) accurately hit the core of Comet Temple 1, with a diameter of less than 6 km, more than 100 million kilometers away from the Earth at a relative velocity of 10.2 km/s
XX-37B space maneuvering vehicle program	From 2010 to 2013, flight experiments of the space maneuvering vehicles (SMV) were carried out by the U.S. Air Force, aiming at developing the fuselage structure, the on-orbit maneuver, the advanced thermal protection system, the autonomous approach and landing, and other key technologies for reusable SMVs. It was also aimed at exploring combat concepts and the capabilities of unmanned spacecraft that have the capability of operating in space for a long period
Phoenix program	In October 2011, the U.S. DARPA proposed the phoenix program, hoping to disassemble the communications antennas from abandoned GEOs and reuse them to provide more economical and sustainable space-based communications services for the U.S. Air Force. The program is predicted to conduct on-orbit demonstration during the 2015–2016 period

orbits. By contrast, special space orbits are exactly designed for these special space missions. For example,

- (1) Hovering orbit: proposed for space missions in which the servicing spacecraft should be kept stationary relative to the target spacecraft;
- (2) Cruising orbit: proposed for the space-based space target surveillance missions;
- (3) Multi-target rendezvous orbit: proposed for space missions in which the servicing spacecraft should conduct orbital rendezvous with several non-coplanar space targets simultaneously;

- (4) Initiative approaching orbit: proposed for missions that require a rapid approach towards a space target;
- (5) Responsive orbit: proposed for missions in which the global coverage period is longer and the access frequency of the spacecraft is higher than those of the typical orbits;
- (6) Earth pole-sitter orbit: proposed for the continuous exploration missions of the Earth's North and South Poles.

2.2 Types of Special Orbit

In accordance with the specific space application needs, six special space orbits will be introduced in this section.

2.2.1 Hovering Orbit

In the 21st century, thanks to the continuous development of space technology, a lot of spacecraft enter into space each year. However, under the influence of the complexity and unpredictability of the space environment, requirements for on-orbit service have been brought forward by an ever increasing number of spacecraft. Generally speaking, it is a necessity that a spacecraft travelling in an orbit should satisfy Kepler's Three Laws, resulting in many problems for on-orbit service. One of the problems is how to keep the servicing spacecraft stationary, relative to the target spacecraft in any orientation.

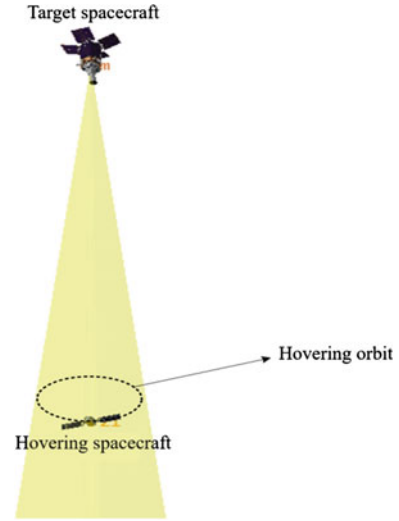
Hovering orbits refer to the orbits on which the servicing spacecraft is kept stationary, or moves within a minimal range, relative to the target satellite during a certain period under the control force, as shown in Fig. 2.3.

The key to the hovering orbits is to realize the hovering of the servicing spacecraft at a certain point or in a certain area in the target orbital coordinate system by adopting orbit control. In this way, the station-keeping of the relative location and orientation between the servicing and the target spacecraft can be achieved when both spacecraft are travelling at high velocities in space, thus laying the foundation for accomplishing space missions such as space maintenance, on-orbit refueling, space-based space target surveillance, and so on.

2.2.2 Cruising Orbit

Space target surveillance and space environment surveillance are the basis for all space activities. However, due to the geographic restrictions and the limited

Fig. 2.3 Schematic figure of hovering orbit



detection range of the ground-based space detection system, it is difficult to realize high-precision detection of a high-orbit spacecraft and certain space environmental elements.

Since the GEO satellites are stationary relative to the Earth's surface, the observation stations deployed on the ground can only observe the GEO satellites above them which are within their visual range all the time. They can never observe the GEO satellites stationed above the other half of the Earth. Moreover, due to the long distances, it is very difficult for the ground stations to identify the high-orbit targets, especially the GEO ones, even if they are detected.

Currently, it is still challenging to image space targets tens of thousands of kilometers away by adopting the ground-based large-scale self-adaptive optical system. In addition, the possible slow tumbling of high-orbit targets makes it even more difficult to achieve fine imaging results. In fact, the current ability to identify high-orbit targets is still immature. Correspondingly, space-based and ground-based research have been simultaneously conducted abroad to tackle the problem. Aiming to enhance its space target surveillance capability, the U.S. has carried out a series of research programs on space-based space target surveillance. On September 25, 2010, the first Space-Based Space Surveillance (SBSS) satellite, i.e., the Pathfinder, was successfully launched at the Vandenberg Air Force Base. As the first SBSS satellite, it is capable of providing preliminary space surveillance service for monitoring space objects in low-Earth orbits. It is projected that a satellite constellation consisting of four SBSS satellites which is equipped with more advanced global space surveillance technology will be deployed in the next phase.

According to the U.S. Air Force's plan, the SBSS system is a LEO (Low Earth Orbit) optical remote sensing satellite constellation, characterized by its strong orbit observation capability, short repeated observation period, and all-weather observation capability. It is expected that the System will substantially enhance the

U.S.'s ability for exploring deep space objects. Allegedly, it will enhance the U.S.'s GEO satellite's tracking ability by 50 %, and shorten the update period of the U.S.'s space targets catalogue information from five days to two days, therefore enormously boosting its Air Force's space situational awareness. The System can detect and track space targets such as satellites and orbital debris, detect in time the tiny targets in deep space, and distinguish whether it is human factors or non-human factors such as the space environment that are damaging the space system. This system prominently outperforms the ground-based space surveillance system which cannot monitor deep-space small objects.

The U.S. Air Force has also planned to develop a space target surveillance satellite that travels in an even higher orbit, i.e., the Orbit Deep Space Imager (ODSI). The envisaged ODSI system is a satellite constellation consisting of optical imaging satellites that travel in the GEO, the major function of which is to provide the images of three-axis stabilized GEO satellites. The ODSI satellites will travel continuously along the GEO and take pictures of the GEO satellites, capturing their high-resolution images. The system can improve not only the ability of U.S.'s space target surveillance system in monitoring high-orbit targets, but also help to acquire the feature information of GEO targets and enhance its capability in identifying these targets.

In addition, the various types of micro-satellites being developed by the U.S. can also be used for space surveillance. The proposed schemes for the application of micro-satellites in space surveillance by the U.S. military forces include:

- ① For emergent space targets with potential hostility, other space surveillance detectors are firstly used to discover, track and identify the targets. When other space- and ground-based space surveillance detectors fail to obtain more detailed information about the targets, micro-satellites used for space surveillance (including on-orbit stay micro-satellites and promptly responsive and launched micro-satellites) can be sent to approach the targets, conducting close observations and taking pictures at short range for more detailed feature data of the targets.
- ② As for its space assets that require special protection, the U.S. armed forces can deploy micro-satellites in the neighborhood, monitoring the surrounding environment, providing early warning and distinguishing between natural destruction and man-made sabotage. A typical application of the micro-satellites is the U.S. MiTEX test.

To sum up, two patterns can be used by the space-based space target surveillance system to monitor the GEOs:

- (1) Monitoring the targets in the GEO by using spacecraft deployed in the medium and low orbits;
- (2) Deploying the surveillance satellites around the GEO orbits and monitoring the targets like a *drifter*.

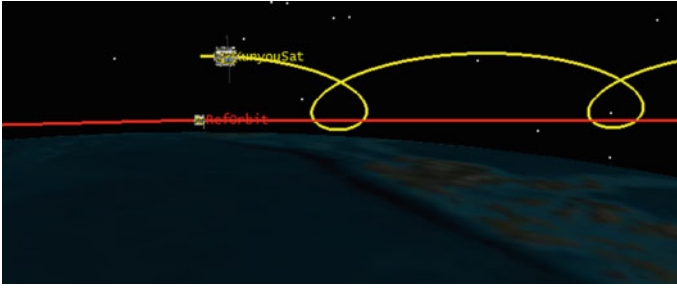


Fig. 2.4 Spiral flying-around orbit

In the above two patterns, the first one is more suitable for general surveys of the GEO targets, allowing the cataloguing of the targets within a short time. However, as a result of the long distance and the large relative velocity between the surveillance satellite and the target spacecraft, it is difficult to acquire abundant detailed information about the targets and meet the demands for target identification, on-orbit service, and others. In the second pattern, however, because of the short distance and the small relative velocity between the surveillance satellite and the target spacecraft, close observation and picture-taking of the targets are feasible. In this way, geometrical morphology, signal features and other detailed information can be obtained.

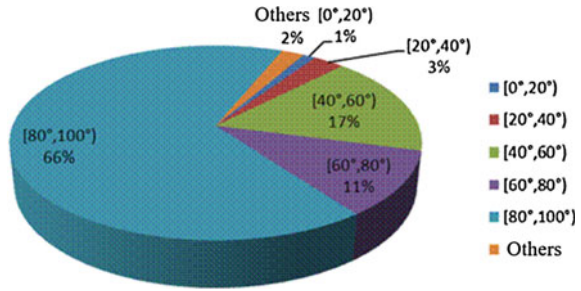
A cruising orbit is a type of relative orbit, in which the cruising spacecraft cruises around the target orbit in a certain pattern, conducting close observation, providing on-orbit service, monitoring nearby space debris and the nearby space environment, and so on, for multiple spacecraft in the target orbit. The spiral flying-around orbit is shown in Fig. 2.4.

Compared to ordinary satellite formation flying such as flying-behind and flying-around, a cruising orbit has obvious advantages in the following aspects: Firstly, the detection target of a cruising orbit is not limited to a single satellite. Given enough time, the orbit can accomplish the detection of all the on-orbit spacecraft in this specific orbit. Secondly, the configuration design of the cruising orbit enables a multi-perspective detection of the target, thus obtaining the detailed description of a specific object. Thirdly, the detectors will not stay around the same object for a long time. Finally, the energy consumption required for multi-target detection is low. If there is no demand for cruising velocity, then the cruising spacecraft can conduct a cruising and detection flight along a free trajectory, which consumes almost no energy theoretically.

2.2.3 Multi-Target Rendezvous Orbit

In April 2007, the space refueling experiment of the U.S. Orbital Express (OE) Project was successfully accomplished. Successively, the Phoenix Program

Fig. 2.5 Distribution of orbit inclinations of LEO satellites



proposed in 2011 put on-orbit maintenance on the agenda. In accordance with the demands of different space missions, spacecraft are usually deployed in different orbit planes in space. According to the statistics of the satellite database of the Union of Concerned Scientists (UCS), there were 521 LEO spacecraft as of June 1, 2013. The distribution of the orbit inclinations of these spacecraft is shown in Fig. 2.5.

Different orbit inclinations inevitably result in differing orbit planes. Changing orbit plane consumes a lot more energy than in-plane maneuvering does. Therefore, it is difficult for a single servicing spacecraft to provide services for multiple target spacecraft travelling in different orbit planes. Taking advantage of the feature that any spacecraft orbit inevitably crosses a random orbit plane in space, scientists have proposed a coplanar multi-target orbital rendezvous method based on traversing point. In this method, the traversing point of the target orbit is considered as the orbit rendezvous point and the traversing time of the target spacecraft as the orbit rendezvous time. In this way, the non-coplanar orbit rendezvous problem is turned into a coplanar orbit rendezvous issue. Moreover, without a restriction on the amount of target spacecraft and orbit distribution, this method realizes, in essence, the one-to-many orbit rendezvous pattern.

2.2.4 Initiative Approaching Orbit

An initiative approaching orbit refers to an orbit in which a spacecraft rapidly or slowly approaches a cooperative or a non-cooperative target through orbit control, thus accomplishing rendezvous and docking, rapid detection, on-orbit service and other space missions. A typical initiative approaching orbit is the orbit in which the U.S. MiTeX (Micro-Satellite Technology Experiment) satellite initiatively approaches and detects the DSP-23 missile early-warning satellite.

According to the U.S. *Aerospace News* on January 14, 2009, the U.S. Department of Defense was inspecting the on-orbit malfunctioning Defense Support Program (DSP)-23 missile early-warning satellite utilizing two Micro-satellites (MiTeX).

This was the first on-orbit inspection mission conducted in a geosynchronous orbit after the U.S. on-orbit maintenance demonstration of the OE satellite in 2007.

The MiTeX Project is a part of the Microsatellite Demonstration Science and Technology Experiment Program (MiDSTEP) jointly implemented by the Defense Advanced Research Projects Agency (DARPA) and the U.S. Air Force. The project, including MiTeX-A, MiTeX-B and three upper stage vehicles that push them into a geostationary orbit, aims to determine, integrate, demonstrate and evaluate micro-satellite technology relevant to GEO maneuvering. Because of the strong propulsion capability and long service life of the upper stage vehicles of the MiTeX Project, the satellites can travel to any location in the geostationary orbit, conduct close-range operations, take pictures, receive all radio communications sent and received by the target satellite. They can even conduct counter operations such as disabling communication networks, discharging propellant in the fuel tank of the target spacecraft, and others.

The DSP-23 satellite was launched on November 10, 2007, but lost touch with the ground control station around October 8, 2008. At that time, the DSP-23 satellite was travelling above the equator in southern Nigeria at longitude 8.5° east. Then the satellite drifted eastwards along the geosynchronous orbit, in accordance with the orbital mechanics law, for around a year and a half, before it reached the space above Australia and then returned to the west. It did this repeatedly. From December 8 to 13, 2008, the MiTeX-A satellite approached DSP-23 from the west towards the east; on December 23, 2008, the MiTeX satellite reached the DSP-23 satellite and established images; on January 1, 2009, the MiTeX-B satellite also approached the DSP-23 satellite.

This experiment demonstrated that the U.S. was already equipped with key capacities in rapid orbital maneuver, space-based object measurement, on-orbit operation service, system comprehensive integration, and so on. The orbit in which the MiTeX satellite operated during its missions is a typical initiative approaching orbit (Fig. 2.6).

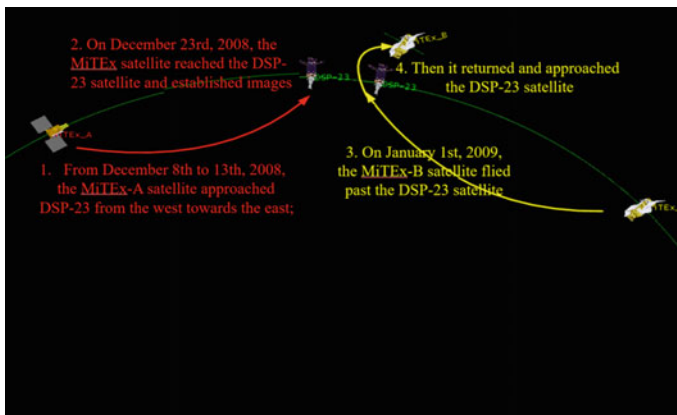


Fig. 2.6 Process of MiTeX satellite initiatives approaching and detecting DSP-23 satellite

2.2.5 Fast Responsive Orbit

To meet the demands of emergent space missions, the U.S. Department of Defense and The Institute for Defense and Disarmament Studies jointly released a research report entitled *Military Space Systems: the Road Ahead* in October 2005. The report put forward the development strategies for Operationally Responsive Space (ORS), which included responsive satellite, responsive carrier and other technologies.

The TacSat Program being conducted by the Office of Force Transformation (OFT), U.S. Department of Defense, is a typical responsive satellite project. The program involves four experimental tactical satellites, which are jointly developed by the U.S. Air Force Research Laboratory, the Naval Research Laboratory, and other collaborative laboratories. It aims to lay the technical foundation for the development of responsive mini-satellites, and demonstrate the affordability of a battlefield that integrates responsive launching, test and systems to support and satisfy the tactical requirements from field commanders by providing them direct access to space assets. The TacSat-3 launched in June 2009 is a mini-satellite developed by the U.S. Air Force Research Laboratory, which is the first responsive satellite that carries a mini-satellite public spacecraft and an optical payload.

A responsive orbit refers to an orbit that can carry out responsive missions. Here, 'responsive time' usually means the period from the time when a mission is proposed to the time when the mission is accomplished. Giving up a number of important indicators such as global coverage, a necessary feature for common spacecraft orbits, and even orbit lifetime, a responsive orbit focuses on its ability to make fast responses to certain space missions.

The most important characteristics of a responsive orbit are:

- Fast response: The responsive time of a responsive orbit is far shorter than that of an ordinary orbit. For example, it takes only a couple of hours for a responsive orbit to send back valid data after being launched into space;
- Low cost: This orbit can be used by small vehicles;
- Tactical application ability: It is specifically used for certain operational missions.

2.2.6 Earth Pole-Sitter Orbit

An earth pole-sitter orbit refers to an orbit that can realize long-term stay above the Earth's poles through orbit control. These types of orbits have two major properties. Firstly, an earth pole-sitter orbit can realize long-term stay above the Earth's poles. By adopting the earth pole-sitter orbit, a single satellite is allowed to cover the high latitude regions in the northern or southern hemisphere (including the North or the South Pole). Apparently, the cost-benefit ratio of an earth pole-sitter orbit is rather high though its security is guaranteed because of the high locations of deployment.

Secondly, the deployment location of the earth pole-sitter orbit is high. The distance from the earth pole-sitter orbit to the Earth's surface is about 0.01 astronomical unit (1 astronomical unit = 1.49597870×10^8 km). Though this may result in a relatively low resolution in ground detection, the orbit can be used for communications and navigation under proper conditions.

2.3 Description of Special Space Orbit

2.3.1 Orbit Element

Generally speaking, a spacecraft orbit can be described with six orbit elements, i.e.,

- Semi-major axis a : Half of the distance between the apogee and the perigee of an elliptical orbit, usually used to describe the size of an elliptical orbit.
- Eccentricity e : The ratio between the focal length and the semi-major axis of an elliptical orbit, usually used to describe the shape of an elliptical orbit, i.e., its non-circular extent;
- Perigee argument ω : The angle measured from the orbital ascending node to the perigee in the motion direction of the satellite in the orbit plane, usually used to describe the orientation of the apsidal line of an elliptical orbit in the orbit plane, i.e., the orientation of the perigee;
- Right ascension of ascending node (RAAN) Ω : The angle measured anti-clockwise from the orientation of the vernal equinox to the orbital ascending node in the equatorial plane, usually used together with the orbit inclination to describe the orientation of an elliptical orbit in space;
- Orbit inclination i : The included angle between an orbit plane and the equatorial plane, or that between the positive normal of an orbit plane and the Earth's North Pole, usually used to describe the inclining degree of the orbit plane relative to the equatorial plane;
- Time of perigee passage τ : The time when a spacecraft passes the perigee while travelling along an elliptical orbit.

Under the postulated conditions of two-body motion, the above six orbit elements are generally constants. Nevertheless, in actual space missions, spacecraft are subject to the influences of the Earth's non-spherical perturbation, atmosphere perturbation, solar radiation pressure perturbation, lunisolar attraction perturbation, and so on. These influences may result in changes to a spacecraft's orbit, i.e., the orbit elements are no longer constants. In order to study the disturbed motion of a spacecraft, concepts such as the osculating orbit and the osculating orbit element will be introduced.

Considering any point in the actual orbit of a spacecraft as a point in a corresponding elliptical orbit (an ideal orbit), then the elliptical orbit would be called an osculating orbit. The osculating orbit is tangent to the actual orbit. On the point of

tangency, the actual velocity of spacecraft equals that of the corresponding point in the osculating orbit. If all the perturbations vanish from this point onwards, then the spacecraft will travel along the osculating orbit.

Osculating orbit elements describe the corresponding orbit elements of the osculating orbit at a certain instant (e.g., time t). Regarding the osculating orbit element of a certain time as the starting point, the precise subsequent orbit motion state can be obtained through numerical integration.

In order to describe more precisely the motion of a spacecraft from a macroscopic view, mean orbit elements can be adopted. The so-called mean orbit elements refer to the orbit elements without the short-period changing term.

The conversion formula between the mean orbit elements and the osculating orbit elements is:

$$E_i = E'_i + \delta E_i(E'_i), \quad i = 1, \dots, 6 \quad (2.2)$$

Here, E_i stands for the i -th osculating orbit element, E'_i refers to the i -th mean orbit element, and δE_i refers to the i -th short-period changing term of the osculating orbit element.

2.3.2 Non Singularity Orbit Elements

In many applications, the spacecraft's orbit is a nearly round one, such as those of the LEO reconnaissance satellite, the GEO satellite (the orbit inclination approximates 0°), and so on. Since the orbit inclination $i \approx 0^\circ$, the right ascension of ascending node (RAAN) shows some singularity; and since the eccentricity $e \approx 0$, the argument of perigee also shows some singularity. The concept of non singularity orbit elements is thus put forward to solve these singularity problems.

For orbits with orbit inclination $i \approx 0^\circ$ and eccentricity $e \approx 0$, there are a number of definitions for non singularity orbit elements, two of which will be introduced in this book. The first definition is:

$$\begin{aligned} a, & \quad h = e \sin(\Omega + \omega), & p = \sin(i/2) \sin \Omega \\ l = \Omega + \omega + M, & \quad k = e \cos(\Omega + \omega), & q = \sin(i/2) \cos \Omega \end{aligned} \quad (2.3)$$

Here, a and l refer to the semi-major axis and the mean longitude respectively; h and k refer to the projections of the eccentricity vectors (whose numerical value equals the orbit eccentricity and the orientation is directed towards the perigee of the orbit) in the XY planes of the Earth centered inertial coordinate system respectively. When we ignore the factor $1/2$, then p and q can be approximately regarded as the projections of the normal vector of the orbit plane into the XY planes of the Earth centered inertial coordinate system. If we take the factor $1/2$ into

account, then the above non singularity orbit element is allowed to be used for an orbit with a large inclination and, in the meantime, avoids singularity when the orbit inclination is 90° .

The second definition of non singularity orbit element is:

$$\begin{aligned} a, & & h = e \sin(\Omega + \omega), & & p = tg(i/2) \sin \Omega \\ l = \Omega + \omega + M, & & k = e \cos(\Omega + \omega), & & q = tg(i/2) \cos \Omega \end{aligned} \quad (2.4)$$

The second definition is more suitable for perturbation calculations.

2.3.3 Rectangular Coordinate Component

Orbit control is regularly adopted in the design of a special space orbit. The equation of spacecraft motion under orbit control is usually described as:

$$\ddot{\vec{r}} = -\frac{\mu}{r^3}\vec{r} + \vec{a} + \vec{a}_T \quad (2.5)$$

Here, \vec{r} , μ , \vec{a} and \vec{a}_T refer to the geocentric distance vector, the Earth's gravitational constant ($\mu = 3.986005 \times 10^{14} \text{ m}^3/\text{s}^2$), the perturbation acceleration, and the controlling acceleration, respectively.

Under orbit control, the motion of a spacecraft can be generally described with rectangular components, which are either components in the Earth centered inertial coordinate system or components in the relative coordinate system.

In space applications, the Earth centered inertial coordinate system usually adopts the Mean Equinox and Equator of J2000.0 Coordinate System, or the J2000.0 Coordinate System for short. The J2000.0 Coordinate System $OX_I Y_I Z_I$ is defined as a coordinate system with the geocentric as its origin O , the OX_I axis pointing towards the J2000.0 mean equinox (at bar centric dynamical time 12:00:00.000 on January 1, 2000, corresponding to the Julian Day 2451545.0), the OZ_I axis pointing towards the J2000.0 mean equator normal, and the OY_I located within the mean equator plane of the J2000.0 and determined by using the right hand rule (Fig. 2.7).

The relative coordinate system refers to the relative motion coordinate system with reference to a certain spacecraft. Here, the origin of the relative motion system s - xyz is fixedly connected with the centroid of the reference spacecraft and moves with it; the direction of axis x overlaps with that of the geocentric vector of the reference spacecraft, pointing from the geocentric to s ; axis y is perpendicular to axis x within the orbit plane of the reference spacecraft and directs towards the motion direction; axis z is determined by using the right hand rule (Fig. 2.8).

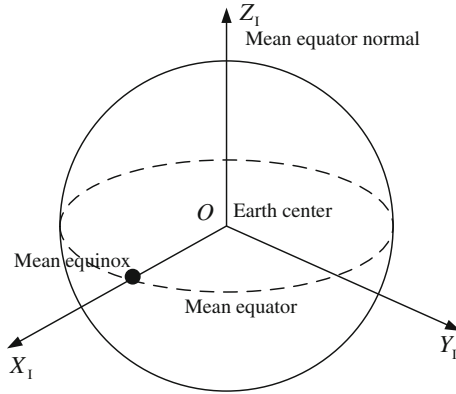


Fig. 2.7 J2000.0 Earth centered inertial coordinate system

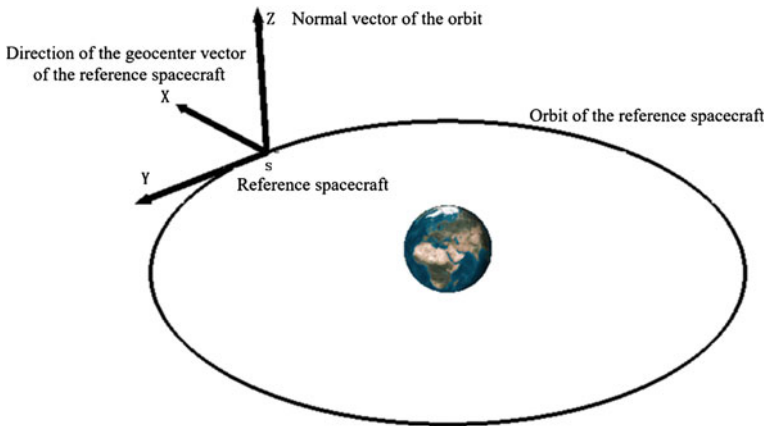


Fig. 2.8 Relative motion coordinate system

2.4 Summary

Special space orbits are proposed amid the development of space technology and the expansion of fields involving space missions. Compared to the more familiar typical orbits, special space orbits mainly demonstrate their distinctive features in orbit design concepts, orbit control application, special space application demands, and so on.

In this chapter, the concept of a special space orbit is introduced, and then the characteristics and applications of six special space orbits, i.e., hovering orbit, spiral cruising orbit, multi-target rendezvous orbit, initiative approaching orbit, responsive

orbit, and earth pole-sitter orbit, are briefly illustrated. Finally, three descriptive approaches of special space orbits including orbit element, non singularity orbit element and rectangular coordinate component are discussed. In the following chapters, we will elaborate on the design concepts and methods of the above six special space orbits.

Chapter 3

Theory and Design Method of Hovering Orbit

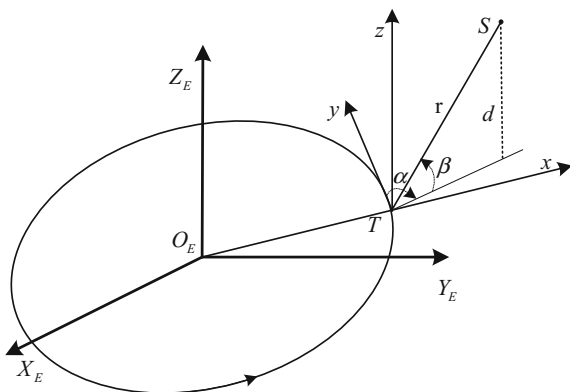
A hovering orbit is the relative motion orbit of a hovering spacecraft which holds still or moves in a minimal range towards its target spacecraft. There are broad application prospects for hovering orbits in missions like space-based space target surveillance, on-orbit service and space rescue.

3.1 Hovering Orbit: Concept

As the name implies, the word “hovering” indicates that the relative position of a hovering spacecraft to its target spacecraft remains still in space. Essentially, a hovering orbit is the orbit of a hovering spacecraft which holds still or moves in a minimal range to its target spacecraft in the orbital coordinate system of the target spacecraft. The value of the relative position is a constant (depending on the specific mission), and the relative velocity and the relative acceleration velocity are both 0. That is to say, the hovering spacecraft remains “relatively static” in relation to its target spacecraft. Based on the dynamics principle of spacecraft orbits, to keep the hovering spacecraft maintaining “relative hovering” to its target satellite in a period of time, an active control force and a control torque should be imposed on the hovering spacecraft.

As is shown in Fig. 3.1, T represents the target spacecraft, and S represents the hovering spacecraft. In the orbital coordinate system of the target spacecraft $T - xyz$, the location parameters of the hovering spacecraft to its target spacecraft can be expressed as r, α, β . Here: r represents the relative distance between the hovering spacecraft and the target spacecraft and is known as the hovering distance; α represents the included angle between the projection of the hovering distance in the target spacecraft’s orbit plane and the motion direction of the target spacecraft, called the hovering azimuth; β represents the included angle between the hovering distance and the orbit plane of the target spacecraft, called the hovering altitude angle or the hovering elevation angle. So, the hovering mission of a hovering

Fig. 3.1 Illustration of configuration relation of hovering orbits' relative position



spacecraft to a target spacecraft can be described as follows: in the hovering process of a hovering spacecraft to its target spacecraft, by imposing active controls to the spacecraft, it keeps the hovering distance r , hovering azimuth α and hovering elevation angle β between the spacecraft and its target spacecraft unchanged.

When $\alpha < 0^\circ$, the hovering spacecraft is below the target spacecraft, and when $\alpha > 0^\circ$, the hovering spacecraft is above the target spacecraft; when $\beta < 0^\circ$, the spacecraft is on the right side of the target spacecraft, and when $\beta > 0^\circ$, the spacecraft is on the left side of the target spacecraft. α, β in Fig. 3.1 are positive values. When $\alpha = -90^\circ, \beta = 0^\circ$, the hovering spacecraft S is directly below the target spacecraft T ; and when $\beta = 0^\circ$, the hovering spacecraft and the target spacecraft are in the same orbit plane. In the ideal hovering process, not only the relative distance between the hovering spacecraft and the target spacecraft remains constant, but also the distance d between the hovering spacecraft and the orbit plane of the target spacecraft keeps unchanged. The trajectory plane of the hovering spacecraft does not pass the Earth-center (except when coplanar hovering), and is parallel to the orbit plane of the target spacecraft.

3.2 Design of Fixed-Point Hovering Orbit

Fixed-point hovering is utilized to maintain a hovering spacecraft at a point in the orbital coordinate system of its target satellite and keep its relative position to the target satellite unchanged. Fixed-point hovering is applicable to on-orbit services and spatial operations which require high accuracy in directivity. Typical operations include spatial rendezvous and docking, on-orbit refueling and on-orbit maintenance. The spatial operations above require high precision on hovering spacecraft control and usually adopt the method of continuous control.

3.2.1 Dynamic Model

In a two-body problem, the velocity V of a spacecraft can be expressed as:

$$V^2 = \mu \left(\frac{2}{r} - \frac{1}{a} \right) \quad (3.1)$$

Here: r represents the position vector of the spacecraft; a represents the semi-major axis of the orbit; G represents the universal gravitation constant; m_E represents the mass of the Earth; m_S represents the mass of the spacecraft, and $\mu = G(m_E + m_S) \approx Gm_E$. Then the horizontal angular velocity of the spacecraft ϖ can be expressed as:

$$\varpi = \sqrt{\frac{\mu}{r^2} \left(\frac{2}{r} - \frac{1}{a} \right)} \quad (3.2)$$

Thus it can be seen that once the orbit is determined, or in other words, the semi-major axis a is determined, the velocity of the spacecraft is only related to the position vector r .

The hovering spacecraft and the target satellite have the same orbital shape, spatial position and dimensional orientation, except their sizes of orbits. That is to say, among the six orbital elements, the eccentricity e , orbit inclination i , right ascension of ascending node (RAAN) Ω , perigee argument ω and true anomaly f are all the same, except the semi-major axis a .

From the orbit equation:

$$r = \frac{a(1 - e^2)}{1 + e \cos f} \quad (3.3)$$

the following can be obtained:

$$\frac{r}{a} = \frac{(1 - e^2)}{1 + e \cos f}$$

Let $\eta = \frac{(1 - e^2)}{1 + e \cos f}$, then:

$$\varpi = \sqrt{\frac{\mu}{r^3} (2 - \eta)} \quad (3.4)$$

That is to say, when the eccentricity e and the true anomaly f of two spacecraft are the same, in other words, η are the same, then the angular velocity of the spacecraft is only related to the value of the position vector r . The farther it is to the Earth, the smaller the angular velocity will be.

It can be seen that the following two steps should be adopted to achieve the hovering to the target satellite:

- Step 1: Transfer the hovering spacecraft into the hovering orbit and satisfy the following conditions, that is, eccentricity e , orbit inclination i , RAAN Ω and perigee argument ω are the same;
- Step 2: To keep the angular velocities of two spacecraft with different semi-major axes the same, it is necessary that, when their true anomalies are the same, an impulse should be imposed on the hovering spacecraft in order to change the initial angular velocity of the hovering spacecraft and make it the same as the angular velocity of the target satellite. Then a continuous thrust should be imposed to keep it in a hovering state, or to keep it in synchronous operation with the target satellite.

Here we assume that the hovering spacecraft has completed step 1, the next part will only discuss the impulse needed to change the initial velocity of the hovering spacecraft and the continuous thrust to keep it hovering.

3.2.1.1 Mathematical Model of the Impulse Thrust

When the hovering spacecraft goes into orbit, its initial velocity is $V_S = \sqrt{\frac{\mu}{r_S}(2 - \eta)}$. To make the angular velocities of the two spacecraft the same, $\varpi_T = \varpi_S$, the velocity of the hovering spacecraft has to be adjusted as follows:

$$V'_S = \frac{r_S}{r_T} \sqrt{\frac{\mu}{r_T}(2 - \eta)} \quad (3.5)$$

We assume the original velocity is positive, then the impulse trust needed is:

$$dV = V'_S - V_S = \left(\sqrt{\frac{r_S^3}{r_T^3}} - 1 \right) \sqrt{\frac{\mu}{r_S}(2 - \eta)} \quad (3.6)$$

It can be seen that, in order to make the two spacecraft have the same angular velocity, when the hovering spacecraft is below the target spacecraft, an impulse dV should be imposed on the hovering spacecraft in the opposite direction to its original velocity.

3.2.1.2 Mathematical Model of Continuous Thrust

In this section, the mechanical analysis method in physics and the “two-body problem” method in celestial mechanics are applied to derive the mathematical model of the continuous thrust respectively.

(1) Mechanical Analysis in Physics

When the velocity vector of the hovering spacecraft is decomposed in the radial direction and the circumferential direction, we can obtain the following:

$$\begin{cases} V_r = \frac{pe \sin f}{(1+e \cos f)^2} \cdot \frac{1}{r} \sqrt{\frac{\mu}{p}}(1+e \cos f) = \sqrt{\frac{\mu}{a(1-e^2)}} e \sin f \\ V_f = r\dot{f} = \sqrt{\frac{\mu}{a(1-e^2)}} e \cos f \end{cases} \quad (3.7)$$

When the initial impulse dV is imposed, the angular velocity of the hovering spacecraft changes to the same angular velocity of the target spacecraft, which is:

$$\begin{cases} V_{Sr} = \frac{r_s}{r_r} V_{Tr} = \frac{r_s}{r_r} \sqrt{\frac{\mu}{a_T(1-e^2)}} e \sin f \\ \quad = \frac{a_s}{a_T} \sqrt{\frac{\mu}{a_T(1-e^2)}} e \sin f \\ V_{Sf} = \frac{r_s}{r_r} V_{Tf} = \frac{r_s}{r_r} \sqrt{\frac{\mu}{a_T(1-e^2)}} (1+e \cos f) \\ \quad = \frac{a_s}{a_T} \sqrt{\frac{\mu}{a_T(1-e^2)}} (1+e \cos f) \end{cases} \quad (3.8)$$

If the motion of the spacecraft is simplified into a two-body motion, i.e., with the Earth as the central gravitation body and the spacecraft rotating around it with the this central force, then the Earth's gravitational acceleration of the hovering spacecraft A_E is the sum of the radial acceleration of the spacecraft and the centripetal force acceleration when doing circumferential rotation.

The radial acceleration A_{Sr} is:

$$\begin{aligned} A_{Sr} &= \dot{V}_{Sr} \\ &= \frac{a_s}{a_T} \sqrt{\frac{\mu}{a_T(1-e^2)}} e \cos f \cdot \dot{f} \\ &= \frac{a_s}{a_T} \sqrt{\frac{\mu}{a_T(1-e^2)}} e \cos f \cdot \frac{1+e \cos f}{r_T} \sqrt{\frac{\mu}{a_T(1-e^2)}} \\ &= \mu \frac{a_s}{a_T r_T^2} e \cos f \end{aligned} \quad (3.9)$$

The centripetal force acceleration generated by circumferential rotation A_{Sf} is:

$$\begin{aligned} A_{Sf} &= \frac{V_{Sf}^2}{r_s} \\ &= \frac{a_s^2 \mu}{r_s a_T^3 (1-e^2)} (1+e \cos f)^2 \\ &= \mu \frac{a_s}{a_T r_T^2} (1+e \cos f) \end{aligned} \quad (3.10)$$

To maintain the spacecraft in the hovering orbit, the impulse acceleration A needed is (radial direction is positive):

$$\begin{aligned}
 A &= A_E - A_{Sf} + A_{Sr} \\
 &= \frac{\mu}{r_S^2} - \mu \frac{a_S}{a_T r_T^2} (1 + e \cos f) + \mu \frac{a_S}{a_T r_T^2} e \cos f \\
 &= \mu \left(\frac{1}{r_S^2} - \frac{a_S}{a_T r_T^2} \right) = \frac{\mu}{r_S^2} \left(1 - \frac{a_S r_S^2}{a_T r_T^2} \right) \\
 &= \frac{\mu}{r_S^2} \left(1 - \frac{r_S^3}{r_T^3} \right) = \frac{\mu}{r_S^2} \left(1 - \frac{a_S^3}{a_T^3} \right)
 \end{aligned} \tag{3.11}$$

(2) Approximate “two-body problem” method

Based on the two-body problem, the motion of the hovering spacecraft accords with Kepler’s Laws. The differential equation of its basic motion is:

$$\ddot{\vec{r}} + \frac{\mu}{r^3} \vec{r} = 0 \tag{3.12}$$

The velocity in orbit is:

$$V = \sqrt{\mu \left(\frac{2}{r} - \frac{1}{a} \right)} \tag{3.13}$$

We establish the trajectory coordinate system in the following manner: the coordinate origin is the centroid of the spacecraft, the x axis points to the spacecraft’s centroid from the Earth’s center-of-mass, the z axis coincides with the angular momentum \vec{h} of the spacecraft’s orbit, the y axis accords with the right-hand coordinate system. It is known therefore that the components of the motional differential equation on the y axis and the z axis are 0, and its component on the x axis is:

$$\ddot{r} + \frac{\mu}{r^2} = 0 \tag{3.14}$$

When an external force F is imposed on the spacecraft on the x axis, we put $A = F/m_S$, then

$$\ddot{r} + \frac{\mu}{r^2} = +A \tag{3.15}$$

If we let $\mu' = \mu - Ar^2$, then

$$\ddot{r} + \frac{\mu'}{r^2} = 0 \quad (3.16)$$

The moving velocity of the spacecraft is:

$$V = \sqrt{\mu' \left(\frac{2}{r} - \frac{1}{a} \right)} \quad (3.17)$$

To achieve the hovering to its target satellite, the hovering spacecraft and its target satellite should be kept in the same angular rate of motion constantly, which is

$$V_S = \sqrt{\mu' \left(\frac{2}{r_S} - \frac{1}{a_S} \right)} = \frac{r_S}{r_T} V_T = \frac{r_S}{r_T} \sqrt{\mu \left(\frac{2}{r_T} - \frac{1}{a_T} \right)} \quad (3.18)$$

It can be derived from the above equation:

$$\mu' = \mu \frac{r_S^2 \left(\frac{2}{r_T} - \frac{1}{a_T} \right)}{r_T^2 \left(\frac{2}{r_S} - \frac{1}{a_S} \right)} = \mu \frac{a_S^4 (2a_T - r_T)}{a_T^4 (2a_S - r_S)} = \mu \frac{a_S^3}{a_T^3} \quad (3.19)$$

If we substitute the above equation into $\mu' = \mu - Ar^2$, then the following can be obtained:

$$A = \frac{\mu}{r_S^2} \left(1 - \frac{a_S^3}{a_T^3} \right) \quad (3.20)$$

Apparently, the result obtained by adopting approximately the two-body problem method is the same as the one obtained by using the mechanical analysis method in physics. Thus the two methods have mutually authenticated the correctness of their derivation processes.

The continuous thrust is known as:

$$F = m_S A \quad (3.21)$$

Therefore, it can be explained from the perspective of physics: In accordance with the law of celestial body movement, when an impulse is imposed to reduce the velocity of the hovering spacecraft, the altitude of the spacecraft will decrease, which is equivalent to imposing a thrust to the spacecraft and “holding” the spacecraft in the hovering orbit. The result obtained by using the approximate “two-body problem” method shows that the orbit of the hovering spacecraft also accords with the First and Second Laws of Kepler. The difference from the Third

Law of Kepler is that the direct proportional coefficient of the square of the spacecraft's operation period to the cubic of the semi-major axis of its elliptical orbit is not earth's gravity μ , but $\mu' = \mu - Ar^2$. It can be interpreted as: the thrust imposed counteracts a part of earth's gravity, or "reduces a part of earth's mass". This kind of orbit can be described as an artificial "sub-keplerian orbit".

3.2.1.3 Feasibility Analysis

Based on the mathematical model of the continuous thrust, it is known that with regard to two orbits with fixed semi-major axis of orbit, the direction of the thrust is consistent with the direction of the spacecraft's position vector, and the thrust value is a function of the position vector. As the value of the position vector of an elliptical orbit changes over time, the orbit control engine should be able to adjust the thrust in real time to achieve the hovering.

With regard to a circular orbit, the value of the position vector remains unchanged. So the continuous thrust needed also keeps the same and the hovering distance $h = r_T - r_S \ll r_T$. Therefore, Eq. (3.20) can be simplified into:

$$A = \frac{3\mu h}{r_T^3}$$

Here, the thrust acceleration is proportional to the hovering distance, and is inversely proportional to the orbit radius of the target satellite.

We assume that the mass of the hovering spacecraft is 1000 kg, the following is an analysis of the hovering conducted in a circular orbit (the orbit of the target satellite).

If the hovering is conducted to a spacecraft in a low orbit (orbit altitude range $1.5 \times 10^5 - 1.0 \times 10^6$ m), the thrust acceleration needed will be relatively big. However, as the orbit of the target spacecraft is relatively low, the hovering distance is definitely not too far. Figure 3.2 shows the acceleration of the continuous thrust needed when the following flying distance is less than 1.5×10^5 m. As to the spacecraft in the near-circular sun-synchronous orbit, to achieve the hovering with a distance of 2.0×10^4 m to a target satellite with an orbit radius of 6.9×10^5 m, the required continuous thrust acceleration is $A = 0.067921$ m/s², and the continuous thrust $F = 67.921$ N.

If the hovering is conducted to a spacecraft in a medium orbit (orbit altitude range $1.0 \times 10^6 - 2.0 \times 10^7$ m), the thrust acceleration needed is shown in Fig. 3.3. For example: To achieve the hovering to a navigation satellite at a distance of 2.0×10^5 m, the acceleration of continuous thrust needed is $A = 0.01313$ m/s², and the continuous thrust $F = 13.13$ N.

If the hovering is conducted to a spacecraft in a high orbit (orbit altitude: over 2.0×10^7 m), the thrust acceleration needed is shown in Fig. 3.4. For example: to achieve the hovering to a geostationary satellite at a distance of 2.0×10^5 m, the

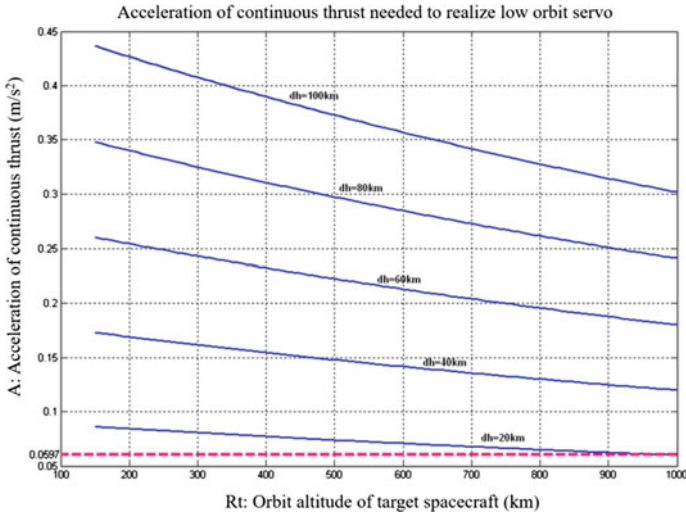


Fig. 3.2 Acceleration of continuous thrust needed to achieve hovering of low-orbit spacecraft

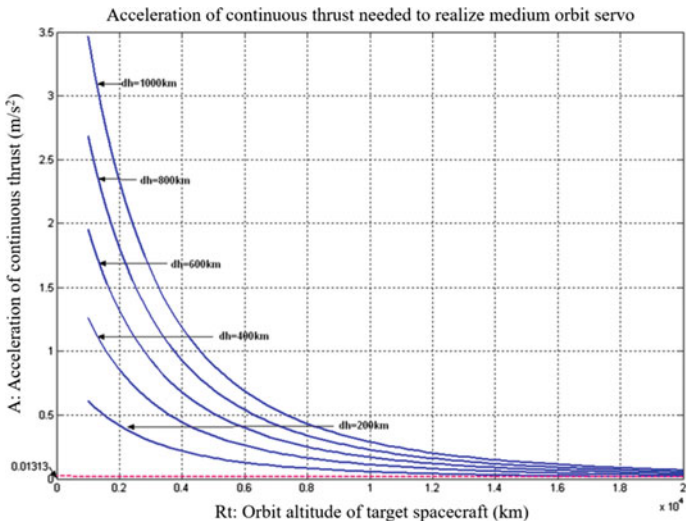


Fig. 3.3 Acceleration of continuous thrust needed to achieve hovering of medium-orbit spacecraft

acceleration of continuous thrust needed is $A = 0.0031573 \text{ m/s}^2$, and the continuous thrust $F = 3.1573 \text{ N}$. When the following flight distance is $1.0 \times 10^6 \text{ m}$, the acceleration of continuous thrust needed is $A = 0.016095 \text{ m/s}^2$, and the continuous thrust $F = 16.095 \text{ N}$.

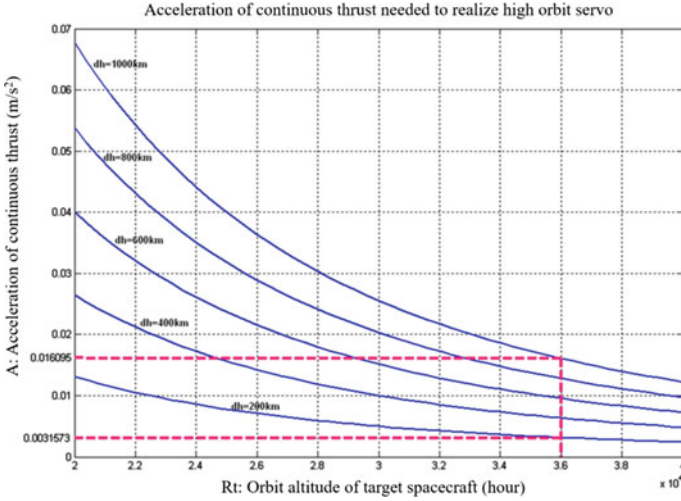


Fig. 3.4 Acceleration of continuous thrust needed to achieve hovering of high-orbit spacecraft

Next, we assume that the operation orbit or the target spacecraft is an elliptical orbit, and its hovering process will be analyzed. It is known that the value of the continuous thrust is related to the spacecraft orbit altitude. Take the Molniya highly elliptical orbit satellite with an orbit period of 12 h as an example: The apogee altitude is about 4.0×10^7 m, the perigee altitude is about 6.0×10^5 m. We assume the difference between the semi-major axis of the hovering orbit and that of the target satellite is 2.0×10^5 m, Fig. 3.5 shows the change in the continuous thrust for hovering during one orbit period. Here, when the spacecraft is at its apogee, the thrust acceleration needed is 0.004207m/s^2 , the value of thrust is 4.207 N; when at its perigee, the thrust acceleration needed is 0.1913 m/s^2 and the value of the thrust is 191.3 N.

From the above analysis, it is thus clear that for a target spaceship with a certain orbit altitude, if a reasonable hovering distance is decided, it will be realizable to conduct hovering and provide the continuous thrust. Especially to a geostationary satellite, an “electric propulsion” engine can help achieve this process. Here, the operation principle of electric propulsion is as follows: Solar energy or nuclear energy transforms into electric energy through a conversion device, then the electric energy heats up the propellant or ionizes the propellant to accelerate the propellant and form high-speed jet propulsion, which ejects out and produces thrust to boost the spacecraft flying capacity. Electric propulsion engines were successfully developed in the 1960s and 1970s and reached a relatively high technical level. Currently, the number of spacecraft launched using electric propulsion exceeds 200. Research on electric propulsion engines is a major trend in the development of propulsion technology.

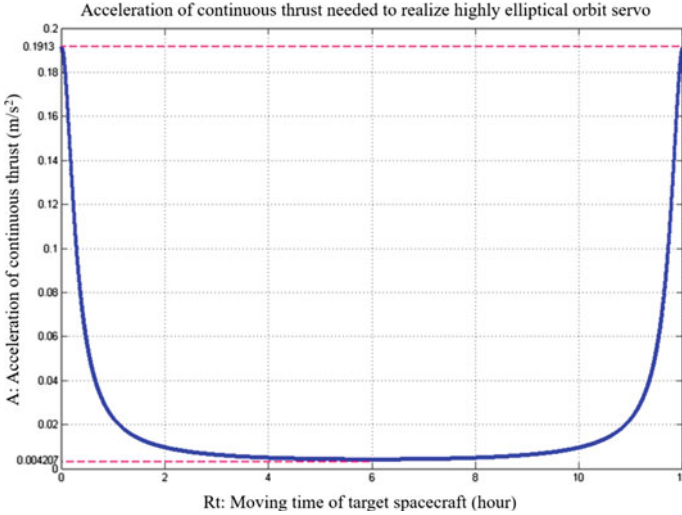


Fig. 3.5 Acceleration of continuous thrust needed to achieve hovering to a highly elliptical orbit

3.2.2 Open-Loop Control

In the orbital coordinate system shown in Fig. 3.6, the hovering spacecraft is located at point A' and the target spacecraft is located at point O . If we assume that the difference of geocentric longitude between the sub-satellite point of point O and any point A on earth is α , the geocentric latitude of point A is β , then the position of point A in the reference system can be described as:

$$(x_{OA}, y_{OA}, z_{OA}) = (R_E \cos \alpha \cos \beta - R, R_E \sin \alpha \cos \beta, R_E \sin \beta) \quad (3.22)$$

Here: R represents the geocentric distance of the target spacecraft, R_E represents the Earth's radius. Thus, in the coordinate system $Oxyz$, the unit vector of vector OA can be obtained as $e_{OA} = \frac{OA}{|OA|}$.

We assume that the distance between A' and O is L , the position of A' in the reference system $Oxyz$ is: $(x, y, z) = L \cdot e_{OA}$, the coordinate position of A' in $O'x'y'z'$ is:

$$(x_{O'A'}, y_{O'A'}, z_{O'A'}) = (x + R, y, z) \quad (3.23)$$

We assume that the unit vector of $O'A'$ is $e_{O'A'} = \frac{O'A'}{|O'A'|}$, the difference between the initial phase of the hovering spacecraft and that of the target spacecraft is:

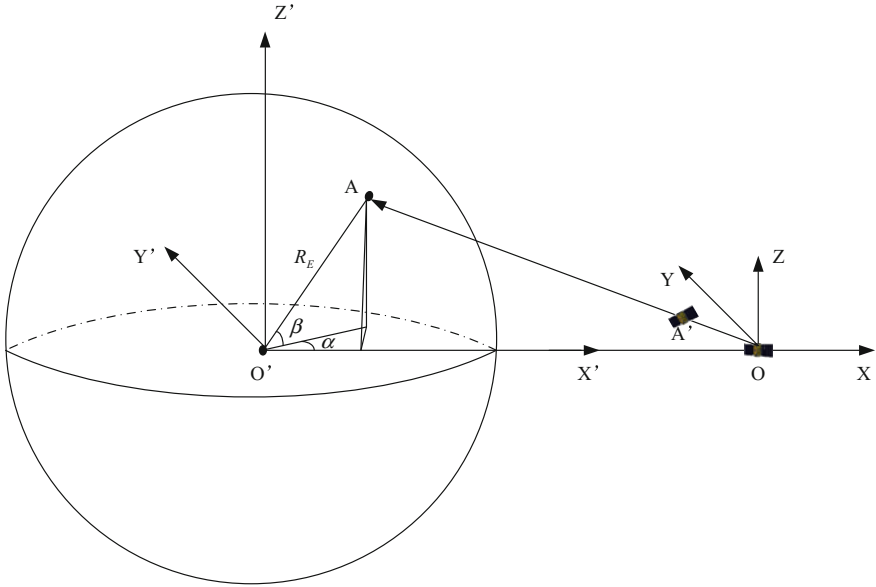


Fig. 3.6 Position of any point in orbital coordinate system

$$\Delta\phi = \arcsin(e_{O'A'}(2)) \quad (3.24)$$

The orbit inclination of the hovering spacecraft i is:

$$i = \arcsin(e_{O'A'}(3)) \quad (3.25)$$

In Eqs. (3.24) and (3.25), $e_{O'A'}(2)$ and $e_{O'A'}(3)$ represent the second and the third components of the unit vector $e_{O'A'}$, respectively.

To keep the hovering spacecraft relatively static in relation to its target spacecraft, the orbital rotational angular rate of the hovering spacecraft must be equal to the angular velocity of the target spacecraft. Moreover, the hovering spacecraft should only have tangential velocity, with velocities in other directions being 0. We assume the angular velocity of the target spacecraft is n , then the orbital tangential velocity of the hovering spacecraft in the reference system $O'x'y'z'$ is:

$$V_m = |O'A'| \cdot \cos(i) \cdot n \quad (3.26)$$

Here, V_m is the value of total velocity of the hovering spacecraft, and the normal velocity in the orbit plane is 0.

We assume that the hovering distance is $L = 100$ km, $\alpha = 127.89^\circ$, $\beta = -16.94^\circ$, then $e_{OA} = (-0.991, 0.0174, 0.128)$. From Eq. (3.23), the coordinates of A' in the reference system $Oxyz$ can be obtained:

$$(x_{A'}, y_{A'}, z_{A'}) = (-99161, 1740.6, 12811 \text{ m})$$

From Eqs. (3.24) and (3.25), in the reference system $O'x'y'z'$, the orbit inclination of the hovering spacecraft A' is $i = 0.035^\circ$, and the difference of its initial phase to that of its target spacecraft is $\Delta\varphi = 0.0048^\circ$.

If the orbit of the target spacecraft is a circular orbit, and the distance between the hovering spacecraft and the target spacecraft is far less than the geocentric distance of the target spacecraft, then the motion of the hovering spacecraft in the reference system $Oxyz$ can be described by the *Hill Equation*:

$$\begin{cases} \ddot{x} - 2n\dot{y} - 3n^2x = f_x \\ \ddot{y} + 2n\dot{x} = f_y \\ \ddot{z} + n^2z = f_z \end{cases} \quad (3.27)$$

Here: n represents the orbital angular velocity of the target spacecraft, (f_x, f_y, f_z) represents the controlling acceleration imposed on each axis of the hovering spacecraft.

As the hovering spacecraft maintains a relatively static position in relation to the target spacecraft, the velocity components and acceleration components on each axis are 0. The mean angular rate of the target spacecraft is $n = 7.2921 \times 10^{-5}$ rad. From Eq. (3.27), in the reference system $Oxyz$, the controlling acceleration component of the hovering spacecraft is obtained:

$$(f_x, f_y, f_z) = (1.585 \times 10^{-3}, 0, -2.1 \times 10^{-5})$$

We assume that the simulation started on *12:00:00, June 1, 2003*. At this moment, relative to the x axis of the J2000 coordinate system, the rotational angular rate of geocentric longitude 0° is 69.518° . Since the phase difference between the hovering spacecraft and the target spacecraft is $\Delta\phi$, it can be obtained that the included angle between the position of the hovering spacecraft and the xoy plane of the J2000 coordinate system is 69.523° .

According to 3-1-3 transfer order, convert the positions and velocities of the two satellites in the orbital coordinate system into the corresponding positions and velocities in the J2000 coordinate system. The position coordinates and velocities on three axes in the J2000 coordinate system are shown in Table 3.1.

The value of the controlling acceleration is 0.001585 m/s^2 . To simplify the programming and controlling process, the body coordinate system of the hovering spacecraft is taken as the reference system and the direction and the value of the

Table 3.1 Initial positions and velocities of target spacecraft and hovering spacecraft

Satellite	Initial position (x, y, z) (km)			Initial velocity $(\dot{x}, \dot{y}, \dot{z})$ (m/s)		
Target spacecraft	-4203.722	3674.850	0	-267.974	-3062.960	0
Hovering spacecraft	-4190.509	3664.473	12.811	-261.47	-2988.6	0

controlling acceleration are kept unchanged in this coordinate system. We take J_2 -perturbation into account, adopt the eight-order Runge-Kutta integrator to solve the satellite's motional equation, set the time step to be 1 s, and the simulation time to be 24 h, generate the orbital data of the target spacecraft and the reference star in one single period (including the position and velocity of the satellites in the J2000 coordinate system).

By calculating the communication link between the target spacecraft and the hovering spacecraft and that between the target spacecraft and a ground station, the changes in the included angle of the two links can be obtained and are shown in Fig. 3.7.

From Fig. 3.7, it can be seen that in the complete orbital operation period, the included angle of the two links changes between 0° and 3.3° , and the maximum of

Fig. 3.7 Changes in the included angle between the hovering spacecraft, target spacecraft and ground station when hovering distance is 100 km

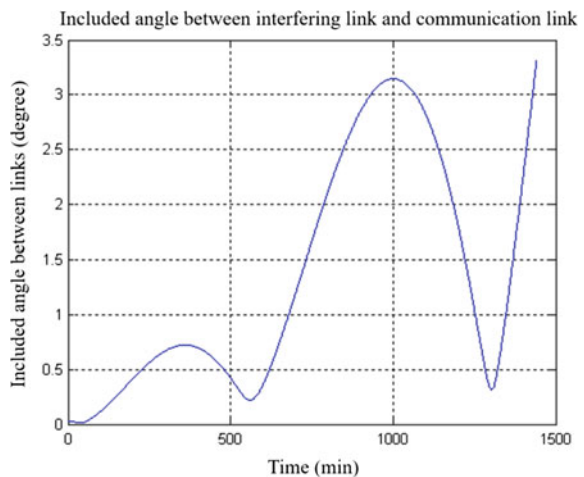
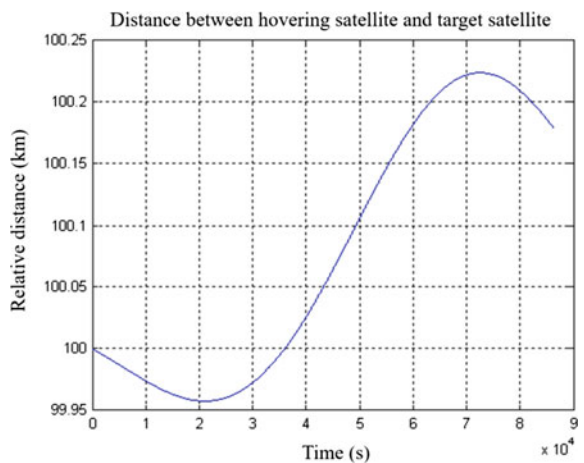


Fig. 3.8 24 h changes in relative distance between hovering spacecraft and target spacecraft when hovering distance is 100 km



the included angle is 3.3° . That is to say, the maximum angle of the hovering spacecraft deviating from the link between the target spacecraft and the ground station is 3.3° .

The changes in the relative distance between the hovering spacecraft and the target spacecraft are shown in Fig. 3.8.

It can be seen that the maximum change value of the distance between the two satellites in one orbit period is 0.225 km, the curve swings around 100 km with its swinging scope increasing, and the relative orbit of the hovering spacecraft to its target spacecraft is a helix.

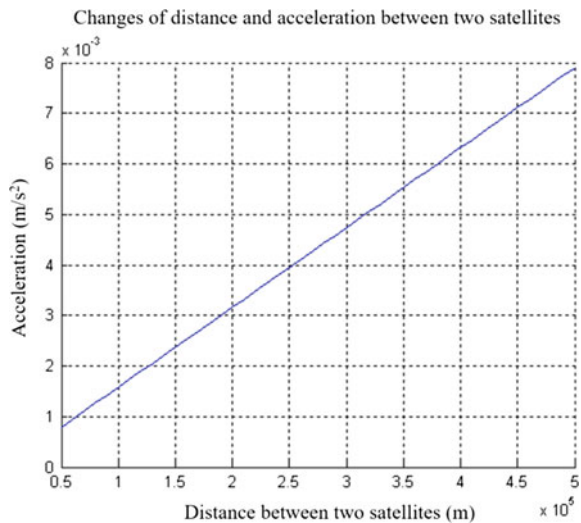
If the distance between the hovering spacecraft and the target spacecraft is set to 50-500 km, the relation between the two spacecraft' distance and the controlling acceleration needed to achieve the hovering can be obtained and is shown in Fig. 3.9.

From Fig. 3.9, when the distance between the two satellites is 50 km, the controlling acceleration needed to maintain the hovering spacecraft on the link is less than 10^{-3} m/s^2 ; when the distance is 500 km, the value of the controlling acceleration is about $8 \times 10^{-3} \text{ m/s}^2$.

From the above analysis, it can be derived that:

- When the hovering spacecraft and the target spacecraft are non-coplanar, the hovering spacecraft weighs 1000 kg and the distance to the target spacecraft is 100 km, a continuous control force of 1.585 N will be able to help the hovering spacecraft hover on a spiral hovering orbit to the target spacecraft.
- Strictly speaking, the hovering spacecraft is not hovering at a fixed point, but drifting along with time. That is because the control force is an open-loop control. If a closed loop control is adopted, fuel loss can be decreased and the hovering spacecraft can be controlled in a certain area precisely.

Fig. 3.9 Changes in spacecraft' distance and controlling acceleration



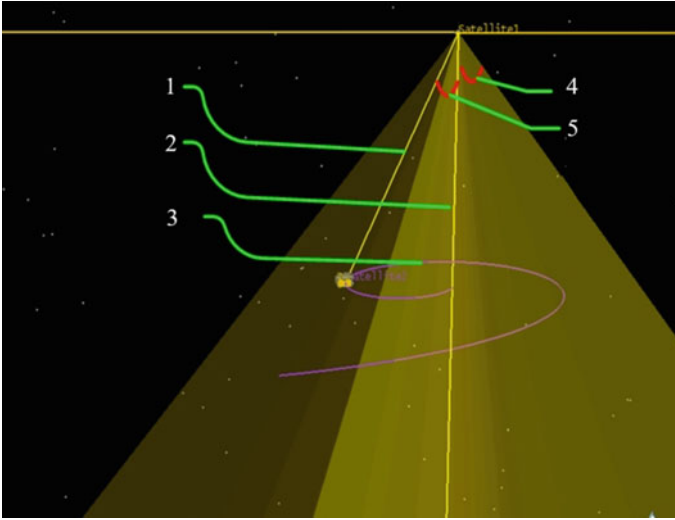


Fig. 3.10 Spiral hovering orbit

In Fig. 3.10:

1. *Direction of inter-satellite link*
2. *Direction of satellite-to-earth link*
3. *24 h relative motion track of hovering satellite and target satellite*
4. *Beam angle of target satellite*
5. *Included angle of links between hovering satellite, target satellite and ground station.*

3.2.3 Closed Loop Control

3.2.3.1 Hovering Control Based on Lyapunov Method

Due to the linearization errors in the Hill Equation, when the hovering spacecraft conducts long-time operation, the accumulative errors will prevent it from maintaining the hovering state. Hence, the linearization errors in simplifying the Hill Equation are considered as disturbances. To solve this, a compensatory controlling acceleration is added to the control process and a feedback control law is designed.

The actual relative motion of the target spacecraft and the hovering spacecraft can be described as follows:

$$\ddot{\vec{r}} = A_1\dot{\vec{r}} + A_2\ddot{\vec{r}} + \ddot{\vec{u}} + \dot{\vec{u}} + c(\vec{r}, \dot{\vec{r}}) \quad (3.28)$$

Here: $A_1 = \begin{bmatrix} 3n^2 & 0 & 0 \\ 0 & 0 & 0 \\ 0 & 0 & -n^2 \end{bmatrix}$, $A_2 = \begin{bmatrix} 0 & 2n & 0 \\ -2n & 0 & 0 \\ 0 & 0 & 0 \end{bmatrix}$; $\dot{\vec{u}}$ represents the compensatory controlling acceleration, $c(\vec{r}, \dot{\vec{r}})$ represents the linearization errors in Hill Equation.

The ideal state equation can be expressed as:

$$\ddot{\vec{r}}^* = A_1\dot{\vec{r}}^* + A_2\ddot{\vec{r}}^* + \ddot{\vec{u}} \quad (3.29)$$

The target of control is to have zero error in a limited time. If we subtract Eq. (3.29) from Eq. (3.28), then:

$$\Delta\ddot{\vec{r}} = A_1\Delta\dot{\vec{r}} + A_2\Delta\ddot{\vec{r}} + \dot{\vec{u}} + c(\vec{r}, \dot{\vec{r}}) \quad (3.30)$$

As the Lyapunov Function is:

$$V = \Delta\dot{\vec{r}}^T K_V \Delta\dot{\vec{r}} + \Delta\vec{r}^T K_r \Delta\vec{r}$$

Here: K_V and K_r are positive definite matrices. Then

$$\dot{V} = 2\Delta\dot{\vec{r}}^T (K_V \Delta\ddot{\vec{r}} + K_r \Delta\dot{\vec{r}}) \quad (3.31)$$

Substituting Eq. (3.30) into (3.31), the following can be obtained:

$$\dot{V} = 2\Delta\dot{\vec{r}}^T (K_V A_1 + K_r) \Delta\dot{\vec{r}} + 2\Delta\dot{\vec{r}}^T K_V A_2 \Delta\ddot{\vec{r}} + 2\Delta\dot{\vec{r}}^T K_V \dot{\vec{u}} + 2\Delta\dot{\vec{r}}^T K_V c(\vec{r}, \dot{\vec{r}}) \quad (3.32)$$

Let

$$\dot{V} = -\Delta\dot{\vec{r}}^T S \Delta\dot{\vec{r}} \quad (3.33)$$

Here: S is a positive definite matrix, therefore, $\dot{V} \leq 0$, which means the system is stable.

When $K_V = I$, it can be obtained from Eqs. (3.32) and (3.33):

$$\dot{\vec{u}} = -(A_1 + K_r) \Delta\dot{\vec{r}} - 0.5(2A_2 + S) \Delta\ddot{\vec{r}} - c(\vec{r}, \dot{\vec{r}}) \quad (3.34)$$

Equation (3.33) has a special case, that is when $\Delta\ddot{\vec{r}} = 0$ and $\Delta\dot{\vec{r}} \neq 0$, we get $\dot{V} = 0$. To prove that the system is also asymptotically stable, substituting Eq. (3.34) into Eq. (3.30) and the following can be derived:

$$\Delta\ddot{\vec{r}} = -K_r\Delta\vec{r} - 0.5S\Delta\dot{\vec{r}} \quad (3.35)$$

Obviously, when $\Delta\dot{\vec{r}} = 0$, $\Delta\vec{r} = 0$, then $\Delta\ddot{\vec{r}} = 0$ can be obtained. So the system is stable.

With regard to Eq. (3.34), $c(\vec{r}, \dot{\vec{r}})$ is a second-order infinitesimal, whose influence on the system is no more than that of the control. There is a positive number K_1 as an infinitesimal and:

$$\|c(\vec{r}, \dot{\vec{r}})\| \leq K_1 \quad (3.36)$$

The following control law is adopted:

$$\dot{\vec{u}} = -(A_1 + K_r)\Delta\vec{r} - 0.5\left(2A_2 + S - K_1I / \|\Delta\dot{\vec{r}}\|\right)\Delta\dot{\vec{r}} \quad (3.37)$$

When we substitute the above Eq. into Eq. (3.32), the following can be derived:

$$\dot{V} \leq -\Delta\dot{\vec{r}}^T \left(S + K_1I / \|\Delta\dot{\vec{r}}\| \right) \Delta\dot{\vec{r}} < 0 \quad (3.38)$$

That is to say, the feedback control law of Eq. (3.37) can stabilize the system.

According to the Hill Equation, during the hovering, in order to keep the position of the hovering spacecraft in the orbital coordinate system of the target satellite unchanged, the relative velocity and the relative acceleration of the hovering spacecraft to the target satellite have to be 0. Therefore, during the hovering, the following control force should be imposed on the hovering spacecraft:

$$\begin{cases} f_x = -3n^2x \\ f_y = 0 \\ f_z = n^2z \end{cases} \quad (3.39)$$

When we combine Eq. (3.39) with (3.37), the three-axis controlling acceleration of the hovering spacecraft will be $(\vec{u} + \dot{\vec{u}})$. Thus, the Lyapunov's theorem has proved that this control law can help a hovering spacecraft achieve long-time stable hovering relative to its target spacecraft.

3.2.3.2 Simulation Analysis

We suppose that the target spacecraft is in the geosynchronous orbit and the hovering spacecraft is 100 km directly under the target spacecraft. So the initial conditions of the two spacecraft in the inertial coordinate system are as follows (Table 3.2).

Table 3.2 Initial conditions of hovering spacecraft and target spacecraft in inertial coordinate system

Satellite	Initial position (x, y, z) (km)			Initial velocity ($\dot{x}, \dot{y}, \dot{z}$) (km/s)		
Target spacecraft	41,164.2	0	0	0	3.0747	0
Hovering spacecraft	42,064	0	0	0	3.0673	0

By adopting the above control law, the result of controlling the hovering spacecraft orbit is shown in Fig. 3.11.

Figure 3.11 shows the result of using fixed-point hovering control, or in other words, the effect of the control obtained after a period of control time. Simulation result indicates that after a period of time, the error on the y axis reduces to 0 and the error on the z axis is always 0, while the error on the x axis stabilizes 1.2×10^{-3} m. The total fixed-point error is about 1.2×10^{-3} m, which is far less than the hovering distance of 100 km. The result shows the control precision is relatively high.

Figure 3.12 illustrates the change curve of the compensatory controlling acceleration needed when the fixed-point hovering is finished. The simulation result shows that after a period of time, the controlling acceleration on the y axis reduces to 0 while the X axis always needs a small compensatory acceleration. That is to say, there is always a force holding the hovering spacecraft.

If the hovering time is 24 h, the increment accumulation of the compensatory controlling acceleration on the X axis is 0.322 m/s^2 , that on the Y axis is 0.027 m/s^2 , and the acceleration on the Z axis is always 0. The total increment of the controlling acceleration is 138.588 m/s^2 , which is apparently feasible.

Fig. 3.11 Relative position errors of three axes

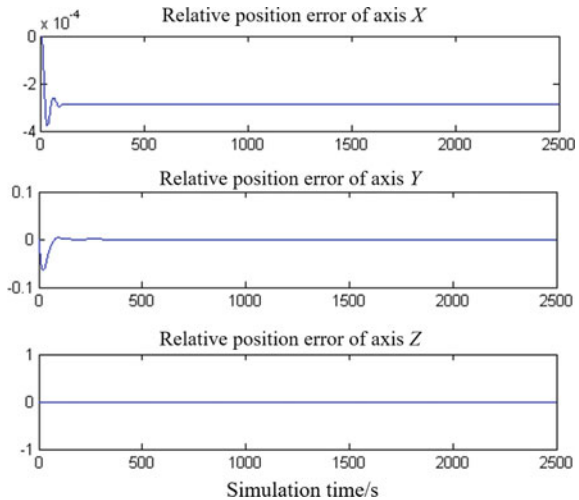
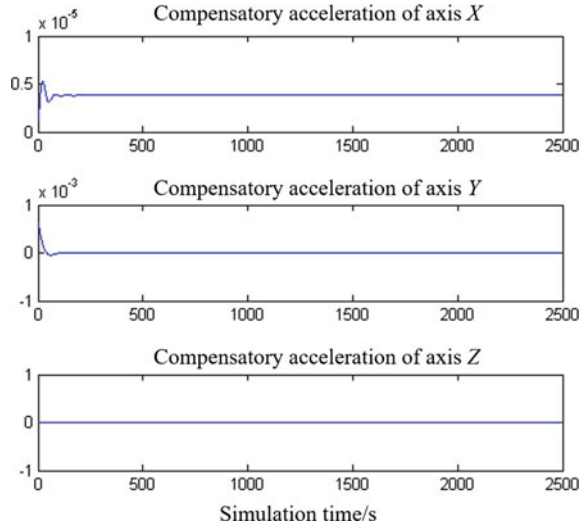


Fig. 3.12 Changes of three-axis compensatory controlling acceleration



3.3 Design of Regional Hovering Orbit

A regional hovering orbit is the relative motion orbit of a hovering spacecraft, subjected to a control system, to its target satellite during a period of time and in a given region. In this kind of relative hovering orbit, orbit control should be conducted only when the hovering spacecraft reaches the boundary of the given region. Compared with the fixed-point hovering, when the hovering spacecraft moves in the confined area, it only needs attitude pointing control and does not require the satellite control system to conduct a continuous control of attitude and orbit coupling, thus realizes the attitude and orbit control separation of the hovering spacecraft. Therefore, a regional hovering orbit can effectively decrease the demands on each subsystem for the satellite when the hovering spacecraft is doing on-orbit services and is beneficial to the implementation of on-orbit autonomous servicing missions.

3.3.1 Analysis of Confined Area Configuration

3.3.1.1 Description of Confined Area Configuration

To obtain the relative motion state of the hovering spacecraft in the confined area, it is necessary to have a proper modeling and description about the space configuration of the confined area to the target satellite. The space configuration of the confined area is shown in Fig. 3.13.

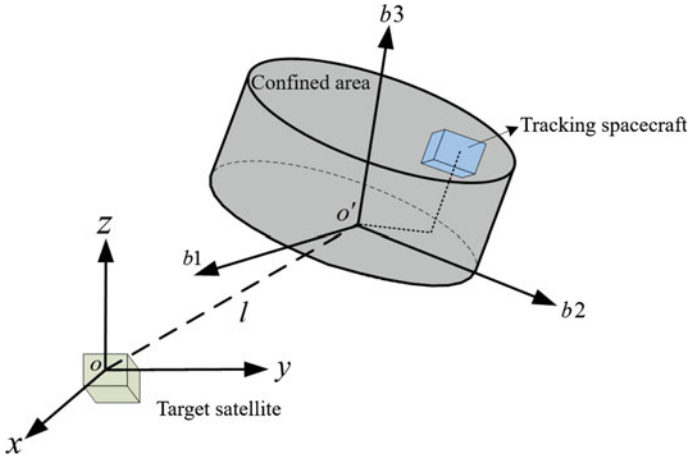


Fig. 3.13 Schematic figure of confined area configuration

Here, $o - xyz$ represents the orbital coordinate system of the target satellite. $o' - b1b2b3$ is defined as a regional rectangular coordinate system to describe the motion state of the hovering spacecraft in the confined area. We suppose the distance between the origin o' and the orbital coordinate origin of the target satellite is l , the azimuth is α , the elevation angle is β , then the coordinates of the origin o' in the orbital coordinate system of the target satellite (x_c, y_c, z_c) can be described as follows:

$$\begin{pmatrix} x_c \\ y_c \\ z_c \end{pmatrix} = \begin{pmatrix} l \cos \beta \cos \alpha \\ l \cos \beta \sin \alpha \\ l \sin \beta \end{pmatrix} \tag{3.40}$$

We suppose that $o' - b1b2b3$ rotates in the order of 3-1-2 for η, ζ, ς respectively and then coincides with the orbital coordinate system of the target satellite, then the transfer matrix of the regional coordinate system $o' - b1b2b3$ and the orbital coordinate system of the target satellite is:

$$T_{o'-b1b2b3}^{RSW} = \begin{bmatrix} \cos \varsigma & 0 & -\sin \varsigma \\ 0 & 1 & 0 \\ \sin \varsigma & 0 & \cos \varsigma \end{bmatrix} \begin{bmatrix} 1 & 0 & 0 \\ 0 & \cos \zeta & \sin \zeta \\ 0 & -\sin \zeta & \cos \zeta \end{bmatrix} \begin{bmatrix} \cos \eta & \sin \eta & 0 \\ -\sin \eta & \cos \eta & 0 \\ 0 & 0 & 1 \end{bmatrix} \tag{3.41}$$

Hence, the transfer formula that is able to transfer the coordinates $(x1, y1, z1)$ in the coordinate system $o' - b1b2b3$ into the coordinates (x, y, z) in the target orbital coordinate system is:

$$\begin{pmatrix} x \\ y \\ z \end{pmatrix} = T_{o'-b1b2b3}^{RSW} \begin{pmatrix} x1 \\ y1 \\ z1 \end{pmatrix} + \begin{pmatrix} x_c \\ y_c \\ z_c \end{pmatrix} \quad (3.42)$$

Thus, the relationship between the regional coordinate system and the orbital coordinate system of the target satellite can be established. And it is very convenient to transfer the coordinates of the hovering spacecraft in the regional rectangular coordinate system into the orbital coordinate system of the target satellite.

3.3.1.2 Typical Confined Area Configurations

Since there are different operation modes and space missions for a hovering spacecraft, the confined area can have multiple configurations. This section will first model some basic 3D configurations, which are sphere, ellipse, cylinder and taper. Then these basic configurations will be used to construct the required confined area configurations in different missions.

(1) Sphere

When the confined area is spherical, in the regional rectangular coordinate system, we suppose the center coordinates in this area are (x_0, y_0, z_0) , the spherical radius is r , then the configuration of the spherical confined area can be expressed as:

$$(x - x_0)^2 + (y - y_0)^2 + (z - z_0)^2 \leq r^2 \quad (3.43)$$

If the coordinates of the sphere center in the spherical area are (50, 50, 50 km), and the radius is 20 km, then the configuration of the confined area is shown in Fig. 3.14.

(2) Ellipse

When the confined area is elliptical, in the regional rectangular coordinate system, we suppose the center coordinates in this area are (x_0, y_0, z_0) , the lengths of the three axes of the ellipse are (x_r, y_r, z_r) , then the configuration of the elliptical confined area can be expressed as:

$$\frac{(x - x_0)^2}{x_r^2} + \frac{(y - y_0)^2}{y_r^2} + \frac{(z - z_0)^2}{z_r^2} \leq 1 \quad (3.44)$$

If the coordinates of the sphere center in the elliptical area are (50, 50, 50 km), and the lengths of the three axes of the ellipse are (20, 50, 10 km), then the configuration of the confined area is shown in Fig. 3.15.

Fig. 3.14 Space configuration of spherical confined area

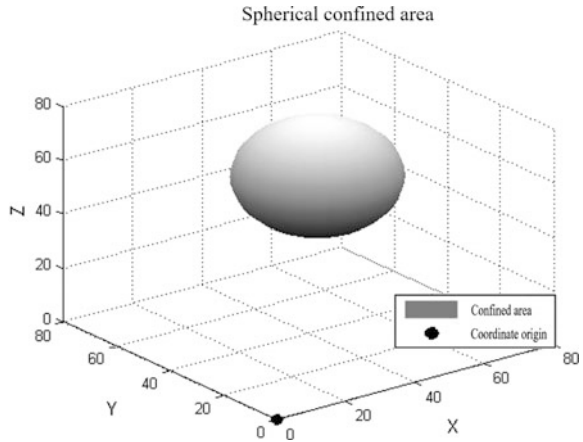
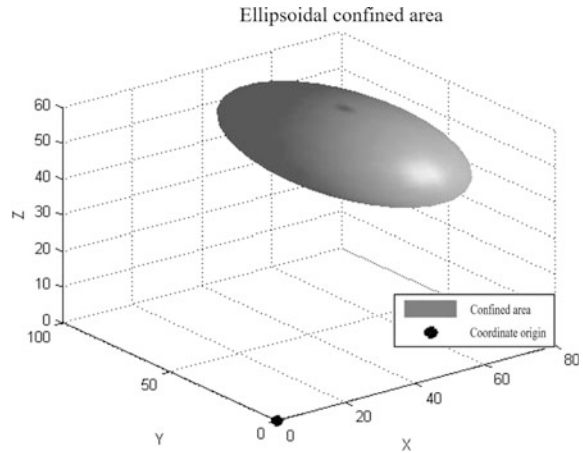


Fig. 3.15 Space configuration of elliptical confined area



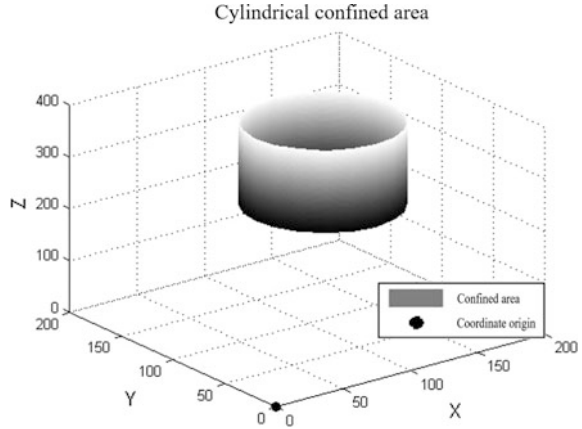
(3) Cylinder

When the confined area is cylindrical, according to different section shapes of the bottom, the cylinder can be divided into a spherical cylinder and an elliptical cylinder. In the regional rectangular coordinate system, the configuration of the cylindrical confined area can be expressed as:

$$\begin{cases} \frac{(x-x_0)^2}{x_r^2} + \frac{(y-y_0)^2}{y_r^2} \leq 1 \\ H_{\min} \leq z \leq H_{\max} \end{cases} \quad (3.45)$$

Here: (x_0, y_0) represents the curve center of the bottom section, (x_r, y_r) represents the chord lengths of the curve, H_{\min} and H_{\max} represent the minimal altitude and the maximum altitude of the cylindrical area respectively. When $x_r = y_r$, the

Fig. 3.16 Space configuration of cylindrical confined area



cylinder is a spherical one; and when $x_r \neq y_r$, the cylinder is an elliptical one. Figure 3.16 illustrates the configuration of the spherical confined area with the bottom surface center being (100, 100, 120 km) and the section radius and altitude being 50 and 160 km, respectively. Likewise, the space configuration of an elliptical confined area can be obtained.

(4) Taper

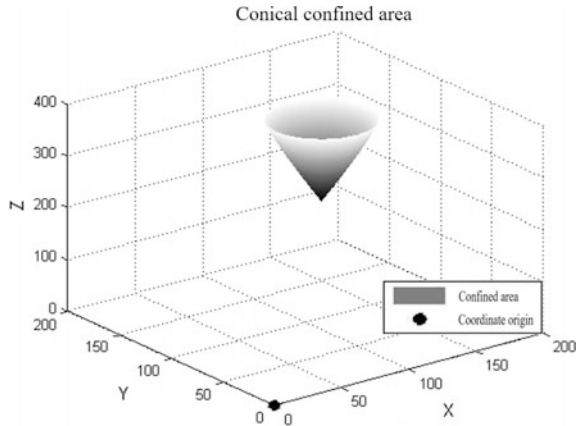
When the confined area is tapered according to different section shapes of the bottom, the taper can be a cone or an elliptical cone. In the regional rectangular coordinate system, the configuration of the tapered confined area can be expressed as:

$$\frac{(x - x_0)^2}{x_r^2} + \frac{(y - y_0)^2}{y_r^2} - \frac{(z - z_0)^2}{z_r^2} \leq 0 \tag{3.46}$$

Here: (x_0, y_0, z_0) represents the position offset of the bottom surface center of the taper relative to the origin, (x_r, y_r) represents the chord lengths of the curve of the bottom section, and z_r represents the altitude of the taper. When $x_r = y_r$, the cylinder is a cone; when $x_r \neq y_r$, the cylinder is an elliptical cone. Figure 3.17 illustrates the configuration of a conical confined area with the bottom surface center being (100, 100, 280 km), and the bottom section radius and altitude being 50 and 160 km, respectively. Likewise, the space configuration of the elliptical cone confined area can be obtained.

Four most basic space area configurations are discussed above. In reality, due to different mission requirements and work modes of target object, the confined area might not be any one of the four types mentioned above, but can be a combination of these four basic space configurations or a transformation of them. For instance, if the confined area is a truncated conical configuration, this configuration can be obtained by two ones cutting each other.

Fig. 3.17 Space configuration of conical confined area



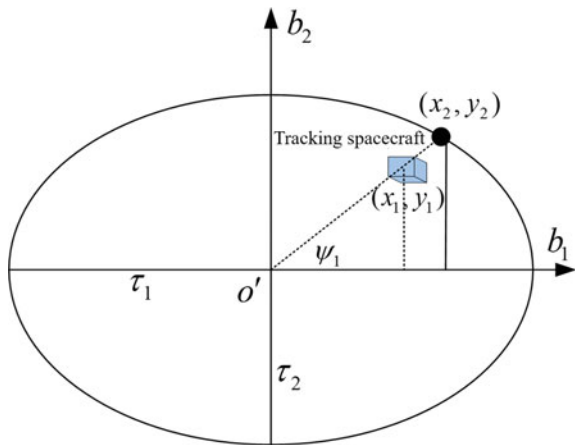
3.3.1.3 Analysis of Confined Area Configuration

According to actual constraint conditions, the hovering spacecraft can only move in a pre-defined confined area to its target satellite. Without the loss of generality, we suppose the confined area is an elliptic cylindrical space configuration, this model can be obtained by changing the size of the bottom section of a cylinder firstly and then rotating the coordinate system.

In the plane $o' - b_1b_2$, the section of the confined area is an elliptical curve. We suppose the semi-major axis of the elliptical curve is τ_1 , the semi-minor axis is τ_2 , as shown in Fig. 3.18.

We suppose the position of the hovering spacecraft in this confined area is expressed as (x_1, y_1) , then

Fig. 3.18 Constraint in confined area plane



$$\psi_1 = \begin{cases} \arctg \frac{y_1}{x_1} & x_1 > 0, y_1 \geq 0 \\ 2\pi + \arctg \frac{y_1}{x_1} & x_1 > 0, y_1 < 0 \\ \pi + \arctg \frac{y_1}{x_1} & x_1 < 0 \end{cases} \quad (3.47)$$

Here: ψ_1 is the included angle between $o'x_1$ and $o'b_1$, representing the phase of the hovering spacecraft in the elliptical area, with the anticlockwise direction being positive. Based on the elliptical formula, the intersection (x_2, y_2) of the straight line $o'x_1$ and the boundary of the elliptical area can be described as:

$$\begin{pmatrix} x_2 \\ y_2 \end{pmatrix} = \begin{pmatrix} \frac{\tau_1 \tau_2 \cos \psi_1}{\sqrt{\tau_1^2 \sin^2 \psi_1 + \tau_2^2 \cos^2 \psi_1}} \\ \frac{\tau_1 \tau_2 \sin \psi_1}{\sqrt{\tau_1^2 \sin^2 \psi_1 + \tau_2^2 \cos^2 \psi_1}} \end{pmatrix} \quad (3.48)$$

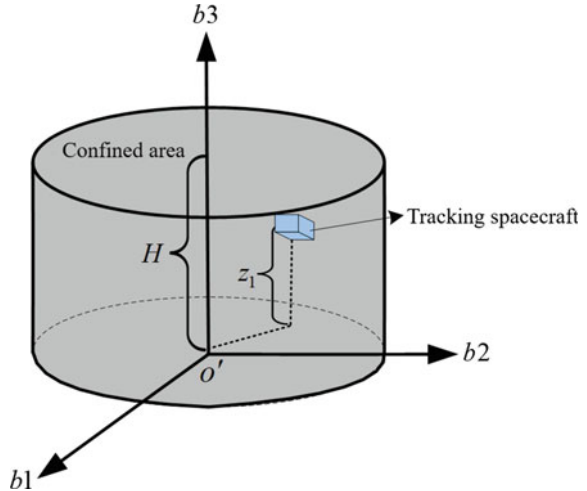
Thus it can be seen that the position parameters of the hovering spacecraft in this plane must meet the following relationship in order to ensure the spacecraft is in this confined area:

$$\begin{cases} x_1^2 + y_1^2 \leq x_2^2 + y_2^2 & x_1 \neq 0 \\ |y_1| \leq |y_2| & x_1 = 0 \end{cases} \quad (3.49)$$

We suppose that the altitude in the confined area is H as is shown in Fig. 3.19, thus the position of the hovering spacecraft z_1 in coordinate system $o' - b_1 b_2 b_3$ cannot be higher than the altitude of the elliptical cylinder H , which is

$$0 \leq z_1 \leq H \quad (3.50)$$

Fig. 3.19 Constraint beyond confined area plane



3.3.2 Control of Regional Hovering Orbit

3.3.2.1 Control Model of Relative Motion

When the hovering spacecraft conducts detailed reconnaissance on the target satellite, compared to the orbit altitude of the target satellite, the relative distance between the hovering spacecraft and the target satellite is an infinitesimal amount. Therefore, the relative motion of the hovering spacecraft to the target satellite can be described by the dynamic model of short-range relative motion as follows:

$$\begin{pmatrix} \rho_i^- \\ \dot{\rho}_i^- \end{pmatrix} = \begin{bmatrix} \Phi_{11}(t_{i-1,i}) & \Phi_{12}(t_{i-1,i}) \\ \Phi_{21}(t_{i-1,i}) & \Phi_{22}(t_{i-1,i}) \end{bmatrix} \begin{pmatrix} \rho_{i-1}^+ \\ \dot{\rho}_{i-1}^+ \end{pmatrix} \quad (3.51)$$

Here: the superscript “-” represents the velocity before the impulse is imposed, the superscript “+” represents the velocity after the impulse is imposed; $(\rho_i, \dot{\rho}_i) = (x, y, z, \dot{x}, \dot{y}, \dot{z})$ represents the relative motion state of the hovering spacecraft at point i ; $t_{i-1,i}$ represents the time of free flight of the spacecraft between point $i - 1$ and point i .

When we let $T = t_{i-1,i}$, then

$$\begin{bmatrix} \Phi_{11} & \Phi_{12} \\ \Phi_{21} & \Phi_{22} \end{bmatrix} = \begin{bmatrix} 4 - 3 \cos nT & 0 & 0 & \frac{\sin nT}{n} & \frac{2(1 - \cos nT)}{n} & 0 \\ 6(\sin nT - nT) & 1 & 0 & -\frac{2(1 - \cos nT)}{n} & \frac{4 \sin nT - 3nT}{n} & 0 \\ 0 & 0 & \cos nT & 0 & 0 & \frac{\sin nT}{n} \\ 3w \sin nT & 0 & 0 & \cos nT & 2 \sin nT & 0 \\ -6n(1 - \cos nT) & 0 & 0 & -2 \sin nT & 4 \cos nT - 3 & 0 \\ 0 & 0 & -n \sin nT & 0 & 0 & \cos nT \end{bmatrix} \quad (3.52)$$

The velocity of the hovering spacecraft after being imposed an impulse at point $i - 1$ is:

$$\dot{\rho}_{i-1}^+ = \Phi_{12}^-(T)[\rho_i - \Phi_{11}(T)\rho_{i-1}] \quad (3.53)$$

It can be expanded and the following can be obtained:

$$\begin{pmatrix} \dot{x}_{i-1}^+ \\ \dot{y}_{i-1}^+ \\ \dot{z}_{i-1}^+ \end{pmatrix} = n \begin{bmatrix} \frac{-4S+3nTC}{8-3nTS-8C} & \frac{2-2C}{8-3nTS-8C} & 0 & \frac{4S-3nT}{8-3nTS-8C} & \frac{-2+2C}{8-3nTS-8C} & 0 \\ \frac{-14+6nTS+14C}{8-3nTS-8C} & \frac{-S}{8-3nTS-8C} & 0 & \frac{2-2C}{8-3nTS-8C} & \frac{S}{8-3nTS-8C} & 0 \\ 0 & 0 & \frac{-C}{S} & 0 & 0 & \frac{1}{S} \end{bmatrix} \begin{bmatrix} x_{i-1} \\ y_{i-1} \\ z_{i-1} \\ x_i \\ y_i \\ z_i \end{bmatrix} \quad (3.54)$$

Here:

$$\begin{cases} S = \sin(nT) \\ C = \cos(nT) \end{cases}$$

We note that the coefficient sign on the right side of Eq. (3.54) y_{i-1} is opposite to that of y_i , so Eq. (3.54) can be expressed as:

$$\begin{pmatrix} \dot{x}_{i-1}^+ \\ \dot{y}_{i-1}^+ \\ \dot{z}_{i-1}^+ \end{pmatrix} = n \begin{bmatrix} \frac{-4S+3nTC}{8-3nTS-8C} & 0 & \frac{4S-3nT}{8-3nTS-8C} & 0 & \frac{-2+2C}{8-3nTS-8C} \\ \frac{-14+6nTS+14C}{8-3nTS-8C} & 0 & \frac{2-2C}{8-3nTS-8C} & 0 & \frac{S}{8-3nTS-8C} \\ 0 & -\frac{C}{S} & 0 & \frac{1}{S} & 0 \end{bmatrix} \begin{bmatrix} x_{i-1} \\ z_{i-1} \\ x_i \\ z_i \\ \Delta y_i \end{bmatrix} \quad (3.55)$$

Here: $\Delta y_i = y_i - y_{i-1}$ represents the relative position between impulsive points i and $i-1$, which means the along-track velocity of the hovering spacecraft after being added an impulse control is only related to its relative position, but not the absolute position.

Similarly, the velocity of the hovering spacecraft before being imposed an impulse at point i is:

$$\begin{aligned} \dot{\rho}_i^- &= \Phi_{21}(T)\rho_{i-1} + \Phi_{22}(T)\dot{\rho}_{i-1}^+ \\ &= \Phi_{21}(T)\rho_{i-1} + \Phi_{22}(T)\Phi_{12}^-(T)[\rho_i - \Phi_{11}(T) \cdot \rho_{i-1}] \end{aligned} \quad (3.56)$$

Then the velocity of the hovering spacecraft before being imposed an impulse at point $i-1$ can be described as:

$$\begin{aligned} \dot{\rho}_{i-1}^- &= \Phi_{21}(T)\rho_{i-2} + \Phi_{22}(T)\dot{\rho}_{i-2}^+ \\ &= \Phi_{21}(T)\rho_{i-2} + \Phi_{22}(T)\Phi_{12}^-(T)[\rho_{i-1} - \Phi_{11}(T) \cdot \rho_{i-2}] \end{aligned} \quad (3.57)$$

We can expand this and obtain:

$$\begin{pmatrix} \dot{x}_{i-1}^- \\ \dot{y}_{i-1}^- \\ \dot{z}_{i-1}^- \end{pmatrix} = n \begin{bmatrix} \frac{-4S+3nT}{8-3nTS-8C} & \frac{-2+2C}{8-3nTS-8C} & 0 & \frac{4S-3nTC}{8-3nTS-8C} & \frac{2-2C}{8-3nTS-8C} & 0 \\ \frac{2-2C}{8-3nTS-8C} & \frac{-S}{8-3nTS-8C} & 0 & \frac{-14+6nTS+14C}{8-3nTS-8C} & \frac{S}{8-3nTS-8C} & 0 \\ 0 & 0 & -\frac{1}{S} & 0 & 0 & \frac{C}{S} \end{bmatrix} \begin{bmatrix} x_{i-2} \\ y_{i-2} \\ z_{i-2} \\ x_{i-1} \\ y_{i-1} \\ z_{i-1} \end{bmatrix} \quad (3.58)$$

Similarly, we can rearrange Eq. (3.58) and obtain:

$$\begin{pmatrix} \dot{x}_{i-1}^- \\ \dot{y}_{i-1}^- \\ \dot{z}_{i-1}^- \end{pmatrix} = n \begin{bmatrix} \frac{-4S+3nT}{8-3nTS-8C} & 0 & \frac{4S-3nTC}{8-3nTS-8C} & 0 & \frac{2-2C}{8-3nTS-8C} \\ \frac{2-2C}{8-3nTS-8C} & 0 & \frac{-14+6nTS+14C}{8-3nTS-8C} & 0 & \frac{S}{8-3nTS-8C} \\ 0 & -\frac{1}{S} & 0 & \frac{C}{S} & 0 \end{bmatrix} \begin{bmatrix} x_{i-2} \\ z_{i-2} \\ x_{i-1} \\ z_{i-1} \\ \Delta y_{i-1} \end{bmatrix} \quad (3.59)$$

Here: $\Delta y_i = y_{i-1} - y_{i-2}$ represents the relative position between impulsive points $i-1$ and $i-2$, which means the along-track velocity of the hovering spacecraft before being added an impulse control is also related to its relative position merely, but not at the absolute position.

Based on Eqs. (3.55) and (3.58), the value of the impulsive control needed at point $i-1$ can be obtained:

$$\Delta v_{i-1} = \dot{\rho}_{i-1}^+ - \dot{\rho}_{i-1}^- = f_3(\rho_{i-1}, \rho_i, t_{i-1,i}, T) \quad (3.60)$$

3.3.2.2 Constraints in Orbit Design

The major constraint in regional hovering orbit design is how to analyze the relative position between the relative motion trajectory of the hovering spacecraft and the confined area. As the relative motion of the hovering spacecraft in and out of the orbit plane of the target satellite is decoupled, the constraints in regional hovering orbit design can be studied from in-plane and out-of-plane of the target satellite's orbit.

(1) In-plane trajectory constraint

In the orbit plane of the target satellite, the relative motion trajectory of the hovering spacecraft between two adjacent impulsive points gradually becomes larger as the time of free flight increases. When the flight time between the two impulsive points becomes long enough, the relative motion trajectory of the hovering spacecraft will go beyond the confined area as is shown in the following figure.

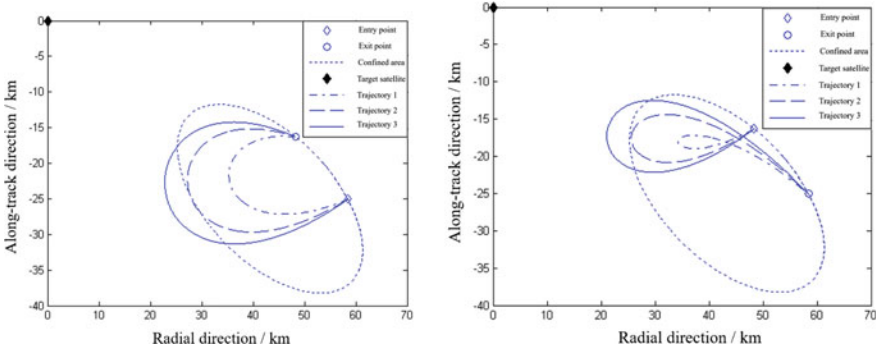


Fig. 3.20 Relative motion trajectory of spacecraft according to different time of flight

In Fig. 3.20, the dotted ellipse represents an elliptical confined area in the orbital coordinate system of the target satellite. In the left figure, the time of flight of trajectories 1, 2 and 3 are $1.5932e+004$ s, $2.0472e+004$ s and $2.2932e+004$ s, respectively; in the right figure, the time of flight of trajectories 1, 2 and 3 are $1.3520e+004$ s, $1.7520e+004$ s and $1.9720e+004$ s, respectively. It is obvious that due to the excessively long time of the free flight, the relative motion trajectory (i.e., trajectory 3) of the tracking spacecraft goes beyond the confined area.

Therefore, with regard to the short-range relative motion under the control of impulse, if T'_{\max} is the maximum permissible free flight time of the hovering spacecraft between two adjacent impulsive points, then only when the free flight time of the hovering spacecraft $T \leq T'_{\max}$, the relative motion trajectory will not go beyond the confined area.

We suppose that the configuration of the confined area is an elliptical area as shown in Fig. 3.21.

Here, $o-xy$ represents the coordinate system in the orbit plane of the target satellite. The direction of axis y is in accordance with the along-track direction of the target and the direction of axis x is in accordance with the radial direction of the target. $o'-x'y'$ is a translational coordinate system and $o'-b_1b_2$ is a rectangular coordinate system in the plane. l_1 represents the distance between the regional center and the target satellite and α represents the azimuth of the regional center in the orbital coordinate system of the target satellite. η represents the rotated angle of $o'-b_1b_2$ relative to $o'-x'y'$. τ_1 and τ_2 represent the size of the elliptical regional configuration. ψ_i represents the phase size of the hovering spacecraft in this area, with the counterclockwise rotation along axis $o'-b_2$ being positive.

We suppose that all the impulsive points are imposed at the boundary of the confined area, then the position coordinates of the impulsive points (x_i, y_i) can be represented by the phase of the hovering spacecraft ψ_i in the confined area. We suppose the phases of any two adjacent impulsive points i and $i+1$ are ψ_i and ψ_{i+1} , respectively, when the configuration of the confined area is given, the corresponding maximum time of a free flight between impulsive points i and $i+1$ is

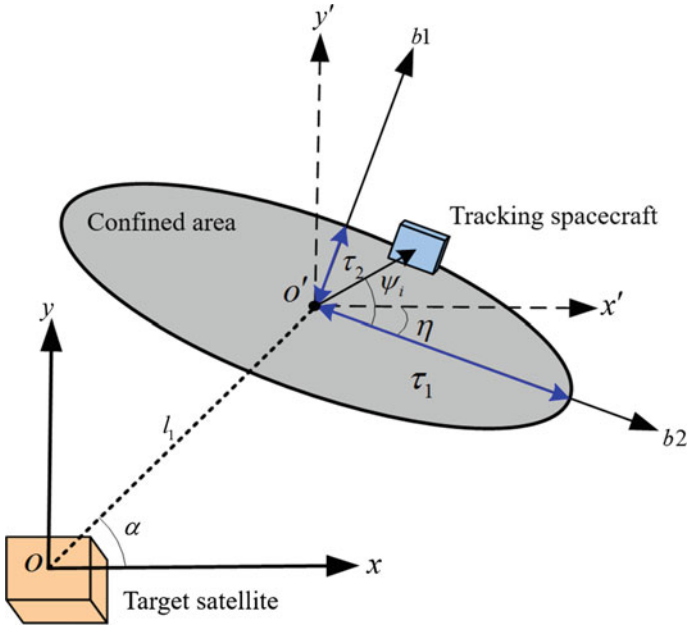


Fig. 3.21 Schematic figure of in-plane constraint of target satellite orbit

$T_{\max}(\psi_i, \psi_{i+1})$. When all the boundary points of the confined area are considered, a distribution curve of the maximum time of the free flight between any adjacent impulsive points can be obtained. The calculation of obtaining the maximum time of the free flight is as follows (Fig. 3.22).

Here, T_{upper} and T_{low} represent the upper and lower limits of the initialized values of the flight time respectively. We can take the observation of a high orbit target satellite as an example. Generally, as the observation time is less than the orbit period of the target satellite, we can set $T_{low} = 0$. Here, T_{upper} represents one single orbit period of the target satellite; tol represents the allowable error.

We can take the target satellite in the geostationary orbit as an example. If the configuration parameters of the confined area are $\alpha = -30^\circ$, $l_1 = 50$ m, $\eta = 30^\circ$, $\tau_1 = 20$ m, $\tau_2 = 10$ m, then between any two points, the distribution curve of the maximum time of a free flight used by the hovering spacecraft is shown in Fig. 3.23.

The left figure shows the distribution curve of the hovering spacecraft's free flight time, and the right figure shows the relative configuration of the confined area in the target orbit plane. The cases shown in Figs. 3.24, 3.25, 3.26 and 3.27 are similar and will be not explained again.

We can take the parameters of the confined area shown in Fig. 3.23 as the reference. A study of the changes related to the size of the elliptical region (τ_1, τ_2), the rotating azimuth η , the distance l_1 and the azimuth α between the regional center

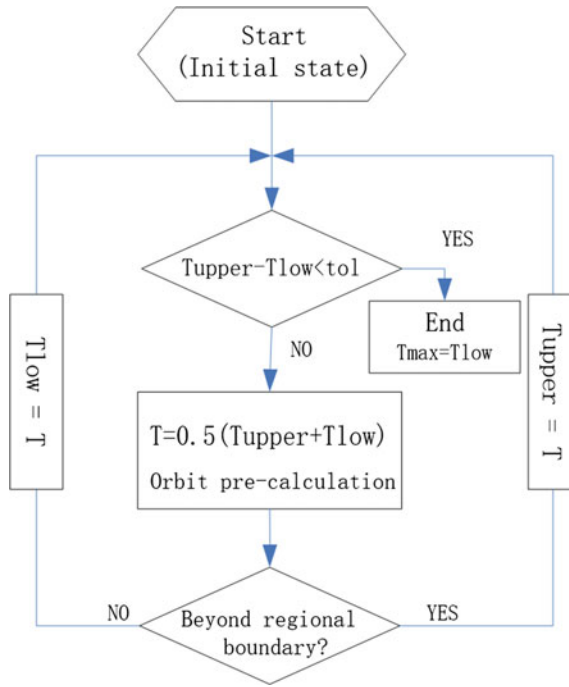


Fig. 3.22 Calculation of flight-time constraint

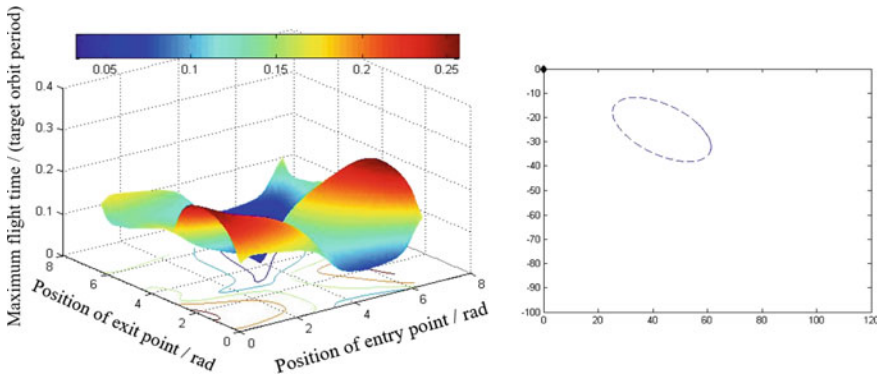


Fig. 3.23 Distribution curve of flight time used by hovering spacecraft

and the target satellite will be conducted below in order to discuss the change law of the distribution curve of the time of the free flight.

- (1) *The influence of the change in the size of the regional relative configuration (τ_1, τ_2) on the distribution of the free flight time.*

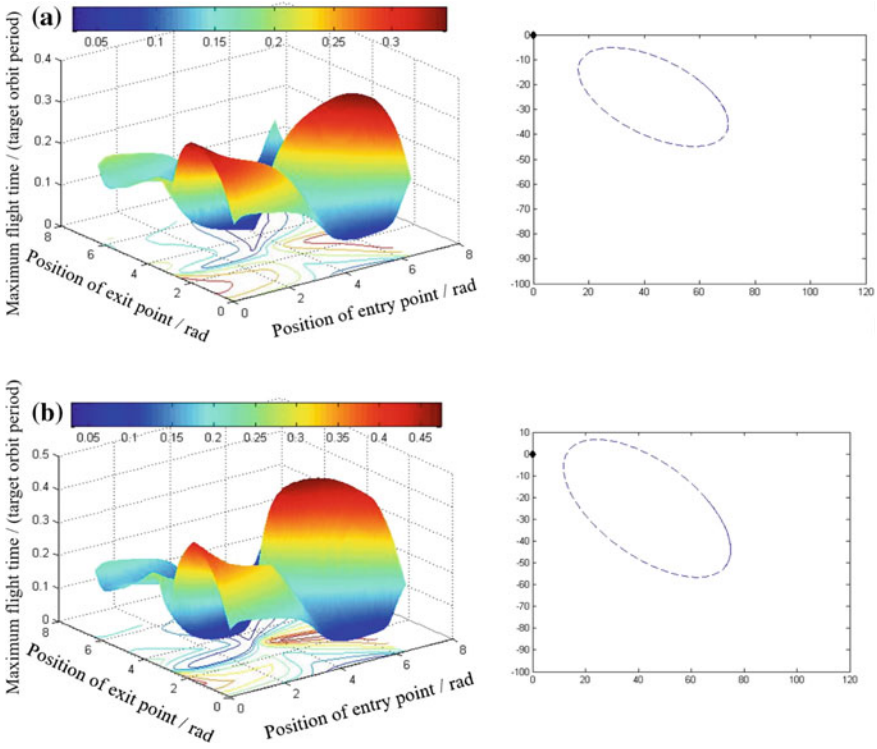


Fig. 3.24 Influence of change in the size of regional configuration on the time of flight

Figure 3.24 shows the influence of the change in the size of the relative configuration of the elliptical confined area (τ_1, τ_2) on the distribution curve of the free flight time. Here, the size of the elliptical configuration in Fig. (a) is $\tau_1 = 30$ m, $\tau_2 = 15$ m, that in Fig. (b) is $\tau_1 = 40$ m, $\tau_2 = 20$ m, the sizes of the elliptical areas are one point five times and twice of the size of the reference parameters respectively.

From the simulation result, it can be seen that when other conditions remain the same, the bigger the configuration of the confined area, the larger the distribution range of the time of the free flight.

- (2) *The influence of the change in the rotation angle of the elliptical area η on the distribution of the free flight time.*

Figure 3.25 shows the influence of the change in the rotation angle of the elliptical confined area on the distribution curve of the free flight time. Here, the rotation angle in Fig. (a) is 45° , that in Fig. (b) is 60° , the sizes of the elliptical areas are one point five times and twice of the size of the reference parameters respectively.

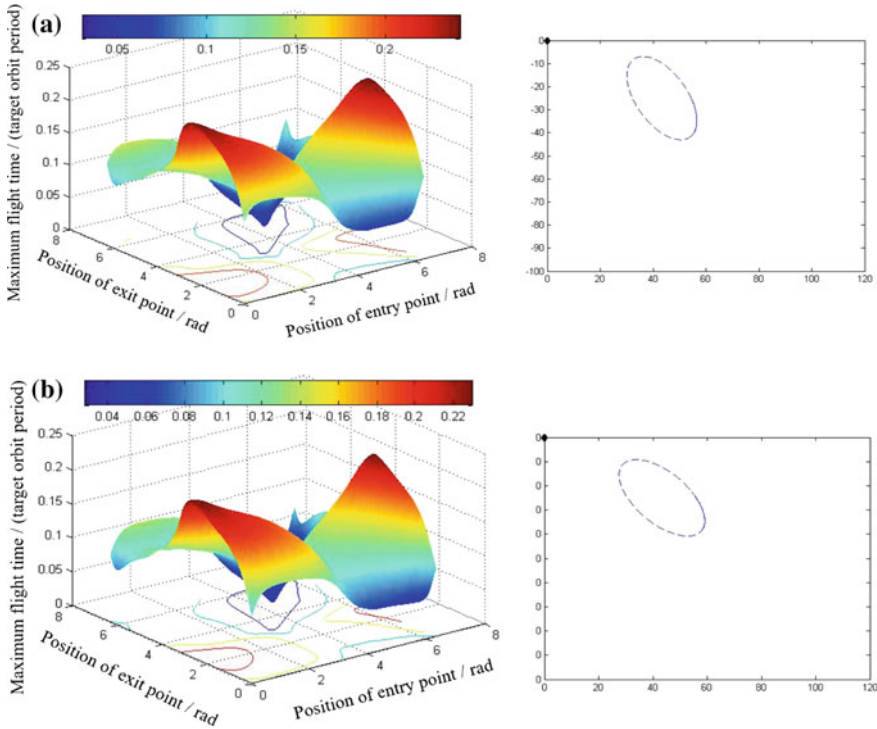


Fig. 3.25 Influence of change in rotation angle of area on time of free flight

From the simulation result, it can be seen that in the fourth quadrant, the bigger the rotated angle is, the larger the distribution range of the time of the free flight is. But compared with other parameters, the rotation angle exerts less influence on the time of free flight.

- (3) *The influence of the change in the distance between the regional center and the target satellite l_1 on the distribution of the free flight time.*

Figure 3.26 shows the influence of the change in the distance between the regional center of the elliptical confined area and the target satellite l_1 on the distribution curve of the free flight time. Here, the distance between the regional center and the target satellite in Fig. (a) is 75 m, that in Fig. (b) is 100 m, and the relative distances are one point five times and twice of the reference parameters respectively.

From the simulation result, it can be seen that when other conditions remain the same, the longer the distance between the regional center and the target satellite, the smaller the distribution range of the time of the free flight.

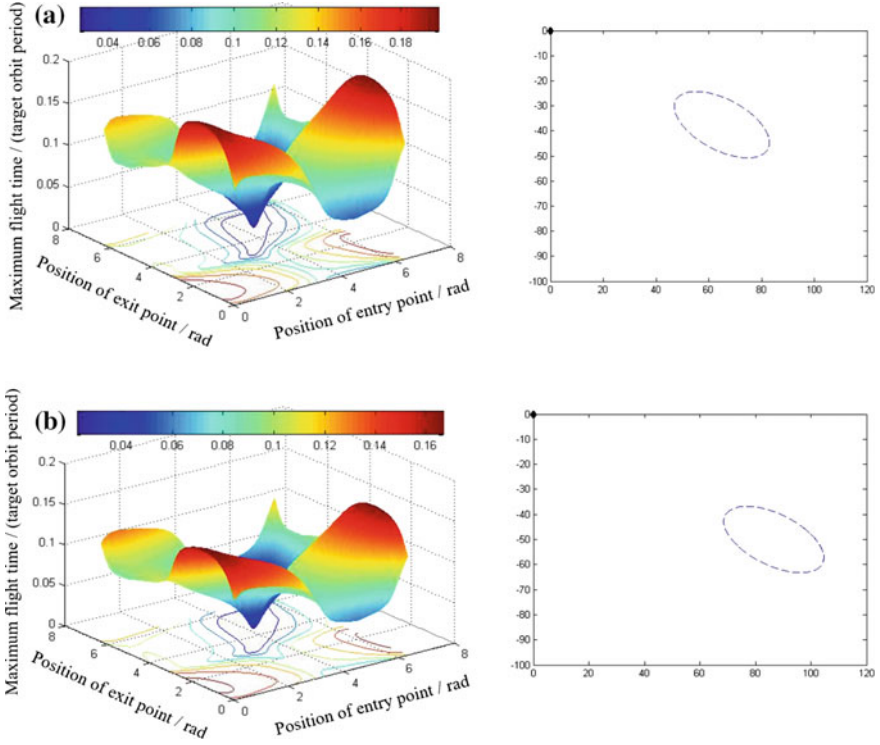


Fig. 3.26 Influence of change in distance between regional center and target satellite on time of free flight

- (4) *The influence of the change in the azimuth of the regional center relative to the target satellite α on the distribution of the free flight time.*

Figure 3.27 shows the influence of the change in the azimuth of the regional center relative to the target satellite α on the distribution curve of the free flight time. Here, the azimuth in Fig. (a) is -45° , that in Fig. (b) is -60° , and the azimuths are one point five times and twice of the size of the reference parameters respectively.

From the simulation result, it can be seen that, the bigger the azimuth of the regional center, the larger the distribution range of the free flight time.

(2) Out-of-plane Trajectory Constraint

Based on the dynamic model of relative motion, the relative motion equation of the hovering spacecraft out of the orbit plane of the target satellite is as follows:

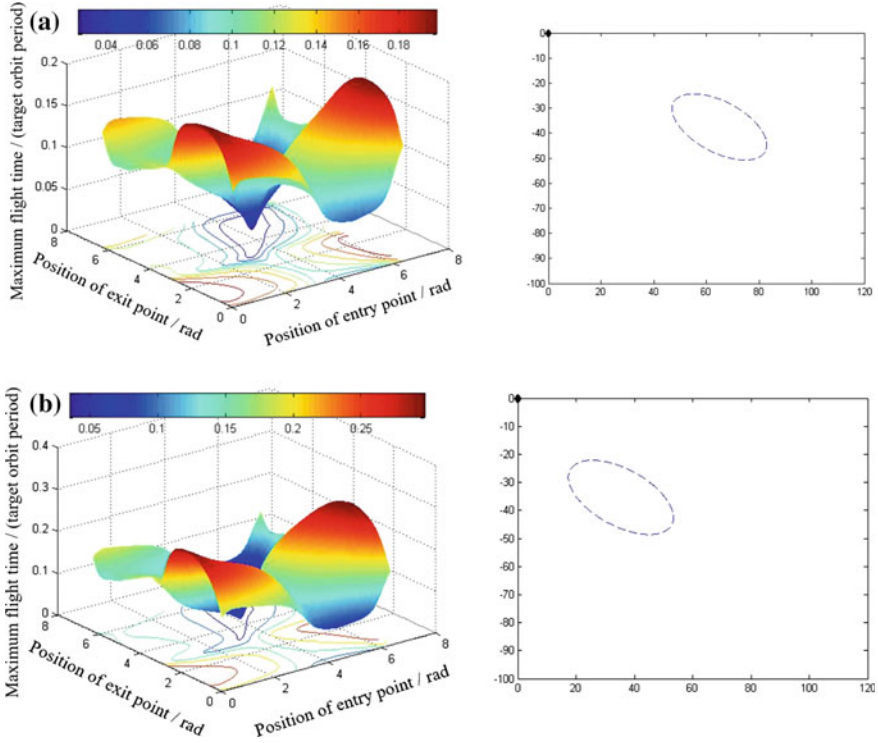


Fig. 3.27 Influence of change in azimuth of the regional center relative to target satellite on flight time

$$\ddot{z} + n^2 z - a_{cz} = 0 \quad (3.61)$$

If the initial position z_0 and the initial velocity \dot{z}_0 of the hovering spacecraft's normal direction in the orbital coordinate system of the target satellite are known, then the solution of Eq. (3.61) is:

$$\begin{cases} z = \frac{\dot{z}_0}{n} \sin nt + z_0 \cos nt = \sqrt{\left(\frac{\dot{z}_0}{n}\right)^2 + (z_0)^2} \sin(nt + \varphi) = Z \sin(nt + \varphi) \\ \dot{z} = \dot{z}_0 \cos nt - n z_0 \sin nt = n \sqrt{\left(\frac{\dot{z}_0}{n}\right)^2 + (z_0)^2} \cos(nt + \varphi) = nZ \cos(nt + \varphi) \end{cases} \quad (3.62)$$

Here, $\tan \varphi = \frac{n z_0}{\dot{z}_0}$, $Z = \sqrt{\left(\frac{\dot{z}_0}{n}\right)^2 + (z_0)^2}$.

Here: when the initial state of the hovering spacecraft is determined, Z represents the longest relative distance between the hovering spacecraft and the target satellite in the orbital coordinate system of the target satellite in the normal direction. From Eq. (3.62), it can be assumed that the motion state of the hovering spacecraft in the

orbital coordinate system of the target satellite in the normal direction is related to its initial relative position and its initial relative velocity in the normal direction. Furthermore, the relative motion is a simple harmonic motion with an amplitude of Z .

The constraint condition of the hovering spacecraft in the orbital coordinate system of the target satellite in the normal direction can be calculated based on the regional configuration parameters. If the regional configuration is as Fig. 3.28 shows:

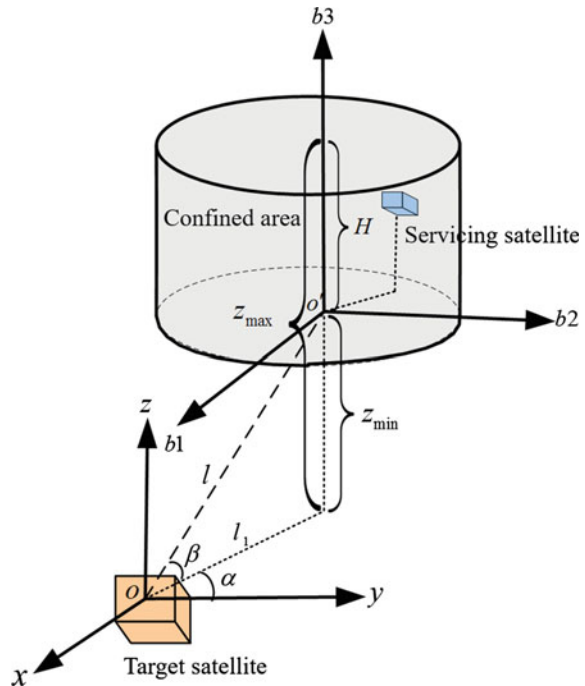
Then:

$$\begin{cases} Z_{\min} = l \sin \beta \\ Z_{\max} = l \sin \beta + H \end{cases} \quad (3.63)$$

Here, H represents the altitude of the confined area in the orbital coordinate system of the target satellite in the normal direction; Z_{\min} and Z_{\max} represent the shortest and the longest distances between the hovering spacecraft and the target satellite in the orbital coordinate system of the target satellite respectively.

When $Z \leq Z_{\max}$, the hovering spacecraft under the uncontrolled condition will not go beyond the farthest end of the confined area. In this case, only the orbit control required when the hovering spacecraft is at the near-end of the confined area should be considered. When the hovering spacecraft moves to the near-end of the confined area and keeps moving towards the target satellite, an impulsive control

Fig. 3.28 Schematic figure of out-of-plane constraint of target satellite orbit



should be imposed to keep the hovering spacecraft in the confined area. At the near-end, the relative motion state of the hovering spacecraft satisfies the following conditions:

$$Z \sin(nt + \varphi) = Z_{\min} \quad (3.64)$$

When this equation is solved, the following can be obtained:

$$\begin{cases} t_1 = \frac{1}{n} \left[\sin^{-1} \left(\frac{Z_{\min}}{Z} \right) - \varphi \right] \\ t_2 = \frac{1}{n} \left[\pi - \sin^{-1} \left(\frac{Z_{\min}}{Z} \right) - \varphi \right] \end{cases} \quad (3.65)$$

Therefore, the time interval between two adjacent impulsive controls is:

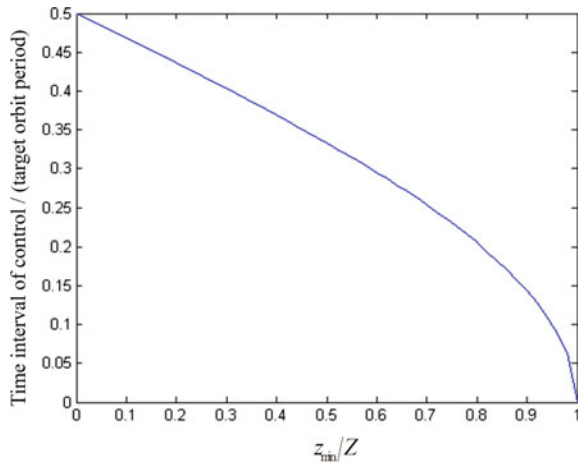
$$\Delta t = t_2 - t_1 = \frac{1}{w} \left[\pi - 2 \sin^{-1} \left(\frac{Z_{\min}}{Z} \right) \right] \quad (3.66)$$

And the impulsive value needed is:

$$\begin{aligned} \Delta v &= \dot{z}_1 - \dot{z}_2 = nZ [\cos(nt_1 + \varphi) - \cos(nt_2 + \varphi)] \\ &= nZ \left[\cos \left(\sin^{-1} \left(\frac{Z_{\min}}{Z} \right) \right) - \cos \left(\pi - \sin^{-1} \left(\frac{Z_{\min}}{Z} \right) \right) \right] \\ &= nZ \left[\cos \left(\sin^{-1} \left(\frac{Z_{\min}}{Z} \right) \right) + \frac{Z_{\min}}{Z} \right] \end{aligned} \quad (3.67)$$

Figure 3.29 illustrates the curve of the two adjacent impulsive controls changing along with Z_{\min}/Z . It can be seen that the bigger the value of Z_{\min}/Z , the shorter the time interval of the control. As shown in Fig. 3.29, when $Z_{\min}/Z = 0$, i.e., when the near-end of the confined area is just in the orbit plane of the target satellite, the

Fig. 3.29 Relation between time interval and Z_{\min}/Z



period of the impulsive control is half of the target orbit period; when $Z_{\min}/Z = 1$, i.e., when the hovering spacecraft is confined at the top of the normal direction of the target orbit, the time interval of the impulsive control is 0, which means a continuous thrust has to be imposed on the hovering spacecraft.

When $Z \geq Z_{\max}$, the hovering spacecraft needs control in the normal direction, and the time of the control is:

$$\begin{cases} Z \sin(nt_1 + \varphi) = Z_{\min} \\ Z \sin(nt_2 + \varphi) = Z_{\max} \end{cases} \quad (3.68)$$

When this equation is solved, the following can be obtained:

$$\begin{cases} t_1 = \frac{1}{n} \left[\sin^{-1} \left(\frac{Z_{\min}}{Z} \right) - \varphi \right] \\ t_2 = \frac{1}{n} \left[\sin^{-1} \left(\frac{Z_{\max}}{Z} \right) - \varphi \right] \end{cases} \quad (3.69)$$

Therefore, the time interval of the control is:

$$\Delta t = \frac{1}{n} \left[\sin^{-1} \left(\frac{Z_{\max}}{Z} \right) - \sin^{-1} \left(\frac{Z_{\min}}{Z} \right) \right] \quad (3.70)$$

Based on the dynamic equation of relative motion, the impulsive value needed in every control can be calculated at the corresponding control node. There is no need for further explanation here.

Figure 3.30 shows the changes of the time interval of the impulsive control along with Z_{\max}/Z and Z_{\min}/Z . From the figure, it can be seen that as Z_{\min}/Z becomes bigger, or as Z_{\max}/Z becomes smaller, the time interval between two

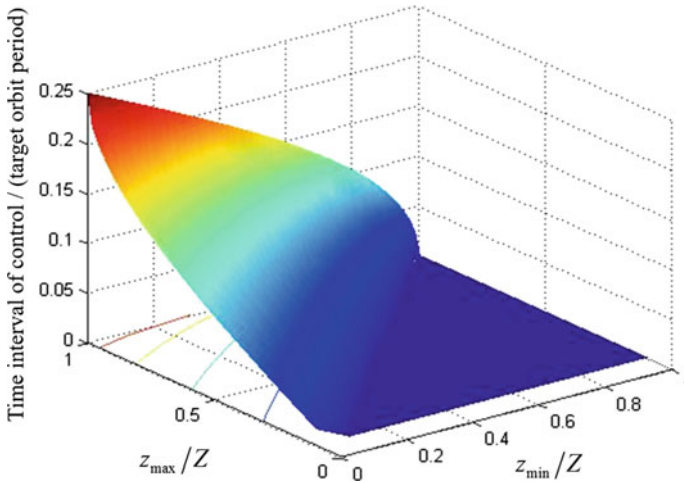


Fig. 3.30 Relation between time interval and Z_{\max}/Z , Z_{\min}/Z

adjacent impulsive controls becomes shorter. It can also be seen that when $Z_{\max}/Z = Z_{\min}/Z$, the time interval of the impulsive control in the normal direction is 0, which means the impulsive control changes into the continuous thrust control.

(3) Other constraints

The design and control of the regional hovering orbit have to meet the constraint on the relative motion trajectory of the spacecraft. At the same time, many other factors also need to be considered. For example, with regard to the design of the confined area's configuration parameters, the requirements on the size and the azimuth of the confined area for a certain mission should be considered; with regard to the control of the regional hovering orbit, it is necessary to take into account the restrictions on the thrust's value and direction needed by the hovering spacecraft in designing the orbit control sequences.

3.3.3 Regional Hovering Orbit of Single-Pulse Thrust

Compared with the complex attitude and orbit coupling control of the fixed-point hovering orbit, the advantage of the regional hovering orbit is that it realizes the separation of orbit control and attitude control. The hovering spacecraft only needs to carry out orbit control at the boundary of the confined area. And when the hovering spacecraft is in the confined area, only attitude pointing control is needed. This kind of separation of attitude control and orbit control brings great benefit to the control of the hovering spacecraft and tremendously enhances the applicability of the regional hovering orbit. This section will be about two optimized control methods of the regional hovering orbit under the control of a single-pulse, which are the minimum rate of energy consuming mode and the fixed time mode.

3.3.3.1 Minimum Rate of Energy Consuming Mode

With regard to some space missions (for example, on-orbit service, key module replacement and repair), the flight time of the hovering spacecraft in the confined area is not pre-set, but becomes longer as the mission extends. Therefore, the minimum energy consuming rate of the hovering spacecraft during the whole mission should be considered as the optimizing index.

The hovering spacecraft enters the confined area from one boundary point (called the entry point) and exits from another boundary point (called the exit point). The position coordinates of the impulsive point in the confined area can be expressed by its phase angle, which means ψ_1 and ψ_2 are used to describe the positions of the entry point and the exit point. We propose that the state (ρ_1, ρ_1^-) of the initial point ψ_1 and the state ρ_2 of the exit point ψ_2 are known, then the time of

the free flight T between adjacent impulsive points can be determined by Eq. (4.60). Here Δv is only the function of variable T and can be expressed as:

$$\Delta v = \dot{\rho}_1^+ - \dot{\rho}_1^- = f(T) \quad (3.71)$$

When we take the variation of the mean velocity of the hovering spacecraft as the optimizing index, the following can be obtained:

$$J = \sum |\Delta v_j| / \sum T_j \quad (3.72)$$

Here: Δv_j represents the velocity increment needed at the j th time in imposing orbit control. As energy consuming has nothing to do with direction, so the following index function is adopted:

$$J = \sum \Delta v_j^2 / \sum T_j \quad (3.73)$$

For the single-pulse control:

$$J = \Delta v_j^2 / T_j = f^2(T_j) / T_j \quad (3.74)$$

Here, $\Delta v_j = (\rho_{i-1}^+)_j - \rho_{i-1}^- = f(T_j)$ represents the velocity variation when the hovering spacecraft imposes control for the j th time at the entry point, and T_j represents the single free flight time of the hovering spacecraft.

Equation (3.74) is a composite function containing inverse circular functions and polynomials with a complicated form. It is hard to give it an explicit expression, though it will not influence the programming of the simulation and the realization of the optimization results. The concrete optimization design model is:

$$J = \min(f^2(T_j) / T_j) \quad (3.75)$$

$$st \begin{cases} f(T_j) = \Delta v_j \\ X(t_0) = \rho_{i-1} \\ X(t_0 + T_j) = \rho_i \\ 0 \leq T_j \leq T_{\max}(i-1, i) \end{cases}$$

The only optimization variable in Eq. (3.75) is T_j . Note that the value of T_j should be smaller than the value of the maximum free flight time $T_{\max}(i-1, i)$.

We propose that the regional configuration parameters are $\alpha = -30^\circ$, $l = 50$ m, $\eta = 30^\circ$, $\tau_1 = 20$ m, $\tau_2 = 30$ m, the position of the entry point of the hovering spacecraft is $\psi_1 = 90^\circ$, the spacecraft's velocity before being imposed an impulse at the initial point in the radial and along-track directions are both 1 m/s, the positions of the exit point ψ_2 of the hovering spacecraft required by the simulation in the regional coordinate system are 0° , 180° , 270° . We use the GA optimization toolbox

Table 3.3 Optimization results

Position of entry point (°)	Position of exit point (°)	Maximum time of free flight(s)	Optimal time of free flight(s)	Average velocity variation (m/s ²)	Minimum velocity increment (m/s)
90	0	2.1794e+4	2.1794e+4	9.3352e-5	2.0345
90	90	1.8231e+4	1.8231e+4	1.1244e-4	2.0499
90	180	1.0683e+4	1.0683e+4	1.8854e-4	2.0142
90	270	1.4426e+4	1.4426e+4	1.3954e-4	2.0130

in MATLAB to obtain their optimal free flight time T respectively, and the results are shown in Table 3.3.

Figures 3.31, 3.32, 3.33 and 3.34 provide the relationship between the index function and the free flight time and the optimal relative motion trajectory under the above four conditions. The left figures show the relations between the index function and the free flight time, and the right figures are the optimal relative motion trajectories.

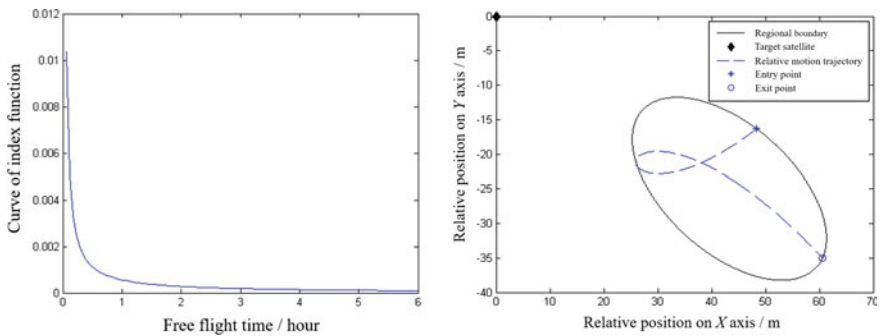


Fig. 3.31 Index function curve of exit point $\psi_2 = 0^\circ$ and relative motion trajectory

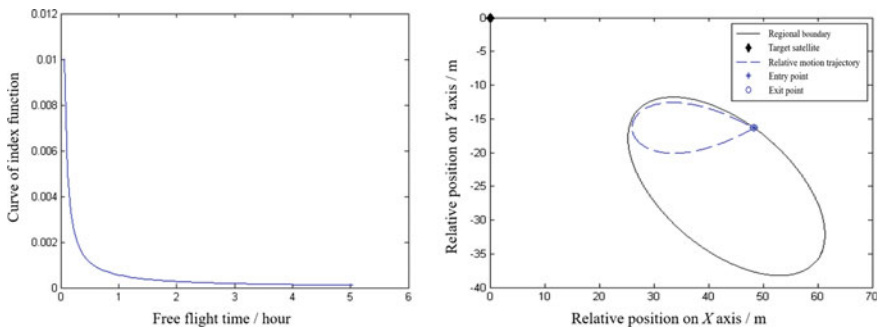


Fig. 3.32 Index function curve of exit point $\psi_2 = 90^\circ$ and relative motion trajectory

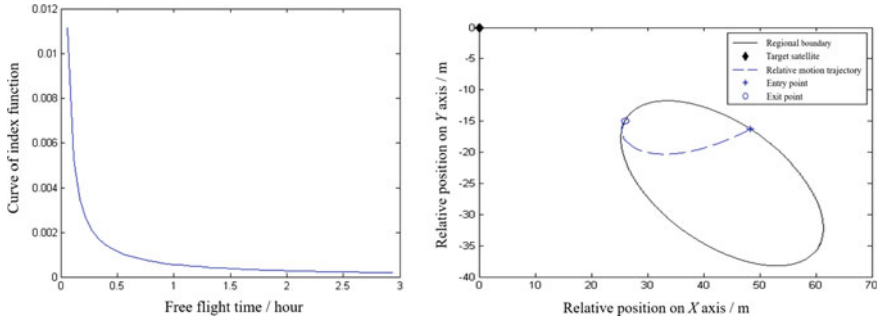


Fig. 3.33 Index function curve of exit point $\psi_2 = 180^\circ$ and relative motion trajectory

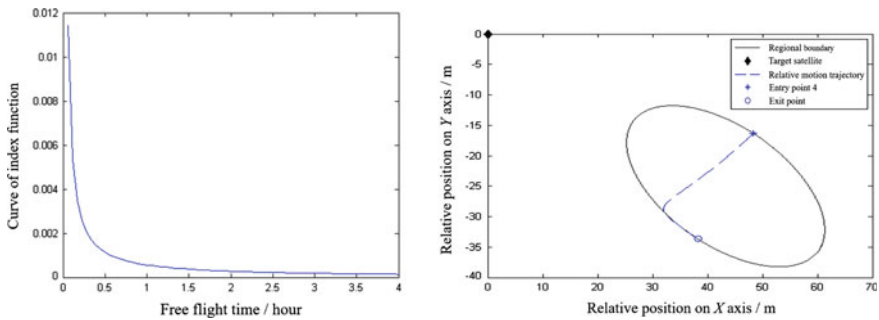


Fig. 3.34 Index function curve of exit point $\psi_2 = 270^\circ$ and relative motion trajectory

It can be seen that under the same conditions, as the free flight time becomes longer, the average velocity increment will gradually decrease. Therefore, the purpose of optimization is to keep the free flight time consumed by the hovering spacecraft in the confined area as long as possible.

Hence, under the minimum rate of energy consumption mode, the longer the free flight time between adjacent impulsive points, the better. As the flight time cannot exceed the constraint on its maximum free flight time, the maximum free flight time between the entry point and the exit point should be taken as the optimal free flight time.

3.3.3.2 Fixed Time Mode

With regard to missions which are time-sensitive (for example, short-range reconnaissance and monitoring), the time nodes for the tasks of the hovering spacecraft are preset. Once a task is completed, the spacecraft has to quit the present task or carry out the next task. As the time of these tasks are fixed, the minimum energy consumption during the whole mission can be taken as the optimizing index.

The hovering spacecraft enters the confined area from a certain point on the boundary and has to leave the area after a period T of interference. Therefore, the known conditions are entry point ψ_1 's position ρ_1 , the velocity before being imposed an impulsive $\dot{\rho}_1^-$ and the mission time T .

We suppose that the spacecraft exits the confined area from point ψ_2 , then it can be known from Eq. (3.60) that Δv is only the function of variable ρ_2 and can be expressed as:

$$\Delta v = \dot{\rho}_1^+ - \dot{\rho}_1^- = f(\rho_2) \quad (3.76)$$

We can take the variation of the total velocity of the hovering spacecraft as the optimizing index:

$$J = \sum \Delta |v_i| \quad (3.77)$$

Here: $\Delta v_i = \dot{\rho}_i^+ - \dot{\rho}_i^-$ represents the velocity variation needed when the hovering spacecraft imposes orbit control at point i . As energy consumption has nothing to do with direction, the following index function is adopted:

$$J = \sum \Delta v_i^2 \quad (3.78)$$

For the single-pulse control:

$$\Delta v^2 = f^2(\rho_2) = E\rho_2^2 + F\rho_2 + G \quad (3.79)$$

Here:

$$\begin{aligned} E &= w^2 B_1^2 + w^2 D_1^2 \\ F &= 2w[(wA_1\rho_1 - \dot{x}_1^-)B_1 + (wC_1\rho_1 - \dot{y}_1^-)D_1] \\ G &= w^2(A_1^2 + C_1^2)\rho_1^2 - 2w(A_1\dot{x}_1^- + C_1\dot{y}_1^-)\rho_1 + \dot{x}_1^2 + \dot{y}_1^2 \end{aligned}$$

$$A_1 = \left[\frac{-4S+3wTC}{8-3wTS-8C} \quad \frac{2-2C}{8-3wTS-8C} \right]$$

$$B_1 = \left[\frac{4S-3wT}{8-3wTS-8C} \quad \frac{-2+2C}{8-3wTS-8C} \right]$$

$$C_1 = \left[\frac{-14+6wTS+14C}{8-3wTS-8C} \quad \frac{-S}{8-3wTS-8C} \right]$$

$$D_1 = \left[\frac{2-2C}{8-3wTS-8C} \quad \frac{S}{8-3wTS-8C} \right]$$

As to a different exit point ρ_2^j :

$$\Delta v_j^2 = E(\rho_2^j)^2 + F\rho_2^j + G \quad (3.80)$$

Here, ρ_2^j represents the position of the j th exit point drafted for the hovering spacecraft. Therefore, the optimizing model can be expressed as:

$$\begin{aligned}
 J &= \min(\Delta v_j^2) \\
 st \quad &\begin{cases} \Delta v = f(\rho_2^j) \\ X(t_0) = \rho_1 \\ X(t_0 + T) = \rho_2^j \\ 0 \leq T \leq T_{\max}(1, j) \end{cases} \tag{3.81}
 \end{aligned}$$

The only unknown quantity in Eq. (3.81) is ρ_2^j . It should be noted here that, as to the position of the optimized exit point ψ_2^j , it has to ensure that the maximum free flight time $T_{\max}(1, j)$ should be longer than the mission time T .

We suppose the regional configuration parameters are $\alpha = -30^\circ$, $l = 50$ m, $\eta = 30^\circ$, $\tau_1 = 20$ m, $\tau_2 = 30$ m, the position of the entry point of the hovering spacecraft is $\psi_1 = 90^\circ$, the spacecraft’s velocity before being imposed an impulsive at the initial point in the radial and along-track directions are both 1 m/s, the mission time are 2, 4 and 6 h, respectively. We use the GA optimization toolbox in MATLAB to obtain the optimal positions of the exit point ψ_2 respectively, and the results are shown in Table 3.4.

It can be seen that the longer the mission, the larger the velocity variation of the hovering spacecraft. Figures 3.35, 3.36 and 3.37 provide the relations between the index function and the exit point and the optimal relative motion trajectories in the three cases. Here, the left figures show the relations between the index function and the position of the exit point, and the right figures show the optimal relative motion trajectories.

Table 3.4 Optimization results

Position of entry point ($^\circ$)	Mission time (h)	Optimal position of exit point ($^\circ$)	Velocity variation (m/s)
90	2	15.70	1.4153
90	4	6.35	1.4176
90	6	357.91	1.4192

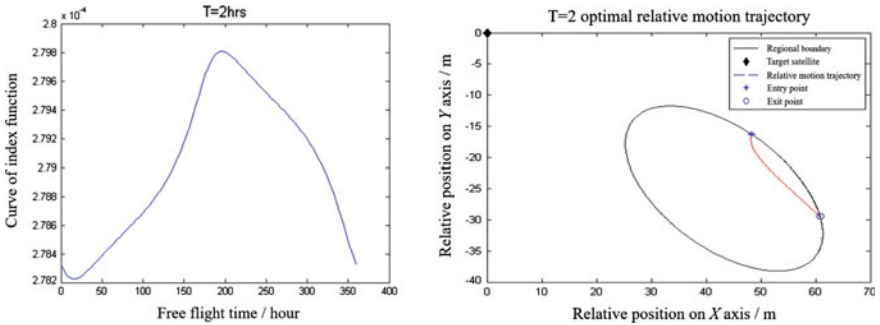


Fig. 3.35 Index function curve and relative motion trajectory when interference time is two hours

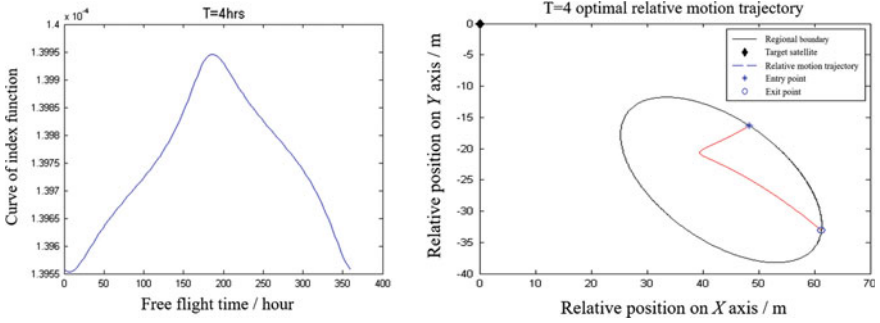


Fig. 3.36 Index function curve and relative motion trajectory when disturbance time is four hours

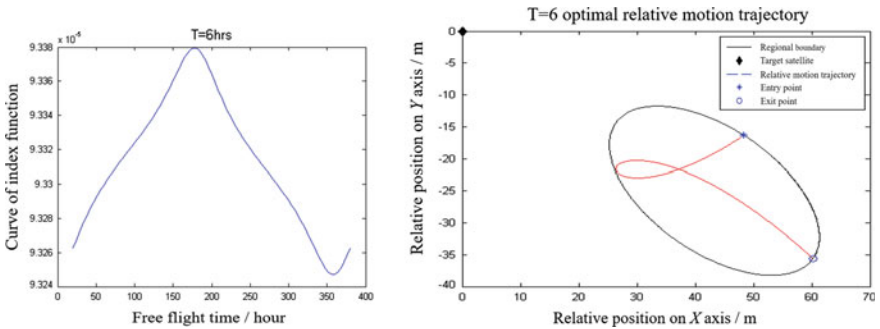


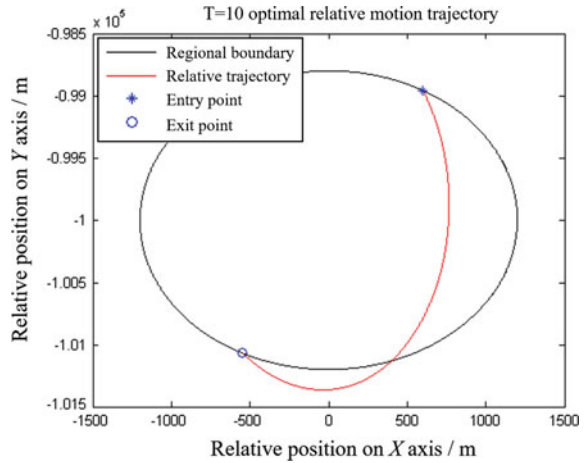
Fig. 3.37 Index function curve and relative motion trajectory when disturbance time is six hours

From the index function curves, it can be known that under every circumstance, the position of the optimized exit point is able to minimize the energy consumption of the hovering spacecraft when it is conducting corresponding missions. It can be known from the above results that the velocity variation of the hovering spacecraft is related to the position of the exit point. Besides, the longer the hovering spacecraft lingers in the confined area, the bigger the velocity variation is and the more the energy consumption is.

3.3.4 Regional Hovering Orbit of Multi-Pulse Trust

Under the control of single-pulse, the flight time of the hovering spacecraft in the confined area is limited as is shown in Sect. 3.3.3. When the lingering time of the hovering spacecraft required by the mission in the confined area exceeds the maximum time, the relative motion trajectory of the hovering spacecraft will go beyond the confined area. As is shown in Fig. 3.38, the mission time is ten hours and that means one single-pulse control cannot meet the requirements of the mission. With regard to missions such as on-orbit services, the mission time is generally unknown and may exceed the maximum free flight time allowed under the single-pulse control.

Fig. 3.38 Relative motion trajectory when hovering time is ten hours



Therefore, in order to increase the free flight time of the hovering spacecraft in the confined area, it is necessary to consider the method of multi-pulse control.

The major factors which influence the regional hovering spacecraft under multi-pulse control are the frequency of pulse control, the position of every impulsive point and the free flight time between adjacent impulsive points. As to the choices of optimizing indexes and control methods under different circumstances, further study can be conducted.

Obviously, compared with the fixed-point hovering orbit, the regional hovering orbit is easier to control and has a broad prospect in on-orbit fault detection and on-orbit monitoring, providing new technical means for spatial operations in the future. We should note that when the hovering time required exceeds the maximum free flight time, the multi-pulse control should be imposed in order to keep the hovering spacecraft remaining in the confined area.

3.4 Design of Displaced Geostationary Orbit

¹As the number of spacecraft in the geostationary orbit (GEO) is growing and the spacecraft is restricted by the deployment in the latitudinal direction, the GEO is getting more crowded. For the sake of this problem, America and other countries have adopted the near-equatorial plane orbit or the equatorial orbit to make up the lack of resources in the GEO.

¹Jeannette Heiligers, Matteo Ceriotti, Colin R. McInnes, et al. Displaced Geostationary Orbit Design Using Hybrid Sail Propulsion [J]. JOURNAL OF GUIDANCE, CONTROL, AND DYNAMICS, 2011, 34(6):1852–1866.

The satellites operating in the GEO are mainly communication satellites and reconnaissance satellites. The orbit period of the GEO is the same as the rotation period of the Earth and the satellites in the GEO keep relative static to their terrestrial points. By utilizing this feature, GEO satellites can provide a continuous communication support to the ground users in a certain region. And because of the advantages brought about by this unique feature, various countries are competing for the precious resources. This makes the GEO become increasingly crowded, especially for the regions over the lands. In order to create new GEO space, in recent years, scholars have proposed some non-Keplerian orbits (NKO) such as the near-equatorial plane orbit and the equatorial orbit, which are also known as the displaced geostationary orbit (displaced GEO). These NKOs use continuous thrust to balance the Earth's gravitational acceleration, and extensive research has been conducted in the existence, stability and control of the orbits. The NKOs have also been proved in many applications, including spatial short-range approaching, reconnaissance and communication in high latitude areas and lunar remote communication, etc.

Displaced orbits are often used to find a balance between two bodies in a rotating reference coordinate system. The method can be specified by the following example. In Fig. 3.39, $R(x_R, y_R, z_R)$ is a rotating coordinate system with an rotation angle of $\omega = \omega \hat{z}_R$, $I(X, Y, Z)$ is a inertial coordinate system with the z_R axis coinciding with the Z axis.

To achieve a displaced orbit, a thrust acceleration \mathbf{a} is needed. Then the motion of the spacecraft in the rotating coordinate system can be described as:

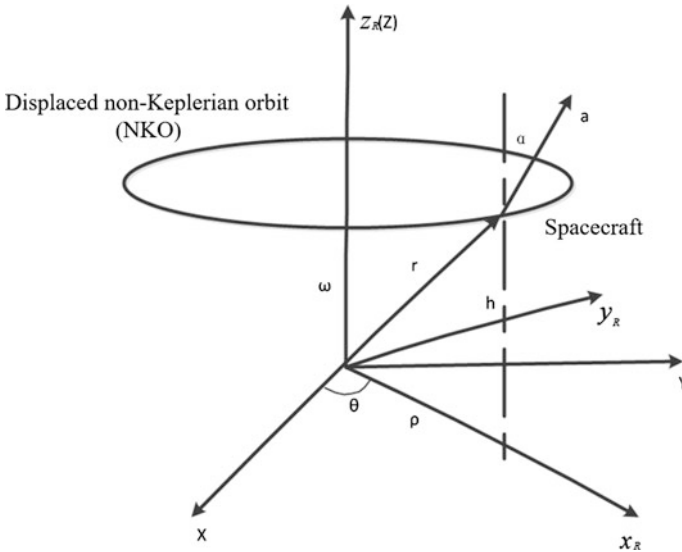


Fig. 3.39 Reference coordinate system of displaced orbit

$$\ddot{\mathbf{r}} + 2\boldsymbol{\omega} \times \dot{\mathbf{r}} + \nabla U = \mathbf{a} \quad (3.82)$$

We assume that μ is the gravitational constant of the central body and U is the common potential function of the central gravitation body and other centripetal acceleration, then

$$U = -(\mu/r) - \frac{1}{2} \|\boldsymbol{\omega} \times \mathbf{r}\|^2 \quad (3.83)$$

If in Eq. (3.82), $\dot{\mathbf{r}} = \ddot{\mathbf{r}} = 0$, when we remove the first two terms, the following can be obtained:

$$\nabla U = \mathbf{a} \quad (3.84)$$

The above directly gives the acceleration needed to maintain the displaced orbit.

As $\boldsymbol{\omega}$ is a fixed value, the vector of the control force needed is in the plane determined by the position vector \mathbf{r} and the Z axis and has no component in its transverse section. The direction of the control force is described by the inclination α , which is

$$\tan \alpha = \frac{\|\mathbf{z}_R \times \nabla U\|}{\mathbf{z}_R \cdot \nabla U} \quad (3.85)$$

Finally, U can be expressed by parameters in the (ρ, θ, h) polar coordinates in Fig. 3.39, which is

$$U = -\left(\frac{1}{2}(\omega\rho)^2 + \frac{\mu}{r}\right) \quad (3.86)$$

When we substitute Eq. (3.86) into Eqs. (3.84) and (3.85), the value and the direction of the thrust acceleration imposed can be obtained as the following:

$$\tan \alpha_{(\rho, \theta, h)} = \frac{\rho}{h} \left(1 - \left(\frac{\omega}{\omega_*}\right)^2\right) \quad (3.87)$$

$$\alpha_{(\rho, \theta, h)} = \sqrt{\rho^2(\omega^2 - \omega_*^2) + h^2\omega_*^4} \quad (3.88)$$

Here, ω_* is the orbital angular velocity of a Keplerian orbit with the same radius, which can be described as:

$$\omega_* = \sqrt{\mu/r^3} = \sqrt{\mu/(\rho^2 + h^2)^{3/2}} \quad (3.89)$$

3.4.1 Displaced Orbit Deviating from Orbit Plane

With regard to the GEO, $\omega = \omega_{GEO} = \sqrt{\mu/r_{GEO}^3}$, $r_{GEO} = 42,164.1696$ km. We further assume the vertical distance h between the spacecraft and the GEO (as shown in Fig. 3.39) is determined, then Eq. (4.81) can be used to find the optimal ρ to minimize the acceleration needed. We take the first derivative of ρ in Eq. (3.88) and obtain:

$$r^6 + \frac{\mu}{\omega^2} r^3 - 3 \frac{\mu}{\omega^2} h^2 r - 2 \left(\frac{\mu}{\omega^2} \right)^2 = 0 \quad (3.90)$$

Then we solve the above 6th-order equation and omit the complex roots and the negative roots. Based on the Descartes Law, Eq. (3.90) has a positive real root. Equation (3.90) cannot be solved by the analytical method, but can be solved by the Newton Method in the numerical method. The solution is shown in Fig. 3.40.

The acceleration in Fig. 3.40 is a dimensionless quantity and is described by the ratio of the acceleration to the rotation acceleration on the Earth's surface. The figure indicates that if the distance between the displaced orbit and the reference orbit plane becomes longer, i.e., the h becomes bigger, the value of the acceleration needed becomes larger; however, in order to prevent the spacecraft in the displaced orbit from affecting the spacecraft in the GEO, the minimum h is often pre-set. When we take into account the related regulations stipulated by the International Telecommunication Union and different countries, we assume the migration heights are 35 km, 75 km and 150 km, respectively. We solve Eq. (3.90) and obtain r .

Fig. 3.40 Outline of minimum acceleration needed when h is given

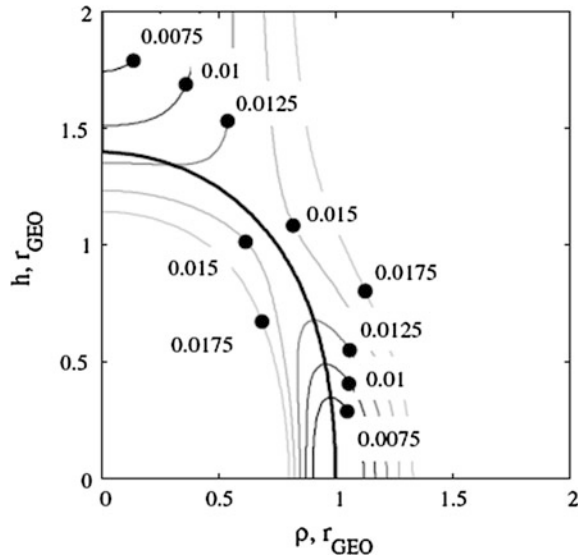


Table 3.5 Corresponding minimum acceleration of different migration heights

h (km)	ρ (km)	α ($^\circ$)	a (mm/s 2)
± 35	42,164.165	0.0476	0.1861
± 75	42,164.147	0.1019	0.3988
± 150	42,164.080	0.2038	0.7976

Then we can obtain the inclination α through Eq. (3.87). The optimized displaced orbit parameters are shown in Table 3.5.

It can be known from Table 3.5 that the inclination α is close to 0. From Eq. (3.87), it can be seen that if $\alpha = 0$ is to be achieved, then $\omega = \omega_*$, or $r = r_{GEO}$ is necessary. If we substitute the above results into Eq. (3.87) and Eq. (3.88), the following can be obtained:

$$\tan \alpha = 0 \tag{3.91}$$

$$a = h\omega_*^2 = \frac{\mu h}{r_{GEO}^3} \tag{3.92}$$

This is called the INKO and the details are shown in Fig. 3.41. Compared with Table 3.5, this orbit needs smaller angular velocity. For example, as to the migration height of 150 km, the maximum of the acceleration needed is only $6.3 \times 10^{-4} \text{ m/s}^2$.

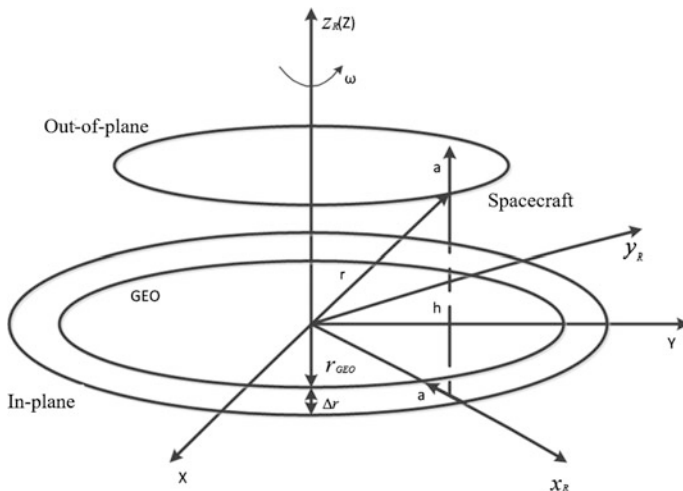


Fig. 3.41 Displaced orbit deviating from orbit plane (out-of-plane) and displaced orbit in orbit plane

3.4.2 Displaced Orbit in Orbit Plane

As is shown in Fig. 3.41, in the displaced orbit in the orbit plane, $h = 0$. We substitute it into Eqs. (3.87) and (3.88) and obtain

$$\alpha = \pm \frac{1}{2} \pi \quad (3.93)$$

$$a = |\rho(\omega_{GEO}^2 - \omega_*^2)| \quad (3.94)$$

Here: $\omega_* = \sqrt{\mu/\rho^3}$, $\rho = r_{GEO} + \Delta r$ and Δr are offsets, $\Delta r < 0$ corresponds to the inner side of the GEO and $\Delta r > 0$ corresponds to the outer side of the GEO.

Based on Eq. (3.93), it can be known that the acceleration needed is in the radial direction and the direction of α depends on Δr , which means when $\alpha < 0$, the direction points to the Earth-center, otherwise the opposite.

3.4.3 Energy Analysis of Orbit Displacement

For the above two displaced orbits, Fig. 3.40 can roughly tell the accelerations needed to maintain the two orbits respectively. When we compare the offsets in the horizontal plane and that in the orbit plane (along the direction of axis Z), we can find that when the offsets are the same, the acceleration needed by the former is three times of the latter. Besides, the acceleration needed by the displaced orbit of $\Delta r > 0$ is slightly superior to that of $\Delta r < 0$.

If three methods, i.e., impulse control, Solar Electric Propulsion (SEP), and the integrated propulsion of SEP and solar sail, are adopted to achieve the displaced orbit deviating from the orbit plane respectively, the control ability of the impulsive control method will be poor. Even for the minimum offset of 35 km, the hold time with this method will be no more than a few months. Therefore, in order to maintain the displaced orbit for a few months to several years when the offsets are 150 and 35 km, the SEP control method should be adopted. However, even though the method is adopted, if the spacecraft carries a payload of 100 kg, the hold time is only a few years with a relatively small offset. If the solar sail is added to the SEP, the SEP can work only at the time when the solar sail is not able to be used (for example, the solar sail cannot provide the thrust facing to the sun). In this way, the fuels can be saved effectively and the lifetime of the spacecraft can be extended or the payload can be increased.

With regard to the displaced orbit deviating from the orbit plane, the control force provided by the solar sail is influenced by seasonal changes. As to the displaced orbit with the migration position in the northern hemisphere, the control effect of the solar sail in winter is better; as to that in the southern hemisphere, the control effect in summer is better. Hence, the displaced orbit can conduct two

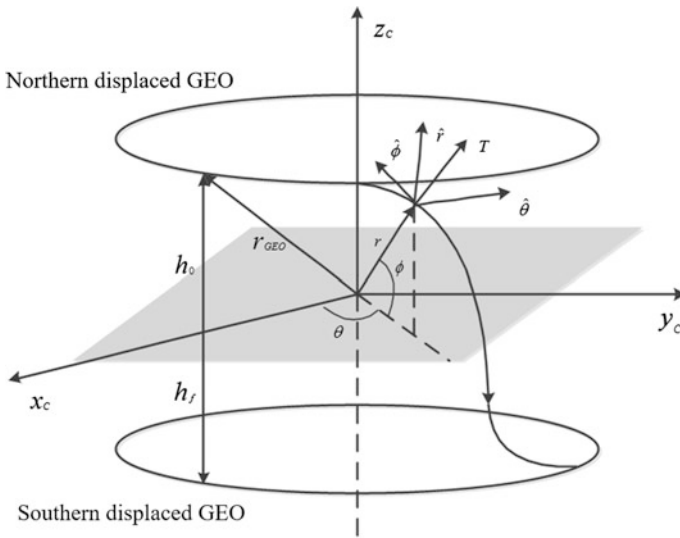


Fig. 3.42 Seasonal shift of displaced orbit

Table 3.6 Mass of propellant for seasonal shift of displaced orbit (g)

m_0/kg	h_0/km			
	± 35	± 75	± 150	
	2912	1020	436	
$\Delta d/\text{km}$	0	2.6	0.96	0.66
	5	243.0	52.6	20.1
	10	—	123.3	42.1
	20	—	—	96.0
	35	—	—	227.4

Note —means the scheme is infeasible

seasonal shifts, which are from north to south in spring and from south to north in fall as shown in Fig. 3.42.

We assume that the maximum thrust the SEP is able to provide is 0.2 N, m_0 is the initial mass of the spacecraft, Δd represents the distance restriction between the spacecraft and the GEO, then the mass of the propellant needed for the shift is shown in Table 3.6.

From the above table, it can be known that the propellant needed for the seasonal shift is quite small, or can even be ignored. The consumption of the propellant is dependent on Δd .

When the seasonal shift is adopted, the lifetime of the spacecraft, which uses single SEP thruster in the displaced orbit with a migration distance of 35 km and carries a payload of 255–487 kg, can be extended to 10–15 years, which is almost

the lifetime of the spacecraft in the GEO of today. And if the number of the SEP thruster is increased, the mass of the payload portable will rise greatly.

Also, these displaced orbits can be used for temporary missions, i.e., a spacecraft can use the displaced orbit when conducting a certain mission and goes back to the GEO for free flight when the mission is completed.

3.5 Summary

This chapter mainly studies the design and control method of the hovering orbit. First of all, the model of the fixed-point hovering orbit is studied through the mechanical analysis in physics and the approximate “two-body problem” method and two control methods, i.e., open-loop control and closed loop control, are provided; secondly, the design and control method of the regional hovering orbit are discussed. The spatial configurations of four confined areas are established and on this basis, the target orbit’s in-plane and out-of-plane design constraints are analyzed. Finally, the concept and design method of the displaced geostationary orbit are elaborated on. The maintenances of the configuration of the displaced orbit in and out of the GEO plane are studied and the energy consumption of the two displaced orbits are analyzed.

Chapter 4

Theory and Design Method of Spiral Cruising Orbit

A spiral cruising orbit is an orbit design method with reference to a target orbit. Spacecraft designed with this method can cruise around the target orbit in a spiral way. Therefore, with only one spacecraft, short-range and high-precision detection of all the spacecraft on the target orbit and the space environment can be achieved.

4.1 Spiral Cruising Orbit: Concept

Space target surveillance and space environment monitoring are the basis of various space activities. However, due to such reasons as the detection range and the deployment position of a ground-based detection network, it is difficult to obtain high-precision detection of all the on-orbit spacecraft, especially that of the high-orbit spacecraft and their space environment.

Spiral cruising orbit is a relative operation orbit with reference to a specific target orbit or a certain arc section of a specific target orbit. Spacecraft operating in a spiral cruising orbit can conduct spiral cruising detection, even spiral round-trip detection, of multiple target spacecraft that are in the target orbit, thus obtaining those target spacecraft's detailed information in multiple perspectives, so as to perform detailed recognition of a target spacecraft.

Spiral cruising orbit, through designing orbit parameters such as eccentricity and orbit inclination of the cruising spacecraft's orbit, enables the cruising spacecraft to move relative to the target orbit in a way similar to spiral precession, thus forming a spiral flying-around relative orbit configuration. Figure 4.1 shows the typical configuration of a spiral cruising orbit.

The mathematical expression of spiral cruising orbit is shown in Table 4.1, in which the first three entries are descriptions about the target orbit of the cruise, its arc sections and key targets in these sections, which are also the basis for the design of a spiral cruising orbit in the future; the last five entries are descriptions about the design parameters of a spiral cruising orbit.

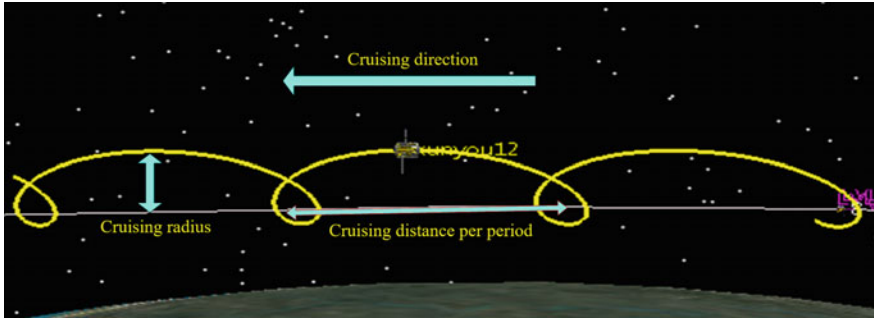


Fig. 4.1 Configuration of spiral cruising orbit

Table 4.1 Description parameters of spiral cruising orbit

Number	Parameter name	Specific descriptions
1	Target orbit	Orbit element of target orbit
2	Cruising orbit arc section	Arc range of cruising target orbit
3	Key target sequence	Key target sequence to be detected on the target orbit
4	Cruising direction	Positive direction: cruising direction is the same as the direction of the target spacecraft Reverse direction: cruising direction is the opposite of the direction of the target spacecraft Round-trip: cruising spacecraft taking round-trip cruising on a specific arc of the target orbit
5	Cruising velocity	Cruised radian per unit time
6	Cruising radius	Maximum distance between the cruising orbit's projection in the target orbit plane and the target orbit
7	Cruising inclination	Inclination of the cruising orbit relative to the target orbit plane
8	Initial phase	Initial position of the cruising spacecraft in the target orbit plane

Cruising velocity largely determines the cruising velocity of the spiral cruising orbit relative to the target orbit, which is directly related to the deviation in semi-major axis between the cruising spacecraft and the target orbit. Cruising radius mainly determines how many details of the target can be obtained by the cruising spacecraft with payload. Cruising inclination mainly determines from which flank the cruising spacecraft will detect the target spacecraft, ensuring the information required in the mission (such as the position of key components and radio signals in a particular direction, and so on) is monitored. The initial phase directly determines the angles formed among the cruising spacecraft, the target spacecraft and the Sun

at the observation moment, thus determining whether the exploratory conditions of the payload in visible light are met.

According to differences in cruising height, cruising radius, cruising direction, and the cruising path, spiral cruising orbits can be classified in multiple ways (Fig. 4.2):

- (1) According to the orbit altitude of the reference orbit (or target orbit), there are high-orbit cruising orbits and Low-Earth-Orbit cruising orbits;
- (2) According to the size of the cruising radius (with satellite warning distance as the separatrix), there are remote cruising orbit and short-range cruising orbit;
- (3) Depending on whether the cruising direction is the same as the direction of the target orbit, there are along-track cruising orbit and cross-track cruising orbit;
- (4) According to different cruising paths, there are traversal cruising orbit, round-trip itinerant orbit, and controllable cruising orbit, etc.

Two concepts are defined in the first place to describe the configuration of a spiral cruising orbit:

- (1) Aiming point: it is the point where the spiral cruising orbit’s trajectory intersects with itself. It is known from the spiral cruising orbit configuration that within one period, the operation trajectory of the platform and its previous cruising path will have at least one intersection point, which is defined as the aiming point.
- (2) Spiral ring: it is the path of the platform as it passes the same aiming point twice during spiral cruising, which is a closed annular relative motion trajectory.

The schematic figure of the aiming point and the spiral ring is shown in Fig. 4.3.

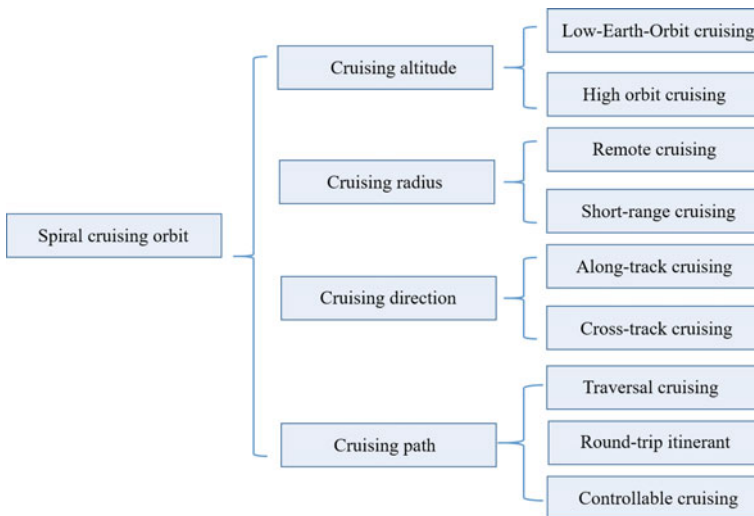


Fig. 4.2 Classification of spiral cruising orbits

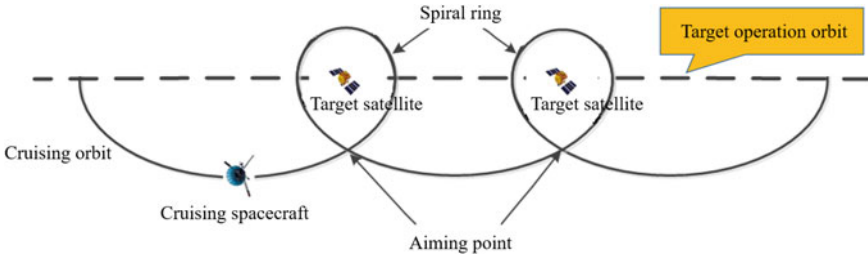


Fig. 4.3 Schematic figure of aiming point and spiral ring

4.2 Precision Analysis of Relative Motion Model

The relative motion dynamics method derives from the basic motion equations described by the absolute motion vectors of a spacecraft. Its study emphasizes solving the nonlinear relative motion differential equations expressed in the target orbit coordinate system. Relative motion dynamics has been well-studied by scholars both at home and abroad. This section starts with the accurate relative motion dynamics equation, and through reasonable hypotheses, obtains the relative motion dynamics model of a cruising spacecraft.

4.2.1 Accurate Relative Motion Dynamics Equation

The motion law of the cruising spacecraft relative to the target satellite can be described by a relative motion dynamics equation. We can suppose that \vec{r}_1 and \vec{r}_2 are the position vectors of the target satellite and the cruising spacecraft in the Earth centered inertial system, respectively, the relative position vector of the cruising spacecraft relative to the target satellite in the Earth centered inertial system is:

$$\vec{r} = \vec{r}_2 - \vec{r}_1 \tag{4.1}$$

It is known that the dynamics equations of the target satellite and the cruising spacecraft in the Earth centered inertial system are:

$$\begin{cases} \vec{r}_1 = -\frac{\mu\vec{r}_1}{r_1^3} + \vec{a}_{p,1} + \vec{a}_{c,1} \\ \vec{r}_2 = -\frac{\mu\vec{r}_2}{r_2^3} + \vec{a}_{p,2} + \vec{a}_{c,2} \end{cases} \tag{4.2}$$

Here, r_1 and r_2 stand for the instantaneous geocentric distances of the target satellite and the cruising spacecraft, respectively; $\vec{a}_{p,1}$ and $\vec{a}_{p,2}$ stand for the sum of all perturbation forces (except earth's gravity) of the target satellite and the cruising spacecraft, respectively; and $\vec{a}_{c,1}$, $\vec{a}_{c,2}$ stand for the sum of controlling accelerations of the target satellite and the cruising spacecraft, respectively.

Therefore, in the Earth centered inertial system, the relative motion dynamics equation of the cruising spacecraft relative to the target satellite is:

$$\ddot{\vec{r}} = \ddot{\vec{r}}_2 - \ddot{\vec{r}}_1 = -\mu \left(\frac{\vec{r}_2}{r_2^3} - \frac{\vec{r}_1}{r_1^3} \right) + \Delta \vec{a}_p + \Delta \vec{a}_c \quad (4.3)$$

In the equation, $\Delta \vec{a}_p = \vec{a}_{p,2} - \vec{a}_{p,1}$ and $\Delta \vec{a}_c = \vec{a}_{c,2} - \vec{a}_{c,1}$ stand for the difference between perturbation forces and the difference between control forces exerted on the cruising spacecraft and the target satellite, respectively.

If the relative motion dynamics equation in the Earth centered inertial system is converted into the target orbital coordinate system, then:

$$\ddot{\vec{r}} + 2\vec{\omega} \times \dot{\vec{r}} + \vec{\omega} \times (\vec{\omega} \times \vec{r}) + \dot{\vec{\omega}} \times \vec{r} = -\mu \left(\frac{\vec{r}_2}{r_2^3} - \frac{\vec{r}_1}{r_1^3} \right) + \Delta \vec{a}_p + \Delta \vec{a}_c \quad (4.4)$$

Here, $\vec{\omega} = [0 \ 0 \ \dot{\nu}]^T$ stands for the rotational angular velocity vector of the target orbital coordinate system relative to the Earth centered inertial system described in the target orbital coordinate system.

If the position vector of the target satellite is $\vec{r}_1 = [r_1 \ 0 \ 0]^T$, the relative position vector is $\vec{r} = [x \ y \ z]^T$, then the position vector of the cruising spacecraft is:

$$\vec{r}_2 = [r_1 + x \ y \ z]^T \quad (4.5)$$

The tangential velocity of the target satellite V_f is:

$$V_f = r_1 \cdot \dot{\nu} = \sqrt{\frac{\mu}{p}} (1 + e \cos \nu) \quad (4.6)$$

Then μ can be expressed as follows:

$$\mu = \frac{r_1^3 \dot{\nu}^2}{1 + e \cos \nu} \quad (4.7)$$

When we substitute Eq. (4.5) to (4.7) into Eq. (4.4), the results are:

$$\begin{cases} \ddot{x} - 2\dot{v}\dot{y} - \ddot{v}y - \dot{v}^2 \left[x + \frac{r_1}{1+e \cos v} - \frac{r_1^3(r_1+x)}{(1+e \cos v)[(r_1+x)^2+y^2+z^2]^{\frac{3}{2}}} \right] - a_{cx} - a_{px} = 0 \\ \ddot{y} + 2\dot{v}\dot{x} + \ddot{v}x - \dot{v}^2 y \left[1 - \frac{r_1^3}{(1+e \cos v)[(r_1+x)^2+y^2+z^2]^{\frac{3}{2}}} \right] - a_{cy} - a_{py} = 0 \\ \ddot{z} + \dot{v}^2 z \left[\frac{r_1^3}{(1+e \cos v)[(r_1+x)^2+y^2+z^2]^{\frac{3}{2}}} \right] - a_{cz} - a_{pz} = 0 \end{cases} \quad (4.8)$$

Here, $[a_{cx}, a_{cy}, a_{cz}]$ and $[a_{px}, a_{py}, a_{pz}]$ stand for the differences in the controlling force and the differences in the perturbation force of the three axes in the target orbital coordinate system between the cruising spacecraft and the target satellite, respectively. Equation (4.8) is the accurate relative motion dynamics equation in the elliptical reference orbit.

If the target orbit is a circular orbit, then

$$\begin{cases} e = 0 \\ \dot{v} = n \\ \ddot{v} = 0 \end{cases} \quad (4.9)$$

We can substitute Eq. (4.9) into Eq. (4.8), then the accurate relative motion dynamics equations in a circular orbit are:

$$\begin{cases} \ddot{x} - 2n\dot{y} - n^2(x+r_1) \left[1 - \frac{r_1^3}{[(r_1+x)^2+y^2+z^2]^{\frac{3}{2}}} \right] - a_{cx} - a_{px} = 0 \\ \ddot{y} + 2n\dot{x} - n^2y \left[1 - \frac{r_1^3}{[(r_1+x)^2+y^2+z^2]^{\frac{3}{2}}} \right] - a_{cy} - a_{py} = 0 \\ \ddot{z} + n^2z \left[\frac{r_1^3}{[(r_1+x)^2+y^2+z^2]^{\frac{3}{2}}} \right] - a_{cz} - a_{pz} = 0 \end{cases} \quad (4.10)$$

4.2.2 Simplification of Relative Motion Dynamics Equation

When the dynamics method is used to describe the relative motion between spacecraft, an accurate relative motion dynamics equation is usually unnecessary. The dynamics equation can be properly simplified according to practical requirements to better solve the problems.

For the nonlinear term $[(r_1+x)^2+y^2+z^2]^{\frac{3}{2}}$ in Eq. (4.8), we perform second-order Taylor expansion and the result is:

$$\left[(r_1 + x)^2 + y^2 + z^2 \right]^{\frac{3}{2}} = r_1^3 \left[1 + \frac{3}{2} \left(\frac{2x}{r_1} + \frac{x^2}{r_1^2} + \frac{y^2}{r_1^2} + \frac{z^2}{r_1^2} \right) + O(x, y, z) \right] \quad (4.11)$$

When infinitesimals above the second-order are ignored, the nonlinear term is simplified as:

$$\left[(r_1 + x)^2 + y^2 + z^2 \right]^{\frac{3}{2}} \approx r_1^3 \left[1 + \frac{3}{2} \left(\frac{2x}{r_1} + \frac{x^2}{r_1^2} + \frac{y^2}{r_1^2} + \frac{z^2}{r_1^2} \right) \right] \quad (4.12)$$

If we substitute Eq. (4.12) into Eq. (4.8), then the following can be obtained:

$$\begin{cases} \ddot{x} - 2\dot{y} - \ddot{y} - \dot{v}^2 \left[x + \frac{r_1}{1+e \cos v} - \frac{r_1^3(r_1+x)}{(1+e \cos v)r_1^3 N} \right] - a_{cx} - a_{px} = 0 \\ \ddot{y} + 2\dot{x} + \ddot{x} - \dot{v}^2 y \left[1 - \frac{r_1^3}{(1+e \cos v)r_1^3 N} \right] - a_{cy} - a_{py} = 0 \\ \ddot{z} + \dot{v}^2 z \left[\frac{r_1^3}{(1+e \cos v)r_1^3 N} \right] - a_{cz} - a_{pz} = 0 \end{cases} \quad (4.13)$$

Here,

$$\begin{aligned} N &= 1 + \frac{3}{2} \left(\frac{2x}{r_1} + \frac{x^2}{r_1^2} + \frac{y^2}{r_1^2} + \frac{z^2}{r_1^2} \right) \\ \dot{v} &= \frac{n(1+e \cos v)^2}{(1-e^2)^{3/2}} \\ \ddot{v} &= \frac{-2n^2 e(1+e \cos v)^3 \sin v}{(1-e^2)^3} \end{aligned}$$

Equation (4.13) is the second-order approximate relative motion dynamics equation in the elliptical reference orbit.

Similarly, when we substitute Eq. (4.9) into Eq. (4.13), the following can be obtained:

$$\begin{cases} \ddot{x} - 2n\dot{y} - 3n^2 x + 3n^4 x^2 - \frac{3}{2} n^4 (x^2 + y^2) - a_{cx} - a_{px} = 0 \\ \ddot{y} + 2n\dot{x} - a_{cy} - a_{py} = 0 \\ \ddot{z} + n^2 z - 3n^4 xz - a_{cz} - a_{pz} = 0 \end{cases} \quad (4.14)$$

Equation (4.14) is the second-order approximate relative motion dynamics equation in the circular reference orbit.

We can simplify the relative motion dynamics equation by ignoring the terms of second-order and above in Eq. (4.11). Then we can get Eq. (4.15):

$$\left[(r_1 + x)^2 + y^2 + z^2 \right]^{\frac{3}{2}} \approx r_1^3 \left(\frac{r_1 + 3x}{r_1} \right) \quad (4.15)$$

When we substitute Eq. (4.15) into Eq. (4.9), then the following simplified relative motion equation can be obtained:

$$\begin{cases} \ddot{x} - 2\dot{y}\dot{y} - \ddot{y}y - \dot{v}^2 \left[x + \frac{2xr_1}{(1+e\cos v)(r_1+3x)} \right] - a_{cx} - a_{px} = 0 \\ \ddot{y} + 2\dot{x}\dot{x} + \ddot{x}x - \dot{v}^2 y \left[1 - \frac{r_1}{(1+e\cos v)(r_1+3x)} \right] - a_{cy} - a_{py} = 0 \\ \ddot{z} + \dot{v}^2 z \left[\frac{r_1}{(1+e\cos v)(r_1+3x)} \right] - a_{cz} - a_{pz} = 0 \end{cases} \quad (4.16)$$

If the cruising spacecraft and the target satellite are close enough, i.e., $r \ll r_1$, then:

$$r_1 + 3x \approx r_1 \quad (4.17)$$

If we substitute Eq. (4.17) into Eq. (4.16), the following can be obtained:

$$\begin{cases} \ddot{x} - 2\dot{y}\dot{y} - \ddot{y}y - \dot{v}^2 x \frac{(3+e\cos v)}{(1+e\cos v)} - a_{cx} - a_{px} = 0 \\ \ddot{y} + 2\dot{x}\dot{x} + \ddot{x}x - \dot{v}^2 y \frac{e\cos v}{(1+e\cos v)} - a_{cy} - a_{py} = 0 \\ \ddot{z} + \dot{v}^2 z \frac{1}{3+e\cos v} - a_{cz} - a_{pz} = 0 \end{cases} \quad (4.18)$$

Equation (4.18) is the first-order approximate relative motion dynamics equation in the elliptical reference orbit.

Similarly, when we substitute Eq. (4.9) into Eq. (4.18), the following can be obtained:

$$\begin{cases} \ddot{x} - 2n\dot{y} - 3n^2x - a_{cx} - a_{px} = 0 \\ \ddot{y} + 2n\dot{x} - a_{cy} - a_{py} = 0 \\ \ddot{z} + n^2z - a_{cz} - a_{pz} = 0 \end{cases} \quad (4.19)$$

Equation (4.19) is the first-order approximate relative motion dynamics equation in the circular reference orbit.

4.2.3 Precision Analysis of Relative Motion Dynamics Model

In this section, the applicability of the first-order relative motion dynamics model and the second-order relative motion dynamics model in orbit design will be analyzed. Through precision analysis of the model, the cruising spacecraft's relative motion dynamics model that meets the orbit design requirement will be confirmed.

As the relative motion error is mainly reflected by the along-track drift error of the target satellite, selections of the cruising spacecraft's initial relative motion state relative to the target satellite are shown in Table 4.2, with a 4-day simulation time.

Table 4.2 Initial relative state parameters of cruising spacecraft

x_0 (m)	y_0 (m)	z_0 (m)	\dot{x}_0 (m/s)	\dot{y}_0 (m/s)	\dot{z}_0 (m/s)
1	2001	1	$7.2922e-6$	0.0401	1

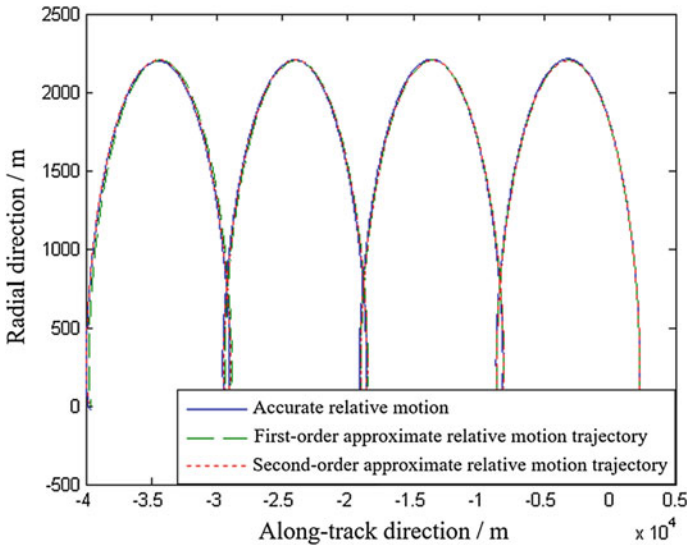


Fig. 4.4 Relative motion trajectories

The motion trajectory of the cruising spacecraft relative to the target satellite within 4 days is as Fig. 4.4 shows. It can be seen that the motion trajectories adopting different relative motion dynamics models have all matched well.

In Fig. 4.5a–d, the first-order and second-order relative motion dynamics models are compared with the accurate dynamics model. It is shown that the relative trajectory errors in radial direction and normal direction are very small (less than 40 m), and the major errors mainly occur on the along-track drift of the target orbit (about 200 m). For the cruising orbit, however, in order to cruise, along-track drift is usually needed. Therefore, by adopting the first-order relative motion dynamics model, requirements for the cruising mission of the cruising spacecraft can be met.

4.2.4 Analysis of Relative Motion Dynamics Model of Cruising Spacecraft

As it meets the orbit design requirements of the cruising spacecraft and has direct analytical solution, the precision of the first-order linear dynamics model has great advantages in the configuration of a relative orbit design.

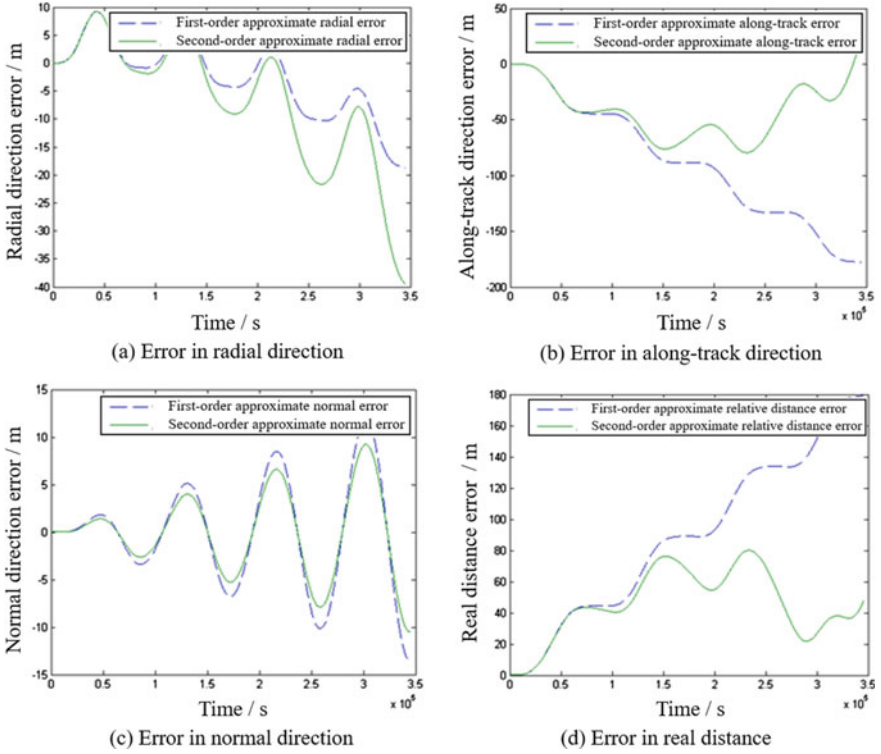


Fig. 4.5 Comparison in precision between different models

$$\begin{cases} \ddot{x} - 2n\dot{y} - 3n^2x - a_{cx} = 0 \\ \ddot{y} + 2n\dot{x} - a_{cy} = 0 \\ \ddot{z} + n^2z - a_{cz} = 0 \end{cases} \quad (4.20)$$

In the condition of non-control, the equations above are turned into the classical C-W Equations, also known as Hill Equation.

$$\begin{cases} \ddot{x} - 2n\dot{y} - 3n^2x = 0 \\ \ddot{y} + 2n\dot{x} = 0 \\ \ddot{z} + n^2z = 0 \end{cases} \quad (4.21)$$

With Laplace transformation, the following can be obtained:

$$\begin{cases} [s^2X(s) - sx_0 - \dot{x}_0] - 2n[sY(s) - y_0] - 3n^2X(s) = 0 \\ [s^2Y(s) - sy_0 - \dot{y}_0] + 2n[sX(s) - x_0] = 0 \\ [s^2Z(s) - sz_0 - \dot{z}_0] + n^2Z(s) = 0 \end{cases} \quad (4.22)$$

Here, $(x_0, y_0, z_0, \dot{x}_0, \dot{y}_0, \dot{z}_0)$ stands for the initial relative motion state of the cruising spacecraft in the orbital coordinate system of the target satellite.

When we transform the equation above to matrix form, the result is:

$$\begin{bmatrix} s^2 - 3n^2 & -2ns & 0 \\ 2ns & s^2 & 0 \\ 0 & 0 & s^2 + n^2 \end{bmatrix} \begin{bmatrix} X(s) \\ Y(s) \\ Z(s) \end{bmatrix} = \begin{bmatrix} sx_0 + \dot{x}_0 - 2ny_0 \\ sy_0 + \dot{y}_0 - 2nx_0 \\ sz_0 + \dot{z}_0 \end{bmatrix} \quad (4.23)$$

Then,

$$\begin{bmatrix} X(s) \\ Y(s) \\ Z(s) \end{bmatrix} = \begin{bmatrix} \frac{(x_0 - \frac{2\dot{y}_0 + 4nx_0}{n})s}{s^2 + n^2} + \frac{(\dot{x}_0)n}{s^2 + n^2} + \frac{2\dot{y}_0 + 4nx_0}{n} \frac{1}{s} \\ \frac{2(\dot{x}_0)s}{s^2 + n^2} + \frac{2(\frac{2\dot{y}_0 + 4nx_0}{n} - x_0)n}{s^2 + n^2} - \frac{3n}{2} \frac{2\dot{y}_0 + 4nx_0}{n} \frac{1}{s^2} + \frac{ny_0 - 2\dot{x}_0}{n} \frac{1}{s} \\ \frac{z_0s}{s^2 + n^2} + \frac{(\dot{z}_0)n}{s^2 + n^2} \end{bmatrix} \quad (4.24)$$

With Laplace inverse transformation, the following can be obtained:

$$\begin{bmatrix} x(t) \\ y(t) \\ z(t) \end{bmatrix} = \begin{bmatrix} [x_0 - \frac{2\dot{y}_0 + 4nx_0}{n}] \cos nt + \frac{\dot{x}_0}{n} \sin nt + \frac{2\dot{y}_0 + 4nx_0}{n} \\ \frac{2\dot{x}_0}{n} \cos nt + 2[\frac{2\dot{y}_0 + 4nx_0}{n} - x_0] \sin nt - \frac{3n}{2} \frac{2\dot{y}_0 + 4nx_0}{n} t + \frac{ny_0 - 2\dot{x}_0}{n} \\ z_0 \cos nt + \frac{\dot{z}_0}{n} \sin nt \end{bmatrix} \quad (4.25)$$

If we take the derivative of Eq. (4.25), then the following can be obtained:

$$\begin{cases} \dot{x}(t) = \dot{x}_0 \cos nt + (2\dot{y}_0 + 3nx_0) \sin nt \\ \dot{y}(t) = -2\dot{x}_0 \sin nt + (4\dot{y}_0 + 6nx_0) \cos nt - (3\dot{y}_0 + 6nx_0) \\ \dot{z}(t) = -nz_0 \sin nt + \dot{z}_0 \cos nt \end{cases} \quad (4.26)$$

It is shown in Eqs. (4.25) and (4.26) that, at time t , the cruising spacecraft's relative position and relative velocity are the functions of its initial relative motion state. When the two equations above are converted to matrix form, the matrix form of the solution of the cruising spacecraft's relative motion equation can be obtained as:

$$\begin{bmatrix} \vec{\rho} \\ \dot{\vec{\rho}} \end{bmatrix} = \begin{bmatrix} \Phi_{11} & \Phi_{12} \\ \Phi_{21} & \Phi_{22} \end{bmatrix} \begin{bmatrix} \vec{\rho}_0 \\ \dot{\vec{\rho}}_0 \end{bmatrix} \quad (4.27)$$

Here,

$$[\vec{\rho}, \dot{\vec{\rho}}] = [x, y, z, \dot{x}, \dot{y}, \dot{z}]$$

$$[\vec{\rho}_0, \dot{\vec{\rho}}_0] = [x_0, y_0, z_0, \dot{x}_0, \dot{y}_0, \dot{z}_0]$$

$$\Phi_{11} = \begin{bmatrix} 4 - 3 \cos nt & 0 & 0 \\ 6(\sin nt - nt) & 1 & 0 \\ 0 & 0 & \cos nt \end{bmatrix}, \quad \Phi_{12} = \begin{bmatrix} \frac{\sin nt}{n} & \frac{2(1 - \cos nt)}{n} & 0 \\ \frac{2(\cos nt - 1)}{n} & \frac{4 \sin nt}{n} - 3t & 0 \\ 0 & 0 & \frac{\sin nt}{n} \end{bmatrix}$$

$$\Phi_{21} = \begin{bmatrix} 3n \sin nt & 0 & 0 \\ 6(\cos nt - 1) & 0 & 0 \\ 0 & 0 & -n \sin nt \end{bmatrix}, \quad \Phi_{22} = \begin{bmatrix} \cos nt & 2 \sin nt & 0 \\ -2 \sin nt & 4 \cos nt - 3 & 0 \\ 0 & 0 & \cos nt \end{bmatrix}$$

It can be seen from the solution of the cruising spacecraft's relative motion dynamics model that its relative motion has the following basic characteristics:

- (1) The cruising spacecraft's motion relative to the target satellite can be decomposed into two independent motions in which one is in the target orbit plane and the other is perpendicular to the plane. The two axes in the orbit plane are in a coupled state.
- (2) The relative motion perpendicular to the orbit plane is a periodic oscillatory motion, whose oscillation amplitude is:

$$Z_{\max} = \sqrt{z_0^2 + (\dot{z}_0/n)^2} \quad (4.28)$$

- (3) In the orbit plane, the phases of x and \dot{x} always lag 90° (a quarter of the orbital period) behind the phases of y and \dot{y} , with the y-axis amplitude twice the x-axis amplitude. Additionally, there is a term on the y-axis that increases linearly with time.

We can set

$$\begin{cases} x_{c0} = \frac{2\dot{y}_0 + 4nx_0}{n} \\ y_{c0} = \frac{ny_0 - 2\dot{x}_0}{n} \\ x = x(t) \\ y = y(t) \end{cases} \quad (4.29)$$

And when we substitute Eq. (4.29) into the first two equations in Eq. (4.25), the following can be obtained:

$$\begin{cases} x - x_{c0} = (x_0 - x_{c0}) \cos nt + \frac{\dot{x}_0}{n} \sin nt \\ \frac{y + \frac{3nx_0}{2}t - y_{c0}}{2} = \frac{\dot{y}_0}{n} \cos nt + (x_{c0} - x_0) \sin nt \end{cases} \quad (4.30)$$

After mathematical transformation, the following can be obtained:

$$[x - x_{c0}]^2 + \frac{[y + \frac{3nx_0}{2}t - y_{c0}]^2}{4} = (x_0 - x_{c0})^2 + \left(\frac{\dot{x}_0}{n}\right)^2 \quad (4.31)$$

When the initial relative motion state of the cruising spacecraft is given, the right side of Eq. (4.31) is a fixed value. We can set

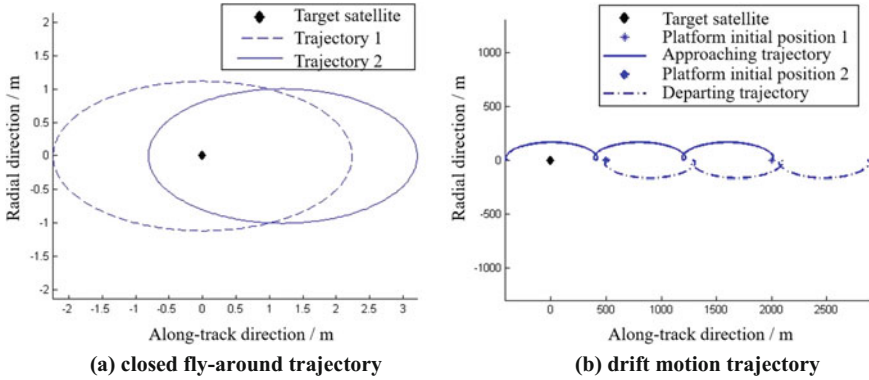


Fig. 4.6 Characteristics of relative motion trajectory

$$b = \sqrt{(x_0 - x_{c0})^2 + \left(\frac{\dot{x}_0}{n}\right)^2} \tag{4.32}$$

then Eq. (4.33) can be obtained:

$$\frac{[x - x_{c0}]^2}{b^2} + \frac{[y + \frac{3nx_0}{2}t - y_{c0}]^2}{4b^2} = 1 \tag{4.33}$$

It is known from Eq. (4.33) that, when $x_{c0} = 0$, the cruising spacecraft flies around the target satellite in a closed ellipse. In this ellipse, the center coordinates are (x_{c0}, y_{c0}) , the semi-major axis is $2b$, the ratio of the semi-major axis to the semi-minor axis is 2:1, the eccentricity $e = \sqrt{3}/2 \approx 0.866$, as Fig. 4.6a shows; when $x_{c0} \neq 0$, the cruising spacecraft's relative motion trajectory in the target satellite's orbit plane is a non-closed spiral motion trajectory, with the value of x_{c0} determining the drift speed of the cruising spacecraft's trajectory center and its plus or minus state determining the along-track drift direction of the cruising spacecraft, as Fig. 4.6b shows.

4.3 Traversal Cruising Orbit: Design

A traversal cruising orbit enables a single spacecraft to accomplish traversal cruising detection of multiple spacecraft that are in the same orbit or in different orbits, which is a typical relative motion. Compared with traditional relative motions such as satellite formation, however, the traversal cruising orbit is designed with reference to a space orbit, rather than a spacecraft. Therefore, it is necessary to find a new or improved orbit design method.

4.3.1 Design Method Based on Hill Equation

According to Hill equation, the relative motion trajectory of the cruising spacecraft in the target plane can be described as:

$$\frac{(x - x_{c0})^2}{b^2} + \frac{(y - y_{c0} + 1.5x_{c0}nt)^2}{(2b)^2} = 1 \quad (4.34)$$

When $x_{c0} \neq 0$, the relative motion trajectory in the plane is an ellipse whose center drifts in the along-track direction of the target orbit. The center's drift velocity is proportional to x_{c0} , and the drift distance in each period is:

$$L = |3\pi x_{c0}| \quad (4.35)$$

The cruising velocity is:

$$V = 1.5x_{c0}n \quad (4.36)$$

The cruising direction is determined by the sign of x_{c0} , that is

$$\begin{cases} x_{c0} < 0 & \text{Positive direction cruising} \\ x_{c0} > 0 & \text{Reverse direction cruising} \end{cases} \quad (4.37)$$

The cruising radius R can be determined by b and x_{c0} as

$$R = b + |x_{c0}| = \sqrt{\left(\frac{2\dot{y}_0}{n} + 3x_0\right)^2 + \left(\frac{\dot{x}_0}{n}\right)^2} + \left|4x_0 + 2\frac{\dot{y}_0}{n}\right| \quad (4.38)$$

The time required for the cruising orbit to complete a traversal cruising to the target orbit is directly related to cruising velocity. The higher the cruising velocity is, the shorter the traversal period will be. The traversal period can be approximately estimated by the following formula.

$$T \approx 2\pi a_T / V \quad (4.39)$$

Here, a_T stands for the semi-major axis of the target orbit.

The relation between the cruising velocity V and the traversal search period T is shown in Fig. 4.7.

It can be seen that when the cruising velocity is fixed, the longer the semi-major axis of the target orbit is, the longer the traversal period will be; when the length of the semi-major axis of the target orbit is fixed, the higher the cruising velocity is, the shorter the traversal period will be. With regard to the same target orbit, there is an approximate inverse relation between the traversal period T and the cruising velocity V .

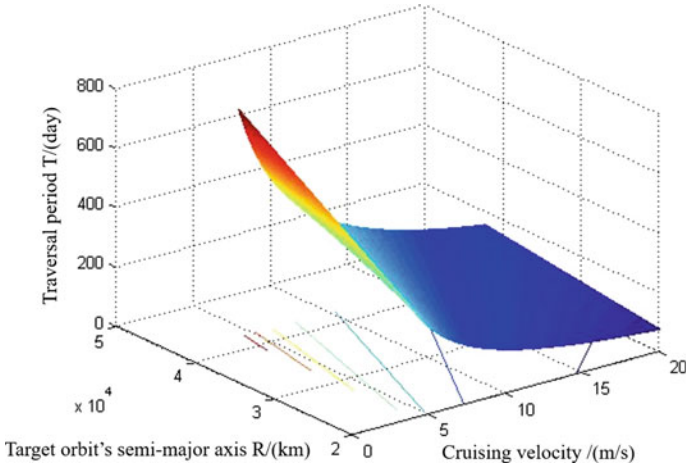


Fig. 4.7 Relation between $a_T - V - T$

As the trajectory center of the traversal cruising orbit is constantly drifting with the change of time, a certain target satellite is usually taken as the reference point in orbit design. We can suppose that at the initial moment, the relative motion state of the cruising spacecraft meets the following condition:

$$y_{c0} = y_0 - \frac{2}{n}\dot{x}_0 = 0 \tag{4.40}$$

The initial position coordinate of the cruising spacecraft in the radial direction is:

$$x_0 = R' \cos \theta \tag{4.41}$$

Here: R' stands for the projection of the traversal cruising orbit's cruising radius R in the target orbit plane; θ stands for the phase angle based on the x axis, with counter-clockwise direction as the positive direction.

Additionally, in the target orbital coordinate system, the initial relative motion state of the cruising spacecraft in the normal direction satisfies:

$$\begin{cases} z_0 = x_0 t g \varphi \\ \dot{z}_0 = \dot{x}_0 t g \varphi \end{cases} \tag{4.42}$$

Here, φ is the angle between the projection of the cruising spacecraft in the $x - z$ plane of the target orbital coordinate system and the x axis.

If the reference orbit element is known, when the cruising velocity of the cruising spacecraft V , the cruising radius R , the phase angle θ and the normal angle φ of the cruising spacecraft in the target orbit plane are given, we can combine the equations from Eq. (4.36) to (4.42), and the initial relative motion state of the

cruising spacecraft in the target orbital coordinate system can be obtained. Then according to the coordinate transformation relation, the position vector and velocity vector of the cruising spacecraft in the Earth centered inertial coordinate system can be obtained.

4.3.2 Design Method Based on E/I Vector Method

When the target orbit is a near-circular orbit, the motion of the cruising spacecraft in the target relative motion coordinate system can be described by the following configuration geometrical parameters.

$$\begin{cases} x = \Delta a - p \cos(u - \varphi) \\ y = l - 1.5\Delta a n t + 2p \sin(u - \varphi) \\ z = s \sin(u - \theta) \\ \dot{x} = np \sin(u - \varphi) \\ \dot{y} = -1.5\Delta a n + 2np \cos(u - \varphi) \\ \dot{z} = ns \cos(u - \theta) \end{cases} \quad (4.43)$$

Here, $(x, y, z, \dot{x}, \dot{y}, \dot{z})$ are the position and velocity components of the cruising spacecraft in the relative motion coordinate system; n is the average motion angular velocity of the target orbit; Δa , l , p , φ , s , and θ are configuration geometrical parameters. By adopting geometrical parameters, the relative motion can be directly described. The details are below:

- Δa is the relative semi-major axis;
- p is the in-plane configuration size (the semi-minor axis of the in-plane configuration ellipse);
- φ is the in-plane configuration phase;
- l is the drift distance of the configuration center along the trajectory;
- s is the out-of-plane configuration size (the configuration lateral amplitude);
- θ is the out-of-plane configuration phase.

The configuration geometrical parameters can be calculated and obtained through the relative orbit elements of the cruising spacecraft and the target satellite.

$$\begin{cases} \Delta a = a_2 - a_1 \\ p = a_1 |\Delta \mathbf{e}| \\ \varphi = \arctan(\Delta e_y, \Delta e_x) \\ l = a_1 (\Delta u + \Delta \Omega \cos i_1) \\ s = a_1 |\Delta \mathbf{i}| \\ \theta = \arctan(\Delta i_y, \Delta i_x) \end{cases} \quad (4.44)$$

Here, a_1 , a_2 , u_1 , u_2 and Ω_1 , Ω_2 stand for the orbit's semi-major axis, the argument of the ascending node and the right ascension of the ascending node

(*RAAN*) of the cruising spacecraft and the target satellite, respectively; other vectors are as follows:

$$\Delta \bar{e} = \bar{e}_2 - \bar{e}_1 = \begin{bmatrix} \Delta e_x \\ \Delta e_y \end{bmatrix} \quad \bar{e}_1 = \begin{bmatrix} e_1 \cos(\omega_1) \\ e_1 \sin(\omega_1) \end{bmatrix} \quad \bar{e}_2 = \begin{bmatrix} e_2 \cos(\omega_2) \\ e_2 \sin(\omega_2) \end{bmatrix} \quad (4.45)$$

$$\Delta \bar{i} = \bar{i}_2 - \bar{i}_1 = \begin{bmatrix} \Delta i_x \\ \Delta i_y \end{bmatrix} \quad \bar{i}_1 = \begin{bmatrix} i_1 \\ \Omega_1 \sin(i_1) \end{bmatrix} \quad \bar{i}_2 = \begin{bmatrix} i_2 \\ \Omega_2 \sin(i_2) \end{bmatrix} \quad (4.46)$$

(1) When $i_1 = 0$, and $\Omega_1 = \Omega_2$, then

$$\bar{i}_1 = \begin{bmatrix} 0 \\ 0 \end{bmatrix} \quad \bar{i}_2 = \begin{bmatrix} i_2 \\ 0 \end{bmatrix} \quad \Delta \bar{i} = \bar{i}_2 - \bar{i}_1 = \begin{bmatrix} i_2 \\ 0 \end{bmatrix} = \frac{s}{a} \begin{bmatrix} \cos \theta \\ \sin \theta \end{bmatrix} \quad (4.47)$$

And we also obtain: $s = a|i_2|$, $\theta = 0^\circ$ or $\theta = 180^\circ$.

(2) When $i_1 = 0$ and $i_2 = 0$, Ω_2 is an arbitrary value (here we set $\Omega_1 = \Omega_2$), then:

$$l = a_1((u_2 - u_1) + (\Omega_2 - \Omega_1) \cos i_1) = a_1 \Delta u \quad (4.48)$$

4.3.3 Design Constraint

In the process of space target surveillance, the surveillance result is susceptible to the relative distance, relative velocity and imaging angle between the surveillance camera and the target. As it is hard to ensure a proper surveillance angle for every target during traversal cruising, in designing a spiral traversal cruising orbit, only the design constraint of the cruising radius and the cruising velocity should be focused on.

(1) Constraint on cruising radius

As for the constraint on the cruising radius, the operating range of the surveillance payload on the cruising spacecraft is a main consideration; another consideration is the responsive ability requirement of the cruising spacecraft.

The selection range of the cruising spacecraft's cruising radius is related to the performance of the CCD visible light camera on it; the effective surveillance range of the camera cannot exceed the maximum operating range of the payload itself. Therefore the working radius of the visible light camera can be described as:

$$R_1 = \frac{R_d D}{2.44 \lambda Q} \quad (4.49)$$

Here, D is the size of the optical aperture of the visible light camera; λ is the working wavelength of the camera (the wavelength range of the visible light wave band is $0.4\text{--}0.7 \mu\text{m}$); Q is the imaging quality factor; R_d is the minimum spatial resolution needed for achieving space target surveillance.

If the optical aperture of the CCD camera carried by the cruising spacecraft is $D = 0.3 \text{ m}$, working wavelength $\lambda = 0.5 \mu\text{m}$, imaging quality factor $Q = 1.1$, $R_d = 0.5 \text{ m}$ then the maximum working distance is about 111.8 km .

If the cruising spacecraft is required to switch from the traversal cruising mode to other modes within a limited time, its responsive ability needs to meet certain requirements. For instance, when the cruising spacecraft travels in the vicinity of a specific target, in order to obtain detailed feature information of the target, it needs to quickly switch from the cruising mode to the small elliptical fly-around mode, the fast circular fly-around mode, or other modes, so as to conduct omnidirectional surveillance of the target. When the mission is accomplished, the cruising spacecraft needs to return to the cruising orbit to continue the collection of information on other targets.

When the cruising spacecraft rapidly approaches the vicinity of the target satellite from a place where the distance to the target spacecraft is L , it is necessary to apply impulses at the initial time and the arrival time, respectively. The total velocity increment to be consumed can be approximately described as (Fig. 4.8):

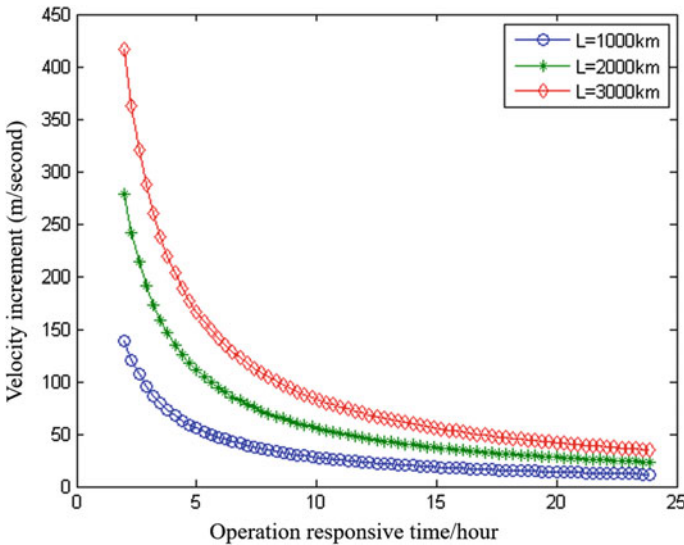


Fig. 4.8 Relations between responsive time and velocity increment required at different distances

$$\Delta V = 2 \frac{L}{\Delta t} \quad (4.50)$$

When we take into full consideration the limitation of available fuel of the cruising spacecraft every time it switches its cruising mode and the requirement for responsive ability, the cruising radius R_2 should meet the following condition:

$$R \leq 0.01H \quad (4.51)$$

Here, H is the orbit altitude of the target orbit.

As is known from Eq. (4.51), if the reference orbit is a geostationary earth orbit (GEO), then the cruising radius should be less than 360 km; if the orbit altitude of the reference orbit is 20,000 km, then the cruising radius should be no more than 200 km.

In summary, if the effective working range of the cruising spacecraft's surveillance payload is R_1 , the constraint of the responsive ability on the cruising radius is R_2 , then the cruising radius of the cruising orbit is:

$$R = \min(R_1, R_2) \quad (4.52)$$

(2) Constraint on cruising velocity

Two aspects need to be considered in designing cruising velocity: one is the requirement of the cruising spacecraft's surveillance payload on cruising velocity; the other is when the cruising radius is given, the constraint of the cruising orbit configuration on cruising velocity.

As the cruising spacecraft is a kind of small-sized spacecraft, the performance configuration of the surveillance payload it can carry is limited. We can suppose that the surveillance payload is a CCD visible light camera. Generally, in order to ensure clear imaging, the linear CCD photo sensor in the focal plane of the camera must meet a certain exposure requirement. The exposure of the linear CCD photo sensor E (in $W \cdot s$) can be expressed as:

$$E = P_D t_i \quad (4.53)$$

Here: P_D is the radiation flux of light received by the camera in W ; t_i is the integration time in s , which is related to the specific performance of the CCD camera. To ensure that there is no omission in camera imaging, the following should be satisfied:

$$t_i \leq r_g / v_g \quad (4.54)$$

Here: r_g is the relative distance between the two spacecraft, and v_g is the relative velocity between them.

The cruising radius and the cruising velocity are both the functions of the relative position velocity; and there exists a coupling relation between the two. When the cruising radius R is given, if a spiral cruising orbit configuration is to be maintained, the cruising velocity V cannot be infinitely large. The relation between the cruising velocity and the cruising radius is:

$$R = b + \left| \frac{2}{3n} V \right| \quad (4.55)$$

Here, refer to Eq. (4.34) for the definition of b .

It can be seen that when the cruising radius R is fixed, as b decreases, the value of $\left| \frac{2}{3n} V \right|$ increases and thus the cruising velocity V also increases. In limiting cases, when $b = 0$, the cruising velocity reaches its maximum value. At this moment, the spiral cruising orbit degrades into a linear cruising orbit. Hence, the cruising velocity of a spiral traversal cruising orbit must meet the following constraint:

$$|V| \leq \frac{3}{2} nR \quad (4.56)$$

Based on Eq. (4.56), the value range of the cruising velocity V , changing with the cruising radius R , can be obtained. An example is presented below. When the target orbit is a GEO, the relation between the cruising velocity and the cruising radius is analyzed. It is shown in Fig. 4.9.

As demonstrated in Fig. 4.9, the higher the cruising velocity is, the larger the corresponding cruising radius will be. This means enhancing the responsive ability of the cruising spacecraft can be achieved at the cost of some surveillance effect. Therefore, in designing a spiral cruising orbit, indexes of the two sides must be balanced so as to achieve an optimal overall effect.

4.3.4 Simulation Analysis

We can suppose that the target orbit is a GEO, and the six elements of the reference target spacecraft are: $a = 42164$ km, $e = 0$, $i = 0^\circ$, $\Omega = 0^\circ$, $w = 0^\circ$, and $M = 0^\circ$. We can set the cruising radius $R = 100$ km, the cruising velocity $V = 4$ m/s; we can also set the initial phase angle of the cruising spacecraft in the target orbit plane $\theta = -90^\circ$, and the initial angle in the normal direction $\varphi = 0^\circ$. It can be calculated that the position vector and the velocity vector of the cruising spacecraft in the Earth centered inertial coordinate system are:

$$\vec{r} = \begin{bmatrix} 42164.1 \\ 103.269 \\ 0 \end{bmatrix} \text{ km} \quad \vec{v} = \begin{bmatrix} -0.00375497 \\ 3.07319 \\ 0 \end{bmatrix} \text{ km/s}$$

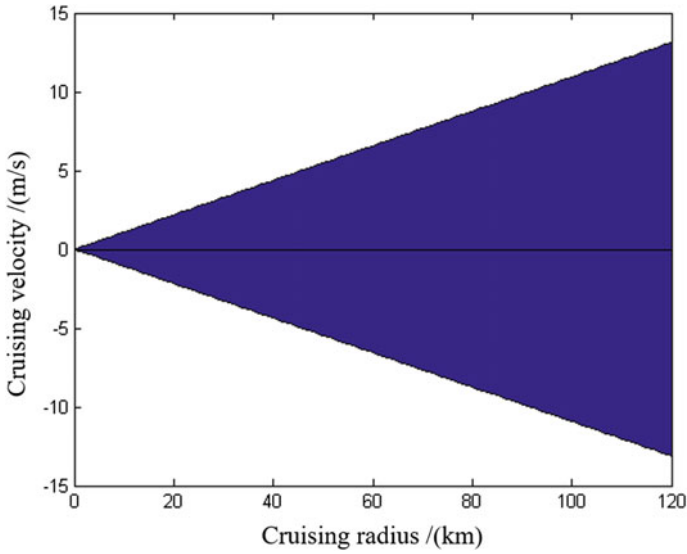


Fig. 4.9 Value range of cruising velocity changing with cruising radius

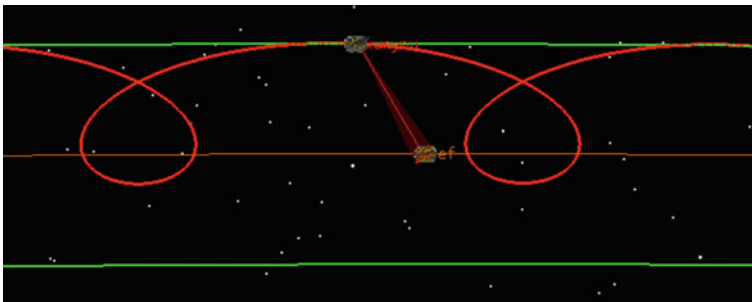


Fig. 4.10 Spiral traversal cruising orbit

The STK software is used to simulate the spiral traversal cruising orbit of the spacecraft. It is shown in Fig. 4.10.

In Fig. 4.10, the orbit in the middle is the GEO, i.e., the target orbit; parallel to the GEO, the two orbits on the top and at the bottom are orbits that are 100 km higher and 100 km lower than the GEO, respectively; the spiral-shaped orbit in the middle is the traversal cruising orbit.

Figure 4.11 shows the changes of the relative distance between the cruising spacecraft and the target orbit in 60 days. As is known from the figure, the cruising radius is within the 100 km distance range required in the design. In this case, the cruising spacecraft can stay in the vicinity of the target orbit for a long time, and can conduct close reconnaissance on and surveillance of all the spacecraft in the target orbit.

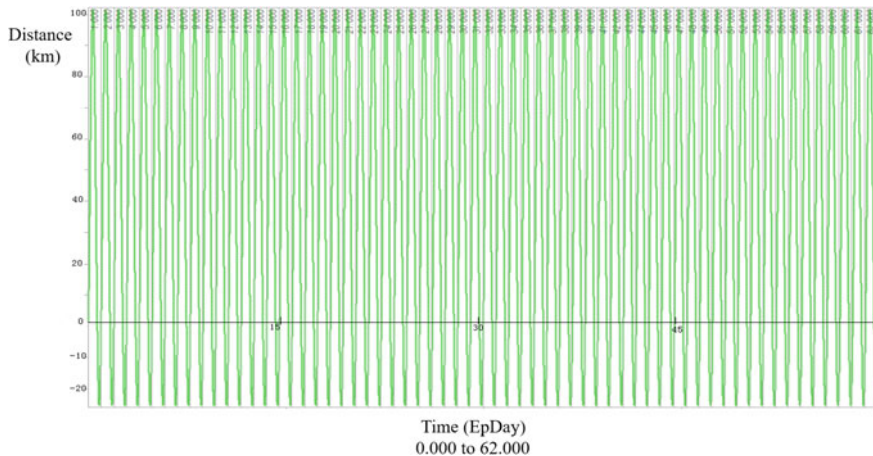


Fig. 4.11 Relative distance between cruising spacecraft and target orbit (in 60 days)

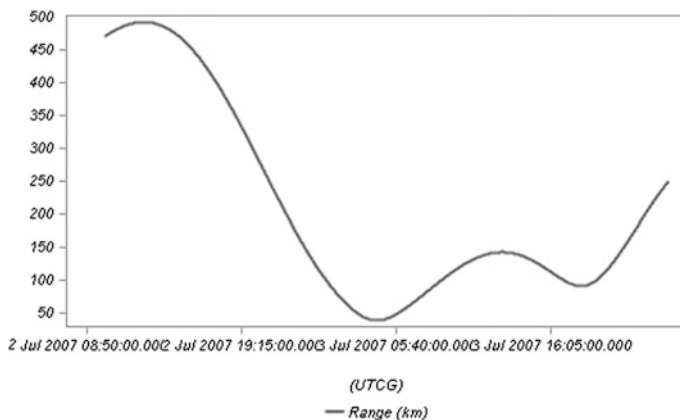


Fig. 4.12 Distance between cruising spacecraft and target spacecraft

We can take a target satellite in the GEO as an example. The abilities of the spiral cruising orbit is explored in three aspects—the change of distance relative to the target, the observation session, and the observation angle. The simulation result is shown in Fig. 4.12.

Figure 4.12 shows the variation curve of the relative distance between the cruising spacecraft and the target spacecraft. It can be seen that the general variation tendency of their relative distance is that the cruising spacecraft slowly approaches the target at first and then gradually moves away from it, without staying in the vicinity of the target for a long time. Therefore it enjoys a high quality of concealment.

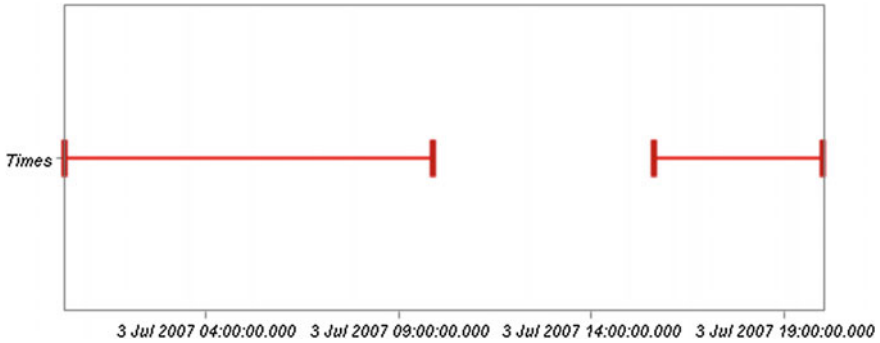


Fig. 4.13 Time period of cruising spacecraft’s surveillance of target spacecraft

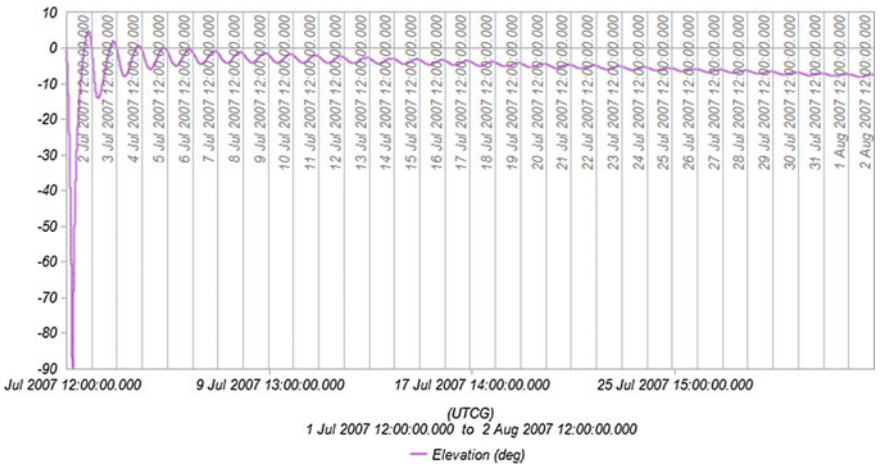


Fig. 4.14 Observation angle of cruising spacecraft relative to target spacecraft

Figure 4.13 shows the time distribution of the cruising spacecraft’s surveillance of the target spacecraft. As is known from the figure, there are two surveillance periods: the first one is [3 Jul 2007 00:20:18.255–3 Jul 2007 09:52:55.208], lasting 9.54 h; the second one is [3 Jul 2007 15:38:12.678–3 Jul 2007 20:00:09.206], lasting 4.36 h. The total effective surveillance time of the cruising spacecraft of the target is about 13.9 h, suggesting that the cruising spacecraft can conduct long-time surveillance of a specific target.

Figure 4.14 shows the variation curve of the observation angle of the cruising spacecraft relative to the target spacecraft. As is known from the figure, the observation angle of the cruising spacecraft relative to the target spacecraft varies within a range of -90° – 5° , indicating that the observation angle of the cruising spacecraft is large and that the target is comprehensively observed.

The time needed for a cruising spacecraft to complete a traversal observation of all the spacecraft in the GEO is:

$$T = 2\pi a_T / V \approx 768 \text{ days}$$

Close-range traversal research on all the spacecraft in the target orbit can be achieved by spiral traversal cruising; and a favorable effect can be achieved on the surveillance of multiple targets. Theoretically speaking, if the cruising mode does not change and effects of factors such as perturbation on the cruising orbit configuration can be neglected, in the process of traversal cruising, the cruising spacecraft does not need to consume fuel, and its operation life is quite long. In spiral traversal cruising, in addition, the traversal period for a high-orbit target is relatively long. Therefore, it is more suitable for long-term on-orbit space target surveillance.

4.4 Design of the Round-Trip Itinerant Orbit

A round-trip itinerant orbit is a spiral-shaped relative orbit along which a spacecraft conducts multi-frequency round-trip surveillance of the target group within a specific arc section of the target orbit. By exerting orbit control on the cruising spacecraft from the boundary of the target group, the direction of the spiral cruise is changed, generally presenting a closed spiral round-trip fly-around configuration as Fig. 4.15 shows.

Similar to the spiral traversal cruising orbit, in designing a spiral round-trip cruising orbit, such requirements as cruising range, observation ability and on-orbit working life also need to be taken into consideration.

4.4.1 Design Method

In designing a spiral round-trip cruising orbit, firstly, the target set is precisely described and the cruising range is defined; next, for the spiral round-trip cruising orbit configuration itself, the cruising velocity and the cruising radius are designed.

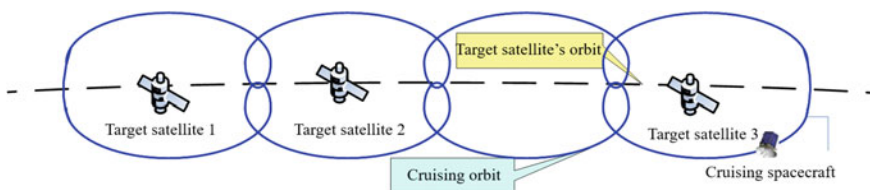


Fig. 4.15 Spiral round-trip cruising orbit

With regard to target groups in the same orbit, a certain satellite can be taken as the reference. With relative state parameters, the target set can be described as:

$$\{\sigma_j, \Delta L_1, \Delta L_2, \dots, \Delta L_n\}$$

Here, σ_j is the orbit element of the reference target j ; ΔL_n is the relative motion state parameter of target n in the orbital coordinate system of target j .

If the target orbit is a GEO, and compared to the radius of the GEO, the distance between two adjacent targets is an infinitesimal amount, then the following approximation can be obtained:

$$y_{c0i} = y_{c0j} + (L_i - L_j)R \quad (4.57)$$

Here, y_{c0i} and y_{c0j} stand for the positions of targets i and j in the reference coordinate system, respectively; L_i and L_j stand for the geographic longitudes of target satellites i and j , respectively; R is the semi-major axis of the target orbit.

The starting point y_s and the terminal point y_e of the spiral round-trip cruising orbit can be approximately determined by the relative position of the target satellites at the two ends of the target set. We suppose that the distance between the target satellites at both ends is ΔL_{\max} , then the round-trip distance ΔL can be approximately obtained:

$$\Delta L = 2|y_e - y_s| = 2\Delta L_{\max} \quad (4.58)$$

According to the relative motion dynamics model, the drift distance d for a cruising spacecraft in one orbital period is:

$$d = 3\pi x_{c0} \quad (4.59)$$

Then the time needed to complete one period of a spiral round-trip cruising can be approximated to the number of orbital period as:

$$T_{\text{go}} = \frac{\Delta L}{d} \quad (4.60)$$

Based on the requirements of the spiral round-trip cruising model, the cruising direction of a cruising spacecraft can be divided into two types: positive and reverse. We suppose that the cruising distances in both directions are the same in each period, and that orbit switch is only conducted on the boundary of the target group without exerting any other control during the cruising process. It is known from the relative motion characteristics of the cruising spacecraft that, its cruising direction is related to the sign of x_{c0} : when $x_{c0} < 0$, it is cruising in the positive direction; when $x_{c0} > 0$, it is cruising in the reverse direction. Therefore, the cruising spacecraft switches its cruising direction mainly via orbit control and changing the value of x_{c0} as Fig. 4.16 shows.

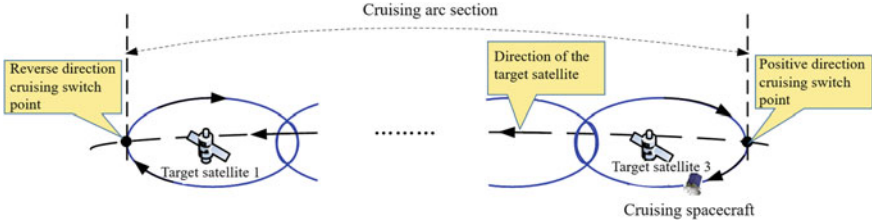


Fig. 4.16 Direction switch of spiral round-trip cruising

After the transformation, x_{c0} can be described as:

$$x_{c0} = \frac{2\dot{y}_0 + 4nx_0}{n} \tag{4.61}$$

We suppose that the cruising spacecraft switches every time at the point where $x_0 = 0$ (according to the relative motion characteristics of the cruising spacecraft, that point always exists), then the following can be obtained:

$$\dot{y}_0 = \frac{1}{2}nx_{c0} \tag{4.62}$$

If, during every switch, only the cruising direction of the cruising spacecraft is changed while its cruising distance in every period remains the same, then it is known from the relative motion dynamics model of the cruising spacecraft that it only needs to apply along-track impulse control to the cruising spacecraft to change the sign of \dot{y}_0 without changing its value. Thus the following can be obtained:

$$\left\{ \begin{array}{l} \text{Positive direction cruising switch : } \Delta V_1 = nx_{c0} \\ \text{Reverse direction cruising switch : } \Delta V_2 = -nx_{c0} \end{array} \right\} \tag{4.63}$$

In one spiral round-trip cruising period, switches in both directions need to be conducted. Therefore, the total velocity increment required in each cruising period is:

$$\Delta V_{total} = 2\Delta V = \frac{2nd}{3\pi} \tag{4.64}$$

It can be seen that the larger the drift distance d is, the greater the velocity increment is required to complete a round-trip cruising period. Figure 4.17 shows the relation between the drift distance of the cruising spacecraft's relative motion trajectory in each period and the velocity increment.

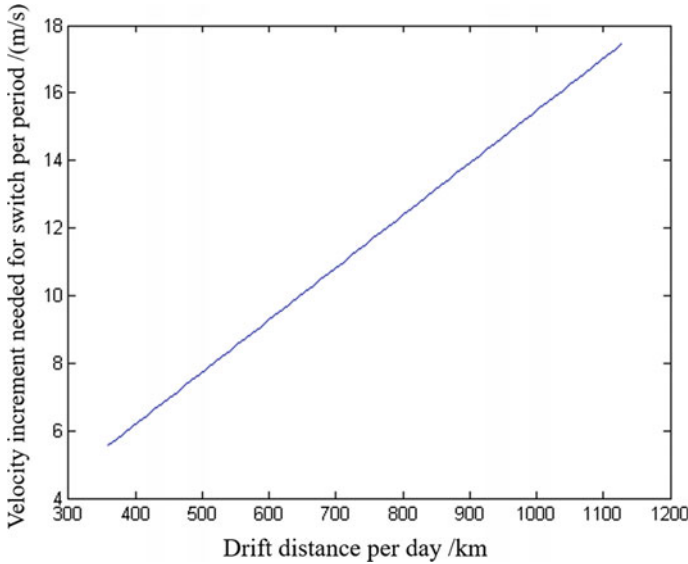


Fig. 4.17 Relation between drift distance and velocity increment per period

4.4.2 Design Constraints

A spiral round-trip cruising orbit is, on the basis of a spiral traversal cruising orbit, a closed relative motion trajectory formed by constantly exerting control on the boundary of the target group and changing the direction of the spiral cruise. As a result, the general constraints on designing a spiral traversal cruising orbit also need to be taken into consideration in designing a spiral round-trip cruising orbit.

Different from the spiral traversal cruising orbit, in designing a spiral round-trip cruising orbit, the constraint of the responsive ability on the orbit design is twofold: one is the constraint of responsive time when the cruising spacecraft switches its cruising mode, i.e., the design constraint of the cruising radius should be considered; the other is, in a round-trip cruise, the time interval between two adjacent reconnaissance by the cruising spacecraft on the same target in a round-trip cruise, or the requirement for the frequency of the cruising spacecraft's surveillance of the same target in a period of time, i.e., the design constraint on the size of the cruising range of the cruising spacecraft should be considered.

4.4.3 Simulation Analysis

In this section, three target satellites (Sat1, Sat2, Sat3) are taken as an example to design a spiral round-trip cruising orbit. A target orbital coordinate system is created with Sat1 as the origin. The target group is described as:

$$\{0, 1.4e + 003 \text{ km}, 2.3e + 003 \text{ km}\}$$

It can be approximately determined that:

$$y_s = 0 \quad y_e = 2.3e + 003 \text{ km}$$

If the maximum cruising radius of the cruising spacecraft is 120 km, then it is known from Eq. (4.60) that the maximum drift distance of the cruising spacecraft per day is $d_{\max} = 753.98 \text{ km}$. If we set $d = 700 \text{ km}$, the round-trip period T is:

$$T > 2\text{INT}\left(\frac{|y_e|}{d}\right) \Rightarrow T > 2\text{INT}(3.3519)$$

If we set eight days as the round-trip period T , then:

$$T = 8 \text{ day}, \quad d = 586.5750 \text{ km}, \quad x_{c0} = 62.2375 \text{ km}$$

It is known from Fig. 4.18 that the relative motion trajectory of the cruising spacecraft is a closed curve consisting of eight drifting ellipses, and that the cruising spacecraft takes round-trip cruises among the three target satellites, with a round-trip period of eight days.

Figures 4.19, 4.20 and 4.21 are the change curves of the relative distances between the cruising spacecraft and the three target satellites in one cruising period, respectively. It can be seen that, the distance between the cruising spacecraft and the target satellite changes periodically with time. In the figures, the value at the dotted line is 120 km, meaning the farthest point at which a cruising spacecraft can perform detailed observation of the target. It is known from the simulation result that in a spiral round-trip cruise, there always exists a certain period of time when the cruising spacecraft can perform short-range surveillance of the three satellites.

Figure 4.22 shows the change curve of the relative distance between the cruising spacecraft and the target orbit.

It is known from Fig. 4.22 that the relative distance between the cruising spacecraft and the target orbit is always within 120 km, suggesting that in the process of a spiral round-trip, the cruising spacecraft can also perform short-range surveillance of other spacecraft in the same arc section.

The drift distance of the cruising spacecraft per day is 586.6 km. It is known from Eq. (4.28) that in each period the velocity increment needed for the cruising spacecraft to switch is 9.1 m/s.

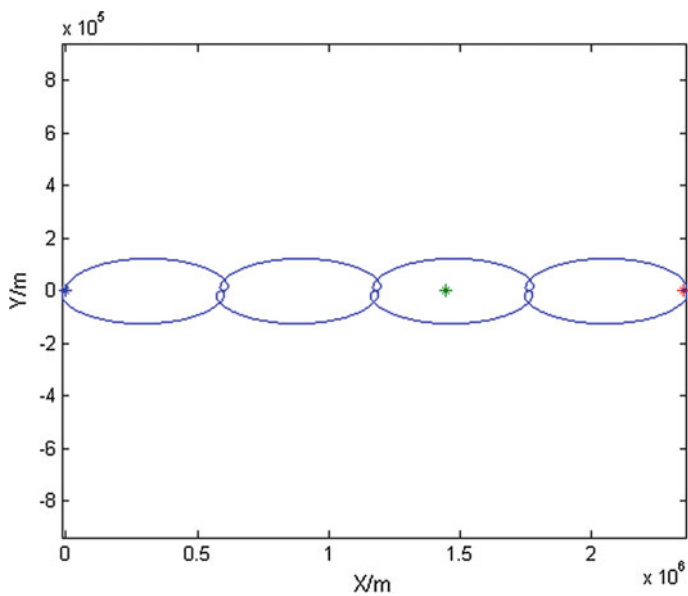


Fig. 4.18 Spiral round-trip cruising trajectory of cruising spacecraft

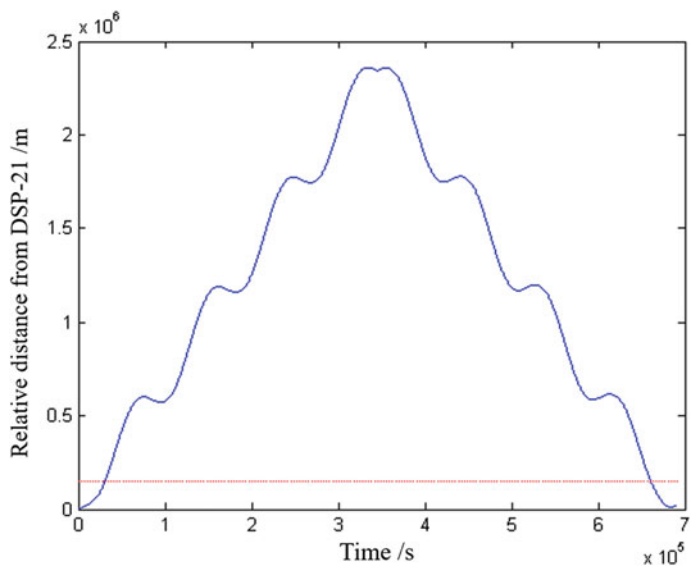


Fig. 4.19 Change curve of relative distance between cruising spacecraft and Sat1

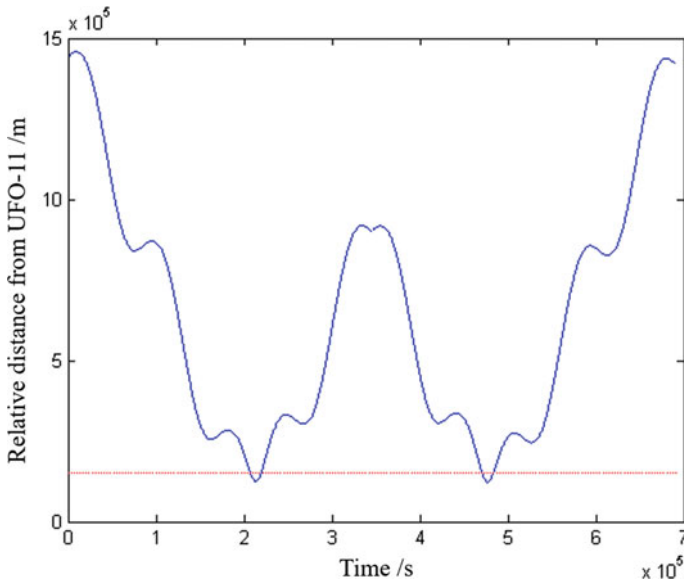


Fig. 4.20 Change curve of relative distance between cruising spacecraft and Sat2

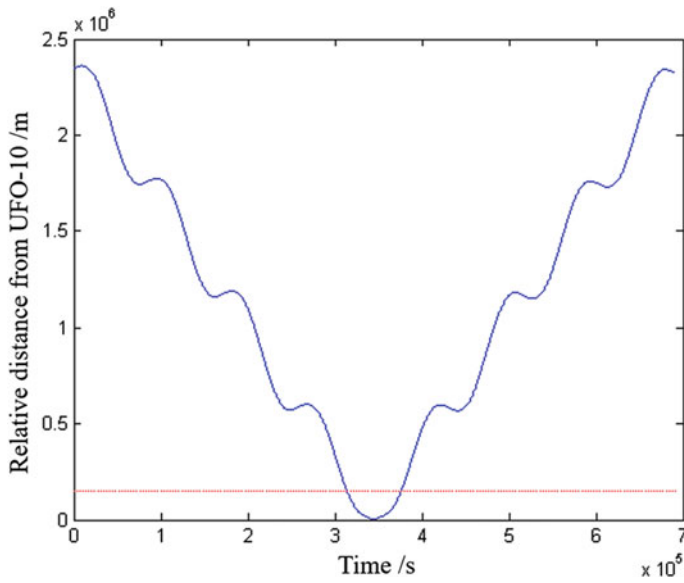


Fig. 4.21 Change curve of relative distance between cruising spacecraft and Sat3

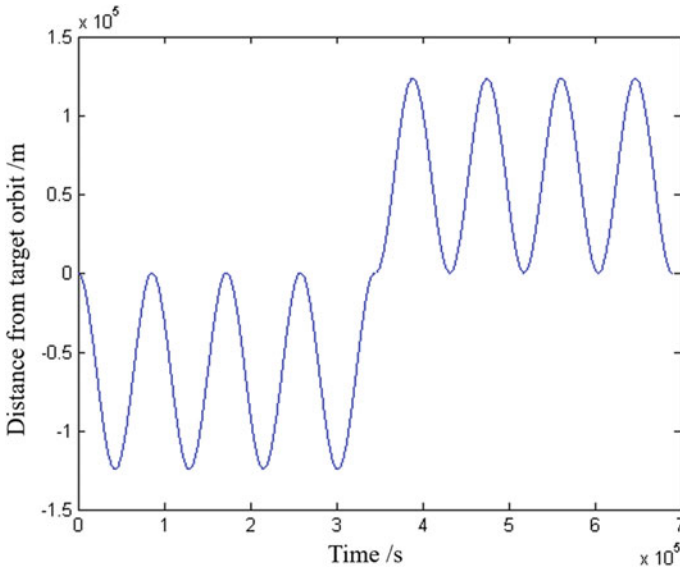


Fig. 4.22 Change curve of relative distance between cruising spacecraft and target orbit

The spiral round-trip cruising method can achieve multi-frequency and short-range round-trip inspection of the target group in the target orbit region. When the round-trip region is relatively small, its round-trip period is relatively short, and the responsive ability is very good. However, orbit control is only applied to the boundary of the target and no control adjustment is conducted during the process. Therefore, with regard to a group of evenly distributed targets, a favorable surveillance effect of every satellite by the cruising spacecraft can be achieved by the reasonable design of the cruising orbit; as for a group of unevenly distributed targets, the cruising spacecraft can only guarantee the intensive surveillance of a few targets in the region, while having difficulty in ensuring the surveillance effect of other targets.

4.5 Controllable Cruising Orbit: Design

Due to influences from factors such as the unevenness in the distribution of space targets and orbit perturbation, it is difficult to obtain the ideal space target surveillance effect by a single orbit configuration. For this purpose, this section will propose a controlled cruising method.

The controllable orbit design combines relative orbit with absolute orbit and applies the method of multiple orbit planning. The goal of the design is, in the process of a spiral motion (one positive direction or reverse direction cruise), the

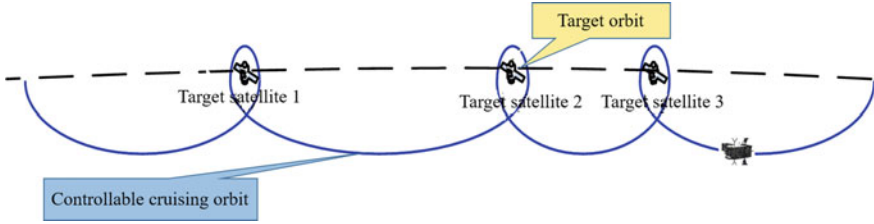


Fig. 4.23 Controllable spiral orbit

cruising spacecraft can conduct at least one or even multiple omnidirectional surveillance of every target of the target group. This is shown in Fig. 4.23.

By adjusting the cruising velocity of the spiral round-trip orbit and the configuration of relative drifting elliptical trajectory, etc., every target is able to be kept on the fly-around trajectory of the spiral round-trip cruising orbit, thus enabling the cruising spacecraft in spiral motion to detect the target satellite at short range. Additionally, in order to guarantee the stability of the imaging quality of the target satellite, we should try our best to ensure that the target satellite is at the center of the spiral fly-around region or in its vicinity so as to obtain the stable imaging effect.

4.5.1 Spiral Ring: Design

We suppose that the number of target satellites needed to be monitored is N . When the cruising spacecraft travels to the vicinity of target satellite i , if short-range fly-around observation is to be performed on the target satellite, then the relative trajectory should meet the following constraint conditions:

- (1) The fly-around trajectory cannot enter the safety zone of the target satellite (i.e., the flight forbidden zone) to avoid collision;
- (2) The fly-around trajectory cannot exceed the effective action range of the imaging payload of the cruising spacecraft.

We suppose that the radius of the target satellite's flight forbidden zone is r_1 , and the effective action distance of the platform's imaging payload is r_2 . In a target satellite orbital coordinate system, we can set the position of the aiming point as x_0 , as Fig. 4.24 shows.

According to the constraint conditions, the following can be obtained:

$$r_1 \leq |x_0| \leq r_2 \quad (4.65)$$

If at moment t_0 , the position of aiming point A, i.e., x_{t_0} , and the fly-around time T (T is the fly-around time of the spiral ring, less than or equal to the orbital period

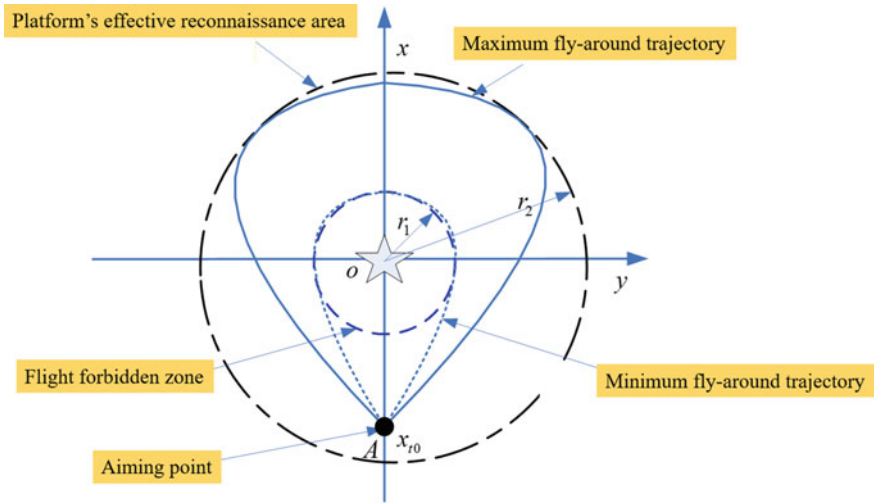


Fig. 4.24 Schematic figure of round-trip imaging trajectory constraint

of the target satellite) are given, by using the dynamics model to perform orbit extrapolation, the spiral ring trajectory of the cruising spacecraft can be obtained. The maximum relative distance between the cruising spacecraft and the aiming point appears at the moment when $t = t_0 + 0.5T$, and

$$h_{\max} = |x_{t_0 + 0.5T} - x_{t_0}| \tag{4.66}$$

Here, h_{\max} stands for the farthest distance between the cruising spacecraft and the aiming point in the spiral ring. Therefore, for the minimum spiral ring, the following constraint should be met:

$$h \geq |x_0| + r_1 \tag{4.67}$$

As for the maximum spiral ring, the following constraint should be met:

$$h \leq |x_0| + r_2 \tag{4.68}$$

The algorithm used to obtain the fly-around time constraint is a dichotomy that solves the nonlinear equation. The flowchart is in Fig. 4.25.

We suppose that the target orbit is a GEO, the effective action distance of the cruising spacecraft with payload is 120 km. Figure 4.26 shows, when the target flight forbidden zones are 100, 500 m, 2, 10, 30, 50 km, respectively, the change curves of the minimum fly-around time as it changes with the position distribution of the aiming point.

We can take Fig. 4.26a as an example. If the peak of the fly-around approaches the forbidden zone of the target satellite from the radial distance, then the minimum

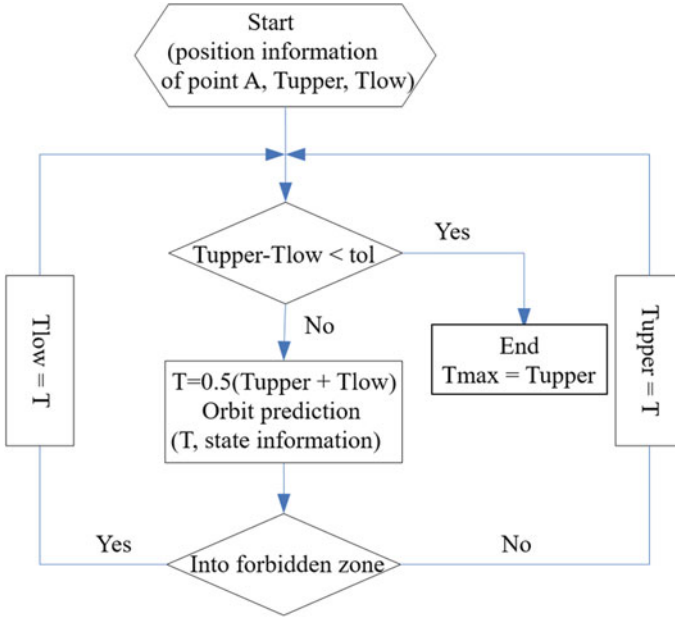


Fig. 4.25 Flow chart of minimum flight period

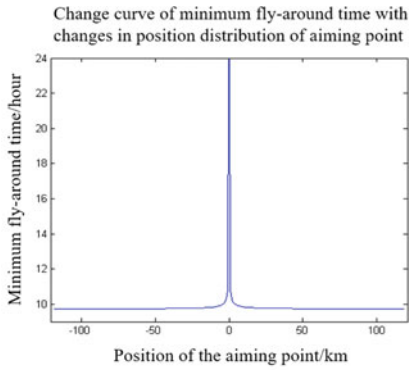
fly-around period is about 24 h; if the radial distance of the fly-around peak is 120 km from the target satellite, the minimum fly-around period is about 9.7 h.

With different position distributions of the aiming point, the variation tendency of the minimum fly-around configuration is shown in Fig. 4.27, in which the forbidden zone of the target is 50 km, the minimum fly-around times are 23.9344, 18.1850, and 15.7811 h, respectively.

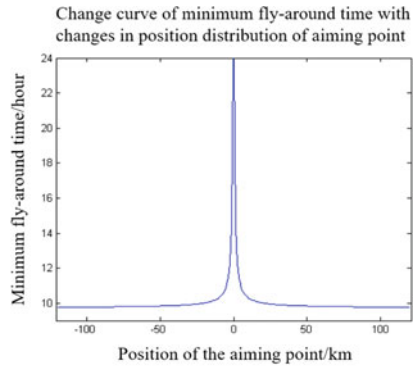
It can be seen that, when the effective action distance of the cruising spacecraft with payload is given, the shorter the radius of the target forbidden zone, the larger the distance between the position of the aiming point and the target, then the less the minimum fly-around time; the longer the radius of the target forbidden zone, the smaller the distance between the position of the aiming point and the target, then the more the minimum fly-around time. In extreme cases, when the aiming point is on the boundary of the target forbidden zone, the minimum fly-around time reaches its maximum value, which is also one orbital period of the target orbit.

4.5.2 Entry Corridor: Design

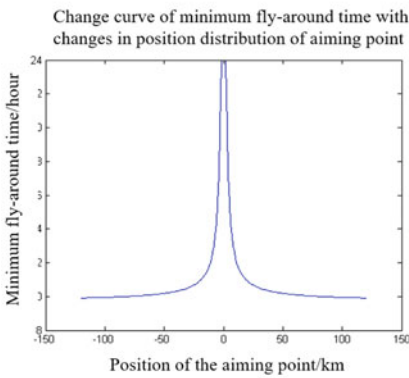
The goal in designing an entry corridor is to enable the cruising spacecraft to perform omnidirectional observation of the target satellite in its vicinity in a natural spiral fly-around way. It therefore does not require extra orbit control.



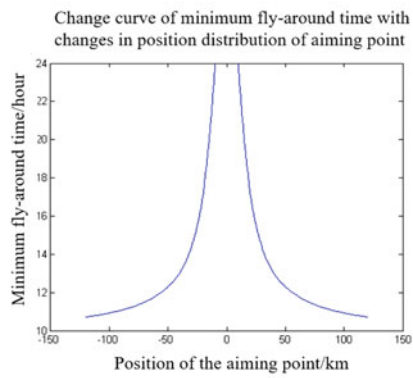
(a) Radius of the target forbidden zone 100m



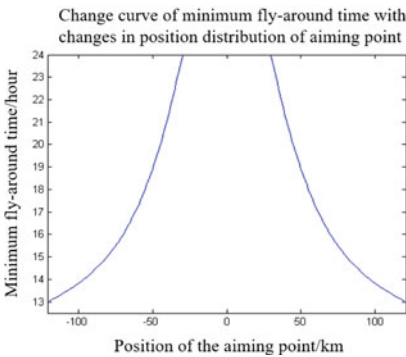
(b) Radius of the target forbidden zone 500m



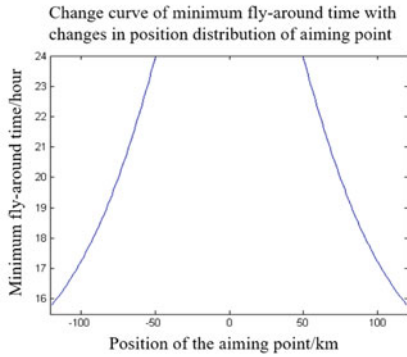
(c) Radius of the target forbidden zone 2km



(d) Radius of the target forbidden zone 10km



(e) Radius of the target forbidden zone 30km



(f) Radius of the target forbidden zone 50km

Fig. 4.26 Change curve of minimum fly-around time with changes in flight forbidden zones and position distribution of aiming point

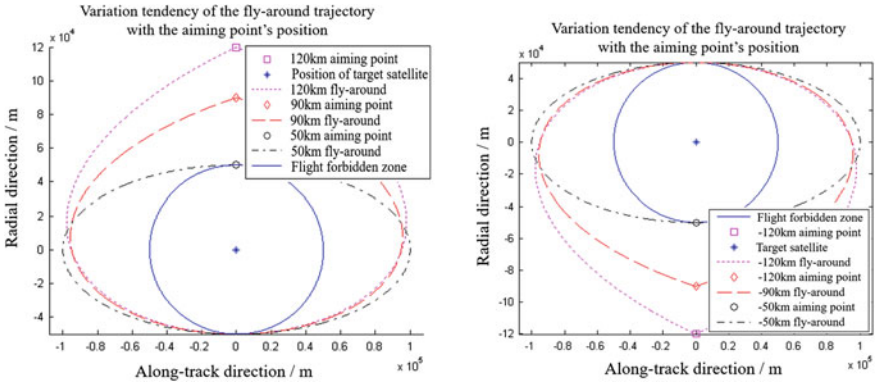


Fig. 4.27 Minimum fly-around trajectory with different aiming points

When the cruising spacecraft performs fly-around observation of the target satellite, its relative distance cannot exceed the working range of its payload; its relative motion trajectory cannot enter the forbidden zones of the target satellite in order to avoid collision. Therefore, when the cruising spacecraft performs spiral fly-around surveillance of a certain target satellite, besides the constraint on the peak of the relative position of the spiral fly-around, its relative initial velocity at the peak of the fly-around must enable the spiral fly-around trajectory of the cruising spacecraft to meet the constraint conditions.

Hence, the spiral fly-around surveillance by the cruising spacecraft of the target satellite is an initial state set of position and velocity, i.e., the “entry corridor”. After the cruising spacecraft completes its surveillance mission of target satellite $i - 1$, planning of surveillance of target satellite i will begin. In approaching target satellite i , once the cruising spacecraft captures the “entry corridor” of target satellite i , it will be able to complete a comprehensive fly-around surveillance of target satellite i with a natural relative fly-around.

The entry corridor can be described as:

$$\begin{aligned}
 S_i &= \cup [\vec{r}_j, \cup (\vec{v}_k)] \\
 st \quad &\begin{cases} x_i^2(t_j) + y_i^2(t_j) \geq r_{jingu}^2 \\ x_i^2(t_j) + y_i^2(t_j) \leq r_{zaihe}^2 \end{cases} \\
 t_j &\in [0, T_j]
 \end{aligned} \tag{4.69}$$

Table 4.3 “Entry corridor” table

	$T_1 = T_{\min}$	T_2	T_3	...	$T_n = T_{\max}$
$r_1 = r_{jinqu}$	$(\dot{x}_{11}, \dot{y}_{11})$	$(\dot{x}_{12}, \dot{y}_{12})$	$(\dot{x}_{13}, \dot{y}_{13})$...	$(\dot{x}_{1n}, \dot{y}_{1n})$
r_2	$(\dot{x}_{21}, \dot{y}_{21})$	$(\dot{x}_{22}, \dot{y}_{22})$	$(\dot{x}_{23}, \dot{y}_{23})$...	$(\dot{x}_{2n}, \dot{y}_{2n})$
r_3	$(\dot{x}_{31}, \dot{y}_{31})$	$(\dot{x}_{32}, \dot{y}_{32})$	$(\dot{x}_{33}, \dot{y}_{33})$...	$(\dot{x}_{3n}, \dot{y}_{3n})$
...	
$r_m = r_{zaihe}$	$(\dot{x}_{m1}, \dot{y}_{m1})$	$(\dot{x}_{m2}, \dot{y}_{m2})$	$(\dot{x}_{m3}, \dot{y}_{m3})$		$(\dot{x}_{mn}, \dot{y}_{mn})$

Here, S_i stands for the entry corridor of target satellite i , a set of a series of initial fly-around peaks \vec{r}_j and initial fly-around velocities \vec{v}_k . For any spiral fly-around peak \vec{v}_k , its fly-around period T_j must meet the following condition:

$$T_j \in [T_{\min}(j), T_{\max}(j)]$$

Here, $T_{\min}(j)$ stands for the minimum fly-around period of the cruising spacecraft at \vec{r}_j ; $T_{\max}(j)$ stands for its maximum fly-around period. $x_i(t_j), y_i(t_j)$ are the relative positions of the cruising spacecraft at moment t_j , satisfying the relative trajectory constraint. As every spiral fly-around peak has a corresponding fly-around period interval, according to the short-range relative motion dynamics model, a series of initial relative fly-around velocities \vec{v}_k at that peak can be obtained. The entire set of positions and velocities $\cup [\vec{r}_j, \cup (\vec{v}_k)]$ constitutes the entry corridor of target satellite i .

Based on the current state and mission requirements, the timing and size of the next control impulse needs to be calculated. The key is that the cruising spacecraft must, according to its predicted state, do iterative computation in real time to see whether the spiral fly-around trajectory meets the mission requirement. Its defects lie in the fact that a long time and a great deal of computing are needed for every iterative computation. Therefore, its defect is that the GNC System sets high requirements on the performance of the cruising spacecraft’s on-board computer. Considering the target group monitored by the cruising spacecraft is quite fixed, based on the features of the target group, the entry corridor of the target satellite can be designed in advance to reduce the real-time computing of the cruising spacecraft. The design pattern of the “entry corridor” table is shown in Table 4.3.

Here, $(\dot{x}_{ij}, \dot{y}_{ij})$ stands for the initial velocity that the cruising spacecraft should have at the spiral fly-around peak r_i when the spiral fly-around period is T_j . In the Table, the position of the fly-around peak r_i and the fly-around period T_j can be reasonably distributed according to actual requirements of the mission.

4.5.3 Single-Pulse Control Strategy

It can be known from Eq. (4.34) that in a relative motion coordinate system, the drifting ellipse parameter b of the relative motion of the cruising spacecraft can be described as:

$$b = \sqrt{\left(\frac{2\dot{y}_0}{n} + 3x_0\right)^2 + \left(\frac{\dot{x}_0}{n}\right)^2} = \sqrt{\left(\frac{2\dot{y}}{n} + 3x\right)^2 + \left(\frac{\dot{x}}{n}\right)^2} \quad (4.70)$$

The drift velocity of the center of the ellipse is:

$$V = 1.5x_{c0}n = 6nx_0 + 3\dot{y}_0 = 6nx + 3\dot{y} \quad (4.71)$$

The distance covered by the cruising spacecraft per day is:

$$L = 1.5x_{c0}nT = 12\pi x_0 + 6\pi\frac{\dot{y}_0}{n} = 12\pi x + 6\pi\frac{\dot{y}}{n} \quad (4.72)$$

Here, $(x_0, y_0, \dot{x}_0, \dot{y}_0)$ is the initial relative motion state of the cruising spacecraft; (x, y, \dot{x}, \dot{y}) stands for the relative motion state of the cruising spacecraft at any one moment.

In a relative motion coordinate system, the control impulses, which need to be applied when the configuration parameters of the spiral orbit are changed according to the requirements of the mission, can be classified into three types: along-track direction Δv_x , radial direction Δv_y , and normal direction Δv_z . When the impulses are applied in different directions, their effect also varies remarkably. For the design of a spiral controllable cruising orbit, due to the decoupling of the control in the normal direction and the control in the target satellite plane, the relative motion control in the normal direction of the target orbit can be designed separately.

(1) Impulse control in the along-track direction

If the velocity increment in the along-track direction is used to change the spiral cruising orbit, for a near-circular target orbit, we differentiate b and the following can be obtained:

$$\Delta b = \Delta \sqrt{\left(\frac{2\dot{y}}{n} + 3x\right)^2 + \left(\frac{\dot{x}}{n}\right)^2} = \frac{2}{nb} \left(\frac{2\dot{y}}{n} + 3x\right) \Delta \dot{y} \quad (4.73)$$

When we substitute the expression of the solution of x and \dot{y} into Eq. (4.73), the following can be obtained:

$$\Delta b = -\frac{2\Delta \dot{y}}{n} \sin(nt + \varphi) \quad (4.74)$$

Here: $\sin \varphi = -\left(\frac{2\dot{y}_0}{n} + 3x_0\right)$, $\cos \varphi = \frac{\dot{x}_0}{nb}$, $\varphi = k\pi + \arctg \frac{-(2\dot{y}_0 + 3nx_0)}{\dot{x}_0}$. When $\sin \varphi > 0$ and $\cos \varphi < 0$, k equals 1; when $\sin \varphi < 0$ and $\cos \varphi > 0$, k equals 0. The following can be obtained:

$$\begin{aligned}
x &= \frac{\dot{x}_0}{n} \sin nt - \left(3x_0 + 2\frac{\dot{y}_0}{n}\right) \cos nt + 2\left(2x_0 + \frac{\dot{y}_0}{n}\right) \\
&= b \sin (nt + \varphi) + 2\left(2x_0 + \frac{\dot{y}_0}{n}\right)
\end{aligned} \tag{4.75}$$

It can be known from Eq. (4.73) that Δb is a sine function of time t . We suppose $|\Delta \dot{y}| = \Delta v$, then the maximum value of Δb is $\frac{2\Delta \dot{y}}{n}$ and the minimum value is $-\frac{2\Delta \dot{y}}{n}$. Therefore, under the effect of the same along-track impulses, the size of the ellipse of the spiral cruising orbit can be adjusted by selecting the time to apply impulse control.

It is known that if $\Delta \dot{y} = \Delta v$, $\Delta b = -\frac{2\Delta v}{n} \sin (nt + \varphi)$, there will be the following conditions:

- (1) When $nt + \varphi = 2k\pi + \frac{1}{2}\pi$, $x = b + 2(2x_0 + \frac{\dot{y}_0}{n})$, i.e., at the highest point in the radial direction of the relative trajectory, the variation of the semi-minor axis of the spiral cruising orbit is $\Delta b = -\frac{2\Delta v}{n}$;
- (2) When $nt + \varphi = 2k\pi + \frac{3}{2}\pi$, $x = -b + 2(2x_0 + \frac{\dot{y}_0}{n})$, i.e., at the lowest point in the radial direction of the relative trajectory, the variation of the semi-minor axis of the spiral cruising orbit is $\Delta b = \frac{2\Delta v}{n}$;
- (3) When $nt + \varphi = k\pi$, $x = 2(2x_0 + \frac{\dot{y}_0}{n})$, i.e., at the midpoint in the radial direction of the relative trajectory, the variation of the semi-minor axis of the spiral cruising orbit is $\Delta b = 0$.

At this moment, $x_{c0} = 4x + 2\frac{(\dot{y} + \Delta v)}{n}$, i.e., the variation of the ellipse center in the radial direction is $\Delta x_c = 2\frac{\Delta v}{n}$; the cruising velocity is changed into $V = 1.5x_{c0}n = 6nx + 3(\dot{y} + \Delta v)$, i.e., the variation of the cruising velocity is $\Delta V = 3\Delta v$; while the variation of the cruising distance in one period is $\Delta L = \frac{6\pi}{n} \Delta v$.

(2) Radial impulse control

If the radial velocity increment is used to change the spiral round-trip orbit, for a near-circular target orbit, we differentiate b and the following can be obtained:

$$\Delta b = \Delta \sqrt{\left(\frac{2\dot{y}}{n} + 3x\right)^2 + \left(\frac{\dot{x}}{n}\right)^2} = \frac{\dot{x}}{nb} \Delta \dot{x} \tag{4.76}$$

When we substitute the expression of the solution of \dot{x} into Eq. (4.76), the following can be obtained:

$$\Delta b = \Delta \dot{x} \sin (nt + \theta) \tag{4.77}$$

Here: $\sin \theta = \frac{\dot{x}_0}{nb}$, $\cos \theta = \frac{2\dot{y}_0 + 3nx_0}{nb}$, $\theta = k\pi + \arctg \frac{\dot{x}_0}{2\dot{y}_0 + 3nx_0}$. When $\sin \varphi > 0$ and $\cos \varphi < 0$, k equals 1; when $\sin \varphi < 0$ and $\cos \varphi > 0$, k equals 0. The following can be obtained:

$$\dot{x} = \dot{x}_0 \cos nt + (2\dot{y}_0 + 3nx_0) \sin nt = nb \sin (nt + \theta) \tag{4.78}$$

It can be known from Eq. (4.77) that Δb is a sine function of time t . We suppose $|\Delta \dot{x}| = \Delta v$, then the maximum value of Δb is $\Delta \dot{x}$ and the minimum value is $-\Delta \dot{x}$. Therefore, under the effect of the same radial impulses, the size of the ellipse of the spiral cruising orbit can also be adjusted by selecting the time to apply impulse control.

It is known that when $\Delta \dot{x} = \Delta v$, $\Delta b = \Delta v \sin(nt + \varphi)$, there are the following conditions:

- (1) When $nt + \theta = 2k\pi + \frac{1}{2}\pi$, $\dot{x} = nb$, $\ddot{x} = 0$, $\dot{y} = -(3\dot{y}_0 + 6nx_0)$, the variation of the semi-minor axis of the spiral cruising orbit is $\Delta b = \Delta v$;
- (2) When $nt + \theta = 2k\pi + \frac{3}{2}\pi$, $\dot{x} = -nb$, $\ddot{x} = 0$, $\dot{y} = -(3\dot{y}_0 + 6nx_0)$, the variation of the semi-minor axis of the ellipse of the spiral cruising orbit is $\Delta b = -\Delta v$;
- (3) When $nt + \theta = k\pi$, $\dot{x} = 0$, the variation of the semi-minor axis of the spiral cruising orbit is $\Delta b = 0$.

At this moment, the initial relative position of the center of the spiral cruising orbit in the along-track direction will drift $\Delta y_c = -\frac{2}{n}\Delta v$; but the center distance of the drifting ellipse in the radial direction, both the cruising velocity V and the cruising distance in one period remain unchanged.

Based on the analysis above, in a spiral controllable cruising orbit, the effect of the control of the drifting ellipse's configuration parameters by applying impulses can be concluded, thus the control strategy of a spiral controllable cruising orbit can be obtained. The selection of the direction to apply impulses and the selection of the control point are shown in Fig. 4.28:

In cases when only along-track control is used:

- (1) When velocity increment is the same, along-track impulses are applied at the highest point and the lowest point in the radial direction of the relative trajectory, and the variation of the semi-minor axis of the spiral cruising orbit is $|\Delta b| = \frac{2\Delta v}{n}$. When velocity increment is the same and along-track impulses are

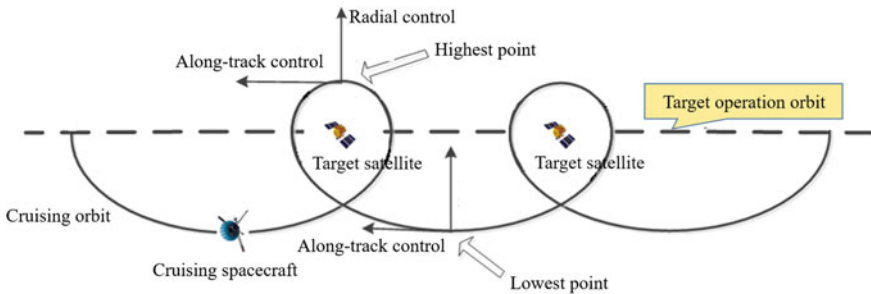


Fig. 4.28 Selection of direction to apply impulses and selection of control point

applied at the radial midpoint of the spiral cruising orbit, the semi-minor axis of the spiral cruising orbit b is not changed.

- (2) The variation of the radial center of the cruising orbit x_{c0} is proportional to the along-track impulse, and $\Delta x_c = 2 \frac{\Delta v}{n}$.
- (3) The variation of the cruising velocity and the cruising distance of the spiral cruising orbit per period are proportional to the along-track impulse, and $\Delta V = 3\Delta\dot{y} = 3\Delta v$, $\Delta L = \frac{6\pi}{n} \Delta v$.
- (4) The along-track impulse does not change the along-track initial relative position of the center of the spiral cruising orbit.

In cases when only radial control is used:

- (1) Radial impulse control does not change the cruising velocity V and the distance of the spiral precession per period L .
- (2) The variation of the initial relative position of the spiral cruising orbit center in the along-track direction is proportional to the radial impulse, i.e., $\Delta y_c = -\frac{2}{n} \Delta v$.
- (3) The maximum variation of the semi-minor axis of the spiral cruising orbit imposed by the radial impulse is $|\Delta b| = \Delta v$. At the highest point and the lowest point of the spiral cruising orbit in the radial direction, applying radial impulse does not change the semi-minor axis of the spiral cruising orbit b .
- (4) Radial impulse control does not change the radial initial relative position of the spiral cruising orbit center x_c .

In summary, for the impulse control method of the configuration parameter of a drifting ellipse, the following control strategies can be adopted:

- When the semi-minor axis of the drifting ellipse is to be adjusted, radial or along-track control is needed, and the along-track control has better effect;
- When the drift velocity of the drifting ellipse center is to be adjusted, along-track impulse control is needed;
- When the radial migration of the drifting ellipse center is to be adjusted, along-track impulse control is needed;
- When the along-track migration of the of the drifting ellipse center is to be adjusted, radial impulse control is needed.

We can take adjusting the orbit parameters of a spiral cruising orbit by using radial control as an example. We select three target satellites (as Fig. 4.29 shows), and the target set is $\{0, 1.4e + 003, 2.3e + 003 \text{ km}\}$. If a natural spiral method is applied, the fly-around observation of target spacecraft 1 and target spacecraft 3 can be achieved, without conducting the fly-around of target spacecraft 2. If the fly-around trajectory of target spacecraft 2 is to be formed, relative orbit control needs to be conducted before the fly-around.

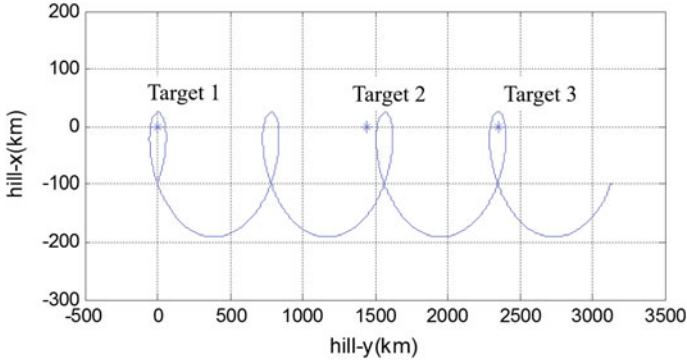


Fig. 4.29 Natural spiral fly-around trajectory of target spacecraft 1 and 3

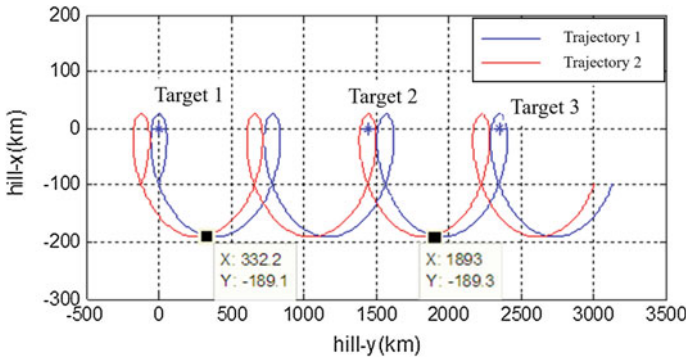


Fig. 4.30 Transfer control point from trajectory 2 to trajectory 1

If we do not change the basic configuration parameters such as the cruising radius of the cruising orbit, target 2 can also be included in the center of the fly-around area of the cruising orbit via changing the along-track initial relative position of the center of the spiral cruising orbit, as Fig. 4.30 shows.

Trajectory 1 is a natural spiral drift configuration without control, while trajectory 2 is a spiral drift configuration with control.

According to the general principle of orbit control, applying impulse control at the intersection of two trajectories can achieve the switch of trajectories. Therefore, applying impulse control at intersection (332.2, -189.1) can achieve control switch from trajectory 1 to trajectory 2; then applying impulse control at intersection (189.3, -189.3) can achieve control switch from trajectory 2 back to trajectory 1. The velocity increment required for the control is 2.8 m/s, with the two controls having opposite directions. After applying the above controls, the trajectory of the spiral cruising orbit eventually obtained is shown in Fig. 4.31.

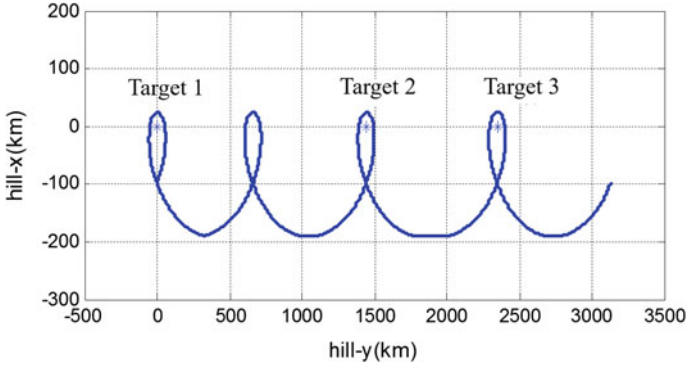


Fig. 4.31 Trajectory curve of entire flight under single impulse control

4.5.4 Fast Cruising Control Strategy

When the natural drifting spiral trajectory method is applied to conduct fly-around observation, relative motion control is easily achieved and the control quantity required, i.e., the fuel consumed, is less; but the moment to apply control quantity must be stipulated, and the time of the transition process of the control is long. In the following part, the control method of adjustable transition time will be studied to enhance the flexibility of the control method of relative motion and to reduce the transition time of configuration control.

It can be known from Eq. (4.27) that when the target orbit is a near-circular orbit, the matrix form of the relative motion equation solution of the cruising spacecraft is:

$$\begin{bmatrix} \vec{\rho} \\ \dot{\vec{\rho}} \end{bmatrix} = \Phi_{xx_0} = \begin{bmatrix} \Phi_{11}(t) & \Phi_{12}(t) \\ \Phi_{21}(t) & \Phi_{22}(t) \end{bmatrix} \begin{bmatrix} \vec{\rho}_0 \\ \dot{\vec{\rho}}_0 \end{bmatrix} \quad (4.79)$$

Equation (4.79) shows the influence that the initial relative position and the relative velocity have on the relative position and the relative velocity at moment t , i.e., the state transfer relation of the relative motion. For example, at moment $-t$, the initial relative position and initial relative velocity can be solved according to the relative position and the relative velocity:

$$\begin{bmatrix} \vec{\rho}_0 \\ \dot{\vec{\rho}}_0 \end{bmatrix} = \Phi_{x_0x} = \begin{bmatrix} \Phi_{11}(-t) & \Phi_{12}(-t) \\ \Phi_{21}(-t) & \Phi_{22}(-t) \end{bmatrix} \begin{bmatrix} \vec{\rho} \\ \dot{\vec{\rho}} \end{bmatrix} \quad (4.80)$$

It is obvious that:

$$\Phi_{xx_0} = \Phi_{x_0x}^{-1} \quad (4.81)$$

We can set time as t , the terminal position as \bar{p}_2 , and the terminal velocity as zero, then the two velocity increments can be obtained as:

$$\bar{p}_2 = \Phi_{\bar{p}\bar{p}}\bar{p}_0 + \Phi_{\bar{p}\dot{\bar{p}}}\dot{\bar{p}}_1 \Rightarrow \dot{\bar{p}}_1 = \Phi_{12}^{-1}(\bar{p}_2 - \Phi_{11}\bar{p}_0) \quad (4.82)$$

And then

$$\Delta\bar{v}_1 = \dot{\bar{p}}_1 - \dot{\bar{p}}_0 = \Phi_{12}^{-1}(\bar{p}_2 - \Phi_{11}\bar{p}_0) - \dot{\bar{p}}_0 \quad (4.83)$$

$$\dot{\bar{p}}_2 = \Phi_{21}\bar{p}_0 + \Phi_{22}\dot{\bar{p}}_1 \Rightarrow \Delta\bar{v}_2 = -\dot{\bar{p}}_2 = -(\Phi_{21}\bar{p}_0 + \Phi_{22}\dot{\bar{p}}_1) \quad (4.84)$$

The three target satellites in Fig. 4.29 are also taken as examples here.

- (1) *From target 1 to target 2: the position of the control starting point is the intersection at the end of the fly-around trajectory for target 1; the position of the terminal point is the intersection at the beginning of the fly-around trajectory for target 2.*

Starting point:

$$\begin{cases} x_1 = \Delta a - p \cos(u_0 + \Delta u - \varphi) \\ y_1 = l - 1.5\Delta a\Delta u + 2p \sin(u_0 + \Delta u - \varphi) \\ \dot{x}_1 = np \sin(u_0 + \Delta u - \varphi) \\ \dot{y}_1 = -1.5\Delta an + 2np \cos(u_0 + \Delta u - \varphi) \end{cases}$$

Terminal point:

$$\begin{cases} x_2 = \Delta a - p \cos(u_0 + 4\pi - \varphi) \\ y_2 = \Delta l + l - 1.5\Delta a4\pi + 2p \sin(u_0 + 4\pi - \varphi) \\ \dot{x}_2 = np \sin(u_0 + 4\pi - \varphi) \\ \dot{y}_2 = -1.5\Delta an + 2np \cos(u_0 + 4\pi - \varphi) \end{cases}$$

We can set the transition time as 1×10^4 s, 3×10^4 s, 5×10^4 s, 7×10^4 s, 9×10^4 s, 11×10^4 s, respectively. The trajectory change curve of the two corresponding impulse control is shown in Fig. 4.32.

In the figure, as the transition time increases, the transition trajectory curve gradually goes up. The corresponding control velocity consumption is shown in Table 4.4.

It can be seen from Table 4.4 that, with different transition time, the corresponding control velocity consumption is different. If the transition time is too short, the corresponding velocity consumption will be huge; but the increase in transition time may not necessarily reduce the velocity consumption. If a suitable transition time is to be selected, then on the one hand, it should be less than the

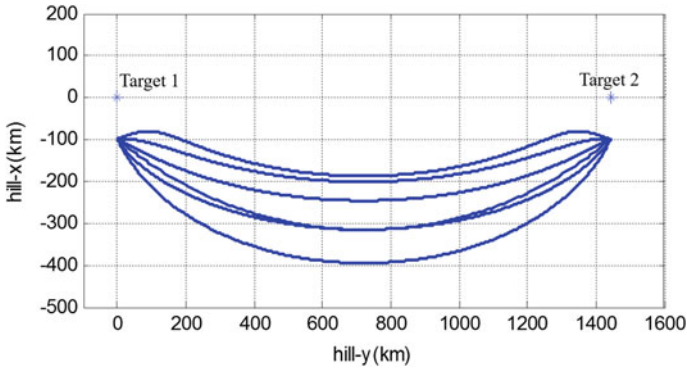


Fig. 4.32 Trajectory curve of transition from target 1 to target 2

Table 4.4 Control velocity consumption corresponding to different transition time

Transition time (s)	1×10^4	3×10^4	5×10^4	7×10^4	9×10^4	11×10^4
Control velocity consumption (m/s)	272.64	57.97	9.86	10.78	17.20	21.71

transition time of a single impulse control; on the other hand, the velocity consumption should not be too much.

- (2) *From target 2 to target 3: the position of the control starting point is the intersection at the end of the fly-around trajectory for target 2; the position of the terminal point is the intersection at the beginning of the fly-around trajectory for target 3.*

Starting point:

$$\begin{cases} x_3 = \Delta a - p \cos(u_0 + 4\pi + \Delta u - \varphi) \\ y_3 = \Delta l + l - 1.5\Delta a(4\pi + \Delta u) + 2p \sin(u_0 + 4\pi + \Delta u - \varphi) \\ \dot{x}_3 = np \sin(u_0 + 4\pi + \Delta u - \varphi) \\ \dot{y}_3 = -1.5\Delta an + 2np \cos(u_0 + 4\pi + \Delta u - \varphi) \end{cases}$$

Terminal point:

$$\begin{cases} x_4 = \Delta a - p \cos(u_0 + 6\pi - \varphi) \\ y_4 = l - 1.5\Delta a6\pi + 2p \sin(u_0 + 6\pi - \varphi) \\ \dot{x}_4 = np \sin(u_0 + 6\pi - \varphi) \\ \dot{y}_4 = -1.5\Delta an + 2np \cos(u_0 + 6\pi - \varphi) \end{cases}$$

We can set the transition time as 2×10^4 s, 3×10^4 s, 4×10^4 s, 5×10^4 s, 6×10^4 s, 7×10^4 s, respectively. The corresponding trajectory change curve is shown in Fig. 4.33.

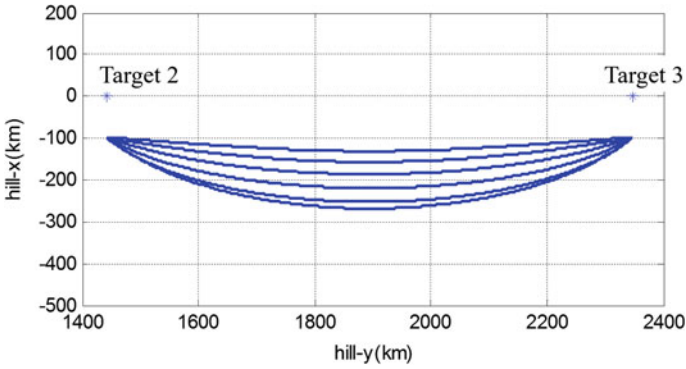


Fig. 4.33 Trajectory curve of transition from target 2 to target 3

Table 4.5 Control velocity consumption corresponding to different transition time

Transition time (s)	2×10^4	3×10^4	4×10^4	5×10^4	6×10^4	7×10^4
Control velocity consumption (m/s)	60.41	22.85	4.18	6.14	11.48	14.27

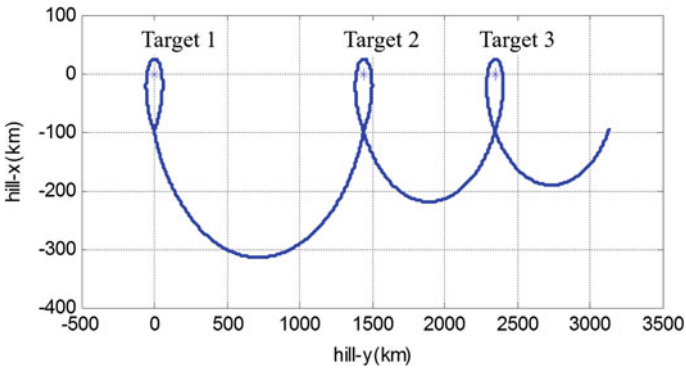


Fig. 4.34 Trajectory curve of entire flight

In the figure, as the transition time increases, the transition trajectory curve gradually goes up. The corresponding control velocity consumption is shown in Table 4.5.

It can be seen from Table 4.5 that, with different transition time, the corresponding control velocity consumption is different. If the transition time is too short, the corresponding velocity consumption will be huge; but the increase in transition time may not necessarily reduce the velocity consumption.

In sum, the transition time from target satellite 1 to target satellite 2 is 5×10^4 s, and the transition time from target satellite 2 to target satellite 3 is 4×10^4 s. The trajectory curve of the entire flight is shown in Fig. 4.34.

4.6 Summary

Different from the traditional orbit design method, the spiral cruising orbit is an orbit that takes the target orbit as the reference. Spacecraft operating in spiral cruising orbit are low in energy consumption (less energy consumed in control) but high in cost-effectiveness (with a single spacecraft being able to achieve the detection of multiple spacecraft in the target orbit). It can carry out multi-perspective (larger than 180° , able to reach 360°), short-range and high-precision detection and is of great application value in the realm of space target surveillance.

In this chapter, starting from different application goals, the design method of three kinds of spiral cruising orbits (traversal orbit, round-trip orbit and controllable orbit) are introduced; and detailed control methods are provided. Finally, combined with typical cases, the feasibility and practicability of the design and control methods of the spiral cruising orbit are analyzed by simulation.

Chapter 5

Theory and Design Method of Multi-Target Rendezvous Orbit Based on Traversing Points

This chapter will propose a new concept—traversing point—to deal with the orbital rendezvous of a servicing spacecraft and multiple target spacecraft. Based on the new concept, it will provide the orbit rendezvous methods for coplanar multi-target spacecraft and non-coplanar multi-target spacecraft. The focus will be on the latter. This method, with the introduction of the concept “traversing point”, turns the orbital rendezvous of non-coplanar multi-target spacecraft into the coplanar multi-point orbital rendezvous. Therefore, it will provide a possibility for the fast and energy-efficient orbit rendezvous of one servicing spacecraft and multiple target spacecraft in different orbits.

5.1 Multi-Target Orbital Rendezvous: Problem Description

As a kind of orbit maneuver, an orbital rendezvous refers to the course in which a tracking spacecraft conducts rendezvous with a target spacecraft at a certain time and place in space. Generally, orbit control is needed in an orbital rendezvous. Thus, the degree of complexity in orbital control and its demand for energy and time should be considered in order to achieve the orbit rendezvous. As we know, among a variety of ways for orbit maneuver, changing the orbit plane requires huge fuel consumption from the spacecraft and its control process is quite complex. So a coplanar orbit plane is usually adopted as a way to achieve an orbit rendezvous. In other words, if the tracking spacecraft and the target spacecraft are in the same orbit plane, then the orbit rendezvous could be achieved simply by a coplanar orbital maneuver of the tracking spacecraft.

With increasing types of space mission, the demand for the capability of an orbital rendezvous is also growing. Because spacecraft manufacturing, launching and operating management are costly, to save cost and improve efficiency, we need

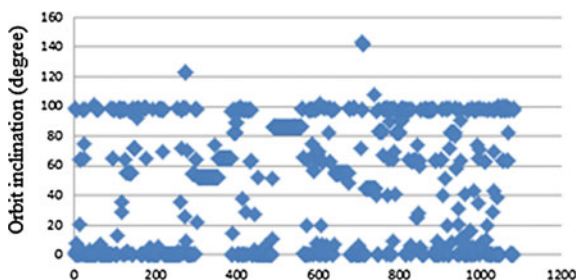
a servicing spacecraft capable of on-orbit serving as many target spacecraft as possible. In other words, a “one-to-many” on-orbit service mode should be adopted. According to statistics, the number of operational on-orbit spacecraft reached 1084 as of September 1, 2013. They are distributed in multiple orbit planes (Fig. 5.1). If those abandoned on-orbit satellites were also included, then the number of orbit planes could be even bigger. When the traditional method of coplanar orbital rendezvous is adopted, even if a servicing spacecraft is able to serve multiple target spacecraft in its own orbit plane, it is still necessary to launch numerous servicing spacecraft into different orbit planes. This is apparently costly. Therefore, to better meet the “one-to-many” on-orbit service requirements and improve its efficiency, how to achieve the orbital rendezvous of multi-target spacecraft, especially those non-coplanar ones, has become an important and urgent issue.

In this chapter, the problems in multi-target orbital rendezvous in space will be divided into two parts: the orbital rendezvous of coplanar multi-target spacecraft and the orbital rendezvous of non-coplanar multi-target spacecraft. On the one hand, orbital rendezvous of coplanar multi-target spacecraft refers to the orbital rendezvous of a servicing spacecraft and multiple target spacecraft in one orbit plane, covering problems in the orbit design and orbit control of the rendezvous orbit. On the other hand, orbital rendezvous of non-coplanar multi-target spacecraft refers to the orbit design and orbit control of the rendezvous orbit when a servicing spacecraft separately conducts rendezvous with multiple target spacecraft in other orbit planes through orbit maneuver.

Generally, orbit design includes the design of a parking orbit and the rendezvous orbit of the servicing spacecraft. Orbit control contains two parts: the first is the orbit control of the servicing spacecraft from the parking orbit to the rendezvous orbit; and the second is the orbit control between the rendezvous orbits of the servicing spacecraft and each of the target spacecraft. It is obvious that, to make the “one-to-many” on-orbit rendezvous mode feasible, the operation procedures of the orbit control should be simplified and the energy consumed in the orbit maneuver should be reduced as much as possible.

Generally speaking, the spacecraft’s operation orbit can be described by six orbit elements $(a, e, i, \Omega, \omega, \tau)$ or geocentric coordinates (x, y, z) . If we assume that the

Fig. 5.1 Distribution map of on-orbit spacecraft orbit inclinations



orbit elements of the servicing spacecraft are $(a_S, e_S, i_S, \Omega_S, \omega_S, \tau_S)$, then its orbital rendezvous positions with n target spacecraft can be written as:

$$\begin{aligned} P_1 &: (t_1, x_1, y_1, z_1) \\ P_2 &: (t_2, x_2, y_2, z_2) \\ &\vdots \\ P_n &: (t_n, x_n, y_n, z_n) \end{aligned}$$

Here, $P_i (i = 1, 2, \dots, n)$ represents the time and positions of orbital rendezvous between the servicing spacecraft and n target spacecraft. Apparently, these n positions with time attributes are supposed to be in the servicing spacecraft's orbit. Figure 5.2 shows what it will be like when $n = 3$.

In Fig. 5.2, the rendezvous orbit conducts rendezvous with three target orbits at points A, B and C, respectively. As we know, two random points in space can be connected by an infinite number of orbits. But when there are three or more points, the orbit which connects them all may not exist unless orbital maneuvers are conducted. Therefore, in orbital design, it is highly unlikely for a rendezvous orbit which can conduct rendezvous with more than three target orbits simultaneously to exist. In that case, orbit control is needed.

For most rendezvous missions in space, a zero distance between the servicing spacecraft and the target spacecraft is not required. It means that we only need to send the servicing spacecraft to the vicinity of the target spacecraft (within a relative distance from several dozens to hundreds of kilometers). Hence, the multi-target orbital rendezvous method studied in this chapter is not only for multi-target rendezvous missions, but also for multi-target orbit interception missions.

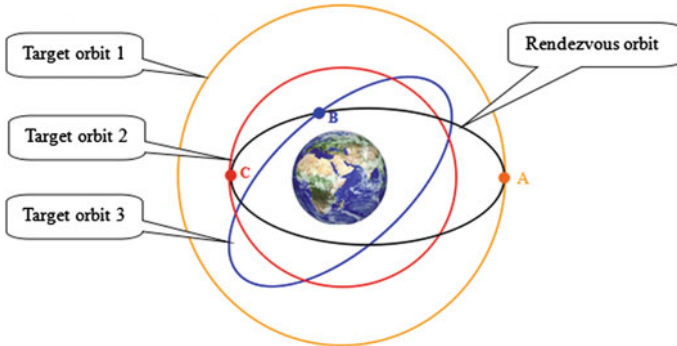


Fig. 5.2 Schematic figure of orbital rendezvous of servicing spacecraft and target spacecraft

5.2 Traversing Point: Concept and Determination Method

5.2.1 Traversing Point: Concept

To reduce the complexity and the cost of orbit control in orbital rendezvous, coplanar orbital maneuver, apparently, becomes a relatively ideal option. However, if the target spacecraft are in different orbit planes, it is obviously impossible for the servicing spacecraft to be coplanar with each target simultaneously. Actually, for an orbital rendezvous to occur, the servicing spacecraft is not required to conduct rendezvous with the target spacecraft's entire orbit, but only with the target spacecraft's orbit at a certain point. That is, all we need is to make the rendezvous point coplanar with the operational trajectory of the servicing spacecraft.

According to Kepler's First Law, the orbit of every spacecraft rotating around the Earth is in the plane passing through the Earth-center. So it is certain that any two spacecraft's orbit planes will intersect. Therefore, if the plane of the parking orbit of the servicing spacecraft is taken as the reference plane, it will intersect all the target orbit planes and the intersection points in the reference plane will be on their intersection lines. It is obvious that the intersection line passes through the Earth-center and the intersection points are on both sides of the Earth-center, as Fig. 5.3 shows.

Figure 5.3 shows the intersection of two orbit planes. The target spacecraft passes through the plane of the parking orbit of the servicing spacecraft (i.e., the reference plane) and there are two intersection points on the intersection line of the two planes. We call the intersection points "traversing points".

Here, the one located in the northern hemisphere of the geocentric celestial sphere is called the north traversing point, and the other in the southern hemisphere—the south traversing point. The phase difference of the two traversing points is 180° .

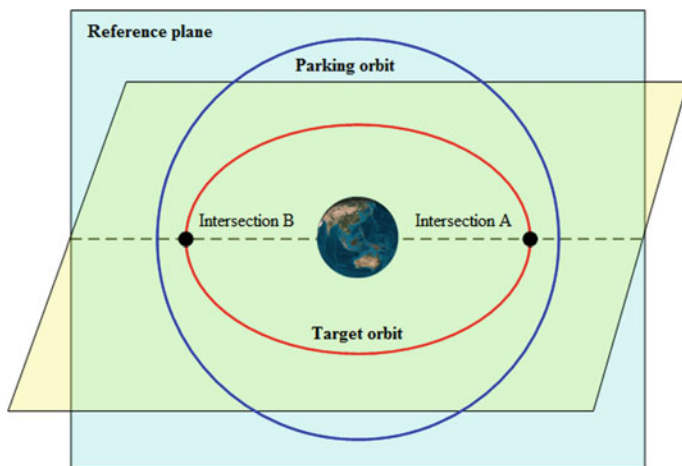


Fig. 5.3 Conceptual figure of traversing points

Clearly, in the orbit plane of the servicing spacecraft, two traversing points will be formed by any target spacecraft that is not coplanar with the servicing spacecraft. And the target spacecraft will continuously pass through the orbit plane of the servicing spacecraft at the two traversing points.

That is, a large number of traversing points are scattered in the orbit plane of the servicing spacecraft. These points are both in the orbit of the target spacecraft and in the orbit plane of the servicing spacecraft. If these traversing points are set as the rendezvous points of the target spacecraft and the servicing spacecraft, then the servicing spacecraft can achieve orbital rendezvous with the target spacecraft by conducting in-plane orbital maneuvers without having to change its orbit plane.

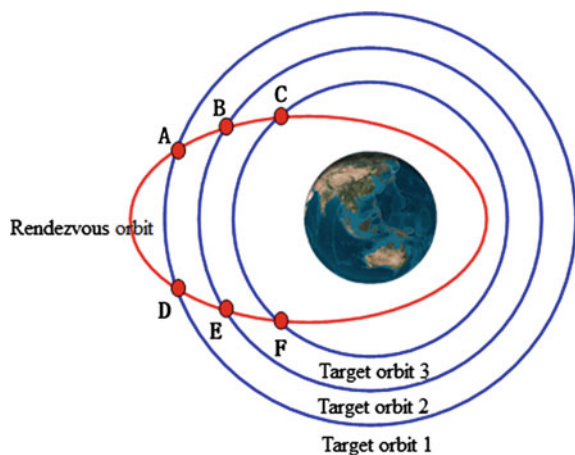
The method of conducting orbital rendezvous of the servicing spacecraft and several target spacecraft at traversing points is what we propose in this chapter—the non-coplanar multi-target orbital rendezvous method based on traversing points.

Using this method, a non-coplanar orbital rendezvous can be turned into a coplanar one. For more than one target spacecraft, this method can also be applied and completely meets the demands of the “one-to-many” orbital rendezvous mode.

In reality, the coplanar rendezvous points can also be taken as the traversing points, as is shown in Fig. 5.4.

In Fig. 5.4, A, B, C, D, E and F are the rendezvous points of the rendezvous orbit with target orbits 1, 2 and 3, respectively. These points can be taken as the traversing points formed by the target spacecraft when it traverses the servicing spacecraft orbit. Clearly, in a coplanar orbital rendezvous, it is the orbit of the servicing spacecraft that the target spacecraft traverses and the traversing points are in the orbit of the servicing spacecraft. However, in a non-coplanar orbital rendezvous, it is the orbit plane of the servicing spacecraft that the target spacecraft passes through and the traversing points are in the orbit plane of the servicing spacecraft. So the traversing points in a coplanar orbital rendezvous can serve as a

Fig. 5.4 Traversing points in coplanar multi-target orbital rendezvous



particular case of the traversing points in a non-coplanar orbital rendezvous. Taking this into consideration, we will focus on the non-coplanar multi-target orbital rendezvous method in this chapter.

5.2.2 Traversing Point: Determination Method

In general, the operation orbit of a spacecraft can be described by six orbit elements $(a, e, i, \Omega, \omega, \tau)$. Here, we can use two orbit elements i, Ω to solely determine the orbit plane in which the spacecraft operates.

According to the definition of the traversing point, there will be two traversing points formed by the orbit of each spacecraft in an appointed orbit plane. It means that we need to first determine the plane through which the spacecraft will pass.

We assume that the orbit plane of the servicing spacecraft, denoted by orbit elements (i_s, Ω_s) , is the rendezvous orbit plane. And we also suppose that a target spacecraft passes through the plane and its orbit elements are $(a_t, e_t, i_t, \Omega_t, \omega_t, \tau_t)$ as Fig. 5.5 shows.

In Fig. 5.5, A and A' are the two rendezvous points of the target spacecraft's orbit and the rendezvous plane, namely, the north traversing point and the south traversing point; point B is the ascending node of the orbit of the target satellite; point C is the ascending node in the rendezvous orbit plane. The coordinates of the traversing point in the rendezvous orbit plane can be denoted as (t, r, ϕ) . Here, t is the time when the target spacecraft passes through the plane; r is the geocentric distance of the traversing point; ϕ is the argument of the ascending node of the traversing point in the rendezvous orbit plane.

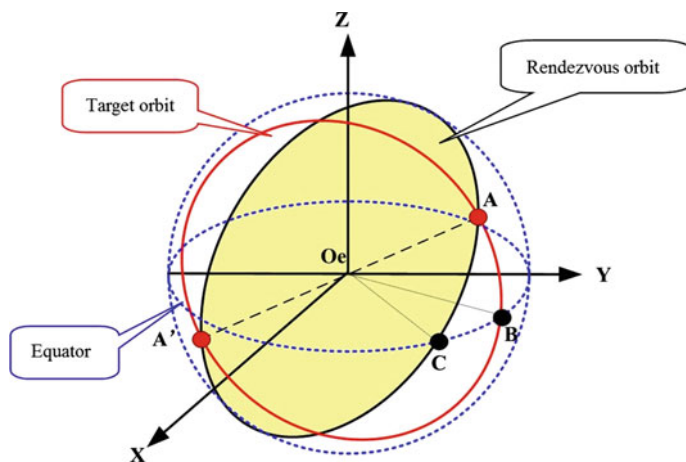


Fig. 5.5 Spatial geometric relationship diagram of traversing points in non-coplanar orbit rendezvous

Thus, the coordinates of north traversing point A are (t_N, r_N, ϕ_N) . Here, t_N is the time when the target spacecraft passes through north traversing point A ; $r_N = O_e A$ is the geocentric distance of north traversing point A ; $\phi_N = \angle A O_e C$ is the argument of the ascending node of traversing point A in the rendezvous plane. Then a spherical triangle is formed by points A , B and C in the geocentric celestial sphere. Using the formula of spherical triangle, we obtain:

$$tg\phi_N = \begin{cases} \frac{\sin(\Omega_t - \Omega_s)}{\cos(\Omega_t - \Omega_s)\cos i_s + \sin i_s ctg(180^\circ - i_t)} & \Omega_t > \Omega_s \\ \frac{\sin(\Omega_s - \Omega_t)}{\cos(\Omega_s - \Omega_t)\cos(180^\circ - i_2) + \sin(180^\circ - i_2)ctg i_t} & \Omega_t < \Omega_s \end{cases} \quad (5.1)$$

Using the orbital equation, we obtain:

$$r_N = \frac{a_t(1 - e_t^2)}{1 + e_t \cos(u_N - \omega_t)} \quad (5.2)$$

Here, u_N is the argument of the ascending node of north traversing point A in the orbit plane of the target spacecraft, and

$$\sin u_N = \frac{\sin \phi_N \sin i_s}{\sin i_t} \quad (5.3)$$

Using Kepler Equation, we obtain:

$$t_N = (E_N - e_t \sin E_N) \sqrt{\frac{a_t^3}{\mu}} + \tau_t \quad (5.4)$$

Here, E_N is the eccentric anomaly of north traversing point A in the orbit plane of the target spacecraft, and

$$tg \frac{E_N}{2} = \sqrt{\frac{1 - e_t}{1 + e_t}} tg \frac{(u_N - \omega_t)}{2} \quad (5.5)$$

Given that north traversing point A is symmetric to south traversing point A' with respect to Earth-center O_e , the coordinates (t_S, r_S, ϕ_S) of south traversing point A' in the rendezvous orbit plane can be obtained:

$$\begin{cases} t_S = (E_S - e_t \sin E_S) \sqrt{\frac{a_t^3}{\mu}} + \tau_t \\ \phi_S = \pi + \phi_N \\ r_S = \frac{a_t(1 - e_t^2)}{1 + e_t \cos(u_S - \omega_t)} \end{cases} \quad (5.6)$$

Here,

$$\begin{cases} E_S = 2\arctg\left(\sqrt{\frac{1-e_t}{1+e_t}}\text{tg}\frac{(u_S-\omega_t)}{2}\right) \\ u_S = \pi + u_N \end{cases} \quad (5.7)$$

It is clear that, for the orbits of different target spacecraft in the same orbit plane, they have the same argument of the ascending node of the north traversing point in the rendezvous plane ϕ_N and the same argument of the ascending node of the south traversing point in the rendezvous plane ϕ_S . They only differ in the distance r_N, r_S , which are related to the size, shape and perigee direction of the target spacecraft.

On the other hand, for traversing moment t_N or t_S , they are not the only moments because the target spacecraft passes through the north traversing point and the south traversing point respectively in every orbit period. And the time interval for traversing is one operation period of the target spacecraft, namely,

$$\begin{cases} t_{mN} = t_N + mT_t \\ t_{mS} = t_S + mT_t \end{cases} \quad m = 0, 1, 2, \dots \quad (5.8)$$

In the above equation, T_t is the orbit period of the target spacecraft; t_{mN} and t_{mS} are the moments when the target spacecraft passes through the north and the south traversing points in its m -th orbit period respectively.

If it is to locate the traversing points in a coplanar orbital rendezvous, the method will be easier, as is shown in Fig. 5.6.

We assume that the orbit elements of the servicing spacecraft and the target spacecraft are $(a_s, e_s, i_s, \Omega_s, \omega_s, \tau_s)$ and $(a_t, e_t, i_t, \Omega_t, \omega_t, \tau_t)$ respectively, and

$$\begin{cases} i_s = i_t \\ \Omega_s = \Omega_t \end{cases}$$

The intersections (i.e., the traversing points) of their orbits are points A and B. The geocentric distances of the traversing points satisfy:

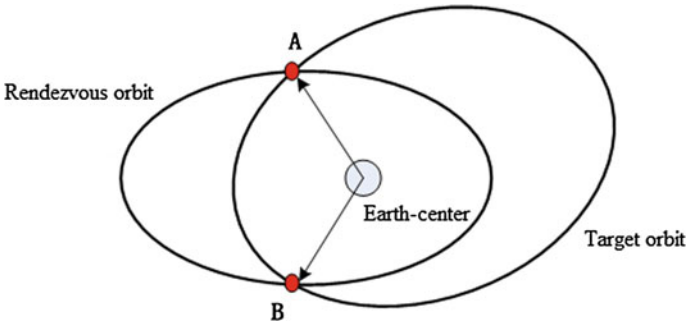


Fig. 5.6 Schematic figure of traversing points in coplanar orbital rendezvous

$$\begin{cases} r_S^A = r_t^A \\ r_S^B = r_t^B \end{cases}$$

Using the orbital equation, we obtain:

$$\begin{cases} \frac{a_t(1-e_t^2)}{1+e_t \cos f_t^A} = \frac{a_s(1-e_s^2)}{1+e_s \cos f_s^A} \\ \frac{a_t(1-e_t^2)}{1+e_t \cos f_t^B} = \frac{a_s(1-e_s^2)}{1+e_s \cos f_s^B} \end{cases} \quad (5.9)$$

Based on it, we can obtain f_t^A and f_t^B , the true anomalies of traversing points A and B in the target orbit respectively, and t_A and t_B , the time when the target spacecraft passes through the two points respectively.

5.3 Orbital Rendezvous: Strategies Based on Traversing Point

5.3.1 Design Principles Based on Traversing Point

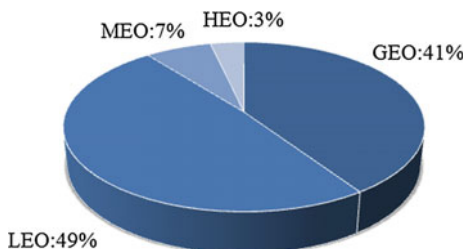
In a non-coplanar orbital rendezvous based on traversing point, traversing points formed by a target spacecraft orbit in the orbit plane of a servicing spacecraft are taken as rendezvous points, thus turning the non-coplanar orbital rendezvous into a coplanar one. In this way, the energy consumption in the non-coplanar orbital rendezvous can be reduced. On the other hand, in a multi-target orbit rendezvous based on traversing point, the servicing spacecraft achieves orbital rendezvous with multiple target spacecraft at the traversing points by multiple maneuverings in its orbit plane. Through sound orbit design and the control of the orbit rendezvous, the servicing spacecraft can even achieve orbital rendezvous with multiple target spacecraft in a single orbit period. Thus, rendezvous time and energy consumption in the process can be greatly reduced.

For the latter method above, the servicing spacecraft and the target spacecraft are not required to be in the same orbit plane, and multiple target spacecraft are not required to be coplanar, either. The main constraining factors are the number of the target spacecraft, the positions of traversing points, the orbital rendezvous time with the target spacecraft and the energy constraint of orbital maneuver of the servicing spacecraft.

At present, on-orbit spacecraft are mainly located in three orbit regions—low earth orbit (LEO; orbit altitude: 200–1500 km), medium earth orbit (MEO; orbit altitude: 19,000–23,000 km) and high orbit (GEO; orbit altitude: 36,000 km). According to the American UCS database,¹ as of May 31, 2013, the number of

¹Union of Concerned Scientists. UCS Satellite Database [EB/OL]. http://www.ucsusa.org/nuclear-weap-ons_and_global_security/space_weapons/technical_issues/ucs-satellite-database.html.

Fig. 5.7 Distribution of on-orbit spacecraft in different orbits



on-orbit spacecraft was 1071, consisting of 523 LEO satellites, 75 MEO satellites, 435 GEO satellites, and 38 highly elliptical Earth orbit (HEO) satellites. Figure 5.7 shows the distribution of on-orbit spacecraft in different orbits.

Therefore, aiming at the target spacecraft in three different orbit regions (LEO, MEO and GEO), we need to design the orbit of the servicing spacecraft separately. For the multi-target orbit rendezvous method based on traversing point, the servicing spacecraft and the target spacecraft are not required to be coplanar. However, if the servicing spacecraft is coplanar with the most important target spacecraft in the target spacecraft group, the chances of the orbital rendezvous between the servicing spacecraft and this target spacecraft will be increased.

5.3.2 *Rendezvous Orbit: Design Method*

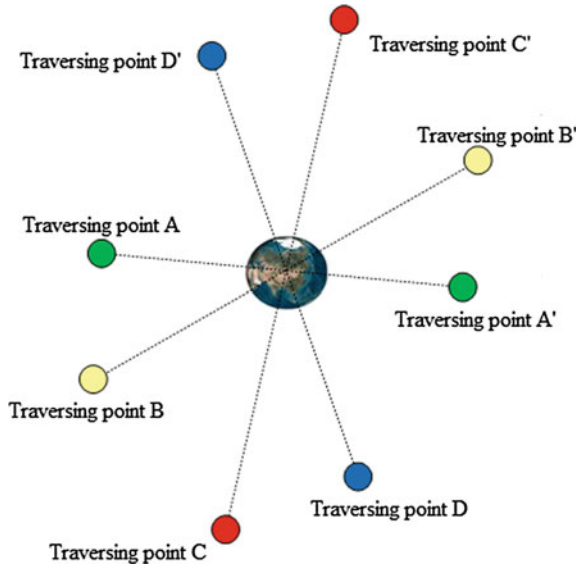
Though the target spacecraft in different orbit regions are not coplanar with the orbit plane of the servicing spacecraft deployed in the regions, according to the concept of traversing point, it is certain that all the target spacecraft in this region will form several pairs of traversing points in the orbit plane of the servicing spacecraft. To achieve the orbital rendezvous of the servicing spacecraft and multiple target spacecraft more effectively, the design of the rendezvous orbit of the servicing spacecraft in this orbit plane should be optimized.

Traversing points are spatial points with time stamps. Therefore, besides passing through these traversing points, the rendezvous orbit of the servicing spacecraft should also pass through them at their marked time. If there are only two traversing points to pass through, according to the Lambert Time Theorem, we can design a rendezvous orbit that passes through them both and the time of passing will also meet the requirement of the marked time. However, if the servicing spacecraft are required to pass through three or more traversing points, then it would be difficult to design a rendezvous orbit. In such a case, an orbit maneuver is needed for the servicing spacecraft.

We assume that there are four target spacecraft, and they will form eight traversing points in the orbit plane of the servicing spacecraft, as is shown in Fig. 5.8.

To make the servicing spacecraft approach these traversing points as close as possible, we first need to conduct orbit fitting for these traversing points. According

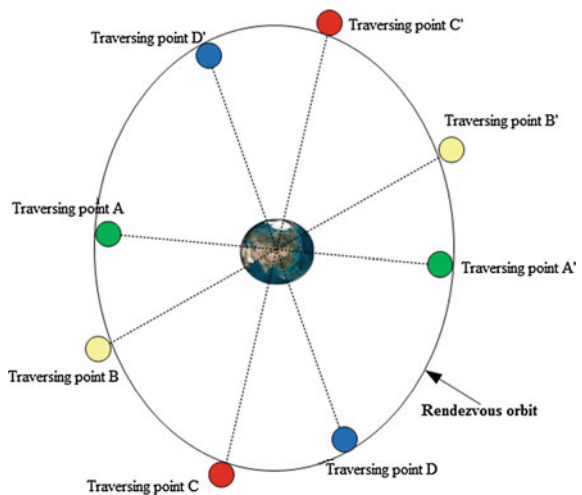
Fig. 5.8 Schematic figure of four target spacecraft and eight traversing points



to orbit dynamics, the fitting orbit should be an elliptic cone curve and the Earth-center should be on a focal point on the fitting curve, as is shown in Fig. 5.9.

After that, we calculate the time when the servicing spacecraft passes through each traversing point respectively according to the fitting orbit. Then we compare the time with the marked time when the target spacecraft pass through these traversing points. By adjusting the initial phase of the servicing spacecraft or the time when the servicing spacecraft passes through the perigee, we can ensure that the servicing spacecraft passes through the traversing points at their marked time as

Fig. 5.9 Rendezvous orbit based on traversing point fitting



punctually as possible. If the servicing spacecraft cannot pass through some traversing points at their marked time, or if it cannot pass through the traversing points with one rendezvous orbit, then the orbital rendezvous at the traversing points can only be achieved by orbit control in the orbit plane.

5.3.3 Orbital Rendezvous: Control Method

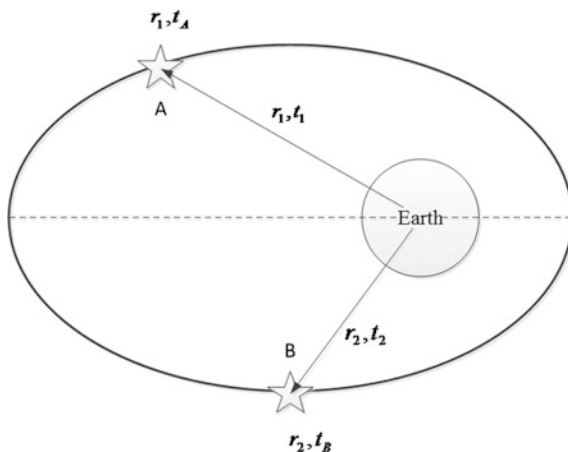
Based on a traversing point set, we can design an optimized rendezvous orbit by curve fitting. However, as traversing points are special positions marked by time stamps, and the optimized rendezvous orbit is designed to have the minimum sum of total distances, we can only ensure that the rendezvous orbit is as close as possible to the traversing point set. However, when the servicing spacecraft in the rendezvous orbit passes through or nears a traversing point, we cannot ensure that the target spacecraft can pass through the traversing point there on time. In general, the target spacecraft is not controllable or even non-cooperative. Therefore, orbit control of the servicing spacecraft is needed to ensure that it reaches the vicinity of a traversing point on time when a target spacecraft passes through it.

In this section, according to the relative position difference of a traversing point and a rendezvous orbit, we will propose three control methods for orbital rendezvous—phase adjustment, time-fixed orbital maneuvering and separate rendezvous trajectory.

(1) Method 1: Phase adjustment

This method is mainly used in multi-target orbital rendezvous missions in which the rendezvous orbit passes through traversing points correctly and the rendezvous time is not strictly required. It is shown in Fig. 5.10.

Fig. 5.10 Time and position relationship among traversing points and rendezvous orbit



In Fig. 5.10, traversing points A and B are both in the rendezvous orbit. By designing the time when the rendezvous orbit passes through the perigee, time t_1 when the servicing spacecraft in the rendezvous orbit reaches point A can be made equal to time t_A when target spacecraft 1 passes through traversing point A . That is, the orbital rendezvous of the servicing spacecraft and the target spacecraft 1 at traversing point A can be achieved without an orbit control. However, time t_2 when the servicing spacecraft reaches traversing point B is different from time t_B when target spacecraft 2 passes through traversing point B . And there is a time difference between them ($\Delta t = t_2 - t_B$). After t_1 , the servicing spacecraft moves along the rendezvous orbit and reaches point B . If it still cannot conduct rendezvous with target spacecraft 2, then orbit control of the servicing spacecraft is required.

By phase adjustment, the time when the servicing spacecraft passes through traversing point B again can be adjusted to $t'_2 = t_2 - \Delta t$, as is shown in Fig. 5.11.

The method of phase adjustment shown above is to conduct orbit maneuver at the apogee of the rendezvous orbit in order to make the servicing spacecraft go into a phasing orbit with the same apogee. As the dotted line shows in Fig. 5.11, t_a is the time when the servicing spacecraft reaches the apogee before phasing, and t'_a is the time when the servicing spacecraft reaches the apogee after phasing. By means of phasing, after completing a period in the phasing orbit, the servicing spacecraft returns to the apogee and then goes back into the original rendezvous orbit through maneuvering. The time when it returns to the apogee ensures that it will conduct rendezvous with the target spacecraft when it moves along the rendezvous orbit and reaches point B . In other words, the relation between time t'_2 when the servicing spacecraft reaches point B and time t_B when the target spacecraft reaches point B is:

$$t'_2 = t_B + nT_2 \tag{5.10}$$

Here, T_2 is the orbit period of target spacecraft 2 and n is an integer that is equal to or greater than 0.

According to the method above, the servicing spacecraft will need many times of phase adjustment as the number of target spacecraft increases. In the most extreme case, for N target spacecraft, the servicing spacecraft will need to conduct $N-1$

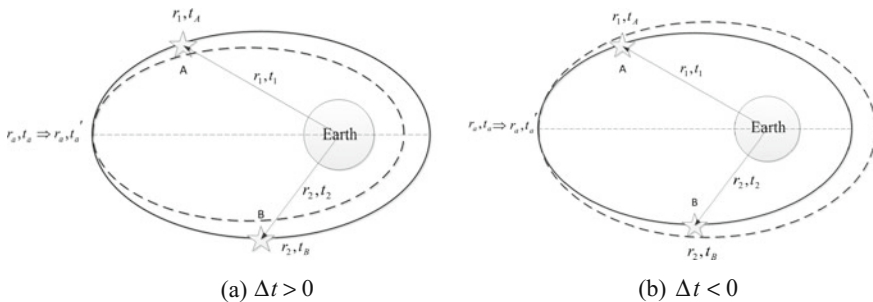


Fig. 5.11 Schematic figure of phase adjustment. a $\Delta t > 0$ b $\Delta t < 0$

times of phase adjustment. Apparently, it means more rendezvous time and multiple times of control. As a result, a fast multi-target spacecraft orbital rendezvous is not possible.

(2) Method 2: Time-fixed orbital maneuvering

This method is mainly applied in multi-target orbital rendezvous missions in which the rendezvous orbit can pass through the traversing points correctly and there are strict requirements for rendezvous time.

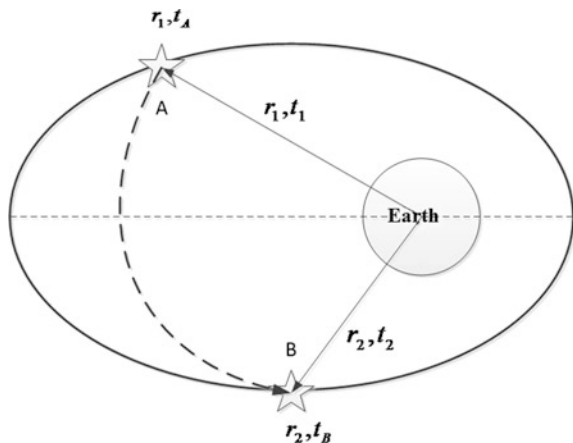
As is shown in Fig. 5.6, the rendezvous orbit passes through traversing points A and B, and the servicing spacecraft conducts a rendezvous with target spacecraft 1 at t_1 and at traversing point A. However, time t_2 when the servicing spacecraft reaches traversing point B is different from time t_B when target spacecraft 2 passes through traversing point B, meaning there is a time difference. If it is required by the mission that the servicing spacecraft should conduct rendezvous with target spacecraft 2 at t_2 , with $\Delta t = t_2 - t_1$ not long enough for a phase adjustment, the servicing spacecraft can only travel from traversing point A to traversing point B along a time-fixed rendezvous orbit, as is shown in Fig. 5.12.

In Fig. 5.12, the dotted line is the trajectory of time-fixed orbital maneuvering. According to this method, the servicing spacecraft will need multiple times of orbit maneuver as the number of target spacecraft increases. In the most extreme case, for N target spacecraft, the servicing spacecraft will need to conduct $N-1$ times of orbit maneuver. Clearly, even though it is conducted in the orbit plane, the maneuver still consumes more energy and needs more orbit control, thus inevitably increasing the complexity of the orbit control.

(3) Method 3: Separate rendezvous trajectory

This method is mainly used in the multi-target orbital rendezvous missions when the traversing points are not in the rendezvous orbit. In this method, it is necessary to separate a rendezvous trajectory from the rendezvous orbit and make it connected

Fig. 5.12 Schematic figure of time-fixed orbital maneuvering



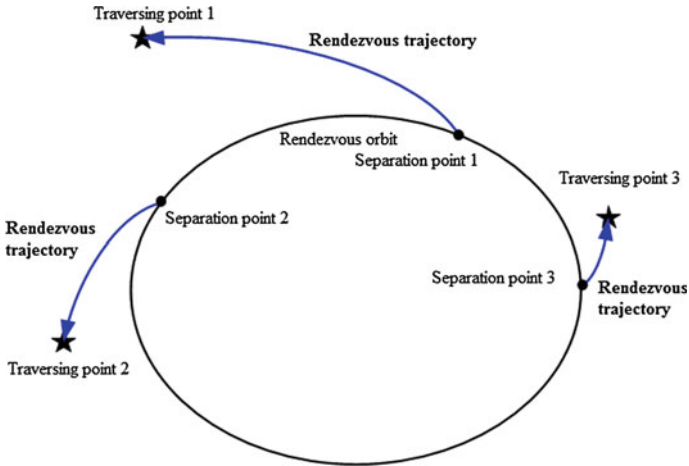


Fig. 5.13 Schematic figure of rendezvous trajectory

to the traversing points which are far away from the rendezvous orbit, as is shown in Fig. 5.13.

In Fig. 5.13, the separation points are in the rendezvous orbit and the trajectories connecting the separation points with the traversing points are called rendezvous trajectories. Here, the term “trajectory” means that it is not a closed curve but a part of a conical curve separated from the rendezvous orbit.

Every traversing point has its time constraint. When separation points are determined, a rendezvous trajectory can be solely determined by the Lambert Time Theorem. Obviously, for a certain traversing point, different separation points will have different rendezvous trajectories.

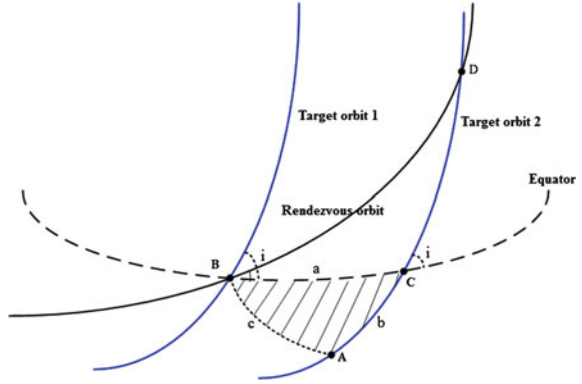
This method differs from the time-fixed orbital maneuvering method in the fact that it aims at achieving the orbital rendezvous with traversing points that are not in the rendezvous orbit.

5.4 Non-Coplanar Homogeneous Multi-Target Rendezvous Orbit: Design Method

A non-coplanar homogeneous multi-target orbital rendezvous refers to the orbital rendezvous of a servicing spacecraft and multiple target spacecraft that are with the same orbit type and altitude and are evenly distributed in space. An example is the case when the target spacecraft are the satellites in a certain Walker Constellation. It is shown in Fig. 5.14.

In Fig. 5.14, target orbits 1 and 2 are orbits in the first and the second orbit planes of a Walker Constellation $N/P/F$ respectively. Point B is the ascending node of target satellite 1 while point C is the ascending node of target satellite 2. When

Fig. 5.14 Spatial geometric relationship among rendezvous orbit and satellite orbits in Walker Constellation



the first satellite in the first orbit plane is at point B , the last satellite in the second orbit plane is at point A . When travelling along a rendezvous orbit from point B to point D , a servicing spacecraft conducts a rendezvous with target satellite 1 at point B , and with target satellite 2 at point D . Then a spherical triangle is formed by points A , B and C .

We assume that A, B, C and a, b, c are the three angles and three sides of the spherical triangle respectively, then:

$$\begin{cases} C = i \\ b = \frac{2\pi}{S} - \frac{2\pi}{N} \cdot F \\ a = \frac{2\pi}{P} \end{cases} \quad (5.11)$$

In Eq. (5.11), i is the orbit inclination of the target orbit; N is the total number of satellites in the Walker Constellation; P is the number of orbit planes in the Walker Constellation; S is the number of satellites in each orbit plane in the Walker Constellation; F is the phase factor.

Using the cotangent four-part formula, we obtain:

$$\begin{cases} \operatorname{tg}A = \frac{\sin C}{\operatorname{ctg}a \cdot \sin b - \cos b \cdot \cos C} \\ \operatorname{tg}B = \frac{\sin C}{\operatorname{ctg}b \cdot \sin a - \cos a \cdot \cos C} \end{cases} \quad (5.12)$$

According to the properties of the Walker Constellation, the two target satellites are both in circular orbits and they are at the same velocity and the following can be obtained:

$$\widehat{BD} = \widehat{CD}$$

In spherical triangle ABD :

$$\angle DBA = \angle DAB = \angle A$$

Then the orbit inclination of the rendezvous orbit is:

$$i_1 = \angle DBC = \angle A - \angle B$$

If we adjust the phase of the servicing spacecraft, the following can be obtained:

$$\Delta f = \frac{2\pi}{S}$$

Then it can conduct rendezvous with adjacent target satellites which are coplanar with the target satellites in the Walker Constellation.

Similarly, for a servicing spacecraft, with each phase adjustment of $m\Delta f (1 \leq m \leq S - 1)$, it will be able to conduct rendezvous with other target satellites in the Walker Constellation. Therefore, when the servicing spacecraft adjusts its phase for $S - 1$ times in the rendezvous orbit plane, it will conduct rendezvous with $3 * S$ target satellites in three adjacent orbit planes in the Walker Constellation. If each phase adjustment can be completed in one orbit period, then the total time needed to achieve an orbital rendezvous will be:

$$T = (S - 1) \times T_m + S \times T_m = (2 \times S - 1)T_m \quad (5.13)$$

In Eq. (5.13), T_m is the orbit period of the target satellite. Here, we will take a Walker Constellation as an example. Its constellation configuration is $24/4/1$, with an orbit inclination of 55° and an orbit altitude of 20,200 km. We will design a rendezvous orbit which can conduct rendezvous with three target satellites—Sat 11, Sat 26 and Sat 41—in the Constellation.

From Eq. (5.11), we know:

$$C = 55^\circ, \quad a = 90^\circ, \quad b = 45^\circ$$

When it is substituted into Eq. (5.12), the following can be obtained:

$$A = 116.341^\circ, \quad B = 39.3227^\circ$$

So the inclination of the rendezvous orbit is:

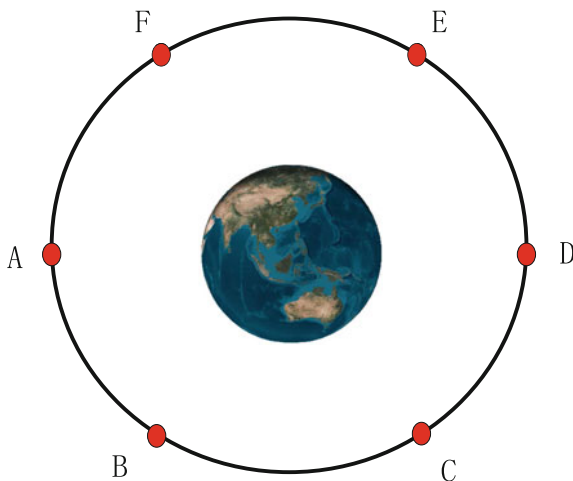
$$i_1 = 77.01^\circ$$

In sum, the orbit parameters of the servicing spacecraft are shown in Table 5.1.

The satellites in the Walker Constellation pass through the rendezvous orbit plane and form six traversing points A, B, C, D, E and F. These traversing points

Table 5.1 Design results of rendezvous orbit

Semi-major axis (km)	Eccentricity	Orbit inclination (deg)	Right ascension of ascending node (deg)	Argument of perigee (deg)	Initial phase (deg)
Re+20,200	0	77.01	Same with sat 11	Same with sat 11	Same with sat 11

Fig. 5.15 Schematic figure of distribution of traversing points

are evenly distributed at 60° intervals in the rendezvous orbit of the servicing spacecraft, as is shown in Fig. 5.15.

With software STK, we can simulate the design result of the rendezvous orbit. The simulation period is 24 h. Figure 5.16 shows the variation in relative distance between the servicing spacecraft and three target satellites in three adjacent orbit planes in the Walker Constellation.

It is clear that, in one orbit period, there are two chances for the rendezvous between the servicing spacecraft and three target satellites.

With a phase adjustment of 60° of the servicing spacecraft, an accurate rendezvous with Sat 12, Sat 21, and Sat 42 can be achieved. Similarly, for each phase adjustment of 60° of the servicing spacecraft, the orbital rendezvous of the servicing spacecraft and three target satellites in three adjacent orbit planes can be achieved respectively. Hence, by five phase adjustments, the servicing spacecraft can achieve rendezvous in its rendezvous orbit plane with 18 target satellites in three orbit planes in the Walker Constellation. If every phase adjustment can be conducted within an orbit period, the total time needed for the orbital rendezvous is:

$$T = 5 \times T_m + 6 \times T_m = 11T_m$$

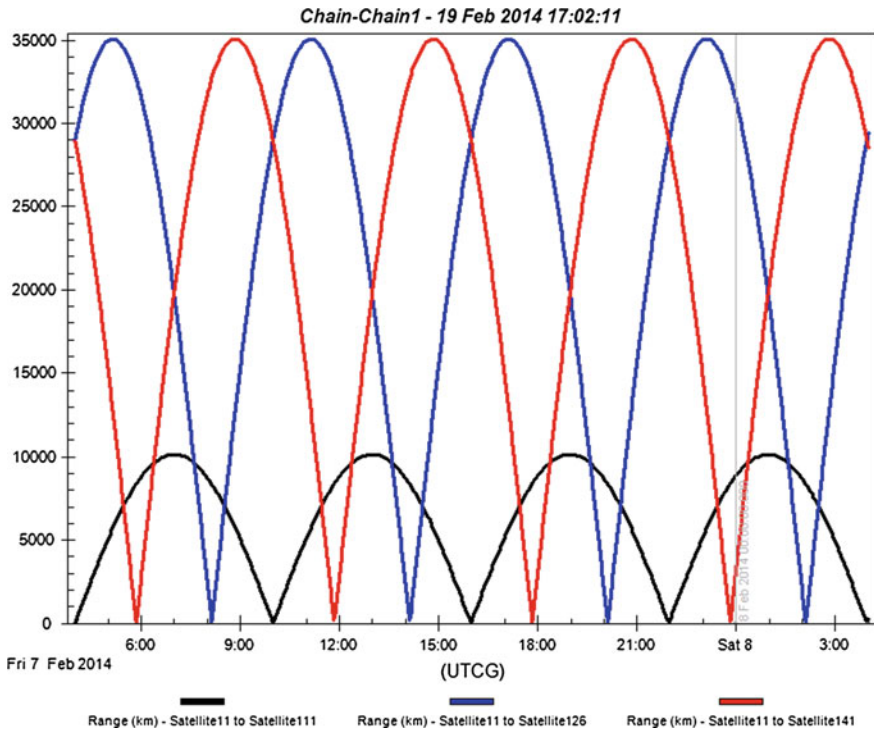


Fig. 5.16 Relative distance between servicing spacecraft and three target satellites

Here, T_m is the orbit period of the target satellite, namely, 12 h. That is to say, the servicing spacecraft can achieve its orbital rendezvous with 18 satellites in the Walker Constellation within 132 h.

5.5 Non-Coplanar Heterogeneous Multi-Target Rendezvous Orbit: Design Method

A non-coplanar heterogeneous multi-target orbital rendezvous refers to the orbital rendezvous of a servicing spacecraft and multiple target spacecraft which differ in orbit parameters such as orbit plane, orbit type, and orbit altitude. An example is when the target spacecraft are operating respectively in circular orbits and elliptical orbits that are non-coplanar.

5.5.1 Design Procedures

The design procedures of a non-coplanar multi-target rendezvous orbit are as follows:

(1) Determine the rendezvous orbit plane and traversing points

As we know, an orbit plane is determined by its orbit inclination and the right ascension of the ascending node. So, if the rendezvous orbit plane is previously determined, we can use the target spacecraft's orbits to directly determine the traversing points of the target spacecraft in the rendezvous orbit plane. If the rendezvous orbit is not previously determined, we then need to optimize the design of the orbit inclination and the right ascension of the ascending node of the rendezvous orbit.

(2) Determine the traversing point set

If no key target is specified particularly, for m target orbits, there will be $2m$ traversing points. Then the traversing point set can have 3^m possibilities. For each possibility, there are three likelihoods—the rendezvous orbit passes through both of the two traversing points or either one of the traversing points, so we need to explore every likelihood through a search method.

(3) Optimize the design of a rendezvous orbit

After we have the traversing point set ready and know the orbit is elliptical, we can determine the shape of the rendezvous orbit by maximum likelihood estimation. The fitting results are semi-major axis, eccentricity and perigee argument.

(4) Optimize the design of a rendezvous trajectory

For the traversing time of each traversing point, in designing the time of perigee passage of a rendezvous orbit, it is necessary that the servicing spacecraft and the target spacecraft reach a traversing point simultaneously. If the fitting rendezvous orbit is quite far away from a certain traversing point, we then need to separate from the rendezvous orbit a rendezvous trajectory which passes through the traversing point. The design of this rendezvous trajectory should be based on the maneuvering capability of the servicing spacecraft and the specific goals of an optimized design. A general design goal could be time optimization or correction speed optimization, or a weighted comprehensive combination of both.

5.5.2 Rendezvous Orbit: Design Method

In essence, rendezvous orbit design is to fit an elliptical orbit that satisfies Kepler's Laws based on traversing points formed by the target spacecraft in the rendezvous orbit plane in order to make the sum of total distances from each traversing point to

the elliptical orbit relatively small. This will ensure the servicing spacecraft's maximum approximation to the target spacecraft in space. Good timing needs to be achieved through the design of the initial phase of the servicing spacecraft (see Sect. 5.5.4).

We assume there are m traversing points in a certain rendezvous orbit plane, and their position coordinates can be expressed as:

$$(r_1, \phi_1), (r_2, \phi_2), \dots, (r_m, \phi_m)$$

We suppose that the orbit parameters of the rendezvous orbit are $(a, e, i, \Omega, \omega, \tau)$, then the position coordinates of the m traversing points above can also be expressed as:

$$(r_1, \omega + f_1), (r_2, \omega + f_2), \dots, (r_m, \omega + f_m)$$

Here, $\phi = \omega + f$.

If the angles are expressed as relative parameters, then the coordinates of the m traversing points above can also be written as:

$$(r_1, \omega + f_1), (r_2, \omega + f_1 + \Delta f_2), \dots, (r_m, \omega + f_1 + \Delta f_m)$$

Here, $f_n = f_1 + \Delta f_n (n = 2, \dots, m)$, as is shown in Fig. 5.17.

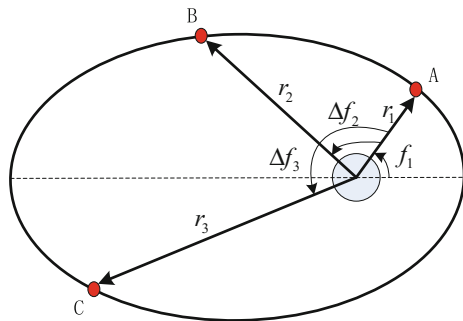
If the rendezvous orbit plane and the positions of the traversing points in the plane are determined, according to two-body motion equations, the rendezvous orbit parameters left to be designed are (a, e, ω) , and

$$\omega = \phi_1 - f_1 \tag{5.14}$$

Here: ϕ_1 is the argument of the ascending node of the first traversing point in the rendezvous orbit plane; f_1 is the corresponding true anomaly of the first traversing point in the rendezvous orbit.

The position coordinates of the traversing points, $(r_1, \phi_1), (r_2, \phi_2), \dots, (r_m, \phi_m)$, are given. In designing the rendezvous orbit, we let $\xi = (a, e, f_1)^T$ be the optimized design parameter. That is, the $2m$ traversing points will all satisfy:

Fig. 5.17 Schematic figure of relative position relationship among traversing points in rendezvous orbit plane



$$r_k = f(\xi, k) = \frac{a(1 - e^2)}{1 + e \cos(f_1 + \Delta f_k)} \quad (1 \leq k \leq 2m) \quad (5.15)$$

The given iterative formula of maximum likelihood estimation is:

$$\xi_{n+1} = \xi_n - (\mathbf{\Gamma}^T \mathbf{\Gamma})^{-1} \mathbf{\Gamma}^T \mathbf{v}(\xi_n) \quad (5.16)$$

Here,

$$\mathbf{\Gamma}(\xi_n) = [\nabla_{\xi}, \mathbf{v}^T(\xi_n)]^T = \begin{bmatrix} -[\nabla_{\xi}, f^T(r_1)]^T \\ \vdots \\ -[\nabla_{\xi}, f^T(r_M)]^T \end{bmatrix}$$

$$\nabla_{\xi} = \left[\frac{\partial}{\partial a}, \frac{\partial}{\partial e}, \frac{\partial}{\partial f_1} \right]^T$$

$$\nabla_{\xi}, f^T(r_k) = \begin{bmatrix} \frac{\partial r_k}{\partial a} \\ \frac{\partial r_k}{\partial e} \\ \frac{\partial r_k}{\partial f_1} \end{bmatrix} = \begin{bmatrix} \frac{1-e^2}{1+e \cos(f_1 + \Delta f_k)} \\ \frac{a(e^2-1) \cos(f_1 + \Delta f_k)}{(1+e \cos(f_1 + \Delta f_k))^2} - \frac{2ae}{1+e \cos(f_1 + \Delta f_k)} \\ \frac{ae(1-e^2) \sin(f_1 + \Delta f_k)}{(1+e \cos(f_1 + \Delta f_k))^2} \end{bmatrix}$$

$$\mathbf{v}(\xi_n) = \begin{bmatrix} [r_1 - f(\xi, 1)] \\ \vdots \\ [r_M - f(\xi, M)] \end{bmatrix}_{M \times 1}$$

In general, the traversing point closest to Earth-center can be approximately seen as the perigee of the rendezvous orbit. The rendezvous orbit is approximately circular, so the initial conditions of iteration are as follows:

$$\begin{cases} a = r_k = \text{Min}(r_i) \\ e = 10^{-8} \\ f_1 = -\Delta f_k \end{cases}$$

It should be noted that in the iterative procedure, the constraint conditions which are needed to be satisfied are:

$$\begin{cases} e \geq 0 \\ 0 \leq f_1 \leq 2\pi \end{cases}$$

The optimized design method of a rendezvous orbit with software MATLAB is given in Appendix A.

5.5.3 Traversing Point Set: Determination Method

According to their properties, traversing points usually appear in pairs with a polar angle difference of 180° . That is, for m target orbits, there should be $2m$ traversing points. The number of traversing points, n , available for use in the design of a rendezvous orbit satisfies $m \leq n \leq 2m$. Apparently, when the number of traversing point sets, n , is different, the rendezvous orbit designed on the basis of this number is very likely to be different.

For example, three target orbits will form six traversing points in a rendezvous orbit plane, as is shown in Table 5.2.

For a rendezvous orbit, we assume that its iteration precision of the semi-major axis, the eccentricity and the perigee argument are 500 m, $1e^{-8}$ and 0.01° , respectively. The optimized design result is:

$$\xi = (7.72545e + 006 \text{ m}, 0.00378887, 0.109803^\circ)^T$$

When the first five traversing points are selected, the optimized design result is:

$$\xi = (7.6466e + 006 \text{ m}, 0.0191879, 0.711686^\circ)^T$$

Apparently, the rendezvous orbits designed on the basis of the two traversing point sets above are different, as is shown in Fig. 5.18.

For one target orbit, there are two traversing points A and B , so there will be three options for a traversing point set: (1) point A only; (2) point B only; (3) point A and point B simultaneously. Similarly, when there are n target orbits, there will be $2n$ traversing points and 3^n possibilities for traversing point sets.

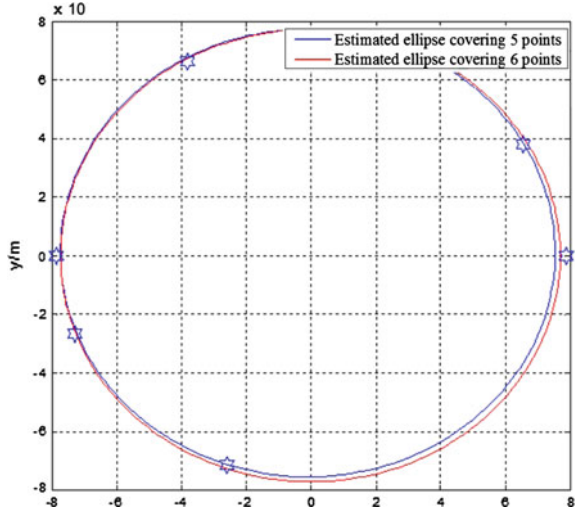
When both of the traversing points of a certain target orbit are selected, the rendezvous orbit to be designed will be closer to the two traversing points and further away from other traversing points. Hence, when we need to determine the traversing point set, the principles below are to be followed:

- (1) For a key target orbit, its two traversing points can be included in the traversing point set.

Table 5.2 Position Coordinates of six traversing points

Serial number of traversing point	Altitude (m)	Polar coordinate angle ($^\circ$)
1	1,200,000.0	30.0
2	1,300,000.0	120.0
3	1,400,000.0	200.0
4	1,250,000.0	250.0
5	1,500,000.0	180.0
6	1,500,000.0	0.0

Fig. 5.18 Comparison of design results of five traversing points and six traversing points



- (2) For a general target orbit, just one of its traversing points is to be selected and included in the traversing point set. The selection of two traversing points depends on the minimum distance between the rendezvous orbit and other traversing points.
- (3) When the target orbits are of the same importance, for every target orbit, one traversing point can be selected. Then the specific traversing point set can be decided by the minimum sum of total distances between the rendezvous orbit and each traversing point in the traversing point set.

5.5.4 Rendezvous Trajectory: Design Method

The design of a rendezvous orbit based on traversing point set can only determine the size and shape of the rendezvous orbit and the direction of perigee. A complete rendezvous orbit can be specified only when the time of perigee passage, τ , is determined.

As to the rendezvous with a single target spacecraft, i.e., when only one traversing point $[r_m, f_m]$ is to be selected, the rendezvous orbit can pass through the traversing point directly. By designing the time of perigee passage of the rendezvous orbit, the servicing spacecraft can pass through the traversing point along the rendezvous orbit exactly when the target spacecraft also passes through it. The requirement is:

$$\tau = t_m - \frac{E_m - e \sin E_m}{n} \tag{5.17}$$

Here, for the rendezvous orbit, a is its semi-major axis, e is its eccentricity, and $n = \sqrt{\frac{\mu}{a^3}}$ is its mean angular rate. E_m is the eccentric anomaly of the traversing point in the rendezvous orbit, and:

$$\operatorname{tg} \frac{E_m}{2} = \sqrt{\frac{1-e}{1+e}} \operatorname{tg} \frac{f_m}{2} \tag{5.18}$$

However, it will be more complicated when it comes to the rendezvous with multiple target spacecraft. Firstly, a single rendezvous orbit may not be able to pass through all traversing points. Secondly, even if it can pass through them all, it may not be able to meet the requirement for the traversing time. Hence, in this section, the control method of orbital rendezvous by separating a rendezvous trajectory proposed above will be adopted to determine the time of the perigee passage of the rendezvous orbit. It is shown in Fig. 5.19.

Apparently, for every traversing point, numerous rendezvous trajectories can be separated from any point of a rendezvous orbit. These trajectories differ from each other only in separation velocity and separation time. If there is a constraint on the separation velocity from the rendezvous orbit, some rendezvous trajectories can be eliminated, yet there are still multiple rendezvous trajectories. In other words, as long as the energy constraint is satisfied, there will be multiple rendezvous trajectories between a point in the rendezvous orbit and a traversing point. And each trajectory has its own separation time, i.e., it corresponds to a time of perigee passage.

We assume a point k expressed as $[r_k, f_k, t_k]$ in the rendezvous orbit, and a traversing point i expressed as $[r_i, f_i, t_i]$. The rendezvous trajectory separated from point k and then reaching traversing point i to conduct rendezvous is only related to time difference $\Delta t_k = t_i - t_k$. We can design the rendezvous trajectory by Lambert

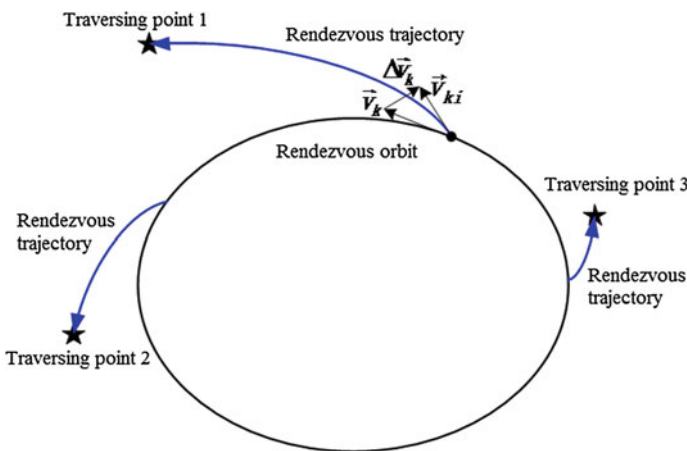


Fig. 5.19 Schematic figure of rendezvous trajectory

Time Theorem, and figure out the velocity increment needed for separating from the trajectory, namely,

$$\Delta \vec{v}_k = \vec{v}_{ki} - \vec{v}_k$$

Here, \vec{v}_k is the velocity vector of point k in the rendezvous orbit, and \vec{v}_{ki} is the velocity vector of point k in the rendezvous trajectory.

If $\Delta \vec{v}_k \leq \Delta V_{\max}$ and ΔV_{\max} is the maximum separation velocity a servicing spacecraft can provide, the rendezvous trajectory will be usable. Then corresponding to t_k , the time of perigee passage τ_k is:

$$\tau_k = t_k - \frac{E_k - e \sin E_k}{n} \quad (5.19)$$

Here, E_k is the eccentric anomaly of traversing point k in the rendezvous orbit, and

$$tg \frac{E_k}{2} = \sqrt{\frac{1-e}{1+e}} tg \frac{f_k}{2} \quad (5.20)$$

Similarly, if we find out all τ_k that meet the requirements above when $0 \leq t_k \leq T_p$, we can construct a set $[\tau_k]$ consisting of all rendezvous trajectories which separate from point k in the rendezvous orbit and then conduct rendezvous with traversing point i on time.

Therefore, for traversing point i , multiple rendezvous trajectories meeting the requirement on energy constraint can be separated from any point in the rendezvous orbit, i.e., there is a time set of perigee passage. They will form a time set of perigee passage for traversing point i and can be written as:

$$[\tau_i] = [\tau_{i1}] \cup [\tau_{i2}] \cup \dots \cup [\tau_{in}]$$

Here, n is the number of separation points available in the rendezvous orbit.

It can be seen that for every traversing point in a traversing point set, there is a time set of perigee passage $[\tau_i] (i = 1, \dots, m)$. Here, m is the number of traversing points in the traversing point set. The time of perigee passage when these traversing points all appear is the intersection of these sets, namely,

$$[\tau] = [\tau_1] \cap [\tau_2] \cap \dots \cap [\tau_m]$$

Finally, from the intersection set, we can choose the time of perigee passage which meets the requirements of the mission to the greatest extent.

Inversely, if τ , the time of perigee passage of the rendezvous orbit, is given, we can also figure out a separable arc section and its corresponding rendezvous trajectory.

Next, we will illustrate the design method above with a simulation case. We assume there are three target orbits. Their traversing point sets in the rendezvous orbit plane are shown in Table 5.3.

Table 5.3 Three target orbits and their corresponding traversing points

Target orbit	Traversing point	Altitude (m)	Angle measured in polar coordinate (°)	Traversing time (s)
1	1	1,500,000.0	30.0	500
	2	1,500,000.0	210.0	7500
2	3	1,400,000.0	200.0	1000
	4	1,400,000.0	20.0	7400
3	5	1,300,000.0	180.0	5000
	6	1,300,000.0	0	12,500

The goal of an optimized design is to minimize the sum of total velocity increments for the rendezvous with the three traversing points, so the objective function is:

$$J = \min \sum_{i=1}^3 \Delta V_i | \Delta V_i \leq V_L$$

Here, $V_L = 3000$ m/s is the maximum separation velocity of each rendezvous trajectory.

To search for possible solutions to the greatest extent, we include all the six traversing points in the traversing point set to design a rendezvous orbit. The result is:

$$\xi = (7771008.7714, 3.4916e - 017, 4.6824)^T$$

The optimized design result at the time of perigee passage is shown in Fig. 5.20.

It can be seen that the time of perigee passage of the optimal rendezvous orbit is 2045.26 s. The corrections of separation velocity of the rendezvous trajectories

Fig. 5.20 Search results of objective function

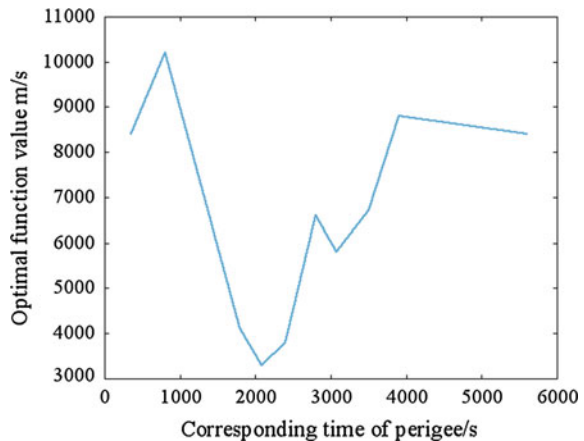
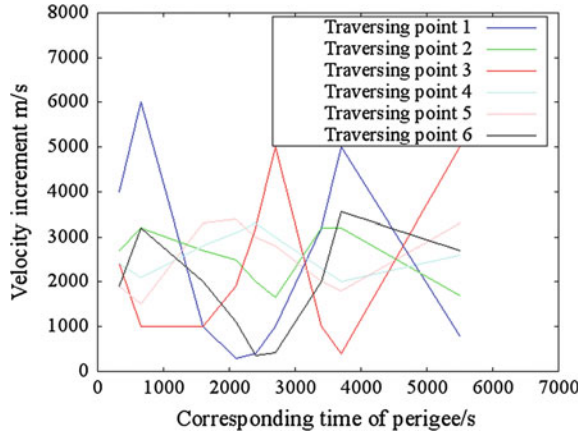


Fig. 5.21 Statistical graph of velocity increments



which conduct rendezvous with traversing points 1, 4 and 6 are 277.732, 965.089, and 2058.28 m/s, respectively (Fig. 5.21).

5.6 Simulation Analysis and Method Correction

5.6.1 Simulation of Orbital Rendezvous Based on Traversing Point

We assume that a servicing spacecraft is to conduct orbit rendezvous with three satellites. The orbit parameters of the three target satellites are shown in Table 5.4.

Requirements of the design: the total rendezvous time with the three target satellites is 24–26 h; the time interval is 2 h; the optimized goal is to minimize the sum of total correction speeds.

We assume that the right ascension of the ascending node is 180° and the orbit inclination of the rendezvous orbit is 45° . The six traversing points formed by the three target orbits in the rendezvous orbit plane are shown in Table 5.5.

Table 5.4 Orbital parameters of three target satellites

Serial number	Perigee (km)	Apogee (km)	Orbit inclination ($^\circ$)	Right ascension of ascending node ($^\circ$)	Perigee argument ($^\circ$)	Time of perigee passage (s)
1	202	1041	97.8	30	270	0
2	264	1050	97.9	90	270	1800
3	200	1000	97.8	150	270	3600

Table 5.5 Traversing points corresponding to target orbits

Serial number	Geocentric distance (m)	Argument (rad)	Time when passing through traversing point (s)	Target orbit period (s)
1	6.76565e+006	3.91172	878.891	5819.16
2	7.18142e+006	0.77013	3981.34	5819.16
3	6.73833e+006	4.8102	2457.2	5863.53
4	7.29589e+006	1.6686	5535.93	5863.53
5	6.78788e+006	5.66912	4562.67	5792.35
6	7.11597e+006	2.52753	7651.68	5792.35

Firstly, we will design a rendezvous orbit based on the six traversing points above. The design result is (Fig. 5.22):

$$\xi = (6.98556e + 006, 0.041125, 5.50577)^T$$

Secondly, we will search for the time of perigee passage of the rendezvous orbit. As the time of perigee passage is different, the separable arc section that can conduct rendezvous with a traversing point along a rendezvous trajectory is also different. Figure 5.23 shows how the separation arc of each traversing point changes as the time of perigee passage varies.

It can be seen from Fig. 5.23 that it is not the case that every time of perigee passage has a corresponding separation arc. Only the solution that covers at least

Fig. 5.22 Search results of objective function

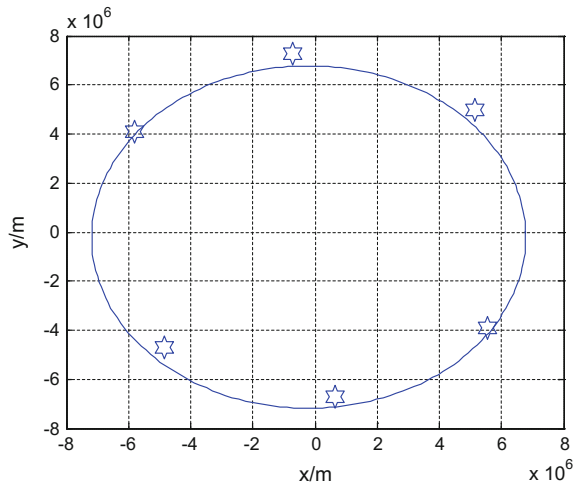
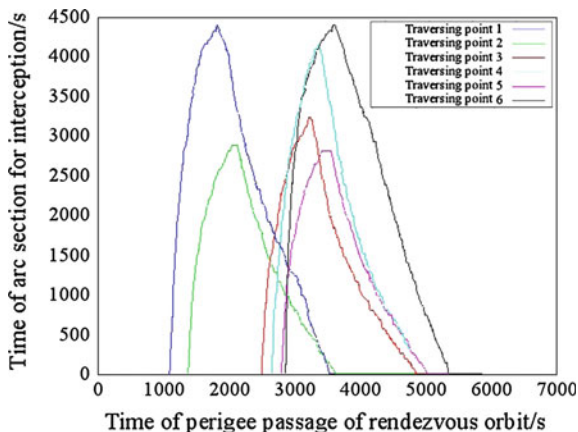


Fig. 5.23 Relationship between time of perigee passage of rendezvous orbit and separable arc section



three traversing points can meet the design requirements for conducting a rendezvous with three target spacecraft separately.

Figure 5.24 shows, when there is a separation arc, the change in minimum correction speeds needed to conduct a rendezvous with each traversing point within the required rendezvous time.

It can be seen from Fig. 5.24 that when there is an appropriate intercepting orbit for a target orbit, the interception of the other two target orbits will usually be poor. Hence, we need to consider the interception as a whole. Figure 5.25 shows how the total correction speed changes when there is a feasible solution for the rendezvous trajectory of all six traversing points.

It can be seen from Fig. 5.25 that the range of feasible solutions is relatively small, mainly between 2700 and 3500 s, and, at the same time, the total correction speed is relatively high.

Fig. 5.24 Minimum correction speeds of six traversing points

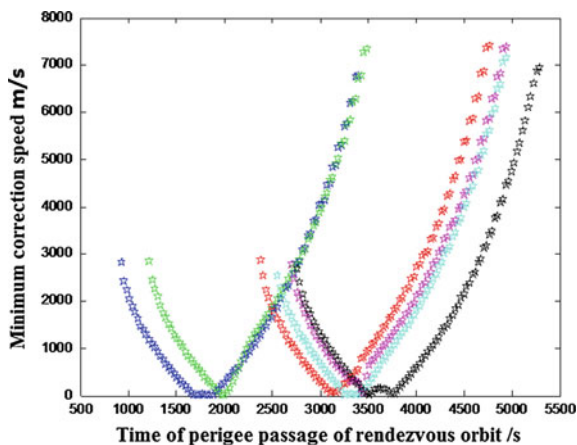
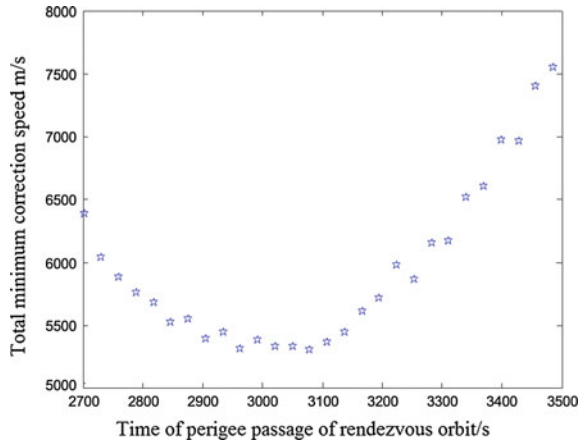


Fig. 5.25 Relationship between total correction speed and time of perigee passage



With all factors taken into account, we can specify that the time of perigee passage corresponding to the optimal rendezvous orbit is 3079.56 s. The optimal solution of the rendezvous trajectory is shown in Table 5.6.

5.6.2 Method Correction of Orbital Rendezvous Based on Traversing Point

From the simulation results in Sect. 5.5, we know that in designing a rendezvous orbit based on traversing point, though the rendezvous orbit is close to every

Table 5.6 Optimal solution of rendezvous trajectory

		Points 2	Points 3	Points 5
Rendezvous trajectory parameters	Semi-major axis (m)	9.86376 e ⁶	6.99999 e ⁶	6.86998 e ⁶
	Flight time (s)	1688.78	2870.2	2827.85
	Geocentric angles (rad)	3.13035	3.05491	2.80862
	Velocity of the orbit maneuver point (m/s)	8791.56	7264.2	7422.62
	Speed inclination of the orbit maneuver point (rad)	0.480838	0.00818902	0.0798481
	Correction speed (m/s)	4281.89	123.884	896.448
	Geocentric distance of the orbit maneuver point (m)	6.77034 e ⁶	7.26614 e ⁶	7.04765 e ⁶
	Geocentric distance of the target point (m)	7.18142 e ⁶	6.73833 e ⁶	6.78788 e ⁶
Separation time (s)	89,580	87,540	88,620	

traversing point, the correction speed needed is relatively high. The reasons are analyzed below:

- The period of the rendezvous orbit is relatively close to that of the target orbit.
- Time range for the rendezvous is relatively small.

Hence, this section suggests that we correct the semi-major axis of the rendezvous orbit to expand the time difference between the rendezvous orbit period and the target orbit period and to expand the time range of the rendezvous. This can help to expand the range of the separable arc section in the rendezvous orbit.

Based on the example in Sect. 5.5, we will increase the semi-major axis of the rendezvous orbit by 300 km and the time range of the rendezvous to 10 h to simulate the optimal design result of a rendezvous with three target satellites.

We assume that the right ascension of the ascending node of the rendezvous orbit is 180° and the orbit inclination is 45° . We also increase the semi-major axis of the rendezvous orbit by 300 km. After the correction, parameters of the rendezvous orbit are:

$$\xi = (7.28556e+006, 0.041125, 5.50577)^T$$

Figure 5.26 shows the separable arc sections in the rendezvous orbit corresponding to each traversing point. It is basically similar to the situation before the semi-major axis is adjusted, yet the separable time for a single traversing point increases.

Figure 5.27 shows, when there are separable arc sections, the minimum correction speed needed for the rendezvous with a target spacecraft passing through every traversing point within the required rendezvous time. It can be seen that the shape is basically similar to that before the correction of the semi-major axis.

Figure 5.28 shows, when conducting rendezvous with all target spacecraft, the change of the total correction speed. It can be seen that there is a relatively large

Fig. 5.26 Separable arc section of rendezvous orbit when semi-major axis increases by 300 km and time range is 10 h

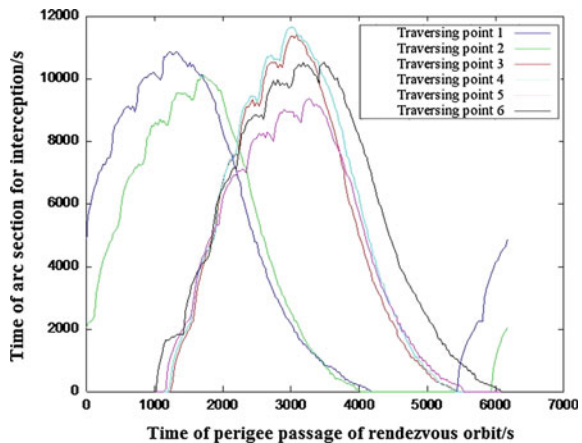


Fig. 5.27 Minimum correction speed when semi-major axis increases by 300 km and attack time range is 10 h

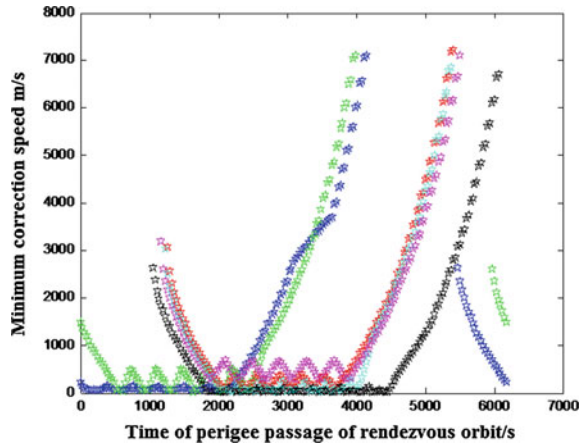
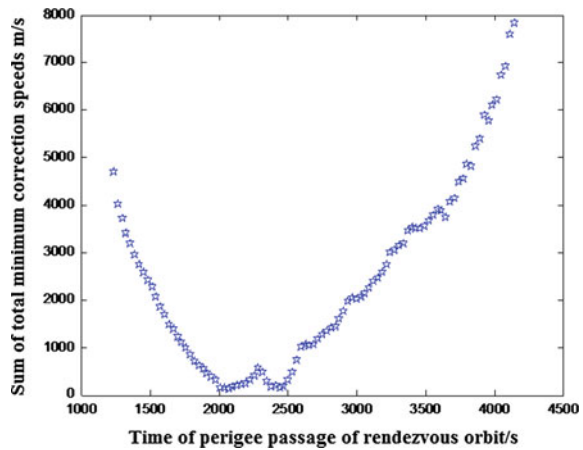


Fig. 5.28 Total correction speed of attack orbit when semi-major axis increases by 300 km and attack time range is 10 h



range for the feasible solutions, which are mainly between 1200 and 4000 s. Besides, compared with the time range of the rendezvous, i.e., 2 h, the range of solutions increases considerably, and the total correction speed decreases greatly.

Based on the simulation result above, we can specify that the time of perigee passage of the optimal rendezvous orbit is 2073.24 s. The optimal rendezvous trajectory is shown in Table 5.7.

Table 5.8 shows the design results when time ranges are 2 and 10 h respectively and the corrected semi-major axis are 100 and 300 km respectively.

It can be seen from Table 5.8 that, for the three non-coplanar target satellites in Low-Earth-Orbit, the optimal rendezvous plan is to increase the semi-major axis of the rendezvous orbit by 300 km under the 10 h rendezvous time constraint. At this time, the total correction speed needed to conduct rendezvous with the three target

Table 5.7 Optimal rendezvous trajectory when semi-major axis increases by 300 km and attack time range is 10 h

		Points 2	Points 4	Points 6
Rendezvous trajectory parameters	Semi-major axis (m)	7.2216 e ⁶	7.14064 e ⁶	7.28886 e ⁶
	Flight time (s)	1747.95	2806.61	2358.58
	Geocentric angles (rad)	1.88574	2.88844	2.53695
	Velocity of the orbit maneuver point (m/s)	7642.86	7614.57	7406.67
	Speed inclination of the orbit maneuver point (rad)	0.0136209	0.0143401	0.0398347
	Correction speed (m/s)	47.5991	72.5752	9.67316
	Geocentric distance of the orbit maneuver point (m)	7.01707 e ⁶	7.00509 e ⁶	7.27738 e ⁶
	Geocentric distance of the target point (m)	7.18142 e ⁶	7.29589 e ⁶	7.11597 e ⁶
Separation time (s)		95,340	120,000	121,140

Table 5.8 Comparison of design results when rendezvous time increases and when semi-major axis is corrected

Time range of rendezvous (h)	Increment in rendezvous orbit's semi-major axis (km)	Total correction speed (m/s)	Total rendezvous time (s)	Serial number of rendezvous traversing point
2	0	5.3022e+003	7.3868e+003	2, 3, 5
	100	4.9143e+003	7.4769e+003	1, 3, 6
	300	4.1431e+003	5.4721e+003	1, 4, 6
10	0	4.8273e+003	7.4411e+003	1, 3, 5
	100	2.8489e+003	7.8552e+003	2, 3, 6
	300	129.8475	6.9131e+003	2, 4, 6

spacecraft is 129.85 m/s. The rendezvous time with the three target spacecraft adds up to 6913 s.

In addition, we also find out from Table 5.8 that, on the one hand, under the 2 h rendezvous time constraint, when the semi-major axis of the rendezvous orbit increases, the total midcourse guidance correction speed slightly decreases. However, the change of the total interception time shows no significant regularity, and the corresponding traversing points of rendezvous are different. On the other

hand, when the time range increases to 10 h, with the increased value of the semi-major axis of the rendezvous orbit, the total midcourse guidance correction speed will decline remarkably. However, the total interception time shows no significant regularity, and the corresponding traversing points of rendezvous are also different.

5.7 Summary

The concept proposed in this chapter, i.e., traversing point, is very effective in solving the problems involved in non-coplanar multi-target orbital rendezvous. The orbital rendezvous method based on traversing point turns the non-coplanar orbital rendezvous problem in space into a coplanar one. This method does not impose any restrictions on the position and the number of orbit planes of the target spacecraft. It is a “one-to-many” orbit rendezvous mode in its real sense. In other words, a servicing spacecraft can conduct orbit rendezvous with multiple non-coplanar target spacecraft without changing its orbit plane. This method greatly reduces the cost of multi-target rendezvous and improves the efficiency of orbital rendezvous. It has broad applications.

According to the different orbit configurations of multiple target spacecraft, this chapter proposes the multi-target orbital rendezvous method for both non-coplanar homogeneous target spacecraft and non-coplanar heterogeneous target spacecraft. Both methods achieve multi-target rendezvous by the traversing points formed by the target spacecraft in the rendezvous orbit plane. For the rendezvous with multiple satellites in the Walker Constellation, a specific design method of the rendezvous orbit is given. For the non-coplanar heterogeneous multi-target orbital rendezvous, after offering the design procedures of the rendezvous orbit, we propose the design methods for the rendezvous orbit and the rendezvous trajectory. Finally, through the analysis of a typical simulation case, we propose a correction method of non-coplanar multi-target orbital rendezvous based on the traversing point. It is achieved by extending the semi-major axis of the rendezvous orbit and the range of rendezvous time. By correcting the rendezvous orbit, the demand for separation velocity can be reduced effectively, thus making the method more practical.

Chapter 6

Theory and Design Method of Initiative Approaching Orbit

With the improvement of space resolution ratio and communication capacity, the spacecraft is becoming heavier, and more costs in manufacturing and launching are required. So on-orbit services for spacecraft have been put on the agenda.

Besides, human space activities are becoming more frequent and over 90 % of space debris is ineffective or uncontrolled, which pose threats to on-orbit spacecraft. Thus, a fast or slow approach to on-orbit cooperative or non-cooperative targets has become the premise and foundation for space missions to carry out on-orbit services and space debris cleaning.

6.1 Initiative Approaching Orbit: Concept

The National Aeronautics and Space Administration (NASA) summarize seven key factors in on-orbit service research in On-Orbit Satellite Servicing Study Project Report¹: service category, executive body, rendezvous and docking, position, time delay, target design and target attitude. Rendezvous and docking means how a servicing spacecraft approaches its target spacecraft which is either cooperative or non-cooperative (Fig. 6.1).

As the mission requires, the servicing spacecraft takes the initiative to approach the target spacecraft through orbit and attitude control and this process is called initiative approach. After this, space missions, such as rendezvous and docking, space target surveillance, on-orbit service, are accomplished.

The initiative approach discussed in this section includes the approach phase in the approaching orbit and the final approach phase in the final approaching orbit. The two spacecraft involved are called the approaching spacecraft and the target spacecraft respectively.

¹NASA Goddard Space Flight Center. On-Orbit Satellite Servicing Study Project Report [EB/OL]. <http://servicestudy.gsfc.nasa.gov/>, retrieved in October 2011.

Service type	Executive body	Rendezvous & docking	Position	Time delay	Target design	Target attitude
...						
Fault maintenance	Robot autonomy	Non-cooperative autonomy	Solar-terrestrial Lagrangian point	Long	Space debris	Rotate
On-orbit assembling	Robot remote control	Cooperative autonomy	Earth-Moon Lagrangian point	Middle	Characteristic body without rendezvous	Controllable
Module replacement	Astronaut		HEO			
Refueling	Astronaut + Mechanical arm	Man-in-the-loop	GEO	Short	Characteristic body with rendezvous	Uncontrollable
Orbit modification			LEO			

Fig. 6.1 Research scope of on-orbit service

The approaching orbits include a phasing orbit and a long-distance approaching orbit. The phasing orbit is used to reduce the orbit phase angle between the approaching spacecraft and the target spacecraft. After phasing, the approaching spacecraft is very close to the target orbit. Then the long-distance rendezvous can be conducted. The long-distance approaching orbit shifts the approaching spacecraft to the first position which is very close to the target spacecraft. This process is called “target seeking”, which aims to further reduce orbit error.

The final approaching orbit is used to further reduce the relative distance between the approaching spacecraft and the target spacecraft to meet the final conditions of service. It should be noted that the non-centroid relative motion of the target spacecraft should be considered in the final approaching phase. It not only depends on the relative position of the spacecraft’s centroids, but also involves the relative spacecraft attitude change.

6.2 Approaching Orbit: Design

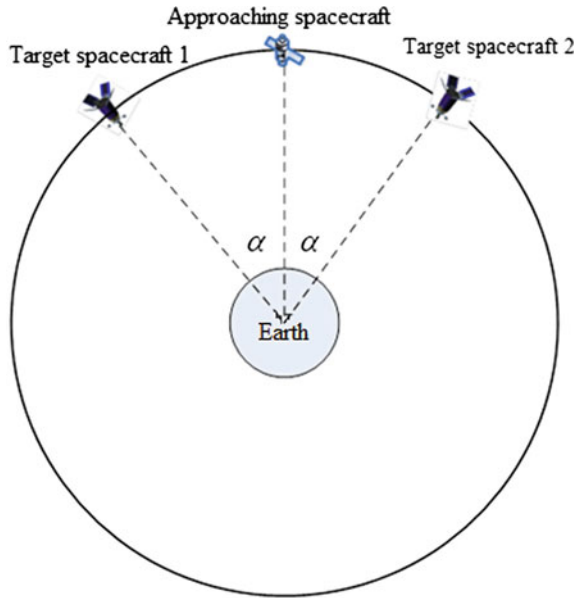
6.2.1 Phasing Orbit

The phasing orbit can move the initiative approaching spacecraft to the vicinity of the target spacecraft and reach the target. We suppose the approaching spacecraft and the target spacecraft are located in different phases of the same orbit as Fig. 6.2.

It can be seen that there are two different relative positions for the target spacecraft and the approaching spacecraft. Next, analyses of the target spacecraft’s phases in Fig. 6.2 are conducted.

In the first case, when the approaching spacecraft is in the front of the target spacecraft (in the direction of motion), there is the advanced angle. Define the phase difference as positive, namely, $\alpha > 0$.

Fig. 6.2 Initial phase of approaching spacecraft and target spacecraft



The phasing elliptical orbit is used to eliminate the phase difference between the two spacecraft. Specifically, the approaching spacecraft is maneuvered to a phasing elliptical orbit, the perigee of which is the initial orbit maneuver point. The geocentric distance of the apogee is larger than the radius R of the initial circular orbit. We suppose dh ($dh = r_a - R > 0$) is the difference in height between the apogee of the phasing orbit and the initial circular orbit. When the approaching spacecraft returns to the perigee after completing one circle in the phasing orbit, the operation phase of target spacecraft along the initial circular orbit can be defined as $2\pi + \alpha$. At this point, an impulse is applied to the approaching spacecraft to make it return to the initial circular orbit as Fig. 6.3.

In the second case, when the approaching spacecraft is behind the target spacecraft, there is the receding angle. The phasing difference is negative, namely, $\alpha < 0$.

The approaching spacecraft is first maneuvered onto a phasing elliptical orbit, the apogee of which is the initial orbit maneuver point. The geocentric distance of the perigee is smaller than the radius of the initial circular orbit. We suppose dh ($dh = r_p - R < 0$) is the difference in height between the phasing orbit's perigee and the initial circular orbit. When the approaching spacecraft returns to the apogee after travelling one circle in the phasing orbit, the operation phase of the target spacecraft along the initial circular orbit is $2\pi + \alpha$. At this point, an impulse is applied to the approaching spacecraft to make the spacecraft return to the initial circular orbit as Fig. 6.4.

Following the two phasing methods above, the phase difference between the approaching spacecraft and the target spacecraft can be eliminated after the

Fig. 6.3 Phasing elliptical orbit used to eliminate advance angle

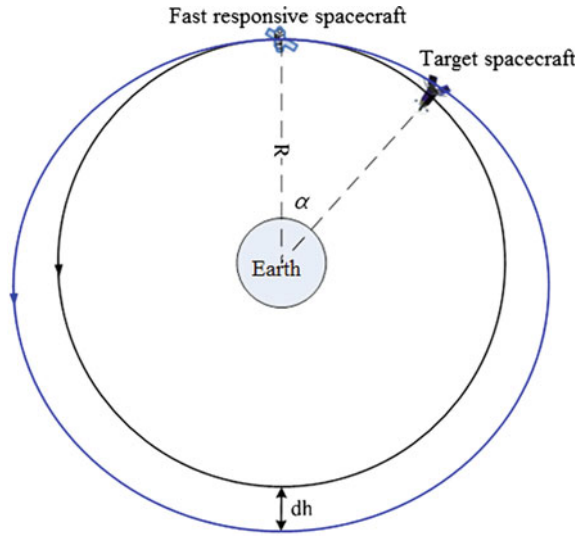
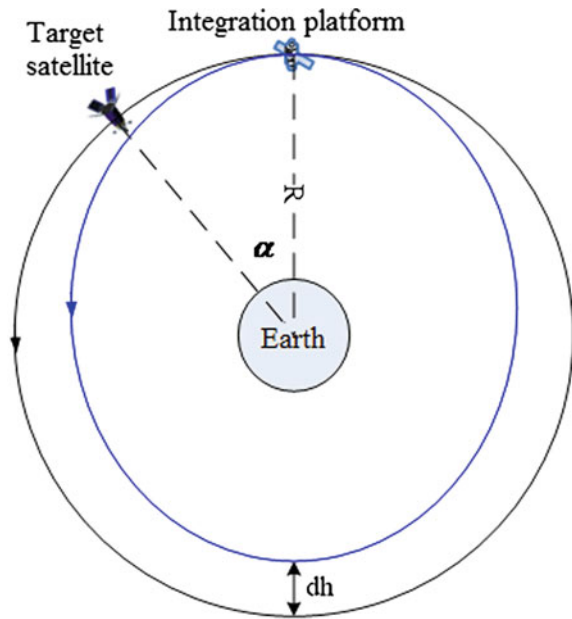


Fig. 6.4 Phasing elliptical orbit used to eliminate receding angle



approaching spacecraft completes one full circle in the phasing orbit. The time spent in this process is exactly the same as the orbit period of the phasing elliptical orbit:

$$t = 2\pi\sqrt{\frac{a^3}{\mu}} \tag{6.1}$$

Here, a is the semi-major axis of the phasing elliptical orbit. That is, $a = R + \frac{dh}{2}$, and

$$t \cdot n = \alpha + 2\pi \tag{6.2}$$

Here, n is the operation angular velocity of the target spacecraft in the initial circular orbit, namely, $n = \sqrt{\frac{\mu}{R^3}}$.

If we combine Eq. (6.1) with Eq. (6.2), the following Eq. (6.3) can be obtained:

$$dh = 2R \cdot \left(1 + \frac{\alpha}{2\pi}\right)^{\frac{2}{3}} - 2R \tag{6.3}$$

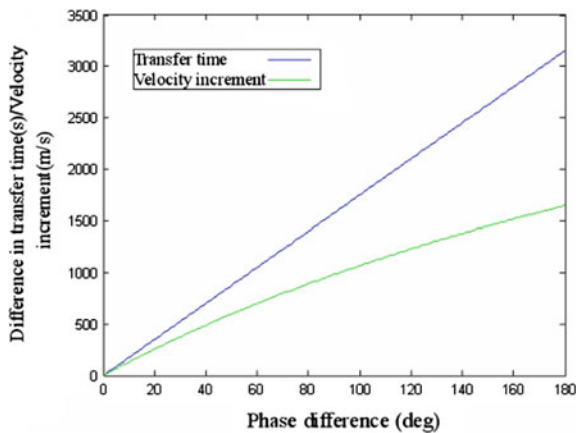
The total velocity increment needed here is:

$$\Delta V = 2 \cdot \left(\sqrt{\mu \left(\frac{2}{R} - \frac{2}{2R + dh} \right)} - \sqrt{\frac{\mu}{R}} \right) \tag{6.4}$$

With the approaching spacecraft and the target spacecraft both in the Geostationary Earth Orbit (GEO), the total velocity increment and the responsive time needed to eliminate the same advance and receding angles are shown in Fig. 6.5.

It can be seen that, when the advance angle is equal to the receding angle, more velocity increment and time are needed to eliminate the advance angle than to eliminate the receding angle.

Fig. 6.5 Difference in phasing time and velocity increment to eliminate same advance and receding angles



6.2.2 Short-Range Approaching Orbit

After the distance between the approaching spacecraft and the target spacecraft is reduced to a certain extent, the relative motion of these two spacecraft can be described with the following state equation:

$$\begin{bmatrix} \vec{r} \\ \vec{v} \end{bmatrix} = \begin{bmatrix} \Phi_{rr} & \Phi_{rv} \\ \Phi_{vr} & \Phi_{vv} \end{bmatrix} \begin{bmatrix} \vec{r}_0 \\ \vec{v}_0 \end{bmatrix} \quad (6.5)$$

The parameters here have been defined in Sect. 4.2.4.

If the initial states \vec{r}_0, \vec{v}_{0-} and the final states \vec{r}_1, \vec{v}_{1+} are given, then an impulse $\Delta\vec{v}_1$ is first applied to the spacecraft at the initial point \vec{r}_1 . After a period of time T , the spacecraft reaches the position \vec{r}_1 where an impulse $\Delta\vec{v}_2$ is applied again to eliminate the terminal velocity error. The solution is as follows:

$$\begin{bmatrix} \vec{r}_1 \\ \vec{v}_{1-} \end{bmatrix} = \begin{bmatrix} \vec{r}_1 \\ \vec{v}_{1+} - \Delta\vec{v}_2 \end{bmatrix} = \begin{bmatrix} \Phi_{rr} & \Phi_{rv} \\ \Phi_{vr} & \Phi_{vv} \end{bmatrix} \begin{bmatrix} \vec{r}_0 \\ \vec{v}_{0-} + \Delta\vec{v}_1 \end{bmatrix} \quad (6.6)$$

When we solve Eqs. (6.6), (6.7) can be obtained:

$$\begin{cases} \Delta\vec{v}_1 = \Phi_{rv}^{-1}(\vec{r}_1 - \Phi_{rr}\vec{r}_0) - \vec{v}_0 \\ \Delta\vec{v}_2 = \vec{v}_{1+} - \Phi_{vr}\vec{r}_0 - \Phi_{vv}\vec{v}_{0+} \end{cases} \quad (6.7)$$

$\Delta\vec{v}_1$, which is obtained from the CW equation, is the velocity increment in the target spacecraft's relative motion coordinate system. When the coordinates are transformed into the J2000 coordinate system, the velocity increment needed in the J2000 coordinate system can be obtained as the following equation shows:

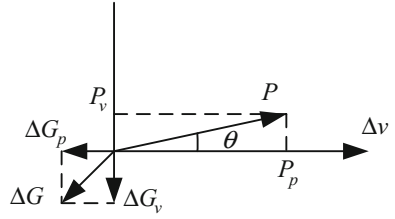
$$\Delta\vec{v} = M_{J2000}\Delta\vec{v}_1 \quad (6.8)$$

We suppose that the operating state of the target spacecraft in the Earth-centered inertial coordinate system is (\vec{X}_e, \vec{V}_e) , and the normal direction of the orbital plane is $\vec{H}_e = \vec{X}_e \times \vec{V}_e$. According to the definition of the target spacecraft's relative motion coordinate system, the transfer matrix M_{J2000r} is:

$$M_{J2000r} = \begin{bmatrix} (X_e \times H_e)_x^0 & X_{ex}^0 & H_{ex}^0 \\ (X_e \times H_e)_y^0 & X_{ey}^0 & H_{ey}^0 \\ (X_e \times H_e)_z^0 & X_{ez}^0 & H_{ez}^0 \end{bmatrix} \quad (6.9)$$

Due to the gravitational difference between the approaching spacecraft and the target spacecraft, a small included angle exists between the direction of theoretical thrust and the direction of velocity increment, as Fig. 6.6.

Fig. 6.6 Schematic figure of thrust direction



It indicates that the thrust is needed to eliminate the gravitational difference's component in the direction which is perpendicular to the velocity increment, and that is:

$$\begin{cases} \Delta \vec{G} = \Delta \vec{G}_{ORS} - \Delta \vec{G}_{T \text{ arg et}} \\ \Delta G_p = \Delta \vec{G} \times \Delta \vec{v}^0 \\ \Delta \vec{G}_v = \Delta \vec{G} - \Delta \vec{G}_p \\ \vec{P}_v = -\Delta \vec{G}_v \\ \theta = \sin^{-1} \left(\frac{P_v}{P} \right) \end{cases} \quad (6.10)$$

Thus the resultant force in the direction of the velocity increment is:

$$F = P \cos \theta - \Delta G_p \quad (6.11)$$

The calculation formula of variable mass velocity increment is known as:

$$\Delta v = I_{sp} \ln \frac{m}{m - \dot{m} \Delta t} \quad (6.12)$$

Then the thrust's duration time is:

$$\Delta t = \frac{m}{\dot{m}} \left(1 - \frac{1}{e^{\Delta v / I_{sp}}} \right) \quad (6.13)$$

Here, I_{sp} is the engine's impulse.

6.3 Dynamics Model of Relative Position and Attitude

We suppose that the approaching spacecraft and the target spacecraft are both rigid bodies. Their relative position in the final approach phase is shown in Fig. 6.7.

Symbols in Fig. 6.7 are defined as follows:

$x_0 y_0 z_0 - CM_0$ represents the body coordinate system which is fixedly connected with the target spacecraft, while $x_1 y_1 z_1 - CM_1$ is the body coordinate system which is fixedly connected with the approaching spacecraft. However, the three axes of

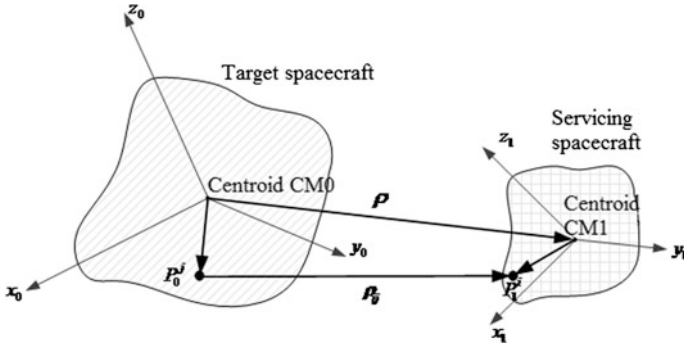


Fig. 6.7 Relative position of approaching spacecraft and target spacecraft

these two coordinate systems are not required to coincide with the corresponding three-inertia principal axes.

P_0^j denotes the position vector of a certain point in the target spacecraft in the $x_0y_0z_0 - CM_0$ system. Assume P_0^j is the optimal capture point in the target spacecraft by the approaching spacecraft, and also the point where the approaching spacecraft detects the target spacecraft.

P_1^i is the position vector of a certain point in the approaching spacecraft in the $x_1y_1z_1 - CM_1$ system. We suppose P_1^i is the front end of the approaching spacecraft's robot arm, and is mounted with a detector.

ρ is the position vector of the approaching spacecraft's centroid relative to the $x_0y_0z_0 - CM_0$ system.

ρ_{ij} is the position vector of P_1^i in the approaching spacecraft relative to P_0^j in the target spacecraft.

We suppose that the target spacecraft rotates at a certain angular velocity. Then in the final approach toward the target without attitude control, the approaching spacecraft needs to keep the attitude tracking to the target spacecraft and ρ_{ij} should be reduced constantly to zero. It can be seen from Fig. 6.2 that ρ_{ij} is not only related to ρ , but also to the relative attitude between these two spacecraft. Therefore, the relative attitude motion and the relative position motion under such circumstance should be analyzed.

6.3.1 Dynamics Model of Relative Attitude

We suppose that the target spacecraft's angular velocity is ω_0 , and the approaching spacecraft's angular velocity is ω_1 . Then their relative angular velocity is:

$$\boldsymbol{\omega} = \boldsymbol{\omega}_1 - \boldsymbol{\omega}_0 \quad (6.14)$$

In the inertial system, the differential form of Eq. (6.14) is:

$$\frac{d^{ECI} \boldsymbol{\omega}}{dt} = \frac{d^{ECI} \boldsymbol{\omega}_1}{dt} - \frac{d^{ECI} \boldsymbol{\omega}_0}{dt} \quad (6.15)$$

The equation above in the target's body coordinate system can be expressed as:

$$\left(\frac{d^{ECI} \boldsymbol{\omega}}{dt} \right)_0 = \mathbf{D} \left(\frac{d\boldsymbol{\omega}_1}{dt} \right)_1 - \left(\frac{d\boldsymbol{\omega}_0}{dt} \right)_0 \quad (6.16)$$

Here, \mathbf{D} is the coordinate transfer matrix from the approaching spacecraft's body coordinate system to the target spacecraft's body coordinate system.

The change rate of $\boldsymbol{\omega}$ observed in the inertial system is the sum of the change rate of $\boldsymbol{\omega}$ in the target's body coordinate system and the vector product $\boldsymbol{\omega}_0 \times \boldsymbol{\omega}$ as Eq. (6.17) shows:

$$\frac{d^{ECI} \boldsymbol{\omega}}{dt} = \frac{d\boldsymbol{\omega}}{dt} + \boldsymbol{\omega}_0 \times \boldsymbol{\omega} \quad (6.17)$$

When we substitute Eq. (6.16) into Eq. (6.17), Eq. (6.18) can be obtained:

$$\frac{d\boldsymbol{\omega}}{dt} = \mathbf{D} \left(\frac{d\boldsymbol{\omega}_1}{dt} \right)_1 - \left(\frac{d\boldsymbol{\omega}_0}{dt} \right)_0 - \boldsymbol{\omega}_0 \times \boldsymbol{\omega} \quad (6.18)$$

The spacecraft's attitude dynamical equation in its body coordinate system is known as:

$$\dot{\boldsymbol{\omega}} = -\mathbf{I}^{-1}[\boldsymbol{\omega} \times (\mathbf{I}\boldsymbol{\omega})] + \mathbf{I}^{-1}(\mathbf{T} + \mathbf{T}_d) \quad (6.19)$$

In Eq. (6.19), \mathbf{I} is the spacecraft's rotation inertia matrix, \mathbf{T} is the spacecraft's control torque, and \mathbf{T}_d is the torque of the interference force applied to the spacecraft. Thus the attitude dynamical equations of the approaching spacecraft and the target spacecraft in their own body coordinate systems are denoted as Eqs. (6.20) and (6.21), respectively.

$$\left(\frac{d\boldsymbol{\omega}_0}{dt} \right)_0 = -\mathbf{I}_0^{-1}[\boldsymbol{\omega}_0 \times (\mathbf{I}_0\boldsymbol{\omega}_0)] + \mathbf{I}_0^{-1}\mathbf{T}_0 \quad (6.20)$$

$$\left(\frac{d\boldsymbol{\omega}_1}{dt} \right)_1 = -\mathbf{I}_1^{-1}[\boldsymbol{\omega}_1 \times (\mathbf{I}_1\boldsymbol{\omega}_1)] + \mathbf{I}_1^{-1}\mathbf{T}_1 \quad (6.21)$$

If we substitute Eqs. (6.15) and (6.21) into Eqs. (6.18) and (6.22) can be obtained:

$$\frac{d\boldsymbol{\omega}}{dt} = \mathbf{D}\mathbf{I}_1^{-1}[\mathbf{T}_1 - \boldsymbol{\omega}_1 \times (\mathbf{I}_1\boldsymbol{\omega}_1)] - \mathbf{I}_0^{-1}[\mathbf{T}_0 - \boldsymbol{\omega}_0 \times (\mathbf{I}_0\boldsymbol{\omega}_0)] - \boldsymbol{\omega}_0 \times \boldsymbol{\omega} \quad (6.22)$$

Therefore the relative attitude dynamical equation in the target's body coordinate system can be expressed as:

$$\begin{aligned} \frac{d\boldsymbol{\omega}}{dt} = & \mathbf{D}\mathbf{I}_1^{-1}[\mathbf{T}_1 - \mathbf{D}^T(\boldsymbol{\omega}_0 + \boldsymbol{\omega}) \times \mathbf{I}_1\mathbf{D}^T(\boldsymbol{\omega}_0 + \boldsymbol{\omega})] - \mathbf{I}_0^{-1}[\mathbf{T}_0 - \boldsymbol{\omega}_0 \times (\mathbf{I}_0\boldsymbol{\omega}_0)] \\ & - \boldsymbol{\omega}_0 \times \boldsymbol{\omega} \end{aligned} \quad (6.23)$$

6.3.2 Dynamics Model of Relative Position

It can be seen from Fig. 6.7 that the relationship of $\boldsymbol{\rho}$, $\boldsymbol{\rho}_{ij}$, \mathbf{P}_0^j and \mathbf{P}_1^i in the target's body coordinate system is:

$$\begin{cases} \mathbf{P}_0^j + \boldsymbol{\rho}_{ij} = \boldsymbol{\rho} + \mathbf{P}_1^i \\ \dot{\mathbf{P}}_0^j + \dot{\boldsymbol{\rho}}_{ij} = \dot{\boldsymbol{\rho}} + \dot{\mathbf{P}}_1^i \\ \ddot{\mathbf{P}}_0^j + \ddot{\boldsymbol{\rho}}_{ij} = \ddot{\boldsymbol{\rho}} + \ddot{\mathbf{P}}_1^i \end{cases} \quad (6.24)$$

Meanwhile:

$$\begin{cases} \dot{\mathbf{P}}_0^j = 0 \\ \ddot{\mathbf{P}}_0^j = 0 \\ \mathbf{P}_1^i = \boldsymbol{\omega} \times \mathbf{P}_1^i \\ \dot{\mathbf{P}}_1^i = \dot{\boldsymbol{\omega}} \times \mathbf{P}_1^i + \boldsymbol{\omega} \times (\boldsymbol{\omega} \times \mathbf{P}_1^i) \end{cases} \quad (6.25)$$

Hence, Eq. (6.24) can be turned into Eq. (6.26):

$$\begin{cases} \boldsymbol{\rho}_{ij} = \boldsymbol{\rho} + \mathbf{P}_1^i - \mathbf{P}_0^j \\ \dot{\boldsymbol{\rho}}_{ij} = \dot{\boldsymbol{\rho}} + \dot{\mathbf{P}}_1^i - \dot{\mathbf{P}}_0^j = \dot{\boldsymbol{\rho}} + \boldsymbol{\omega} \times \mathbf{P}_1^i \\ \ddot{\boldsymbol{\rho}}_{ij} = \ddot{\boldsymbol{\rho}} + \ddot{\mathbf{P}}_1^i - \ddot{\mathbf{P}}_0^j = \ddot{\boldsymbol{\rho}} + \dot{\boldsymbol{\omega}} \times \mathbf{P}_1^i + \boldsymbol{\omega} \times (\boldsymbol{\omega} \times \mathbf{P}_1^i) \end{cases} \quad (6.26)$$

We suppose that the rotational angular velocity in the target's body coordinate system relative to the target's orbit coordinate system is approximately $\boldsymbol{\omega}_0$, and the transfer matrix from the target's orbit coordinate system to the target's body coordinate system is \mathbf{H} , then,

$$\begin{cases} \mathbf{H}^{TOF}\boldsymbol{\rho} = \boldsymbol{\rho} \\ \mathbf{H}^{TOF}\dot{\boldsymbol{\rho}} = \dot{\boldsymbol{\rho}} + \boldsymbol{\omega}_0 \times \boldsymbol{\rho} \\ \mathbf{H}^{TOF}\ddot{\boldsymbol{\rho}} = \ddot{\boldsymbol{\rho}} + \dot{\boldsymbol{\omega}}_0 \times \boldsymbol{\rho} + 2\boldsymbol{\omega}_0 \times \dot{\boldsymbol{\rho}} + \boldsymbol{\omega}_0 \times (\boldsymbol{\omega}_0 \times \boldsymbol{\rho}) \end{cases} \quad (6.27)$$

Equation (6.28) can be obtained based on Eqs. (6.27) and (6.26):

$$\begin{cases} \dot{\rho}_{ij} = \mathbf{H}^{TOF} \dot{\rho} - \omega_0 \times \rho + \omega \times \mathbf{P}_1^i \\ \ddot{\rho}_{ij} = \mathbf{H}^{TOF} \ddot{\rho} - \dot{\omega}_0 \times \rho - 2\omega_0 \times \dot{\rho} - \omega_0 \times (\omega_0 \times \rho) + \dot{\omega} \times \mathbf{P}_1^i + \omega \times (\omega \times \mathbf{P}_1^i) \end{cases} \quad (6.28)$$

It can be turned into a state matrix as follows:

$$\begin{bmatrix} \dot{\rho}_{ij} \\ \ddot{\rho}_{ij} \end{bmatrix} = \begin{bmatrix} \mathbf{H} & \mathbf{0} \\ \mathbf{0} & \mathbf{H} \end{bmatrix} \begin{bmatrix} {}^{TOF}\rho_{ij} \\ {}^{TOF}\dot{\rho}_{ij} \end{bmatrix} + \begin{bmatrix} -\omega_0 \times \rho + \omega \times \mathbf{P}_1^i \\ -\dot{\omega}_0 \times \rho - 2\omega_0 \times \dot{\rho} - \omega_0 \times (\omega_0 \times \rho) + \dot{\omega} \times \mathbf{P}_1^i + \omega \times (\omega \times \mathbf{P}_1^i) \end{bmatrix} \quad (6.29)$$

The C-W state equation is known as:

$$\dot{\mathbf{X}} = \mathbf{A}\mathbf{X} + \mathbf{B}u \quad (6.30)$$

Its transfer matrix \mathbf{A} is:

$$\mathbf{A} = \begin{bmatrix} 0 & 0 & 0 & 1 & 0 & 0 \\ 0 & 0 & 0 & 0 & 1 & 0 \\ 0 & 0 & 0 & 0 & 0 & 1 \\ 0 & 0 & 0 & 0 & 0 & 2n \\ 0 & n^2 & 0 & 0 & 0 & 0 \\ 0 & 0 & 3n^2 & -2n & 0 & 0 \end{bmatrix} = \begin{bmatrix} \mathbf{0} & \mathbf{I} \\ \mathbf{A}_{21} & \mathbf{A}_{22} \end{bmatrix} \quad (6.31)$$

The input matrix \mathbf{B} is:

$$\mathbf{B} = \begin{bmatrix} 0 & 0 & 0 \\ 0 & 0 & 0 \\ 0 & 0 & 0 \\ 1 & 0 & 0 \\ 0 & 1 & 0 \\ 0 & 0 & 1 \end{bmatrix} = \begin{bmatrix} \mathbf{0} \\ \mathbf{I} \end{bmatrix} \quad (6.32)$$

Then in the target orbit coordinate system,

$$\begin{bmatrix} {}^{TOF}\dot{\rho}_{ij} \\ {}^{TOF}\ddot{\rho}_{ij} \end{bmatrix} = \mathbf{A} \begin{bmatrix} {}^{TOF}\rho_{ij} \\ {}^{TOF}\dot{\rho}_{ij} \end{bmatrix} + \begin{bmatrix} \mathbf{0} \\ {}^{TOF}\gamma \end{bmatrix} \quad (6.33)$$

We can substitute Eq. (6.33) into Eq. (6.29), and obtain Eq. (6.34):

$$\begin{bmatrix} \dot{\rho}_{ij} \\ \ddot{\rho}_{ij} \end{bmatrix} = \mathbf{S}_1 + \mathbf{S}_2 + \mathbf{S}_3 \quad (6.34)$$

Here,

$$\begin{cases} \mathbf{S}_1 = \begin{bmatrix} \mathbf{H} & \mathbf{0} \\ \mathbf{0} & \mathbf{H} \end{bmatrix} \begin{bmatrix} \mathbf{0} & \mathbf{I} \\ \mathbf{A}_{21} & \mathbf{A}_{22} \end{bmatrix} \begin{bmatrix} {}^{TOF}\dot{\rho} \\ {}^{TOF}\ddot{\rho} \end{bmatrix} \\ \mathbf{S}_2 = \begin{bmatrix} -\dot{\omega}_0 \times \rho - 2\omega_0 \times \dot{\rho} - \omega_0 \times (\omega_0 \times \rho) + \dot{\omega} \times \mathbf{P}_1^i + \omega \times (\omega \times \mathbf{P}_1^i) \\ -\omega_0 \times \rho + \omega \times \mathbf{P}_1^i \end{bmatrix} \\ \mathbf{S}_3 = \begin{bmatrix} \mathbf{H} & \mathbf{0} \\ \mathbf{0} & \mathbf{H} \end{bmatrix} \begin{bmatrix} \mathbf{0} \\ {}^{TOF}\gamma \end{bmatrix} \end{cases} \quad (6.35)$$

According to Eq. (6.27), \mathbf{S}_1 in Eq. (6.35) can be further transformed into:

$$\begin{aligned} \mathbf{S}_1 &= \begin{bmatrix} \mathbf{0} & \mathbf{H} \\ \mathbf{HA}_{21} & \mathbf{HA}_{22} \end{bmatrix} \begin{bmatrix} \mathbf{H}^T \dot{\rho} + \mathbf{H}^T (\omega_0 \times \rho) \\ \dot{\rho} + \omega_0 \times \rho \end{bmatrix} \\ &= \begin{bmatrix} \mathbf{HA}_{21} \mathbf{H}^T \rho + \mathbf{HA}_{22} (\mathbf{H}^T \dot{\rho} + \mathbf{H}^T (\omega_0 \times \rho)) \end{bmatrix} \end{aligned} \quad (6.36)$$

We suppose that the two vectors' vector product can be transformed into dot product using the following method:

$$\mathbf{a} \times \mathbf{b} = (\mathbf{a}^\times) \mathbf{b} = \begin{bmatrix} 0 & -a_x & a_y \\ a_z & 0 & -a_x \\ -a_y & a_x & 0 \end{bmatrix} \mathbf{b} \quad (6.37)$$

Equation (6.38) can be derived from Eq. (6.26) and Eqs. (6.35)–(6.37):

$$\begin{aligned} \begin{bmatrix} \dot{\rho}_{ij} \\ \ddot{\rho}_{ij} \end{bmatrix} &= \begin{bmatrix} \mathbf{0} & \mathbf{I} \\ \{\mathbf{HA}_{21} \mathbf{H}^T + \mathbf{HA}_{22} \mathbf{H}^T (\omega_0^\times) - (\dot{\omega}_0^\times) - (\omega_0^\times) (\omega_0^\times)\} & \{\mathbf{HA}_{22} \mathbf{H}^T - 2(\omega_0^\times)\} \end{bmatrix} \begin{bmatrix} \rho_{ij} \\ \dot{\rho}_{ij} \end{bmatrix} \\ &+ \left\{ \begin{array}{l} \mathbf{0} \\ -\mathbf{HA}_{21} \mathbf{H}^T (\mathbf{P}_1^i - \mathbf{P}_0^j) - \mathbf{HA}_{22} \mathbf{H}^T (\omega \times \mathbf{P}_1^i) - \mathbf{HA}_{22} \mathbf{H}^T (\omega_0^\times) (\mathbf{P}_1^i - \mathbf{P}_0^j) \\ + (\dot{\omega}_0^\times) (\mathbf{P}_1^i - \mathbf{P}_0^j) + 2(\omega_0^\times) (\omega \times \mathbf{P}_1^i) + (\omega_0^\times) (\omega_0^\times) (\mathbf{P}_1^i - \mathbf{P}_0^j) \\ + \dot{\omega} \times \mathbf{P}_1^i + \omega \times (\omega \times \mathbf{P}_1^i) \end{array} \right\} \\ &+ \begin{bmatrix} \mathbf{0} \\ \mathbf{H}^{TOF} \gamma \end{bmatrix} \end{aligned} \quad (6.38)$$

6.4 Ultimate Approaching Orbit: Design

In the final approach phase, the non-centroid relative motion of the target spacecraft needs to be considered. It not only depends on the relative position of the spacecraft's centroids, but also involves the spacecraft's relative attitude change. There are mainly two cases:

1. The target spacecraft with attitude control

Currently, most of the spacecraft which are worthy of on-orbit repair are three-axis-stabilized, in addition, their attitude change rate is usually not higher than $0.1^\circ/\text{s}$. The final approach strategy for the cooperative rendezvous of those three-axis-stabilized target spacecraft is generally the $V\text{-bar}$ straight-line approximation or the $R\text{-bar}$ straight-line approximation, like the final approach towards the International Space Station (ISS) by American space shuttles, European ATV and Japanese HTV. However, the target spacecraft may not be able to provide effective information for cooperation in some space missions like on-orbit service and maintenance. For this kind of non-cooperative autonomous rendezvous, straight-line approximation in random directions should be considered and docking and capture should be conducted within a certain range around the capture point.

2. The target spacecraft without attitude control

The target spacecraft without attitude control is commonly a piece of space debris or some dysfunctional satellites with a faulty attitude and orbit control system. The uncontrolled target spacecraft rotates around its largest inertia principal axis. Its attitude change rate is usually not lower than $1^\circ/\text{s}$. For these targets, the approaching spacecraft should achieve the tracking and control of the attitude and position relative to the target spacecraft simultaneously, and reduce the relative angular velocity to zero. Meanwhile, the approaching spacecraft should gradually approach the capture point along a certain capturing axis in the target spacecraft's body coordinate system. However, for those spacecraft with a higher rotating angular velocity and without attitude control, the straight-line approximation along the target's rotation axis can be adopted.

6.4.1 *The Final Approach for Three-Axis-Stabilized Target Spacecraft*

As is shown in Fig. 6.8, the approaching spacecraft in the target's orbit coordinate system is in the initial position r_0 when $t = 0$, and then arrives at the capture and docking point within the transfer time T (when $t = T$).

In Fig. 6.8, the dotted line from r_0 to r_T is the reference trajectory of the straight-line approximation, which is denoted with the vector ρ , while the real trajectory (the bold solid line in Fig. 6.8) under the control thrust may change back

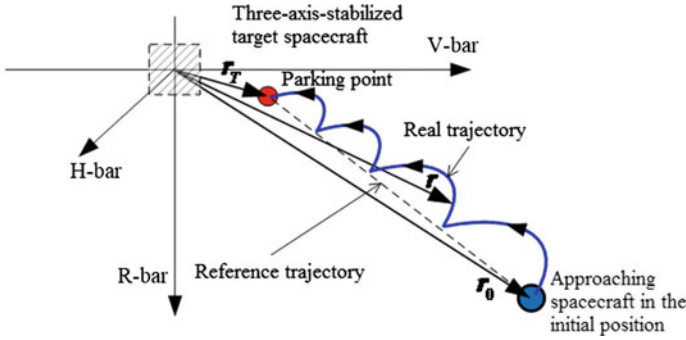


Fig. 6.8 Schematic figure of straight-line approximation for three-axis-stabilized target spacecraft

and forth around the reference trajectory. \mathbf{r} represents the position of the approaching spacecraft at the time t in the target’s orbit coordinate system, and $\boldsymbol{\rho} = \mathbf{r} - \mathbf{r}_T$.

We suppose that the target spacecraft is three-axis-attitude-stabilized, and the approaching spacecraft is ultimately to dock at a certain point in the vicinity of the target spacecraft, so this section only discusses the control of the approaching spacecraft’s relative position.

With the sliding-mode variable structure control, the switching function can be expressed as:

$$s_i = \mathbf{k}_1(\mathbf{r} - \mathbf{r}_d) + \mathbf{k}_2\dot{\mathbf{r}} \tag{6.39}$$

Here, \mathbf{r} is the position vector of the approaching spacecraft in the target’s orbit coordinate system, and \mathbf{r}_d represents the expected position vector in the target’s orbit coordinate system and is same as \mathbf{r}_T , the position vector of the capture and docking point after the final approach is completed. \mathbf{r} and $\dot{\mathbf{r}}$ can be obtained based on the C-W equation. If components of control parameters \mathbf{k}_1 and \mathbf{k}_2 in the target’s orbit coordinate system are both positive, then Eq. (6.39) will satisfy:

$$\begin{cases} \lim s_i \dot{s}_i = 0 \\ s_i(0, \dots, 0) = 0 \end{cases} \tag{6.40}$$

It indicates that the sliding-mode motion is asymptotic stable.

The external force acceleration γ_i in the C-W equation is set as the following switching control acceleration constants:

$$\gamma_i = \begin{cases} -T, & s_i > 0 \\ 0, & s_i = 0 \\ T, & s_i < 0 \end{cases} \tag{6.41}$$

We suppose that a thrust can be applied to all of the three axes in the target’s orbit coordinate system. If the component of the approaching spacecraft’s relative position vector \mathbf{r} in the x axis is larger than the expected value ($s_i > 0$), then the control thrust should be applied along the x axis in the negative direction. If the component of the approaching spacecraft’s relative position vector \mathbf{r} in the x axis is equal to the expected value, then no thrust is applied along the x axis. If the component of the approaching spacecraft’s relative position vector \mathbf{r} in the x axis is smaller than the expected value, then the control thrust is applied along the x axis in the positive direction.

According to the above analysis, the Simulink model of the straight-line approximation under sliding-mode control can be constructed in MATLAB as is shown in Fig. 6.9.

In Fig. 6.9, the C-W module is the relative motion model constructed based on the C-W equation; the Simulink module is the model under sliding-mode control constructed based on Eq. (6.39); and the Switch module switches the control acceleration based on the value of s_i in Eq. (6.39).

The straight-line approximation simulation conditions for three-axis-stabilized target spacecraft are set as:

1. The angular velocity of the target orbit:

$$n = 7.292 \times 10^{-5} \text{ rad/s,}$$

$$\mathbf{r}_0 = [104 \ 10 \ 60]^T \text{ m,}$$

$$\dot{\mathbf{r}}_0 = [0 \ 0 \ 0]^T \text{ m/s,}$$

$$\mathbf{r}_d = [5 \ 0 \ 2]^T \text{ m.}$$

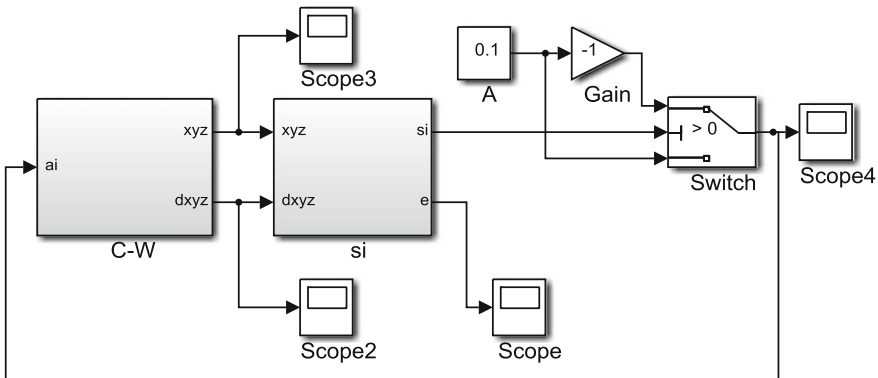


Fig. 6.9 Simulink model under sliding-mode control

2. Control parameters:

$$\begin{aligned} k_1 &= \text{diag}(0.2 \quad 0.2 \quad 0.2), \\ k_2 &= \text{diag}(5 \quad 5 \quad 5), \\ T &= 0.1 \text{ ms}^{-2}. \end{aligned}$$

3. Simulation time: 1000 s.

The variation of the relative velocity and position with time is shown in Fig. 6.10.

It can be seen from Fig. 6.10 that the change curve of the relative velocity and the relative position under sliding-mode control can converge quickly in the first 300 s. When it arrives at r_d around the 140th second, the approaching spacecraft's velocity is nearly zero in the target's orbit coordinate system. Ultimately, the approaching spacecraft can keep in the expected docking position. When we extract data of the relative position and draw a three-dimensional curve, then the straight-line approximation simulation trajectory of the approaching spacecraft in the final approach phase can be obtained as Fig. 6.11.

Figure 6.11 shows that, except the initial phase, the approaching spacecraft can approach the docking point along the straight line trajectory in the final approach phase. Therefore the sliding-mode variable structure control discussed in this section can achieve the straight-line approximation and control for the high-orbit, three-axis-stabilized and non-cooperative target spacecraft in the final approach phase of autonomous rendezvous.

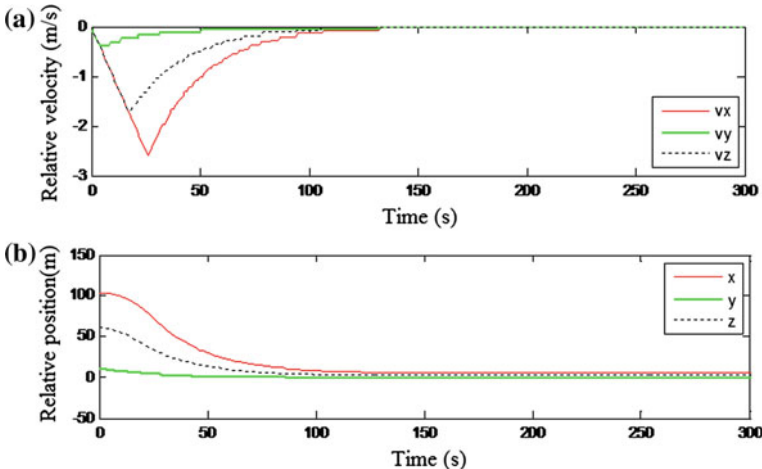


Fig. 6.10 Change curve of relative velocity and position under sliding-mode control with time

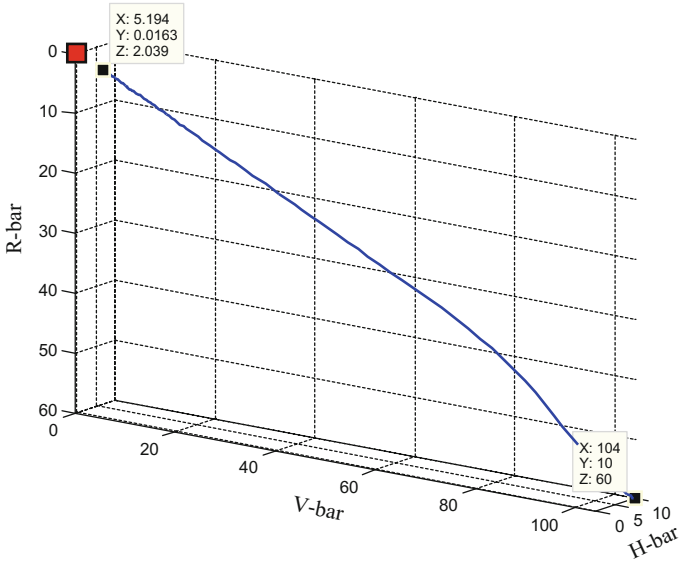


Fig. 6.11 Final approaching trajectory of approaching spacecraft under sliding-mode control

6.4.2 Final Approach to the Target Without Attitude Control

The control process of the position and attitude tracking and approaching in the final approach phase is: firstly, according to the estimation of the relative position and attitude, we suppose the current values of the relative attitude, the relative attitude angular velocity, the relative position and the relative velocity are obtained. Then, by comparing the current values with the nominal values, the deviation value between them is obtained. Finally, based on the feedback control law, the control quantity is generated to eliminate the difference.

For the controlled targets with relatively large inertia, the dynamic characteristics in system adjustment can be improved via Proportion-Differentiation Control (PD control). The transfer function under PD control is:

$$G_c(s) = K_P + K_P\tau s \tag{6.42}$$

Here, K_P is the proportional coefficient, and τ is the differential time constant. The output signal of the PD controller can be denoted as:

$$u(t) = K_P e(t) + K_P\tau \frac{de(t)}{dt} \tag{6.43}$$

1. Relative attitude and tracking control

We suppose all of the unknown quantities in the relative attitude motion are interference torque T_d , and then Eq. (6.25) can be reduced to:

$$\frac{d\omega}{dt} = DI_1^{-1}T_1 - DI_1^{-1}\omega_1 \times I_1\omega_1 - T_d \tag{6.44}$$

Therefore, the law of the attitude tracking PD control of the approaching spacecraft to the target spacecraft can be expressed as follows:

$$T_c = \omega_1 \times I_1\omega_1 - I_1D^T(K_1\Delta q + K_2\omega) \tag{6.45}$$

According to Eqs. (6.20) and (6.21), the Simulink model of spacecraft’s attitude dynamics can be constructed as shown in Fig. 6.12.

Figure 6.12 shows the attitude dynamic model of the approaching spacecraft, which can ultimately output the approaching spacecraft’s angular velocity ω_1 . Similarly, the attitude dynamic model of the target spacecraft can also be obtained. It should be noted that T_c in Fig. 6.12 is the control torque output of the attitude tracking PD controller in Eq. (6.45) and can be obtained from the Simulink model in Fig. 6.14. However, there is no corresponding input in the target spacecraft’s attitude dynamic model.

Based on the Simulink model in Fig. 6.11 and Eq. (6.23), the Simulink model of relative attitude calculation can be constructed as Fig. 6.13.

Five inputs are needed in the model in Fig. 6.13. Input 1 is the attitude dynamics of the target spacecraft; input 2 is the attitude dynamics of the approaching spacecraft; input 3 is the direction cosine form of the target spacecraft’s angular velocity; input 4 is the direction cosine form of the approaching spacecraft’s angular velocity, and D in Fig. 6.13 is the coordinate transfer matrix from the approaching spacecraft’s body coordinate system to the target spacecraft’s body coordinate system; input 5 is the angular velocity of the target spacecraft. According to Eq. (6.10), the relative attitude dynamics in the target system can be acquired with these five inputs above.

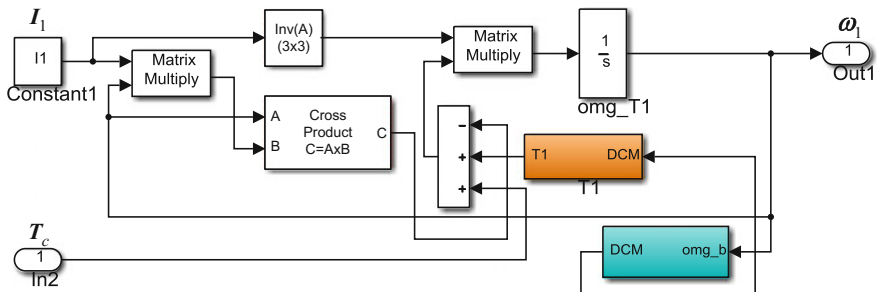


Fig. 6.12 Simulink model of approaching spacecraft’s attitude dynamics

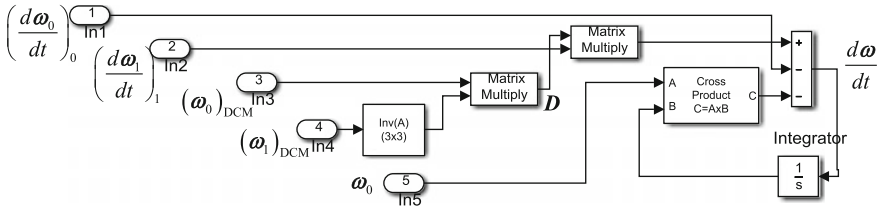


Fig. 6.13 Simulink model of relative attitude dynamics calculation

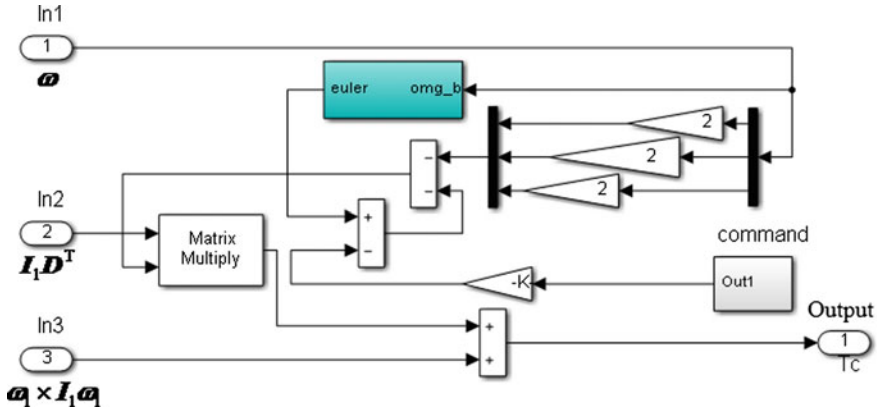


Fig. 6.14 Simulink model of relative attitude tracking PD control

Based on Eq. (6.45) and the Simulink model in Fig. 6.13 and 6.12, the Simulink model of the approaching spacecraft’s relative attitude tracking PD controller can be constructed. The model can output the control torque T_c to control the approaching spacecraft’s attitude dynamics as Fig. 6.14.

2. Relative position and tracking control

We suppose that the unknown quantities in the relative position motion are also interference factors, and that the target spacecraft is in slow rotation. To simplify the problem, if the relative attitude has already been already tracked, through controlling the relative position of the approaching spacecraft’s centroids, the relative position motion between the robot arm’s front end P_1^j and the capture point P_0^j can be realized indirectly. Thus Eq. (6.38) can be further simplified as:

$$\begin{bmatrix} \dot{\rho}_{ij} \\ \ddot{\rho}_{ij} \end{bmatrix} = \begin{bmatrix} \mathbf{0} & \mathbf{I} \\ \mathbf{H}A_{21}\mathbf{H}^T & \mathbf{H}A_{22}\mathbf{H}^T \end{bmatrix} \begin{bmatrix} \rho_{ij} \\ \dot{\rho}_{ij} \end{bmatrix} + \begin{bmatrix} \mathbf{0} \\ \mathbf{H}^{TOF}\gamma \end{bmatrix} \quad (6.46)$$

Then the law of the relative position tracking PD control of the approaching spacecraft to the target spacecraft is:

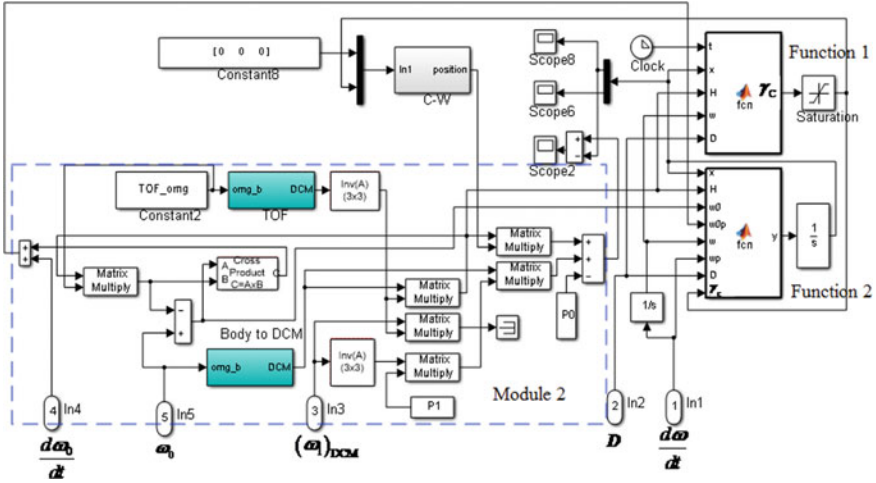


Fig. 6.15 Simulink model of relative position tracking control

$$\gamma_C = -A_{21}H^T \rho_{ij} - A_{22}H^T \dot{\rho}_{ij} - H^T (K_1 \Delta \rho_{ij} + K_2 \dot{\rho}_{ij}) \quad (6.47)$$

The Simulink model of the approaching spacecraft's relative position tracking control is shown in Fig. 6.15.

6.4.3 Simulation and Realization

We suppose that there is a capture axis in the target spacecraft fixedly connected with its body coordinate system. In its tracking and approaching under the closed loop control, the approaching spacecraft needs to conduct the final approach along this axis from 50 meters away. In its final approach, the spacecraft's relative velocity is 0.1 m/s and it keeps a stable relative attitude.

We also set the target spacecraft's orbit angular velocity $n = 7.292 \times 10^{-5} \text{ rad/s}$, its angular velocity of rotation is $1^\circ/\text{s}$, and

$$P_0 = (2 \ 4 \ 0)^T \text{ m}$$

$$P_1 = (3 \ 4 \ 5)^T \text{ m}$$

$$I_0 = [100 \ 0 \ 0; 0 \ 50 \ 0; 0 \ 0 \ 50]^T \text{ kg m}^2$$

$$I_1 = [10 \ 0 \ 0; 0 \ 10 \ 0; 0 \ 0 \ 10]^T \text{ kg m}^2$$

With the Simulink model above, we set 500 s as the simulation time and 0.1 s as the step size, then several curves can be obtained (as is shown in Figs. 6.16, 6.17 and 6.18), including the variations of the target spacecraft's attitude Euler angle,

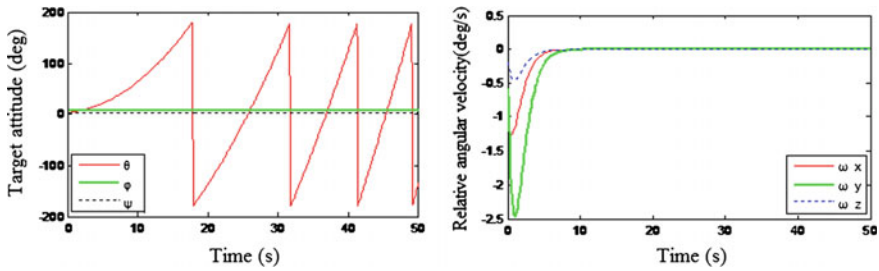


Fig. 6.16 Variation curves of target spacecraft's attitude Euler angle and relative angular velocity

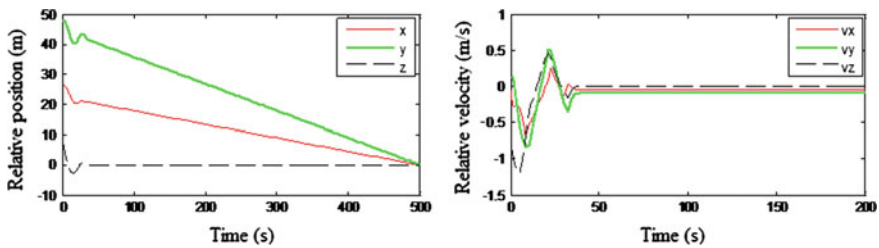


Fig. 6.17 Variation curves of relative position and relative velocity

relative angular velocity, relative position, relative velocity, the approaching spacecraft's control acceleration and control torque.

It can be seen from the curve of the target attitude that the target spacecraft is not motionless but rolls and rotates around the x axis of its body coordinate system. The curve of the relative angular velocity in Fig. 6.16 indicates that the relative angular velocity of the approaching spacecraft and the target spacecraft converges to nearly zero ultimately, and attitude tracking is achieved.

It can be seen from Fig. 6.17 that the relative position can finally converge to about zero, indicating that the front end of the approaching spacecraft's robot arm reaches the capture point. The initial fluctuation of the curve is caused by the limiting of the control acceleration. The relative velocity of the approaching spacecraft and the target spacecraft converges finally and keeps at about 0.1 m/s.

Figure 6.18 shows that, with the convergence of the relative position and the synchronization of the attitude, the control acceleration reduces from around 0.1 m/s^2 to about 0.01 m/s^2 . The control torque first varies from -1 N m to about 1 N m , and then converges to around zero.

To create a simulation scene in STK, it's necessary to set up the target spacecraft's attitude and orbit data. Meanwhile, according to the simulation data about the relative position and relative attitude, an approaching spacecraft is also set up to conduct visual simulation. This is shown in Fig. 6.19.

In Fig. 6.19, the target spacecraft is rotating around the grey dotted line in bold—the rotation axis, the red fine dotted line here is the capture axis fixedly connected

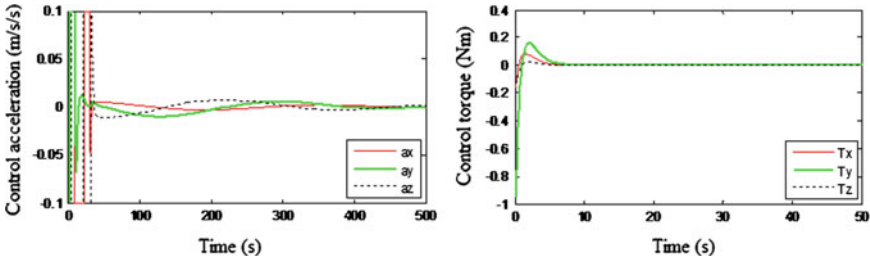
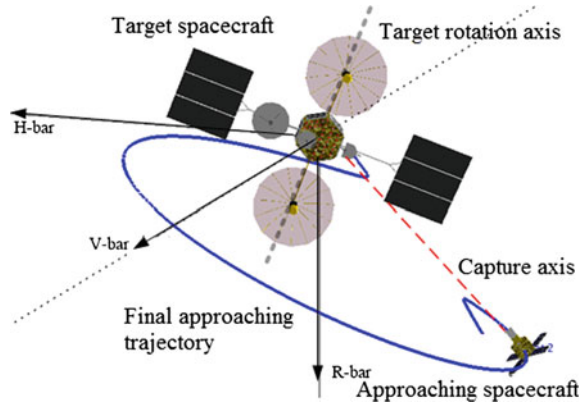


Fig. 6.18 Variation curves of control acceleration and control torque

Fig. 6.19 STK simulation of position and attitude tracking and approaching



with the target’s body coordinate system, and it also rotates around the target spacecraft’s rotation axis. The blue solid line in bold is the final approach trajectory of the approaching spacecraft in the target orbit coordinate system.

In the final approach phase, the approaching spacecraft approaches the target spacecraft along the capture axis in the target’s body coordinate system, forming a trajectory of encircling approach to the target capture point in the target’s orbit coordinate system. It shows that the approaching spacecraft successfully tracks and approaches the target without attitude control and reaches the effective capture point.

6.5 Summary

In the initiative approaching process, an approaching spacecraft, with a target spacecraft being the target, through the maneuver control of the relative orbit and relative attitude, finally approaches the target in a specific way. The design of the initiative approaching orbit is an important part in the research on debris clearance and on-orbit services.

This chapter first introduces the concept of the initiative approaching orbit, and then presents the target approaching orbit from two aspects: the design of the phasing orbit and the short-range approach. Furthermore, specific algorithms of orbit control are provided. Finally, dynamic models of the relative attitude and relative position between the approaching spacecraft and the target spacecraft are constructed, and for the three-axis-stabilized target spacecraft and the target spacecraft without attitude control, strategies for attitude and orbit control are put forward. Besides, simulation and analysis are conducted to verify the correctness and feasibility of them.

Chapter 7

Theory and Design Method of Responsive Orbit

An orbit which meets the demands of fast responsive missions is called a fast responsive orbit. Fast responsive missions mainly aim at emergent geological hazard, earthquake, nuclear leakage, and military conflict. These emergencies are generally unexpected and very destructive and cause huge losses if we cannot get information timely and act decisively. This chapter will start with the concept of the responsive orbit, and then focus on the theories and design methods of several typical responsive orbits such as the fast access orbit and the fast phasing orbit.

7.1 Fast Responsive Orbit: Concept

A response is a system's reaction to incentives. It starts when the system receives incentives and ends when the system responds. In aerospace application, the responsive time is usually defined as the period of time from the proposal of the mission to the moment the mission's demands are satisfied.

Due to the constraint from the Keplerian orbit, once the spacecraft's orbit is determined, its operation law in space and its motion relative to the ground are both fixed. Many natural and man-made disasters are highly unexpected. For example, the sea to the east of Miyagi-ken, a prefecture in northeastern Japan, was struck by a 9.0-magnitude earthquake on March 11, 2011, triggering a mega tsunami and causing mass casualties. Consequently, power outage occurred successively in the six units of the Fukushima Daiichi Nuclear Plant. Alternate diesel-generators were destroyed, the cooling systems were no longer effective, and then reactors exploded in succession. Because the resultant nuclear leakage damaged the environment seriously, the detection personnel could hardly enter the disaster-stricken area. In addition, owing to the territorial sky and sea restrictions, some countries directly involved in this disaster, like China, had no access to first-hand data. If a fast responsive spacecraft was available then, near real-time information of high

accuracy could be obtained, providing firsthand data to aid in the fast formulation of counter-measures.

This is the case in the civil field. The same is true in the military field. As a matter of fact, the concept of “the responsive space” was first put forward by the U.S. military. In 1999, the United States Air Force (USAF) introduced the concept of “the responsive space” for the first time in its Operational Responsive Space-lift Mission Needs Statement, or ORSMNS in short. Afterwards, this concept was constantly modified and enriched. In the memorandum of the Deputy Secretary of Defense on July 9, 2007, the ORS is defined as “assured space power focused on timely satisfaction of Joint Force Commanders’ needs, the capability of fast and accurate deploying in space and near space, and the operation of national and military assets with affordable costs.”

The ORS strikes a balance between the emergent space requirements of the Joint Force Commanders and the requirements of other users. Meanwhile, the ORS provides “capacity to respond to unexpected loss or degradation of selected functions and/or to provide timely availability of tailored or new capabilities” (NSPD-40, American Space-lift Strategy). The strategic or long-term demand is not the focal point of ORS, however.

According to the U.S. Joint Space Operation Regulations, the ORS synchronizes and integrates space technologies and other forces available to the Joint Force Commanders in a timely and proactive way.

The advantages include:

- Rapid response to the new or improved space technologies required by Joint Force Commanders.
- Fast improvement and strengthening of existing space technologies as desired.
- Fast restructure or complement of key space technologies to ensure the operation, and provide continuous space forces for Joint Force Commanders.

The limitations are:

- The shortened time limit which presents challenges to all aspects of the development and deployment process, and also increases risks.
- The Congress limits maximum expenses and requires detailed explanation of Joint Force Commanders’ needs, which may lead to a technical scheme that is “just adequate”.

An orbit that meets the demand of a fast responsive mission is called a fast responsive orbit. The foremost goal in the design of a responsive orbit is to accomplish the mission quickly. The design also takes into account the Keplerian orbit constraint, the service life and the follow-up application of the spacecraft.

The fast responsive orbits designed for different responsive missions can be divided into several categories. This chapter will mainly introduce the fast fly-around orbit and the fast access orbit.

1. Fast fly-around orbit

Flying around means a spacecraft travels around another spacecraft. These two spacecraft are called the flying-around spacecraft and the target spacecraft, respectively. The period of the natural flying around is usually equal to the orbital period of the target spacecraft. For example, it takes 24 h for the target spacecraft in the earth-synchronous orbit to fly in a complete circle around the Earth. This natural flying around is designed on the basis of the orbit's mechanical characteristics and the short-range relative motion equation. Relevant studies have recently matured.

The period of the natural flying around is equal to the orbital period of the target spacecraft, which is inconvenient in practical uses such as in the comprehensive observation of GEO satellites and the fast checking and maintenance of space stations. With the natural flying around, 24 h is needed for a 360° observation of the GEO satellite. Owing to the characteristics of the GEO, the spacecraft is in the shadow area for a while (a few minutes to an hour), so the visible light camera can't form images. With the fast flying around, only a few hours is needed to finish the observation and the shadow area can also be avoided. This can even be done in tens of minutes. So the fast flying around method is more practical.

In addition, to inspect and maintain the space station quickly, the inspecting spacecraft is required to fly around the target in a very short time so that the problem can be fixed rapidly. The XSS-10 satellite of the US XSS plan is a typical case of the fast flying around method.

The XSS plan aims to develop a micro satellite under fully-autonomous control. This kind of satellite can be used for on-orbit inspection, rendezvous and docking, and short-range maneuver around the on-orbit target. The XSS satellite will ultimately enhance the ability of the US Air Force Space Command (AFSPC) in space repair and maintenance, and other special space missions. The XSS-10 satellite, the first micro satellite of the XSS plan, was launched into orbit by the Delta-2 rocket on January 29, 2003. The XSS-10 satellite was in service for only 24 h and mainly worked to demonstrate and verify the short-range inspection between spacecraft and the autonomous navigation technology. It successfully conducted the demonstration and verification test of the fast flying around in the 10-minute period (Fig. 7.1).

2. Fast access orbit

If there is an emergency but no appropriate spacecraft to deal with it, a new spacecraft must be launched from the ground. That is to say, the spacecraft must be tested and launched into orbit as soon as possible and then arrive at the region of interest or the vicinity of the target spacecraft at the appointed time so that it can obtain highly accurate information and support the decision making on the ground. For instance, the responsive orbit in Fig. 7.2 can be applied in covering the Fukushima area in Japan. After being launched into the responsive orbit, the satellite can arrive at the space over Fukushima and conduct the first reconnaissance within ten minutes and then the second reconnaissance after one and a half hours.

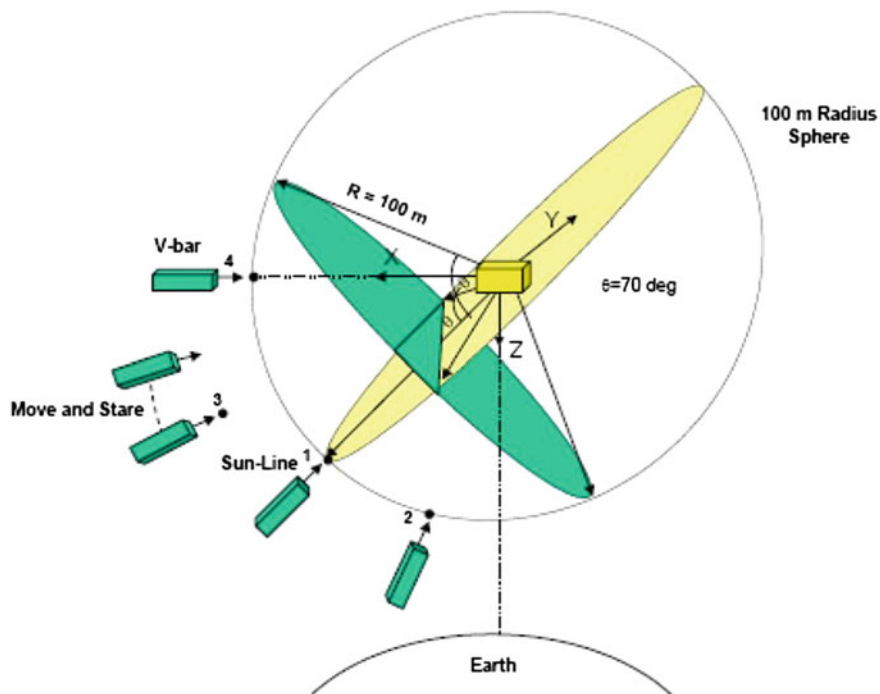


Fig. 7.1 Mission of XSS-10

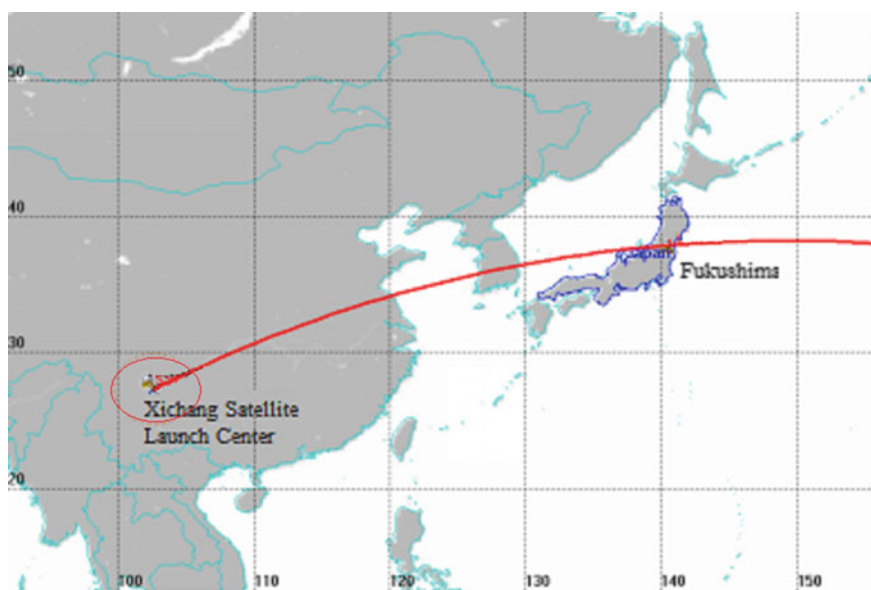


Fig. 7.2 Responsive orbit designed for Fukushima

The reconnaissance result can be transmitted back to the ground in real time using the data relay satellite and provide decision support for the formulation of countermeasures on the ground.

7.2 Circular Fast Flying-Around Orbit

Generally speaking, a natural fly-around doesn't need an external force and the fly-around relative trajectory is elliptical. The fly-around period is also fixed (equal to the orbital period of the target spacecraft). However, a circular fast fly-around requires an external force. In this case, the fly-around spacecraft can fly with the target spacecraft periodically along the circular fly-around trajectory within a short designated time.

7.2.1 Circular Fast Flying-Around Orbit: Design

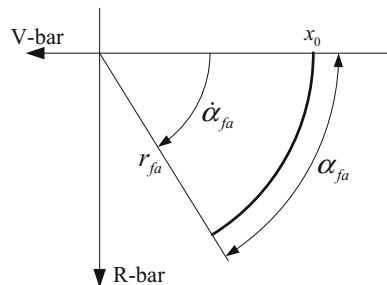
When the initial state of the fly-around spacecraft meets certain conditions, the elliptical natural flying around the target spacecraft can be achieved. But it takes an orbital period to fly a circle. If the fly-around spacecraft needs to fly around the target spacecraft in a shorter time, or must keep a constant distance to the target spacecraft for some special reasons, the circular fast fly-around method is adopted. It can be divided into in-plane circular fast fly-around and out-of-plane circular fast fly-around.

1. In-plane circular fast fly-around

The in-plane circular fast fly-around means that the fly-around trajectory of the fly-around spacecraft is in the orbit plane of the target spacecraft and the trajectory is circular.

As is shown in Fig. 7.3, r_{fa} is the fly-around radius, $\dot{\alpha}_{fa}$ is the fly-around angular velocity, and $\alpha_{fa} = \dot{\alpha}_{fa}t$.

Fig. 7.3 Schematic figure of in-plane circular fast fly-around



We assume that the in-plane clockwise circular fly-around starts from the $-V$ -bar, and the motion equations are:

$$\begin{cases} x = -r_{fa} \cos(\dot{\alpha}_{fa}t) \\ z = r_{fa} \sin(\dot{\alpha}_{fa}t) \end{cases} \quad (7.1)$$

The fly-around spacecraft needs to meet the following condition at the initial fly-around point.

$$(x_0 \quad z_0 \quad \dot{x}_0 \quad \dot{z}_0) = (-r_{fa} \quad 0 \quad 0 \quad r_{fa}\dot{\alpha}_{fa}) \quad (7.2)$$

If we ignore the influence of perturbation, the thrust acceleration applied to the fly-around circle is:

$$\begin{cases} \gamma_x = -r_{fa}\dot{\alpha}_{fa}(2\omega - \dot{\alpha}_{fa}) \cos(\dot{\alpha}_{fa}t) \\ \gamma_z = -r_{fa}(\dot{\alpha}_{fa}^2 - 2\omega\dot{\alpha}_{fa} + 3\omega^2) \sin(\dot{\alpha}_{fa}t) \end{cases} \quad (7.3)$$

Here, ω is the angular velocity of the target spacecraft's orbit. The instantaneous velocity at any point on the fly-around circle is:

$$\begin{cases} \dot{x} = r_{fa}\dot{\alpha}_{fa} \sin(\dot{\alpha}_{fa}t) \\ \dot{z} = r_{fa}\dot{\alpha}_{fa} \cos(\dot{\alpha}_{fa}t) \end{cases} \quad (7.4)$$

Given that the fly-around radius r is 120 m, and the angular velocity of the fast fly-around is k ($k = 2, 3, 4$) times that of the target's orbit, the change curve of the thrust acceleration with time can be shown in Fig. 7.4.

It can be seen that the variation of the thrust with time follows a periodical sine curve, and the period is $\frac{1}{k}$ that of the target's orbit. Meanwhile, as the value of

Fig. 7.4 Relation between thrust acceleration and fly-around velocity in in-plane circular fly-around

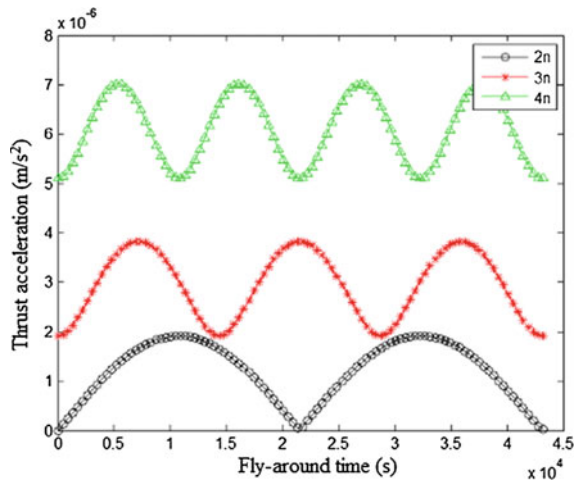
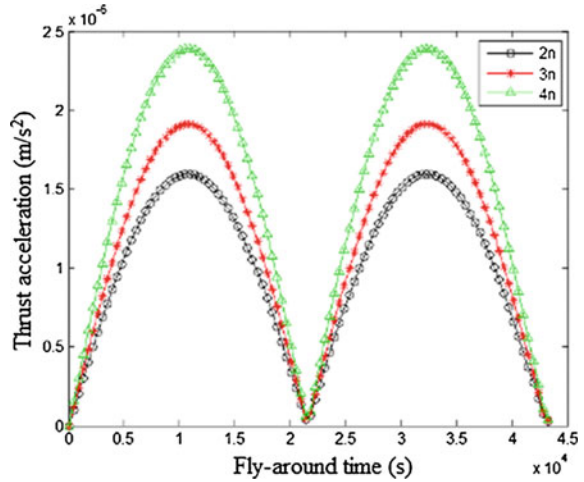


Fig. 7.5 Relation between thrust acceleration and fly-around radius in in-plane fly-around



k becomes bigger, the maximum and minimum values of the thrust acceleration within a fly-around period will both increase.

We suppose $k = 2$, namely, the fly-around velocity is twice the angular velocity of the target spacecraft’s orbit. With different fly-around radiuses (100, 120, and 150 m), the change curves of the thrust acceleration with time can be shown in Fig. 7.5.

It is clear that, with the increase of the fly-around radius, the maximum value of the thrust within a period becomes bigger.

2. Out-of-plane circular fast fly-around

In the out-of-plane circular fast fly-around, there is an included angle between the fly-around trajectory of the fly-around spacecraft and the orbit plane of the target spacecraft, and the trajectory is circular.

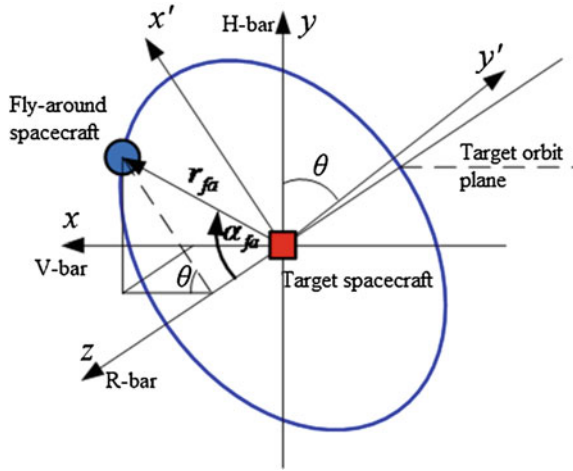
We assume that the initial point of the out-of-plane circular fly-around is on the $+R$ -bar, the distance between it and the target is r_{fa} , the fly-around angular velocity is $\dot{\alpha}_{fa}$, and the fly-around angle (the angle the fly-around spacecraft travels on the fly-around circle from the initial point) is α_{fa} . The fly-around trajectory intersects with the R -bar, and the included angle between the fly-around plane and the x - z plane is θ .

As the geometrical relationship in Fig. 7.6 shows, the motion equations of the fly-around spacecraft in the target orbit coordinate system can be expressed as:

$$\begin{cases} x = r_{fa} \cos \theta \sin(\alpha_{fa}) \\ y = r_{fa} \sin \theta \sin(\alpha_{fa}) \\ z = r_{fa} \cos(\alpha_{fa}) \end{cases} \quad (7.5)$$

Then the fly-around spacecraft needs to satisfy the following condition at the initial point:

Fig. 7.6 Schematic figure of out-of-plane fast circular fly-around



$$(\dot{x}_0 \quad \dot{y}_0 \quad \dot{z}_0 \quad \ddot{x}_0 \quad \ddot{y}_0 \quad \ddot{z}_0) = (0 \quad 0 \quad r_{fa} \quad r_{fa} \cos \theta \quad r_{fa} \sin \theta \quad 0) \quad (7.6)$$

A continuous thrust must be imposed onto the spacecraft, and the thrust acceleration is:

$$\begin{cases} \gamma_x = -r_{fa} \dot{\alpha}_{fa}^2 (\cos \theta \sin(\dot{\alpha}_{fa} t) - 2n \cos(\dot{\alpha}_{fa} t)) \\ \gamma_y = -r_{fa} \sin \theta \sin(\dot{\alpha}_{fa} t) (\dot{\alpha}_{fa}^2 \sin \theta + n^2) \\ \gamma_z = -r_{fa} \cos(\dot{\alpha}_{fa} t) (\dot{\alpha}_{fa}^2 - 2n \cos \theta + 3n^2) \end{cases} \quad (7.7)$$

The instantaneous velocity at any point on the fly-around circle is:

$$\begin{cases} \dot{x} = r_{fa} \dot{\alpha}_{fa} \cos \theta \cos(\dot{\alpha}_{fa} t) \\ \dot{y} = r_{fa} \dot{\alpha}_{fa} \sin \theta \cos(\dot{\alpha}_{fa} t) \\ \dot{z} = -r_{fa} \dot{\alpha}_{fa} \sin(\dot{\alpha}_{fa} t) \end{cases} \quad (7.8)$$

We suppose that the included angle between the fly-around plane and the x - z plane is 30° , the fly-around radius r is 120 m, and the angular velocity of the fast fly-around is k ($k = 2, 3, 4$) times that of the target's orbit. The variation curve of the thrust acceleration with time is shown in Fig. 7.7.

As revealed in Fig. 7.7, in the out-of-plane fly-around, the fly-around velocity has little effect on the thrust acceleration. This is mainly because the thrust acceleration is used to support the out-of-plane motion, namely, the motion in the Z direction. Figure 7.8 shows the relation between the thrust acceleration in the Z direction and the fly-around velocity.

We suppose $k = 2$, namely, the fly-around velocity is twice that of the target spacecraft. With different fly-around radiuses (100, 120, and 150 m), the change curve of the combined thrust acceleration with time is shown in Fig. 7.9.

Fig. 7.7 Relation between thrust acceleration and fly-around velocity in out-of-plane circular fast fly-around

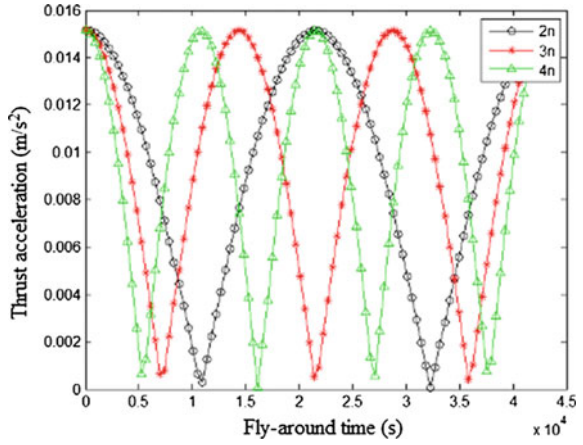


Fig. 7.8 Relation between thrust acceleration in Z direction and fly-around velocity in out-of-plane fly-around

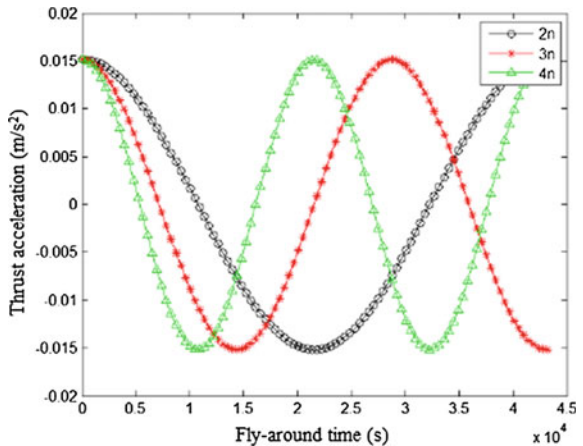
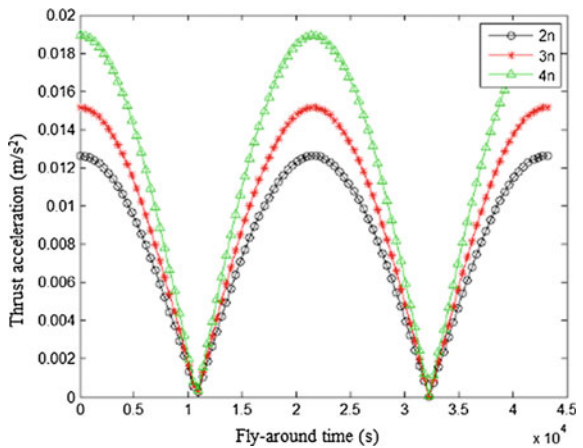


Fig. 7.9 Relation between thrust and fly-around radius in out-of-plane fly-around



It is clear that, as the fly-around radius increases, the maximum value of the thrust in a period will also increase, but the change is small.

7.2.2 Target Forbidden Zone: Definition

The target forbidden zone, also known as the safety zone of the target spacecraft, is an important factor in determining whether the fly-around trajectory is safe or not. The target forbidden zone can be expressed by a sphere with the target spacecraft as its center. Its radius r_{KOZ} observes the following condition:

$$r_{SR} \geq r_{KOZ} \geq r_{TE} + 2(r_{SE} + \Delta_{GNC} + \Delta_{PM}) \tag{7.9}$$

Here, r_{SR} is the valid detection scope of the fly-around spacecraft’s detection payload. r_{TE} is the maximum one among the extended radiuses of the target spacecraft’s body, its solar array and the parabolic antenna. r_{SE} is the fly-around spacecraft’s envelope radius. Δ_{PM} is the fly-around spacecraft’s position measuring precision. Δ_{GNC} is the control precision of the fly-around spacecraft’s GNC system.

If the spherical forbidden zone is projected into the x - z plane of the target orbit coordinate system, a corresponding circular forbidden zone can be obtained. It is shown in Fig. 7.10.

We can take the TDRS-1 satellite in the GEO as an example. The extended lengths of its solar array and parabolic antenna are about 11 m and 7 m, respectively. Therefore, assumptions about the factors which influence its target forbidden zone can be made, as is shown in Table 7.1.

When we substitute the values in Table 7.1 into Eq. (7.9), then the value range of r_{KOZ} is: $20 \text{ km} \geq r_{KOZ} \geq 47 \text{ m}$.

Due to the strong sensitivity of the high-orbit environment to collisions, the target forbidden zone should have adequate safety boundaries. Thus the target forbidden zone’s radius in high-orbit fast circular fly-around orbit is usually designed as: $r_{HKOZ} = 2r_{KOZ}$.

Fig. 7.10 Schematic figure of circular forbidden zone

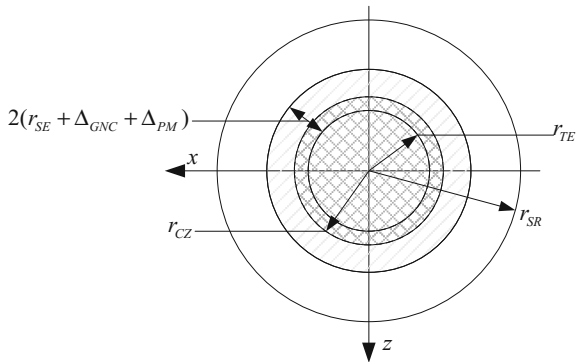


Table 7.1 Assumptions about factors that influence TDRS-1 target forbidden zone

r_{TE}	r_{SR}	Δ_{PM}	Δ_{GNC}	r_{SE}
12 m	20 km	5 m	5 m	8 m

7.2.3 Safety Analysis

It is known from the fly-around radius that, to achieve safe fly-around in the x - z orbit plane, the following condition must be satisfied:

$$x^2 + z^2 \geq r_{KOZ}^2 \quad (7.10)$$

If a continuous thrust is applied according to Eq. (7.7), the fast circular fly-around can achieve active safety. To test the passive safety of this fast circular fly-around, the situation of whether the fly-around spacecraft will enter into the target forbidden zone after the thrust disappears should be considered.

We suppose that the thruster fails after the fly-around spacecraft arrives at a certain point on the fly-around circle. At this moment, the angle the spacecraft has covered is $\alpha_{failure}$. According to Eqs. (7.1) and (7.4), the state of the fly-around spacecraft at the thrust failure point can be expressed as follows:

$$\mathbf{X}_{failure} = \begin{bmatrix} -r_{fa} \cos(\alpha_{failure}) \\ r_{fa} \sin(\alpha_{failure}) \\ \dot{\alpha}_{fa} r_{fa} \sin(\alpha_{failure}) \\ \dot{\alpha}_{fa} r_{fa} \cos(\alpha_{failure}) \end{bmatrix} \quad (7.11)$$

According to the state above, the free flight trajectory of the fly-around spacecraft after the thruster fails is:

$$\mathbf{X}_{free} = \Phi_{x-z}(\tau) \mathbf{X}_{failure} \quad (7.12)$$

The free flight trajectory after the thruster fails is simulated and calculated with MATLAB. In the reference trajectory of the circular fly-around, eight points, from 0° and at an interval of 45° , are selected as the failure points. We assume the radius of the target forbidden zone is 100 m, the fly-around radius is 120 m, and the angular velocity of the circular fly-around is still n . Ignoring the influence of perturbation, the simulation result is shown in Fig. 7.11.

It can be seen that, if the angular velocity of the circular fly-around is n , the trajectory is closed only when $\alpha_{failure} = 0^\circ, 180^\circ$. In this case, the closed trajectory enters into the target forbidden zone, so its safety is low. However, at other failure points, it can always stay far away from the reference trajectory, and its safety is guaranteed. But it is not easy for the fly-around spacecraft to return to the reference trajectory after the problem is solved.

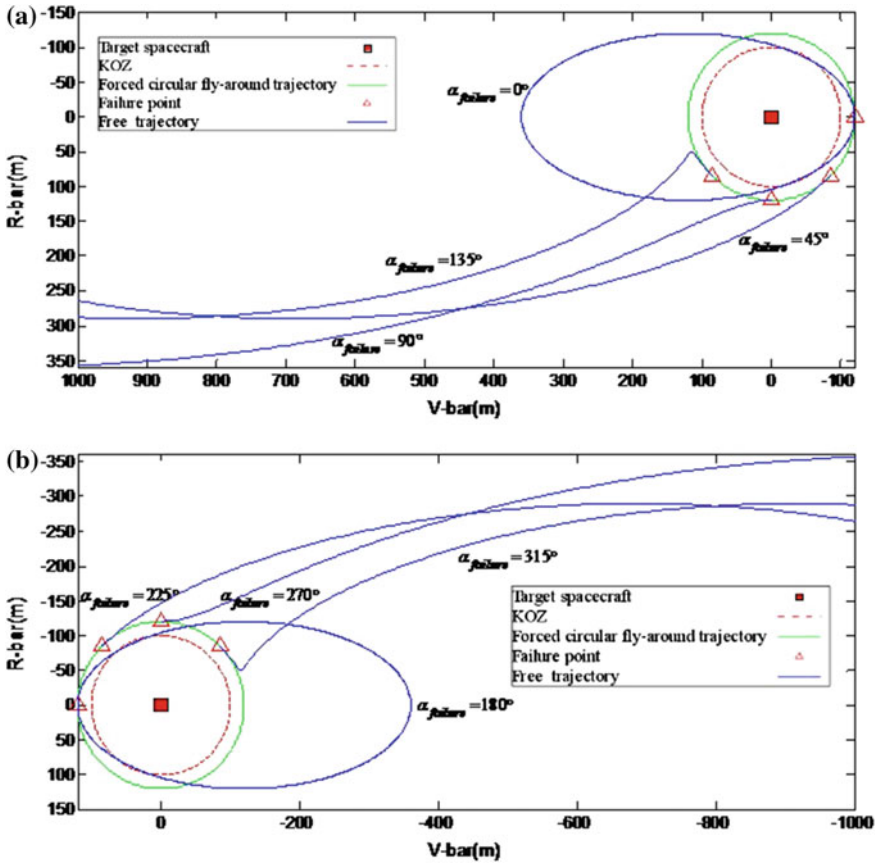


Fig. 7.11 Trajectory simulation after thruster fails at failure points in fast circular fly-around

Below, the impact of different fly-around angular velocities on the free trajectories when $\alpha_{failure} = 0^\circ, 45^\circ, 90^\circ, 135^\circ$ will be analyzed. It is shown in Fig. 7.12.

It is clear from Fig. 7.12 that, when the fly-around angular velocity $\dot{\alpha}_{fa} = 2n$, the trajectories of the failure points are all elliptical. Next, a mathematical derivation of this case will be conducted.

The free flight trajectories when $\alpha_{failure} = 180^\circ, 225^\circ, 270^\circ, 315^\circ$ are centrosymmetric with those when $\alpha_{failure} = 0^\circ, 45^\circ, 90^\circ, 135^\circ$. So the analysis will not be repeated.

We suppose that the angular velocity of the circular fly-around is:

$$\dot{\alpha}_{fa} = 2n \tag{7.13}$$

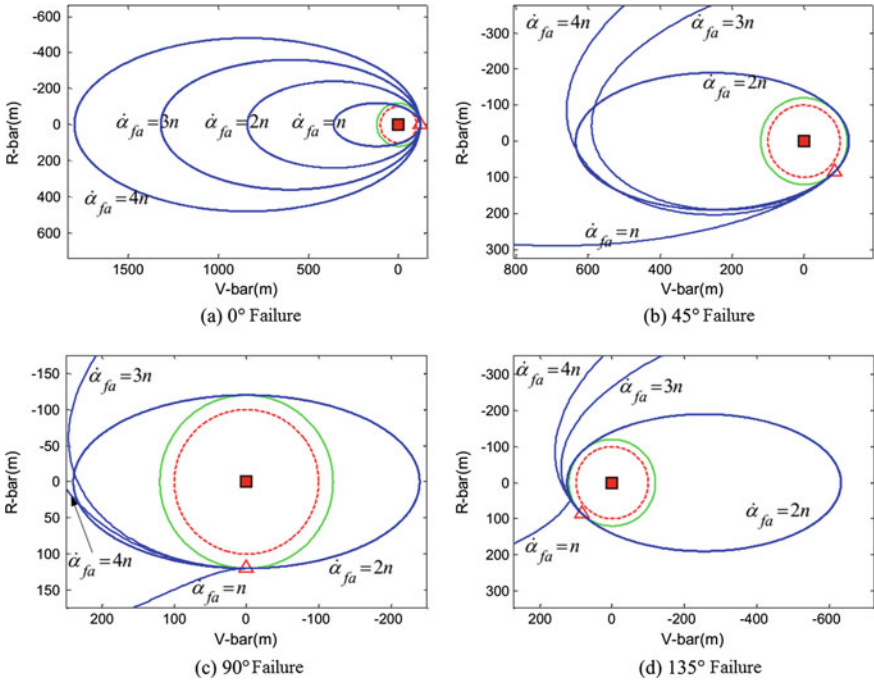


Fig. 7.12 Free trajectories with different failure points as fast fly-around angular velocity increases

When we expand Eq. (7.12), the following can be obtained:

$$\begin{cases} x_{free} = 3r_{fa} \cos(\alpha_{failure}) + 2r_{fa} \sin(\alpha_{failure}) \sin(n\tau) - 4r_{fa} \cos(\alpha_{failure}) \cos(n\tau) \\ z_{free} = r_{fa} \sin(\alpha_{failure}) \cos(n\tau) + 2r_{fa} \cos(\alpha_{failure}) \sin(n\tau) \end{cases} \quad (7.14)$$

When we reorganize Eq. (7.14), the following can be obtained:

$$\begin{cases} \frac{x_{free} - 3r_{fa} \cos(\alpha_{failure})}{2r_{fa}} = \sin(\alpha_{failure}) \sin(n\tau) - 2 \cos(\alpha_{failure}) \cos(n\tau) \\ \frac{z_{free}}{r_{fa}} = \sin(\alpha_{failure}) \cos(n\tau) + 2 \cos(\alpha_{failure}) \sin(n\tau) \end{cases} \quad (7.15)$$

If we square both sides of the above equations and add them, the following can be obtained:

$$\frac{(x_{free} - 3r_{fa} \cos(\alpha_{failure}))^2}{(2r_{fa})^2} + \frac{(z_{free})^2}{(r_{fa})^2} = 1 + 3 \cos^2(\alpha_{failure}) \quad (7.16)$$

It can be seen from Eq. (7.16) that, when the angular velocity of the circular fly-around is $2n$, the free trajectory is always elliptical wherever the thruster of the fly-around spacecraft fails in the fast fly-around circle. It accords with the simulation result. Therefore, the free trajectory in such a case is called a “free ellipse”.

The center of the free ellipse is on the V-bar. Its x coordinate is $3r_{fa} \cos(\alpha_{failure})$. The semi-major axis is $2r_{fa} \sqrt{1 + 3 \cos^2(\alpha_{failure})}$, and the semi-minor axis is $r_{fa} \sqrt{1 + 3 \cos^2(\alpha_{failure})}$. The free ellipse is tangent to the reference trajectory, and the coordinates of the tangency point are:

$$\begin{bmatrix} x_{tan} \\ z_{tan} \end{bmatrix} = \begin{bmatrix} -r_{fa} \cos(\alpha_{failure}) \\ \pm r_{fa} \sin(\alpha_{failure}) \end{bmatrix} \quad (7.17)$$

Equation (7.17) shows that, if $\alpha_{failure} = 0, \pi$, then there is only one tangency point within a single period between the free ellipse and the reference trajectory, and it is $(r_{fa} \ 0)$ or $(-r_{fa} \ 0)$. If $\alpha_{failure} \neq 0, \pi$, then there are two tangency points within a single period between the free ellipse and the reference trajectory.

It can be seen from the above analysis that, because the free ellipse is tangent to the reference trajectory of the circular fly-around, as long as the reference trajectory is designed according to Eq. (7.10), the free ellipse can also satisfy Eq. (7.10). In this way, the passive safety of the fly-around spacecraft along the trajectory can be guaranteed even if the thruster fails at any point.

Once the fly-around spacecraft is restored and back to normal, it can return to the reference trajectory utilizing this tangency relationship if a continuous thrust is imposed on the position denoted by Eq. (7.17). It can be derived from Eq. (7.3) that the continuous thrust only has a component in the radial direction and it is:

$$\gamma_z = \begin{cases} -3r_{fa}n^2 \sin(\alpha_{failure} + 2nt) & (\text{return at } \alpha_{failure}) \\ 3r_{fa}n^2 \sin(\alpha_{failure} - 2nt) & (\text{return at } 2\pi - \alpha_{failure}) \end{cases} \quad (7.18)$$

It can be seen that, if the fly-around angular velocity is twice that of the target spacecraft's orbit, the balance between safety, fuel and time can be achieved, that is:

- Its fly-around period is only half of the natural fly-around period, and the fly-around spacecraft can keep a constant distance to the non-cooperative target (s) so that the detector can work in a stable way.
- The reference trajectory will not enter into the target forbidden zone. Once the thruster fails, the free trajectory of the fly-around spacecraft is an ellipse tangent to the reference circle and will not enter into the target forbidden zone. In this way both active and passive safety are achieved.
- The fly-around spacecraft doesn't need to move far away before it conducts maneuver and returns. It can go back to the pre-set circular fly-around mission through the tangency point between the free ellipse and the reference circle.

Similar to the in-plane fly-around, to achieve the safe out-of-plane fly-around, the following condition is required:

$$x^2 + y^2 + z^2 \geq r_{KOZ}^2 \quad (7.19)$$

Likewise, we can assume the thruster of the fly-around spacecraft fails at a certain point on the fly-around circle and the angle it has covered at this time is $\alpha_{failure}$. The state of the fly-around spacecraft at the failure point can be obtained according to Eqs. (7.5) and (7.8).

$$\begin{bmatrix} r_{fa} \cos \theta \sin(\alpha_{failure}) \\ r_{fa} \sin \theta \sin(\alpha_{failure}) \\ r_{fa} \cos(\alpha_{failure}) \\ r_{fa} \dot{\alpha}_{fa} \cos \theta \cos(\alpha_{failure}) \\ r_{fa} \dot{\alpha}_{fa} \sin \theta \cos(\alpha_{failure}) \\ -r_{fa} \dot{\alpha}_{fa} \sin(\alpha_{failure}) \end{bmatrix} \quad (7.20)$$

According to Eq. (7.20), the free trajectory after the thruster fails is:

$$\mathbf{X}_{free} = \mathbf{\Phi}_{xyz}(\tau) \mathbf{X}_{failure} \quad (7.21)$$

To ensure the passive safety of the free trajectory at the failure point, the following condition is required:

$$x_{free}^2 + y_{free}^2 + z_{free}^2 \geq r_{KOZ}^2 \quad (7.22)$$

The free trajectory after the thruster fails is also simulated and computed with MATLAB. In the fast fly-around reference trajectory, eight points from 0° at an interval of 45° are selected as failure points. We suppose the radius of the target forbidden zone is 100 m, θ is 45° , the fast fly-around radius is 120 m, and the angular velocity of the fast fly-around is still n . Ignoring the influence of perturbation, the simulation result is shown in Fig. 7.13.

It can be seen that, the trajectories in the out-of-plane fly-around are far more complex than those in the in-plane fly-around. It is hard to obtain from Fig. 7.13 the relation between the free trajectory and the target forbidden zone after thrust failure. So next, the relative distances between free trajectories and the target forbidden zone (100 m) after the thrust failure at different angular velocities will be illustrated in Fig. 7.14.

According to Fig. 7.14, when $\theta = 45^\circ$, the free trajectory can stay out of the target forbidden zone within two orbital periods as the fly-around angular velocity increases. In such cases, the out-of-plane fast circular fly-around enjoys relatively high passive safety.

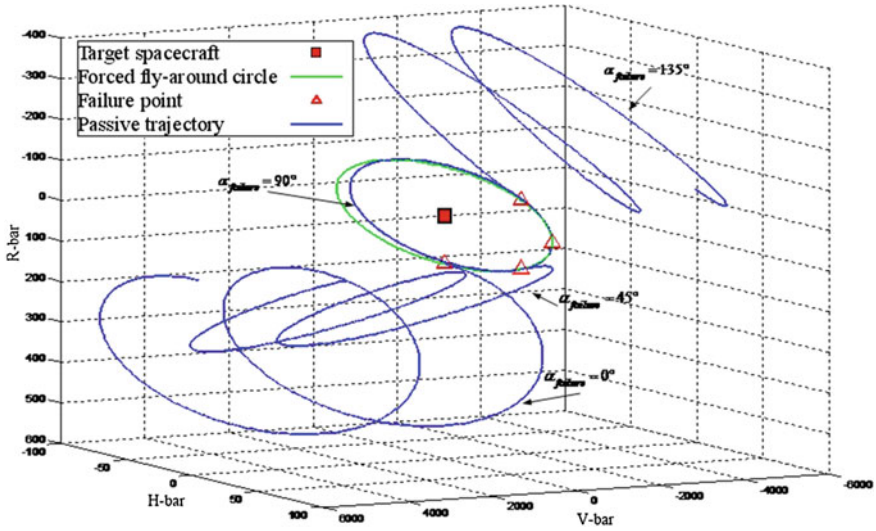


Fig. 7.13 Trajectory simulation with different failure points in out-of-plane fast circular fly-around

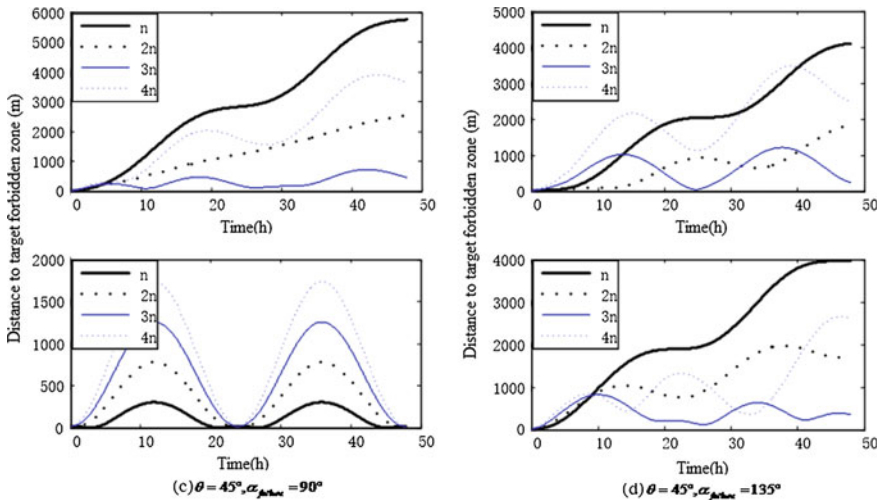


Fig. 7.14 Relative distances at different fly-around angular velocities when $\theta = 45^\circ$

As revealed in Eq. (7.20), if r_{fa} is determined, the trajectory after the thruster fails at a point in the out-of-plane fast circular fly-around is related to $\dot{\alpha}_{fa}$, θ and $\alpha_{failure}$. Obviously, their relationship is quite complicated. We know the failure point cannot to be predicted. The free trajectory of the fly-around spacecraft enters into

the target forbidden zone as long as the thruster fails at a certain point on the fly-around circle, namely,

$$\rho_{in} = \min\left(\sqrt{x_{free}^2 + y_{free}^2 + z_{free}^2} - r_{KOZ}\right) < 0 \quad (7.23)$$

The fast fly-around circle cannot be considered passively safe. Hence, we need to analyze the passive safety of the fly-around spacecraft's free trajectories with different values of $\dot{\alpha}_{fa}$ and θ .

Therefore, if r_{fa} is determined, a triple-loop structure can be designed, and the loops from the outside to the inside are: the first one is the for loop of the fast fly-around angular velocity $\dot{\alpha}_{fa}$ from low to high; the second one is the for loop of the included angle between the fly-around plane and the $x-z$ plane from low to high; the last one is the for loop of $\alpha_{failure}$ from low to high. The flow chart of this process is as follows Fig. 7.15.

It should be noted that this is similar to the in-plane fly-around. When the value of $\alpha_{failure}$ varies from 0° to 360° , the free trajectory in the first half 180° is symmetric with that in the second half 180° relative to the origin of the TOF coordinate system. When the value of θ varies from 0° to 360° , the free trajectory in the first half 180° is symmetric with that in the second half 180° relative to the $x-z$ plane. Hence, we only need to consider the cases when the values of $\alpha_{failure}$ and θ vary from 0° to 180° .

In simulation and computing, the fly-around radius r_{fa} is 120 m, and the target's orbit angular velocity is 7.292×10^{-5} rad/s. Ignoring the influence of perturbation, the free flight trajectory after the thruster fails is expanded by two orbital periods. According to the final results, a surface color map and a plane color map are drawn as Figs. 7.16 and 7.17 show respectively.

In Figs. 7.16 and 7.17, each color block indicates how far the free trajectory determined by the corresponding $\dot{\alpha}_{fa}$ and θ enters into the forbidden zone, namely, ρ_{in} in Eq. (7.23). The bigger the color block's value, the smaller the value of ρ_{in} . This indicates that the free trajectory enters more deeply into the target forbidden zone and the passive safety of the fly-around circle is lower. It can be seen that, when $r_{fa} = 120$ m, the bigger the angular velocity of the fast fly-around and the included angle between the fly-around plane and the $x-z$ plane, the higher the passive safety of the fast fly-around. However, the free trajectory may enter into the target forbidden zone when the thruster fails under some circumstances, which is denoted by the color blocks of high value in Figs. 7.16 and 7.17. Therefore, $\dot{\alpha}_{fa}$ and θ corresponding to the color blocks of small value should be selected in practical application.

There is a precondition for the above analysis, i.e., $r_{fa} = 120$ m. If the fly-around radius changes, the values of ρ_{in} brought about by different $\dot{\alpha}_{fa}$, θ and $\alpha_{failure}$ should also be calculated. The results are as follows Fig. 7.18.

It can be seen that, as the fly-around radius constantly increases, the value of ρ_{in} becomes bigger and the less free trajectory enters into the target forbidden zone. r_{fa} is proportional to ρ_{in} as follows:

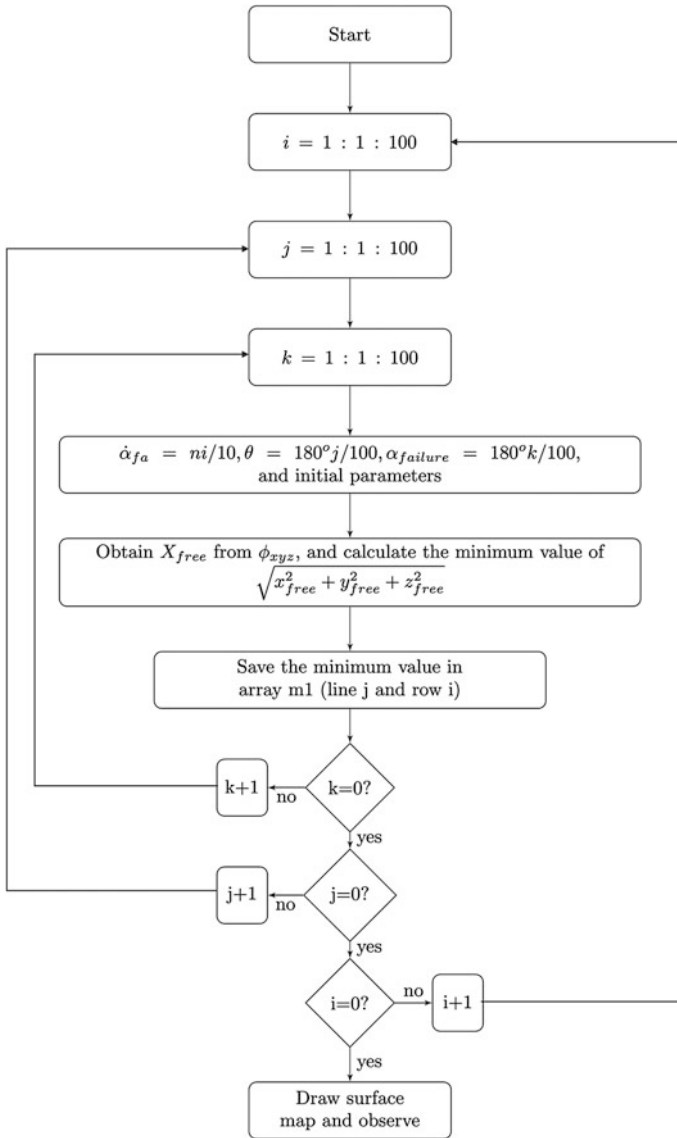


Fig. 7.15 Flow chart designed to determine whether free trajectory enters into target forbidden zone

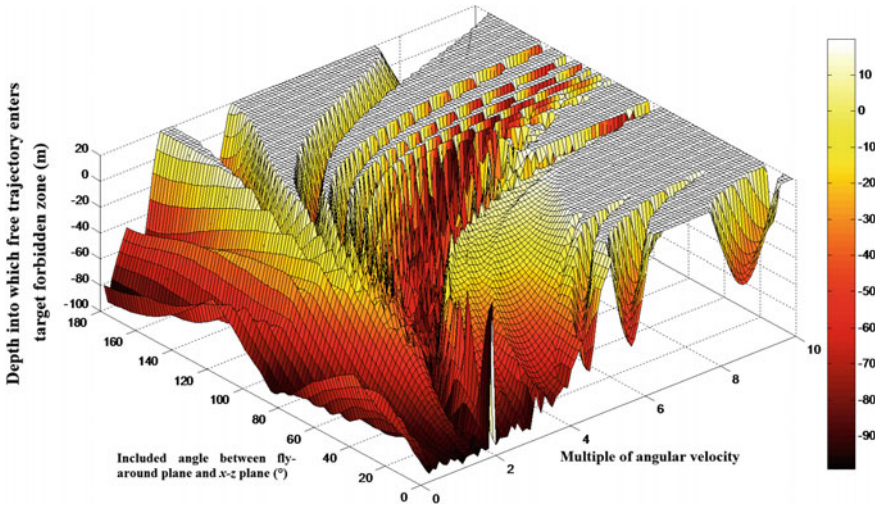


Fig. 7.16 Surface color map the free trajectory enters into target forbidden zone when $r_{fa} = 120$ m

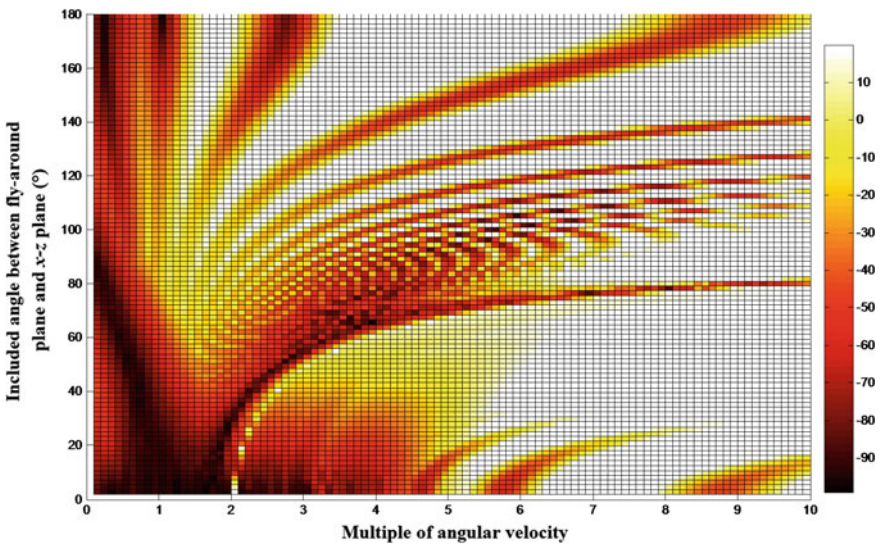


Fig. 7.17 Plane color map the free trajectory enters into target forbidden zone when $r_{fa} = 120$ m

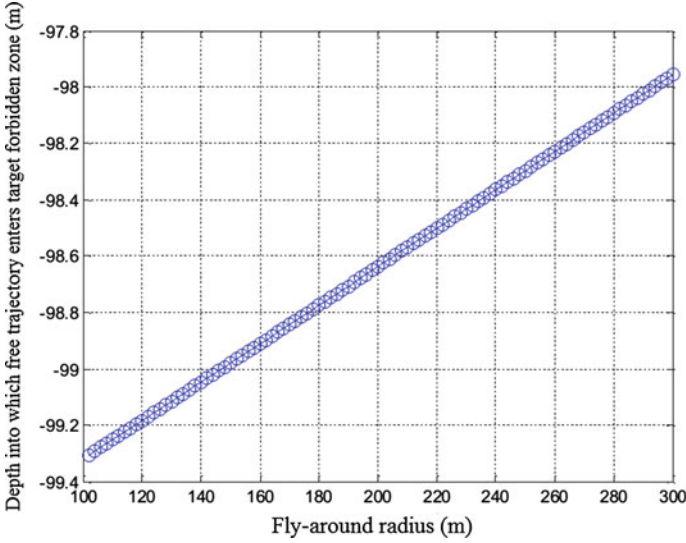


Fig. 7.18 Depths to which free trajectory enters into target forbidden zone as r_{fa} changes

$$\rho_{in} = 0.00675r_{fa} - 99.975 \quad (7.24)$$

Thus in the high-orbit non-cooperative autonomous rendezvous, we should try to make $\rho_{in} \geq 0$. In other words, only when the value of r_{fa} is bigger than 14.8 km can we guarantee that the fly-around spacecraft in the fast circular fly-around will not enter into the target forbidden zone under any circumstances.

7.3 Fast Access Orbit

When disasters like earthquakes, nuclear leakages and military conflicts happen, to have a timely understanding of the emergency, some new spacecraft need to be launched from the ground. If the spacecraft can reach the space orbit rapidly, the observation data regarding the region of interest can be obtained as quickly as possible. Therefore, the most salient feature of a fast access orbit is its rapid responsiveness. After an emergency occurs, a fast access orbit can transmit the information to users within just a few hours.

The response time of the fast access orbit is defined as:

$$T_{Response} = T_{Prepare} + T_{WaitWindow} + T_{LaunchTime} + T_{OrbitMission} \quad (7.25)$$

Here, $T_{Prepare}$ is the launch preparation time; $T_{WaitWindow}$ is the waiting time for launch window; $T_{LaunchTime}$ is the time from launching the spacecraft to its entering

into the predetermined orbit; $T_{\text{OrbitMission}}$ is the orbit response time which starts when the spacecraft enters into the orbit and ends when the ground receives the first batch of data, or the communication and navigation services begin.

7.3.1 Low-Earth-Orbit Fast Access Orbit: Design

The Low-Earth-Orbit (LEO) fast access orbit was first put forward by Microcosm, which aimed to acquire firsthand information as soon as possible in order to respond timely to an emergency. The LEO fast access orbit is mainly used for reconnaissance on sensitive regions. Its design principle is shown in Table 7.2.

For any launch site, if the launching azimuth is not considered, two fast access orbits can be designed to cover any point on Earth. One is antero-grade and the other is retrograde as shown in Fig. 7.19.

For an appointed target, the orbit can be determined by selecting a launching azimuth. The major steps are:

- Set a launch site and obtain its longitude and latitude;
- Select a target and obtain its longitude and latitude;
- Determine the observation requirements, including the resolution of ground imaging and the regression period. Determine the altitude and eccentricity of the orbit.
- According to the launch time $T_{\text{LaunchTime}}$, and the positions of the launch site and the target, obtain the orbit elements of the LEO fast access orbit.

We can use an example here. If the launch site is in Xichang, China, the target is Fukushima, Japan, and the orbit is a recursive circular orbit with 15 days as a period, then the design is shown in Fig. 7.20.

Limited by the minimum elevation in optical reconnaissance (30°), the fast access orbit thus designed covers the target area as Fig. 7.21.

It can be seen that the satellite in the fast access orbit can cover the target area twice a day, satisfying the design requirements.

Table 7.2 Design principle of LEO fast access orbit

Serial number	Design principle	Method
1	Cover the target within 90 min after being launched	Enters into the orbit covering the target in the first circle
2	Repeatedly observe per day	Via recursive orbit
3	Observe twice a day if possible	Observed once when the orbit ascends and once when it descends

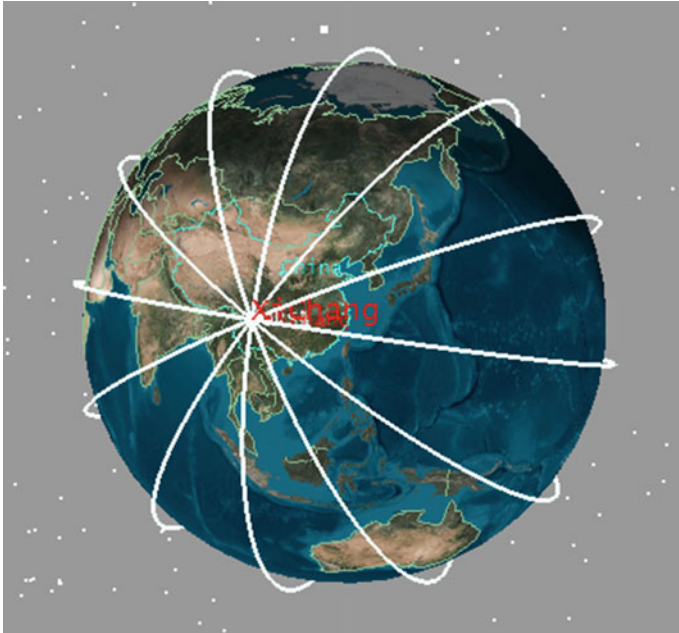


Fig. 7.19 Coverage of any point on Earth from any launch site

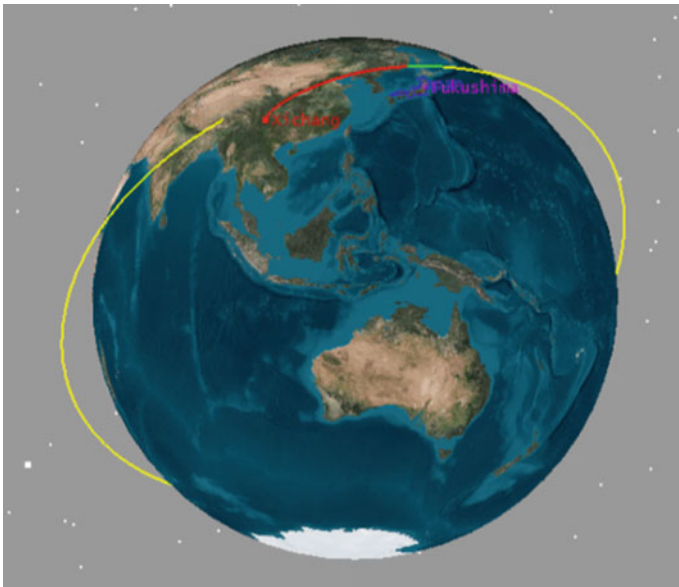


Fig. 7.20 Fast access orbit designed for Fukushima

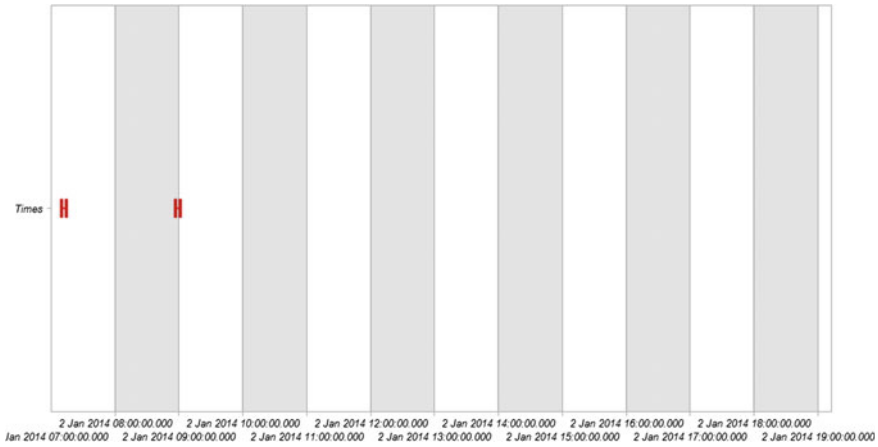


Fig. 7.21 Time on observing Fukushima

7.3.2 Cobra Orbit: Design

The Cobra orbit was first brought up by John Draim, aiming to provide highly efficient communication support for middle-longitude regions. Through reasonable design, a Cobra orbit can cover regions of specific longitude and latitude at a specific communication time. The Cobra orbit has big eccentricity (800 km × 27,000 km). Its orbit inclination is the critical inclination (63.4°), so its apogee and perigee do not revolve. Hence the Cobra orbit can keep stable for a long time.

We can take the communication coverage of China as an example. The design steps of a Cobra orbit is as follows:

- Design the orbit: the altitudes of the apogee and the perigee are 27,000 and 800 km, respectively; the orbit inclination is 63.4°;
- Determine the region of interest, and set the orbit’s apogee over this region;
- Set the time when the satellite passes the apogee as the expected time.

Following the steps above, the Cobra orbit used to provide communication coverage for China can be designed as Figs. 7.22, 7.23.

We suppose that the minimum elevation required in communication is 10°. The spacecraft in the Cobra orbit can support the communication for seven hours in an eight-hour orbital period (Fig. 7.24).

According to the Cobra orbit’s coverage, a network formed by three to four spacecraft in the Cobra orbit can achieve continuous coverage of China, so it is very practical.

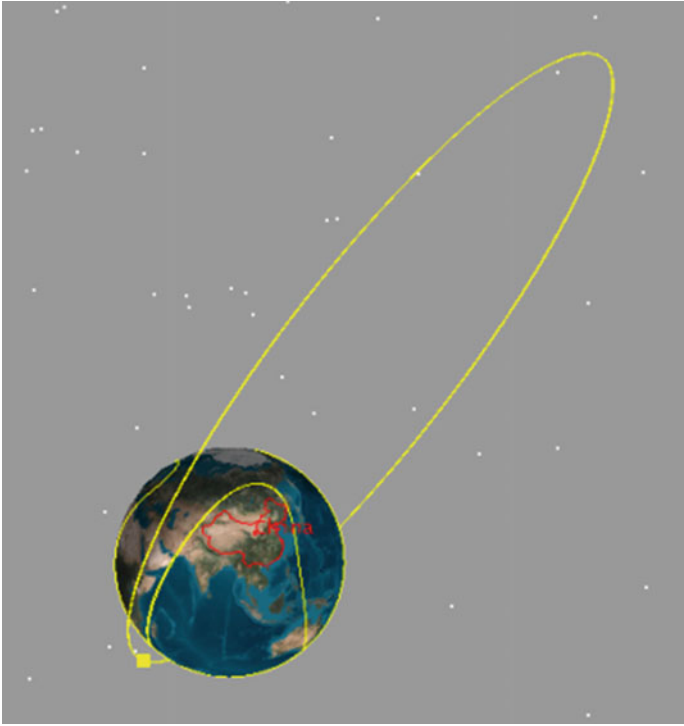


Fig. 7.22 Cobra orbit designed to provide communication coverage for China

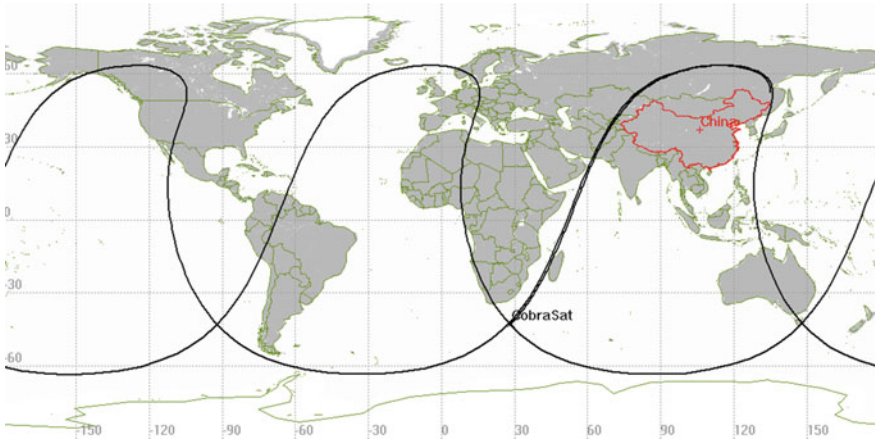


Fig. 7.23 Ground track of Cobra orbit

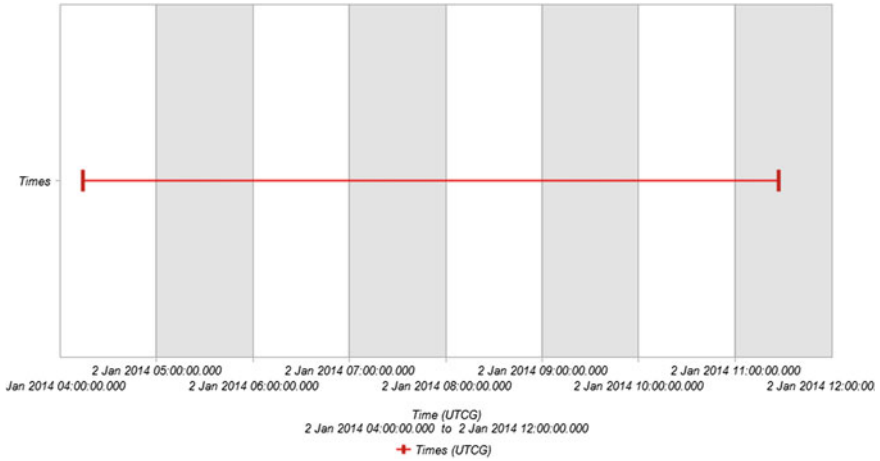


Fig. 7.24 Coverage of China from spacecraft in Cobra orbit (within one period)

7.4 Summary

The fast responsive orbit significantly shortens the response time at the cost of some traditional performance indexes like coverage and service life, which makes it superior in carrying out emergent space missions. The fast responsive orbit is directly related to space missions, so it is highly oriented. This chapter mainly focuses on two such responsive orbits, i.e., the fast fly-around orbit and the fast access orbit. There are other types not dealt with here. Readers can come up with other fast responsive orbits according to their practical demands.

Chapter 8

Theory and Design Method of Earth Pole-Sitter Orbit

During the late 1970s and the early 1980s, inspired by the science fiction work *Two Planets*, Driver described a spacecraft which was able to hover over the Earth's poles for a long time, and the earth pole-sitter orbit is exactly the orbit designed for this spacecraft.

8.1 Earth Pole-Sitter Orbit: Concept

An earth pole-sitter is a spacecraft that hovers over the South Pole or the North Pole of the Earth and flies in the earth pole-sitter orbit. The ground track of the spacecraft is always around the South Pole or the North Pole, and in this way, the spacecraft achieves the long-time coverage of the South Pole or the North Pole.

The spacecraft operating in the earth pole-sitter orbit are on the rotation axis of the Earth. Seen from space, the spacecraft seems to be residing on the South Pole or the North Pole of the Earth. If the distance between the spacecraft and the South Pole or the North Pole remains unchanged, then in the Earth-fixed coordinate system, the spacecraft will remain static.

At present, the continuous coverage of the Earth's surface is mainly achieved by the GEO. But as the orbit inclination of the GEO is 0° , the coverage of high latitude regions and Polar Regions is unrealizable. Therefore, with regard to the coverage of Polar Regions, multiple low and medium-orbit satellites with a large inclination are often used to constitute a constellation to achieve the coverage. However, the arc of the satellite when it is passing through the observation region is limited, so when the number of satellites in the constellation is restricted, continuous coverage is not able to be achieved and the frequency of the coverage depends on the number of

Matteo Ceriotti, Colin R. McInnes. An Earth Pole-Sitter Using Hybrid Propulsion [C]. AIAA/AAS Astrodynamics Specialist Conference. Canada: AIAA/AAS Astrodynamics Specialist Conference, 2010:1–29.

satellites in the constellation and the configuration of the constellation. Moreover, if the constellation consists of imaging satellites, in order to obtain the observation result with a full field of view, the reconstruction of multiple images must be done.

If the earth pole-sitter orbit is adopted, one spacecraft will be enough to achieve the continuous coverage of the Polar Regions. It is not only beneficial to real-time reconnaissance, monitoring and communication with a full field of view, but also provides weather observation data with moderate precision, instead of the traditional periodic data, to the meteorological departments.

8.2 Earth Pole-Sitter Orbit: Design Method

8.2.1 Dynamic Model in Circular Restricted Three-Body Problem

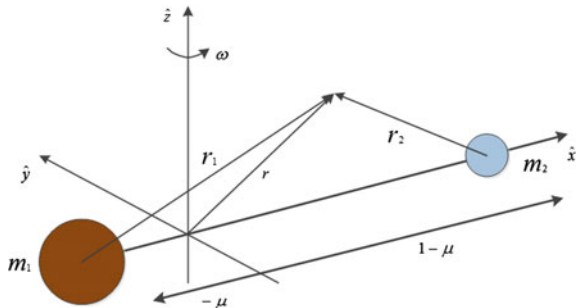
The circular restricted three-body problem is to study the motion of an object (the spacecraft) with a very small mass under the universal gravitation of two large celestial bodies, i.e., the circular motion around the centers of mass of the two celestial bodies. This model ignores the gravitation of the spacecraft to the two large celestial bodies.

We assume that the masses of the two large celestial bodies P_1 and P_2 are m_1 and m_2 respectively, and they move in a circular motion around each other with a rotational angular velocity of ω . Now we define the centroid rotation coordinate system as $Oxyz$, which is shown in Fig. 8.1.

- The origin represents the centroid of the two-body system consisting of two large celestial bodies P_1 and P_2 ;
- $x - y$ Plane represents the motion planes of P_1 and P_2 ;
- x axis is fixed with the line connecting P_1 and P_2 , points to the smaller celestial body P_2 , and does a circular motion with it.
- z axis is consistent with the rotation axis of the system;

$$\ddot{\mathbf{r}} + 2\boldsymbol{\omega} \times \dot{\mathbf{r}} + \boldsymbol{\omega} \times (\boldsymbol{\omega} \times \mathbf{r}) = -\nabla V + \mathbf{a} \tag{8.1}$$

Fig. 8.1 Centroid rotation coordinate system in restricted three-body problem



Here: \mathbf{r} is the position vector; \mathbf{a} is the non-gravitational acceleration, such as the thrust; V is the gravitational potential function of the large celestial bodies, and

$$V(r) = -\left(\frac{1-\mu}{r_1} + \frac{\mu}{r_2}\right), \mu = \frac{m_2}{m_1+m_2} \quad (8.2)$$

Then, the gravitational constants of the two celestial bodies are:

$$\begin{aligned} Gm_1 &= 1 - \mu \\ Gm_2 &= \mu \end{aligned}$$

Here: G represents the universal gravitational constant.

We will use a normative dimensionless form in the following equations, i.e., we assume $\omega = 1$ and the unit of distance is the distance between the two celestial bodies. In this way, the coordinate of m_1 on X axis is $-\mu$, that of m_2 is $1 - \mu$. If the large celestial body m_1 represents the Sun and m_2 represents the Earth, then $\mu = 3.0404 \times 10^{-6}$ and $\mathbf{r}_1, \mathbf{r}_2$ are the radius vectors of the spacecraft to the two large celestial bodies m_1, m_2 , then

$$\begin{cases} \mathbf{r}_1 = \mathbf{r} + [0 \ 0 \ \mu]^T \\ \mathbf{r}_2 = \mathbf{r} - [0 \ 0 \ 1 - \mu]^T \end{cases} \quad (8.3)$$

If we define $\Phi(\mathbf{r}) = -\frac{1}{2}(x^2 + y^2)$, then $\boldsymbol{\omega} \times (\boldsymbol{\omega} \times \mathbf{r}) = \nabla\Phi$; and if we let $U = V + \Phi$, then Eq. (8.1) can be changed into:

$$\ddot{\mathbf{r}} + 2\boldsymbol{\omega} \times \dot{\mathbf{r}} = -\nabla U + \mathbf{a} \quad (8.4)$$

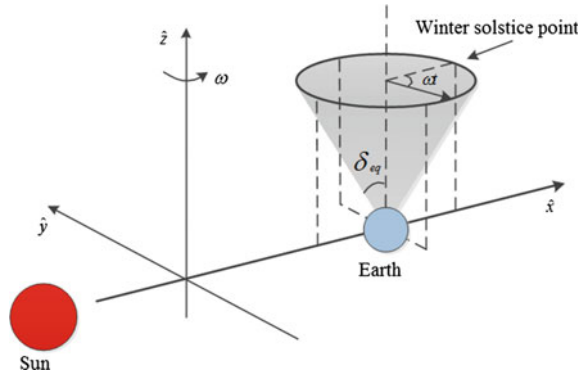
It is already known that the spacecraft in the earth pole-sitter orbit remains on the rotation axis of the Earth during the whole mission. If the Earth's pole shift and nutation are ignored, then the rotation axis of the Earth will not go through rotation and other changes when the Earth revolves around the Sun. Hence, in the rotation coordinate system mentioned above, the rotation axis of the Earth rotates at a velocity opposite to that of the three-body system, and the rotational angular velocity is $-\boldsymbol{\omega}$. In this way, after a one-year rotation, the rotation axis of the Earth will form a cone as is shown in Fig. 8.2.

In order to keep the spacecraft on the rotation axis of the Earth all the time, we assume that at the moment when $t_0 = 0$, the spacecraft is at the winter solstice point in Fig. 8.2, then the position vector of the spacecraft can be described as:

$$\mathbf{r}(t) = \begin{bmatrix} d(t) \sin \delta_{eq} \cos \omega t + (1 - \mu) \\ -d(t) \sin \delta_{eq} \sin \omega t \\ d(t) \cos \delta_{eq} \end{bmatrix} \quad (8.5)$$

Here: $d(t)$ represents the distance between the center of the Earth and the spacecraft, and is often a continuous function of time. When we substitute Eq. (8.5)

Fig. 8.2 Motion of Earth's rotation axis in three-body system



into Eq. (8.4), the value and the direction of the controlling acceleration required in completing the earth pole-sitter orbit control can be obtained.

8.2.2 Design of Earth Pole-Sitter Orbit with Fixed Residence Distance

We assume that the combination control by SEP/solar sail is adopted, the initial position of the spacecraft is at the winter solstice point, the initial mass is 1000 kg, and the geocentric distance is 0.01AU. Then we use the dynamic model of the spacecraft in the earth pole-sitter orbit formulated in the previous section to simulate the operation of the spacecraft in one year. The simulation result is shown in Fig. 8.3.

Figure 8.3 illustrates the controlling accelerations (the illumination of the solar sail $\beta_0 = 0.05$) needed for a one-year earth pole-sitter mission. The black bold arrows, which are in proportion, represent the value and direction of the acceleration needed to stay in the orbit; the green arrows represent the normal direction of the solar sail's surface. As the solar sail adopted in the calculation is not ideal, the direction is not totally consistent with the direction of the controlling force (the blue arrows) produced in practice by the solar sail; the black arrows represent the acceleration provided by the solar electric propulsion.

From Fig. 8.3, it can be seen that on the whole, the gravitational accelerations point to the $-\hat{z}$ axis, so the thrust imposed has to be in the opposite direction; the direction of the accelerations provided by the solar sail has a component in the direction of the $+\hat{z}$ axis, and obviously, it has a component in the direction of the $+\hat{x}$ axis (i.e., the direction of the line connecting the Sun and the spacecraft). Therefore, the direction of the accelerations provided by SEP mainly supplements the acceleration in the direction of the $+\hat{z}$ axis, and offsets the remaining components in the direction of \hat{y} .

Fig. 8.3 Controlling acceleration needed for one-year earth pole-sitter mission

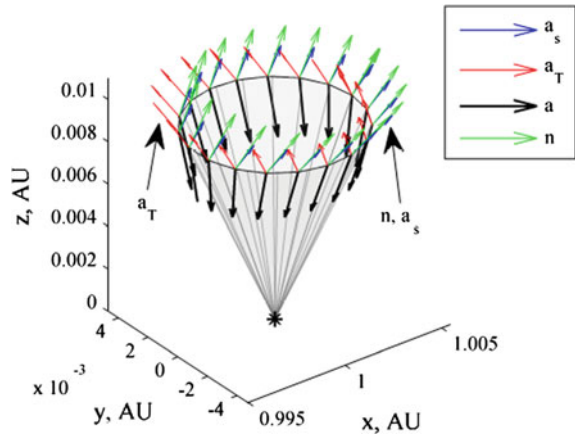


Fig. 8.4 Thrust acceleration provided by SEP and solar sail

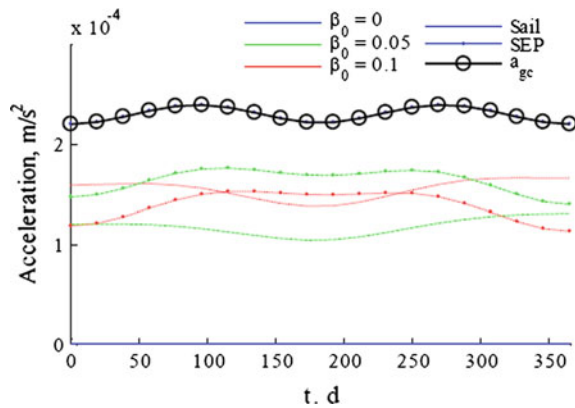


Figure 8.4 illustrates the value of the acceleration (the dotted line) provided by the solar sail and SEP. In the figure, the line with circles represents the value of the acceleration needed to complete the earth pole-sitter mission; $\beta_0 = 0$ indicates that the acceleration provided by the solar sail is 0 and there is only SEP to provide the controlling acceleration; the green line represents the controlling acceleration provided by the solar sail and SEP when $\beta_0 = 0.05$; the red line represents the controlling acceleration provided by the solar sail and SEP when $\beta_0 = 0.1$.

From Fig. 8.4, it can be seen that the controlling acceleration needed from SEP around summer solstice ($t \in [100, 250]$) is relatively big.

Figure 8.5 illustrates the changes in the mass of the spacecraft, mainly the consumption of propellant during the propulsion control by SEP.

Figure 8.6 illustrates the influence of the residence distance of the spacecraft (the distance between the spacecraft and the earth center) on propellant consumption. From Fig. 8.6, it can be seen that as the residence distance becomes shorter, the gravitation of the Earth starts to take the leading role and fuel consumption

Fig. 8.5 Changes in spacecraft's mass

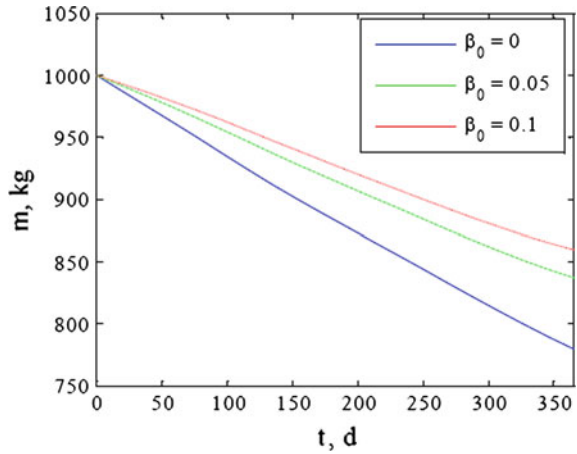
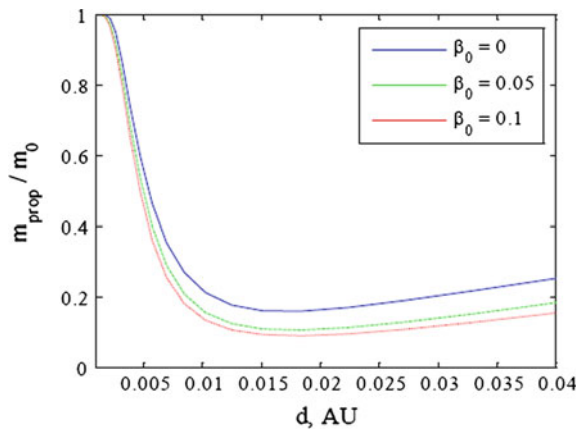


Fig. 8.6 Residence distance and propellant consumption



increases sharply. And when the geocentric distance $d \cong 0.017AU$, the consumption of propellant reaches the lowest point.

8.2.3 Design of Earth Pole-Sitter Orbit with Unfixed Residence Distance

If there are fewer constraints on the residence distance and an inclined orbit is adopted, the solar sail might be better utilized and thus we can decrease propellant consumption and extend residence time.

We assume the residence geocentric distance of the spacecraft at the winter solstice point is d_1 and that at the summer solstice point is d_2 , the changes in residence height in one year is shown in Fig. 8.7.

Fig. 8.7 Changes in residence position

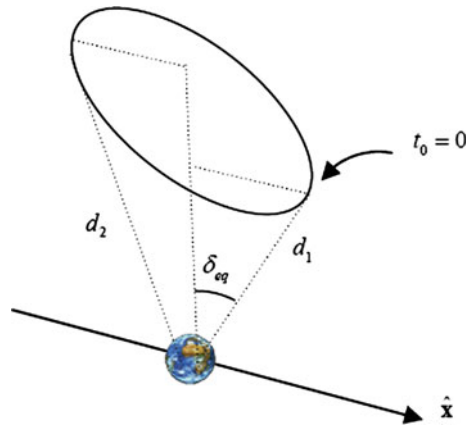
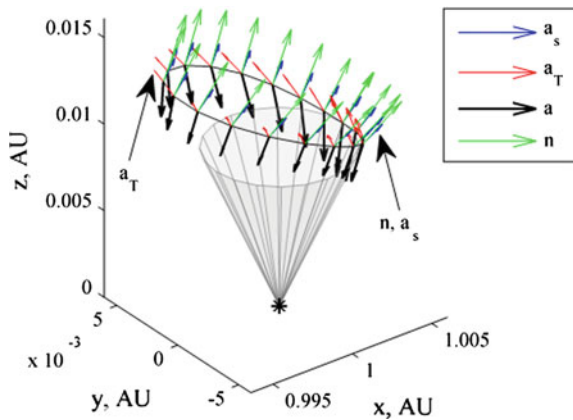


Fig. 8.8 Controlling acceleration needed for one-year residence (with changing residence heights)



With regard to the residence method mentioned above, the following equations can be obtained:

$$d(t) = d_1 + (d_2 - d_1) \frac{\cos(\omega t + \pi) + 1}{2} \tag{8.6}$$

$$\mathbf{r}(t) = \begin{bmatrix} d(t) \sin \delta_e \cos \omega t + (1 - \mu) \\ -d(t) \sin \delta_e \sin \omega t \\ d(t) \cos \delta_e \end{bmatrix} \tag{8.7}$$

We assume $d_1 = 0.01AU$, $d_2 = 0.015AU$. Through simulation, the controlling acceleration ($\beta_0 = 0.05$) needed for a one-year earth pole-sitter mission can be obtained as Fig. 8.8 shows.

The accelerations provided by the solar sail and SEP respectively in one year are shown in Fig. 8.9. In the figure, the dotted line represents the acceleration provided

Fig. 8.9 Thrust acceleration provided by SEP and solar sail (with changing residence heights)

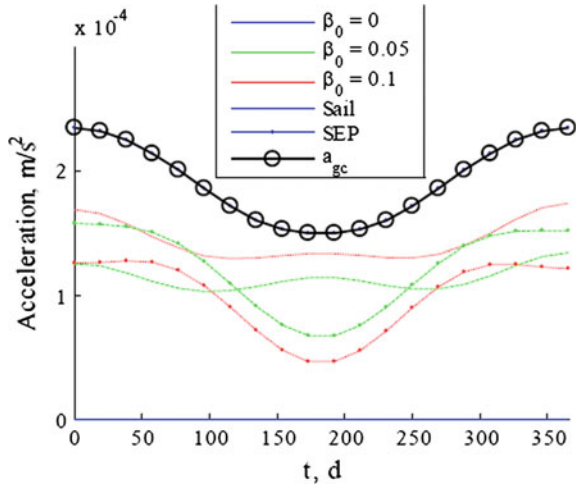
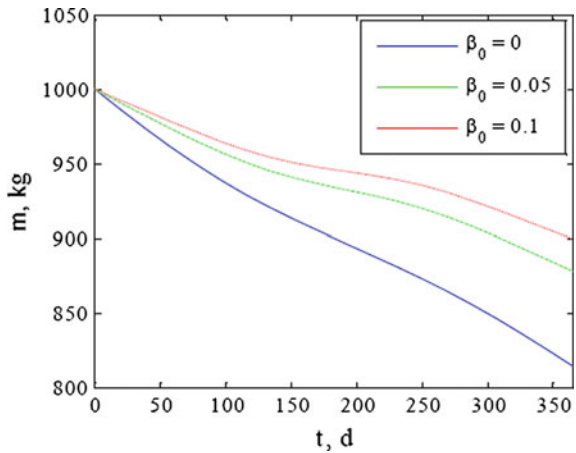


Fig. 8.10 Changes in spacecraft’s mass (with changing residence heights)



by SEP and the line with circles represents the total controlling acceleration needed in completing the earth pole-sitter mission.

It can be seen that the controlling acceleration needed from SEP decreases substantially around summer solstice and this can save the propellant remarkably.

Figure 8.10 illustrates the changes in the spacecraft’s mass along with time. Compared with the situation when the residence height is unchanged, the propellant is quite obviously saved.

It is worth noting that the saving in propellant is not because the residence height becomes higher during the summer only. The more important fact is that inclined residence is adopted. Generally, with regard to the north pole-sitter mission, keeping shorter residence distance in winter and longer residence distance in summer will save more propellant.

8.3 Optimization Design of Earth Pole-Sitter Orbit

It can be known from the above analysis that, by means of designing the residence distance of the spacecraft, the propellant needed in the control of the earth pole-sitter spacecraft can be saved effectively. In practical application, we should, on the basis of the specific requirement of the payload on the spacecraft, choose between the fixed residence height and the changing residence height. If the requirement of the payload is not considered, then an optimal change law of the spacecraft’s residence distance can be found through optimization in order to save the propellant as much as possible.

We take $\beta_0 = 0, 0.05, 0.1$ and $d_{\max} = 0.1AU$, and pick 60 sampling points in one year to optimize them. The variation in the geocentric distance of the spacecraft when energy is saved most is shown in Fig. 8.11.

Figure 8.12 illustrates the variation of the spacecraft’s geocentric distance under three conditions, i.e., $\beta_0 = 0, 0.05, 0.1$. Under the first condition, the spacecraft is

Fig. 8.11 Optimal paths when $\beta_0 = 0, 0.05, 0.1$

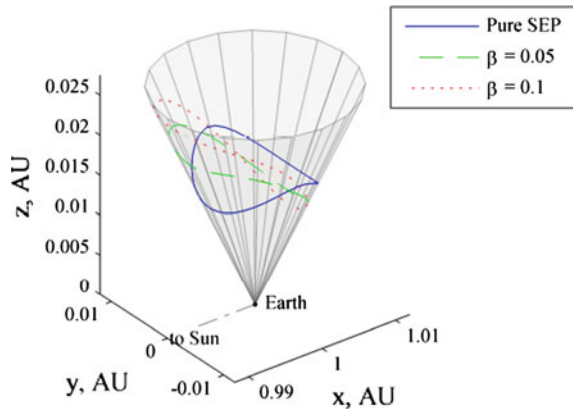
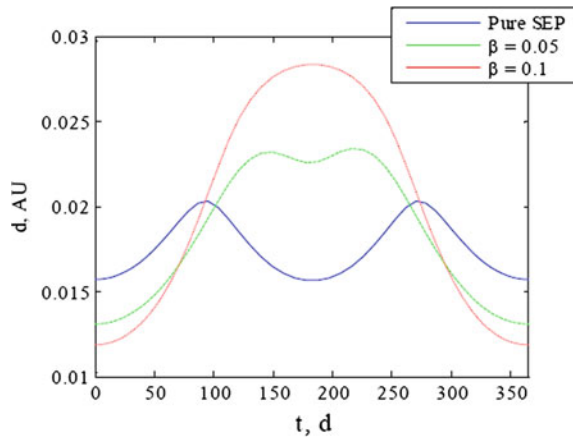


Fig. 8.12 Variation of the spacecraft’s geocentric distance



solely propelled by SEP (i.e., $\beta_0 = 0$), the optimal path is symmetric in summer and winter, and as β_0 increases, the residence orbit becomes closer to the geo-center in winter and becomes farther from the geo-center in summer; when $\beta_0 = 0.1$, the distance in summer is two times of that in winter.

Figures 8.13 and 8.14 illustrate the controlling acceleration needed from the solar sail and SEP with the optimal path and the variation in the spacecraft's mass respectively.

From Fig. 8.13, it can be known that under the sole control of SEP (i.e., $\beta_0 = 0$), the controlling acceleration includes two regions: one passes the summer solstice point and one passes the winter solstice point. In the two regions, the controlling acceleration provided by SEP is almost constant. The two regions are divided by two narrow V shapes at the vernal equinox and the autumnal equinox. In the two V-shaped regions, the controlling acceleration needed from SEP becomes very small, the motion of the spacecraft along the direction of the \hat{z} axis will reverse, i.e., the minimum controlling acceleration appears when the spacecraft is farthest from the geo-center.

If $\beta_0 = 0.05$, less acceleration provided by SEP will be needed in the V-shaped regions. Meanwhile, the thrust region around the summer solstice point becomes smaller and the two regions with weaker thrust become larger.

If $\beta_0 = 0.1$, the thrust region around the summer solstice point disappears, the two ballistic arcs merge, i.e., from spring all the way to autumn.

From Fig. 8.14, it can be known that adopting the solar sail can reduce the consumption and loss of propellant effectively. We can take one year as a period, and it can be seen that the control solely by SEP consumes 158 kg of propellant. But if a solar sail of $\beta_0 = 0.05$ is adopted, the propellant consumption is reduced to 97 kg.

Table 8.1 provides the parameter comparison of the three optimal paths when $\beta_0 = 0, 0.05, 0.1$.

Here, T_{\max} is the maximum control force provided by SEP.

Fig. 8.13 Controlling acceleration provided by solar sail and SEP with optimal path

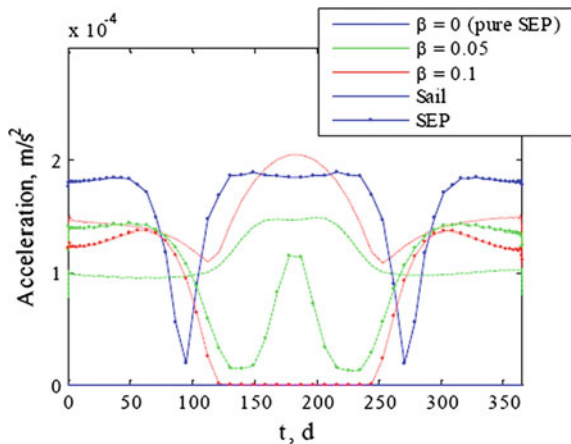


Fig. 8.14 Variation of spacecraft's mass with optimal path

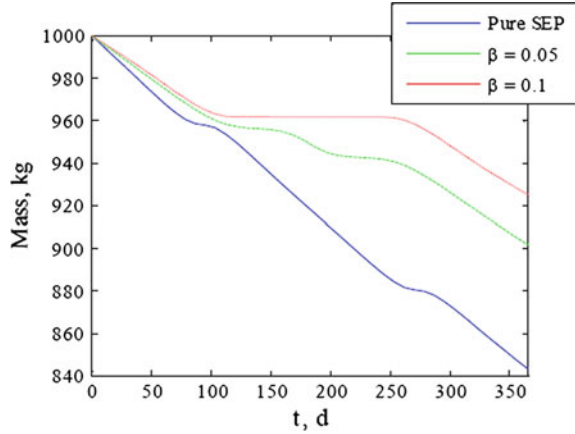


Table 8.1 Parameter comparison of three optimal paths when $\beta_0 = 0, 0.05, 0.1$

β_0	$\min_t d(t), AU$	$\max_t d(t), AU$	m_f, kg	m_{prop} / m_0	T_{max}, N
0.0	0.015675	0.020332	843.430417	0.156570	0.180648
0.05	0.013116	0.023422	901.896219	0.098104	0.141085
0.1	0.011896	0.028363	925.192867	0.074807	0.134256

8.4 Summary

The geostationary orbit (GEO) is not able to achieve the coverage of high latitude regions and Polar Regions. So generally, in order to achieve the continuous coverage of these regions, multiple spacecraft should be used to form a constellation and the number of the spacecraft has to be large. The earth pole-sitter orbit uses orbit control to achieve the long-term residence of the spacecraft at the Earth's poles. Therefore, with only one spacecraft, the coverage of the high latitude regions in the northern or southern hemisphere (including the North Pole or the South Pole) can be achieved. This has significant application values in navigation, communication, meteorological reconnaissance, and other areas.

Of course, from the above analysis, it can be seen that the defects of this orbit are also quite obvious. As the orbit is very far from the Earth's surface, it is difficult for it to be used in reconnaissance that has a high demand for precision and in other fields.

Appendix A

Optimization Design of Rendezvous Orbit with MATLAB

We assume that there are n target spacecraft whose orbits are all circular orbits, which means they will form $2n$ traversing points in the rendezvous orbit plane. According to the determination method of traversing points, the positions of the $2n$ traversing points can be expressed as:

$$(r_1, \phi_1), (r_1, \phi_1 + \pi), (r_2, \phi_2), (r_2, \phi_2 + \pi), \dots, (r_n, \phi_n), (r_n, \phi_n + \pi)$$

And the positions are shown in Fig. A.1.

Fig. A.1 illustrates four pairs of traversing points, i.e., eight traversing points formed when the four orbits of the target spacecraft passing through the rendezvous orbit plane, and they are $(A1, A1')$, $(A2, A2')$, $(A3, A3')$, $(A4, A4')$ respectively. The phase angles of these points relative to the direction of the ascending node of the rendezvous orbit are $(\phi_1, \phi_1 + \pi)$, $(\phi_2, \phi_2 + \pi)$, $(\phi_3, \phi_3 + \pi)$, $(\phi_4, \phi_4 + \pi)$ respectively. Obviously, through curve fitting, an elliptical curve can be fitted and it is realizable to require one of the focuses on the elliptical curve to be at the spherical center of the Earth. The relation between the direction of the perigee and the direction of the ascending node is shown in Fig. A.2.

If the orbit plane of the rendezvous orbit is determined, which means the two orbit elements of the rendezvous orbit, i.e., the orbit inclination i and the right ascension of the ascending node Ω , are already known. Then, the remaining orbit elements needed to be determined are the size, the shape and the direction of the rendezvous orbit in the orbit plane, i.e., the semi-major axis a , the eccentricity e and the argument of perigee ω .

According to Kepler's First Law, it can be known that the rendezvous orbit is an elliptical curve and the Earth is at one of the focuses of the ellipse. We define a two-dimensional reference coordinate system $o - xy$ and a two-dimensional translational coordinate system $o' - x'y'$ in the rendezvous orbit plane. Here, ox points to the direction of the ascending node. And then, we define another coordinate system $o' - x''y''$ along the rendezvous orbit, with $o' - x''$ pointing to the direction of the perigee of the rendezvous orbit. This is shown in Fig. A.3.

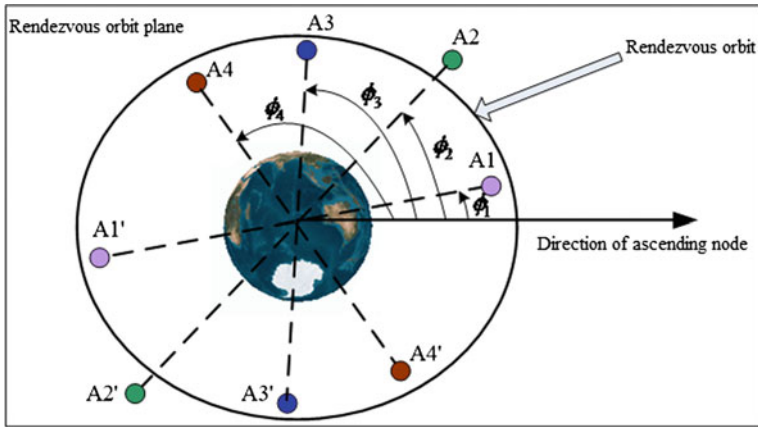


Fig. A.1 Distribution of traversing points in rendezvous orbit plane

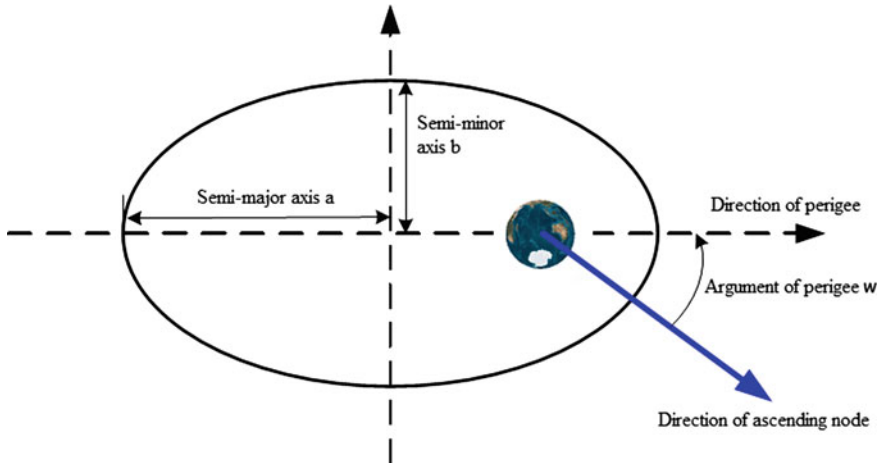


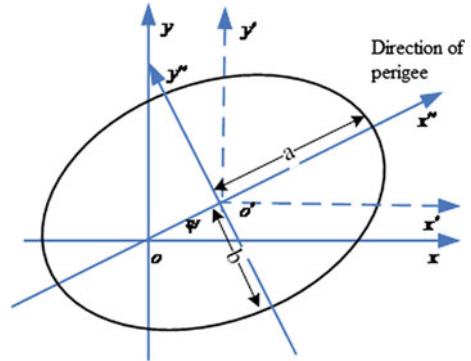
Fig. A.2 Schematic figure of parameters of rendezvous orbit

It can be seen that the included angle ψ between the ox axis and the $o'x''$ axis is the argument of perigee ω of the elliptical orbit. When we assume the semi-major axis of the ellipse is a , the semi-minor axis is b , and the coordinates of the ellipse's center in $o - xy$ are (x_{c0}, y_{c0}) , then the following equation can be obtained:

$$a^2 - b^2 = c^2 = x_{c0}^2 + y_{c0}^2 \tag{A.1}$$

It is already known that in the $o' - x''y''$ coordinate system, the rendezvous orbit can be described by the following elliptic equation:

Fig. A.3 Schematic figure of rendezvous orbit



$$\frac{x''}{a^2} + \frac{y''}{b^2} = 1 \tag{A.2}$$

Now we convert Eq. (A.2) into the $o - xy$ coordinate system, and the conversion relationship is:

$$\begin{bmatrix} x'' \\ y'' \end{bmatrix} = \begin{bmatrix} \cos(\psi) & \sin(\psi) \\ -\sin(\psi) & \cos(\psi) \end{bmatrix} \begin{bmatrix} x - x_{c0} \\ y - y_{c0} \end{bmatrix} \tag{A.3}$$

When we rearrange the equations, the following constraint conditions can be obtained:

$$\psi = \begin{cases} \arctan\left(\frac{y_{c0}}{x_{c0}}\right), & x_{c0} > 0, y_{c0} > 0 \\ \pi + \arctan\left(\frac{y_{c0}}{x_{c0}}\right), & x_{c0} < 0, y_{c0} > 0 \\ \pi + \arctan\left(\frac{y_{c0}}{x_{c0}}\right), & x_{c0} < 0, y_{c0} < 0 \\ 2\pi + \arctan\left(\frac{y_{c0}}{x_{c0}}\right), & x_{c0} > 0, y_{c0} < 0 \end{cases} \tag{A.4}$$

We now substitute Eq. (A.3) into Eq. (A.2), and the following can be obtained:

$$A'x^2 + B'y^2 + C'xy + D'x + E'y + F' = 1 \tag{A.5}$$

Here:

$$\begin{cases} A' = \frac{\cos^2 \psi}{a^2} + \frac{\sin^2 \psi}{b^2}, & B' = \frac{\sin^2 \psi}{a^2} + \frac{\cos^2 \psi}{b^2}, & C' = 2 \cos \psi \sin \psi \left(\frac{1}{a^2} - \frac{1}{b^2}\right) \\ D' = \frac{1}{a^2} (-2x_{c0} \cos^2 \psi - 2y_{c0} \cos \psi \sin \psi) + \frac{1}{b^2} (-2x_{c0} \sin^2 \psi + 2y_{c0} \cos \psi \sin \psi) \\ E' = \frac{1}{a^2} (2x_{c0} \cos \psi \sin \psi - 2y_{c0} \sin^2 \psi) + \frac{1}{b^2} (2x_{c0} \cos \psi \sin \psi - 2y_{c0} \cos^2 \psi) \\ F' = \frac{1}{a^2} (x_{c0}^2 \cos^2 \psi + y_{c0}^2 \sin^2 \psi + 2x_{c0}y_{c0} \cos \psi \sin \psi) \\ \quad + \frac{1}{b^2} (x_{c0}^2 \sin^2 \psi + y_{c0}^2 \cos^2 \psi - 2x_{c0}y_{c0} \cos \psi \sin \psi) \end{cases}$$

It can be seen that A', B', C', D', E', F' contain five parameters $(a, b, \psi, x_{c0}, y_{c0})$. When we let

$$A = \frac{A'}{1 - F'}, B = \frac{B'}{1 - F'}, C = \frac{C'}{1 - F'}, D = \frac{D'}{1 - F'}, E = \frac{E'}{1 - F'}$$

the rendezvous orbit can be expressed in the general form of an elliptic equation:

$$Ax^2 + By^2 + Cxy + Dx + Ey = 1 \quad (\text{A.6})$$

And when we combine Eq. (A.1) with Eq. (A.4), it can be found that the A, B, C, D, E in Eq. (A.6) are only related to three parameters (b, x_{c0}, y_{c0}) .

Based on different mission requirements and the distribution of traversing points, various rendezvous orbits can be designed. In this section, we take the minimum sum of total distances between every traversing point and the rendezvous orbit as the optimization index to design an optimal rendezvous orbit. The design method is as follows.

We assume that there is a group of given traversing points $(x_1, y_1) \dots (x_n, y_n)$, and record the minimum distance between the i -th traversing point and the rendezvous orbit as L_i , then the question can be described as.

Find a rendezvous orbit, i.e., find a group of A, B, C, D, E where $\min \sum_{i=1}^n L_i$. As A, B, C, D, E are the functions of parameters (b, x_{c0}, y_{c0}) , the question is now transformed into looking for a group of parameters (b, x_{c0}, y_{c0}) where $\min \sum_{i=1}^n L_i$. In other words, the optimization design of a rendezvous orbit is the optimization design of multiple parameters under constraint conditions.

Here we take the four low-orbit satellites as an example and try to find a rendezvous orbit by which fast approaching detection can be achieved according to the above design method. The orbit parameters of the four target satellites are shown in Table A.1.

We assume the orbit inclination of the rendezvous orbit plane is 45° and the right ascension of the ascending node is 100° , then the traversing points of the four target satellites formed in the rendezvous orbit plane are shown in Table A.2.

Table A.1 Orbit parameters of four target satellites

Serial number	Orbit altitude (km)	Orbit inclination	Right ascension of ascending node
1	715	57°	30°
2	800	63°	40°
3	850	99°	60°
4	1100	63°	70°

Table A.2 Coordinates of traversing points in rendezvous orbit plane

	Traversing point 1	Traversing point 2	Traversing point 3	Traversing point 4
Geocentric distance r (km)	7093.1	7178.1	7228.1	7478.1
Argument of ascending node ϕ (deg)	76.976	89.554	315.481	296.756
	Traversing point 5	Traversing point 6	Traversing point 7	Traversing point 8
Geocentric distance r (km)	7093.1	7178.1	7228.1	7478.1
Argument of ascending node ϕ (deg)	25.6976	26.9554	135.481	116.756

Table A.3 Parameters of rendezvous orbit in orbit plane

Semi-major axis a	Semi-minor axis b	x_{c0}	y_{c0}	Argument of perigee ω
7209.903 km	7209.88 km	15.18 km	-9.63 km	327.898 deg

Table A.4 Orbit elements of rendezvous orbit

Orbit inclination i	Right ascension of ascending node Ω	Argument of perigee ω	Semi-major axis a	Eccentricity e
45 deg	100 deg	327.898 deg	7209.903 km	0.00249

Now we use the optimization toolbox in MATLAB and take the minimum sum of total distances between the traversing points and the rendezvous orbit as the optimization index to design the orbit parameters of the rendezvous orbit in the orbit plane. The orbit parameters are shown in Table A.3.

If we convert the parameters into orbit elements and combine them with the parameters of the rendezvous orbit plane, then the orbit parameters of the rendezvous orbit are shown in Table A.4.

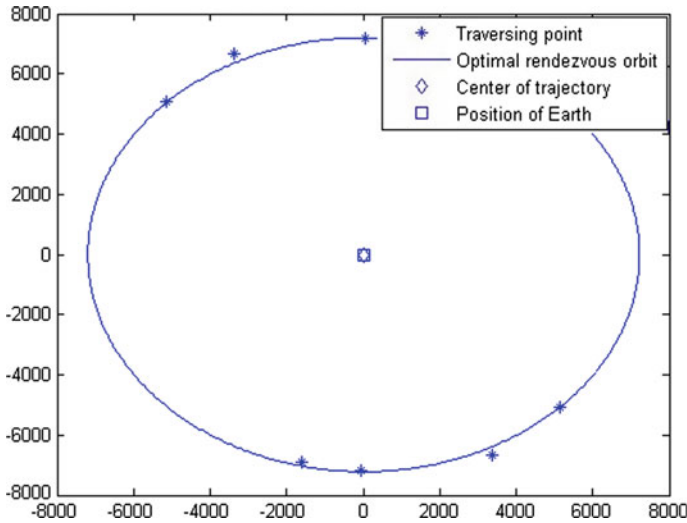


Fig. A.4 Schematic figure of traversing points and rendezvous orbit

Table A.5 Minimum distances between traversing points and rendezvous orbits

Serial number	Traversing point	Coordinates of traversing point (km)	Minimum distance (km)
1	Traversing point 1	(1598.5, 6910.6)	110.8348
2	Traversing point 2	(5587.5, 7177.9)	22.24078
3	Traversing point 3	(5153.8, -5068.0)	0.6784
4	Traversing point 4	(3366.6, -6677.4)	252.752
5	Traversing point 5	(-1598.5, -6910.6)	122.7575
6	Traversing point 6	(-5587.5, -7177.9)	41.2657
7	Traversing point 7	(-5153.8, 5068.0)	35.8368
8	Traversing point 8	(-3366.6, 667.74)	283.6231

The distribution of the eight traversing points in the rendezvous orbit plane and the optimal rendezvous orbit designed are shown in Fig. A.4.

The rectangular coordinates of the eight traversing points in the rendezvous orbit plane and their minimum distances to the rendezvous orbit are shown in Table A.5.

References

- Classification of Geosynchronous objects, issue 15. European Space Agency, European Space Operations Center (2013)
- Heiligers J, Ceriotti M, McInnes CR et al (2011) Displaced geostationary orbit design using hybrid sail propulsion. *Journal of Guidance, Control, and Dynamics* 34(6):1852–1866
- Matteo C, McInnes CR (2010) An earth pole-sitter using hybrid propulsion. In: AIAA/AAS astrodynamics specialist conference. Canada, pp 1–29
- NASA Goddard Space Flight Center. On-Orbit Satellite Servicing Study Project Report [EB/OL]. <http://servicingstudy.gsfc.nasa.gov/> (2011–2010)
- Union of Concerned Scientists. UCS Satellite Database [EB/OL]. http://www.ucsusa.org/nuclear_weap-ons_and_global_security/space_weapons/technical_issues/ucs-satellite-database.html
- Wertz JR, Microcosm (2005) Coverage, responsiveness, and accessibility for various “responsive orbits”. In: 3rd responsive space conference. Los Angeles